l'université nantes angers le mans
PÔLE DE RECHERCHE ET D'ENSEIGNEMENT SUPÉRIEUR

UNIVERSITÉ DE NANTES

Thèse de Doctorat

Rodrigue DÉCATOIRE

Mémoire présenté en vue de l'obtention du
grade de Docteur de l'Université de Nantes
sous le label de L'Université Nantes Angers Le Mans

École doctorale : SPIGA

Discipline : *Science de l'ingénieur*
Spécialité : *Génie civil*
Unité de recherche : *GeM*

Soutenue le *10 Décembre 2015*
Thèse N° :

Optimisation des campagnes d'inspection dans le cadre de processus stochastiques de dégradation : Application aux structures en béton armé

JURY

Rapporteurs :	**Alan O'CONNOR**, Associate Professor, Trinity College of Dublin (Irlande) **John Dalsgaard SØRENSEN**, Professor, University of Aalborg (Danemark)
Examinateurs :	**Alaa CHATEAUNEUF,** Professeur, Institut Pascal Clermont-Ferrand **Frédéric DUPRAT**, Professeur, INSA/LMDC Toulouse
Directeur de Thèse :	**Franck SCHOEFS**, Professeur, Université de Nantes
Co-directeur de Thèse :	**Sidi Mohammed ELACHACHI**, Maître de conférence HDR, Université de Bordeaux
Co-encadrant de Thèse :	**Thierry YALAMAS**, Docteur, Phimeca Engineering

l'université nantes angers le mans
PÔLE DE RECHERCHE ET D'ENSEIGNEMENT SUPÉRIEUR

UNIVERSITÉ DE NANTES

Thèse de Doctorat

Rodrigue DÉCATOIRE

Optimisation des campagnes d'inspection dans le cadre de processus stochastiques de dégradation : Application aux structures en béton armé

Optimisation of inspection plans for structures submitted to a stochastic degradation context: application on RC structures

Résumé

La gestion des structures en béton armé dans le but d'assurer leur sécurité et leur durabilité est devenu un challenge économique d'importance notable. La réponse à ce challenge tient en partie dans la recherche d'un plan d'inspection, de maintenance et de réparation (IMR) optimisé en fonction de contraintes de sureté.
Ce travail est placé dans un cadre de maintenance préventive, où les dégradations du béton considérées peuvent amener à la corrosion des armatures, non à la défaillance structurelle. Les modèles de dégradation concernés sont placés dans un cadre probabiliste où la variabilité spatiale de l'exposition environnementale et des propriétés matériaux du béton sont prises en comptes. Sur la base de ces prédictions, un plan d'expérience adaptatif permet d'identifier, à une date donnée, où il est intéressant d'inspecter la structure pour évaluer son état qui conditionnera la décision de maintenance ou de réparation.
Un arbre de décision permet ensuite de prédire l'évolution probabiliste de cet état incluant les effets des maintenances et réparations. Ce modèle est enfin utilisé dans une procédure d'optimisation qui vise à déterminer quand et avec quel outil cette structure doit être inspectée pour optimiser l'espérance du budget de suivi d'une structure ou d'un parc ainsi que les incertitudes associées liées aux erreurs de mesure, tout en prenant en compte les diverses contraintes spécifiques des gestionnaires d'ouvrages.

Mots clés
Optimisation, Variabilité spatiale, Inspection, Maintenance, Actualisation Bayésienne

---

Abstract

The development of modern societies has seen the construction of several structures and infrastructures built in reinforced concrete. The management of those structures, potentially large and subjected to important pathologies, aiming at ensuring and guaranteeing their safety and durability has become a true economical challenge. Looking for an optimal inspection, maintenance and repair plan according to safety constraints is one of the possible solutions to address this challenge.
This work is bounded by a preventive maintenance context where the concrete degradations may lead to the corrosion of the reinforcements and not to structural failure. The corresponding degradation models are put in an uncertainty context where the spatial variability of the environmental exposure and the concrete properties are accounted for. Based on such predictions, an adaptive design of experiments helps to identify, at a given time, where the structure should be inspected in order to evaluate its degradation state which will indicate the need for maintenance or a repair action.
A decision tree therefore allows to predict the probabilistic evolution of the structure state, including the effect of maintenance and repairs. This tree is then used in an optimisation process which aims at finding where and with which inspection technique the structure is to be inspected to minimise both the expectation of the exploitation costs and the associated uncertainties due to the measurement errors, accounting for the stakeholder's constraints.

Key Words
Optimisation, Spatial variability, Inspection, Maintenance, Bayesian statistics

---

Optimisation of inspection plans for structures submitted to a stochastic degradation context : application on RC structures

A thesis submitted by **Rodrigue DÉCATOIRE**
in partial fulfillment of the requirements for
the degree of doctor of philosophy

UNIVERSITÉ DE NANTES

Nantes, France

defended publicly on December 10, 2015 in front of a jury made up of:

Pr. Alaa CHATEAUNEUF	Institut Pascal, Clermont-Ferrand	Examiner
Pr. Frédéric DUPRAT	INSA/LMDC, Toulouse	President of the jury
Dr. Mohammed ELACHACHI	Université de Bordeaux, Bordeaux	Co-supervisor
Dr. Alan O'CONNOR	Trinity College Dublin, Irlande	Reviewer
Pr. Franck SCHOEFS	Université de Nantes, Nantes	Supervisor
Pr. John Dalsgaard SØRENSEN	Université d'Aalborg, Danemark	Reviewer
Dr. Thierry YALAMAS	Phimeca Engineering S.A., Paris	Co-supervisor

RÉSUMÉ ÉTENDU

Les structures en béton armé et leur plan d'inspections

Introduction

L'expansion des pays développés et la croissance rapide de leur population depuis le 19ème siècle ont conduit à la construction de nombreuses structures et infrastructures en béton armé afin de répondre aux besoins en :

- Énergie ;
- Logements ;
- Infrastructures routières et ferroviaires.

En France, ces infrastructures routières et ferroviaires sont composées de :

- 280 000 ponts ;
- 50 000 murs de soutènement ;
- 1 000 kilomètres de tunnels.

L'électricité est produite entre autres à 80% par 60 réacteurs nucléaires et à 5% par 450 barrages hydrauliques. 62% des 4 millions d'habitations à loyer modéré ont été construites avant les années 80. En considérant l'importance économique et sociale de ces structures et infrastructures, il ne fait aucun doute qu'assurer leur fiabilité est un challenge majeur pour chaque pays développé. D'autant plus que dans l'environnement économique actuel, ces structures tendent à avoir une durée de vie étendue afin d'éviter de coûteuses reconstructions. C'est pourquoi la conservation d'un niveau de fiabilité donné impose que ces structures soient inspectées et maintenues de façon régulière, en accord avec des plans d'inspection, de maintenance et de réparation (IMR). Cependant le coût de ces plans IMR, bien que plus faible qu'un coût de reconstruction, n'est pas pour autant négligeable.

D'un autre côté, les politiques de développement durable sont devenues un sujet de préoccupation majeur ces 10 dernières années. Cela implique d'appliquer les plans IMR dans un contexte de maintenance préventive afin de réduire au maximum les coûts associés aux actions de maintenance et de s'affranchir du besoin de reconstruction.

Traiter de ces aspects nécessite une procédure optimisé pour concevoir les plans IMR visant à réduire également le coût d'inspection à long terme de ces structures et infrastructures.

Les processus de dégradation physico-chimique du béton armé

Le vieillissement des structures en béton armé trouve ses origines dans des processus de dégradation physico-chimiques liés à l'environnement extérieur. Chaque structure en béton armé est au minimum exposée au dioxyde de carbone, noté CO_2, qui est la source du processus de carbonatation du béton. Le dioxyde de carbone pénètre à l'intérieur du béton par la porosité et réagit avec la chaux du béton pour former du carbonate de calcium, comme illustré Figure 1, ce qui conduit à une baisse du pH de la solution interstitielle.

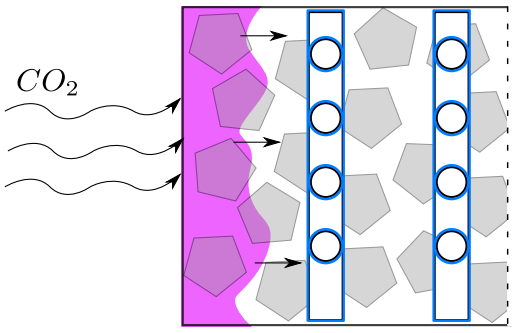

FIGURE 1 – Représentation du processus de carbonatation du béton. L'aire rose représente la partie carbonatée. Les barres et cercles bleus représentent les armatures ainsi que leur protection contre la corrosion.

La cinétique du processus de dégradation, relativement lente, dépend principalement de la porosité du béton, de son humidité relative et de la concentration de CO_2 dans l'atmosphère qui varie entre 0.03% et 0.2% en atmosphère urbaine.

Les structures proches d'un environnement marin sont également exposées aux chlorures. Comme le montre la Figure 2, ce processus est similaire à la carbonatation puisque les ions chlorures pénètrent également via la porosité du béton. Leur présence entraîne une baisse du pH de la solution interstitielle.

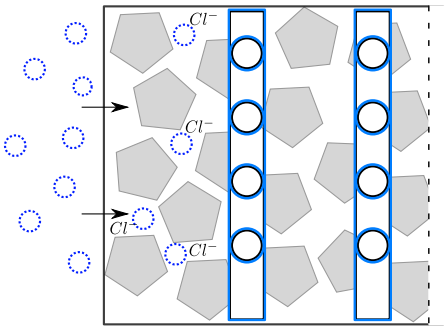

FIGURE 2 – Représentation du processus de pénétration des ions chlorures dans le béton armé.

La solution interstitielle du béton armé est alcaline, son pH étant compris entre 12 et 13. Dans ces conditions de pH un film passif (représenté en bleu dans les Figures 1 et 2) protège les armatures de la corrosion. Si la pénétration des ions chlorures et la carbonatation n'occasionnent pas directement une baisse des propriétés mécaniques du béton armé, ces processus de dégradation détruisent la protection des armatures contre la corrosion en baissant le pH de la solution interstitielle. L'apparition de la corrosion pouvant amener vers la défaillance structurelle par fissuration du béton armé.

✓ *Ces processus de dégradation et leurs modélisations sont introduits dans le Chapitre 1.*

Bilan sur les approches d'optimisation

De l'analyse de Faber et Stewart (2003) sur la généralisation des méthodologies d'optimisation de plan d'inspections résultent d'intéressantes conclusions comme par exemple :

- Les ingénieurs n'apparaissent pas complètement convaincus de l'utilité de ces méthodologies qu'ils jugent "trop compliquées", "trop mathématiques" pour évaluer le risque d'un évènement jamais observé ;
- La prudence générale et une longue expérience amènent à privilégier l'usage de méthodes standardisées pour la définition des plans d'inspections. Cependant ces méthodes peuvent ne pas être appropriées.

Basés sur ces observations et sur une revue de la littérature de ce sujet, les objectifs de la thèse sont :

1. De proposer une méthodologie d'optimisation des plans d'inspections :
    - Non dédiée à un unique objectif ;

- Aussi indépendante que possible des différentes hypothèses qui peuvent être faites sur la modélisation des inspections, des maintenances et des défaillances ;
- Capable d'être appliquée sur des structures de différentes tailles, soumises ou non à des processus de dégradation présentant une corrélation spatiale ;
- Indépendante du processus de dégradation considéré et de l'indice de dégradation correspondant ;
- Aussi simple que possible avec un coût de calcul acceptable.

2. De permettre l'utilisation de données existantes qui s'avéreraient pertinentes pour calibrer ou actualiser le modèle de dégradation pour affiner le plan d'inspections conçu par la méthodologie d'optimisation.

✓ *La revue bibliographique évoquée est disponible dans le Chapitre 1.*

Prédire l'évolution d'un indice de dégradation

Modèle de prédiction de l'indice de dégradation

Pour proposer une méthodologi.e capable de répondre aux objectifs de la thèse, l'utilisation d'un arbre de décision comme modèle prédictif de l'évolution d'un indice de dégradation incluant l'effet des inspections, des maintenances et des réparations, dénoté ci-après *IMRM*, est apparue plus appropriée. Cet arbre de décision illustré Figure 3 est capable de répondre aux objectifs de la thèse puisque :

- Le noeud d'inspection conduit à l'estimation de deux probabilités, fonction d'un indice de dégradation D :
  - La probabilité de réparer (ou probabilité de défaillance) définie par :
    $$\tilde{\mathscr{P}}_f = \tilde{\mathscr{P}}\left[D >= d_c\right], \tag{1}$$
    où d_c est le seuil de défaillance relatif à l'indice de dégradation D ;
  - La probabilité de maintenance définie par :
    $$\tilde{\mathscr{P}}_{Ma} = \tilde{\mathscr{P}}\left[D >= d_{pm} \mid D < d_c\right], \tag{2}$$
    avec d_{pm} le seuil de maintenance relatif à l'indice D. La probabilité de maintenance est conditionnée par le non-franchissement du seuil de défaillance.

  Aucune hypothèse n'est nécessaire concernant la méthode d'inspection menant à l'estimation de ces probabilités ;
- Maintenir et réparer mènent uniquement à la prochaine inspection, sans hypothèse sur la technique de réparation (parfaite ou non, modifiant la cinétique de dégradation, ...).

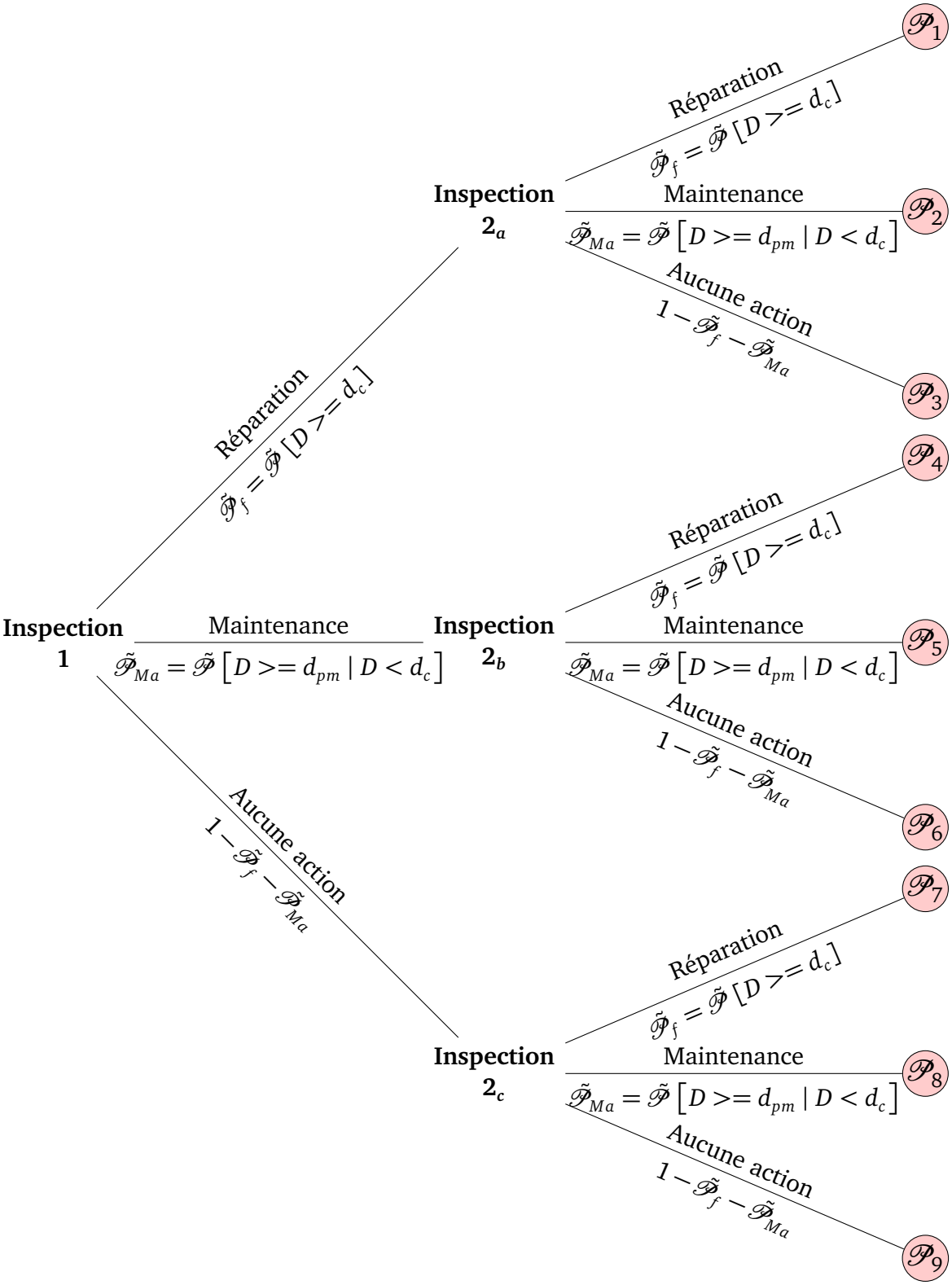

FIGURE 3 – Arbre de décision avec deux inspections. $\mathscr{P}_\circ$ est la probabilité de la branche $\circ$.

Plan d'expérience adaptatif

En définissant l'indice de dégradation D tel que :

$$D = \frac{|L_d - L_t|}{L_t},$$

où L_d est la longueur d'armatures potentiellement dépassivées et L_t la longueur totale d'armatures. À partir des simulations du modèle de dégradation considéré, la probabilité, notée $\mathscr{P}[D \geq d]$, que cet indice de dégradation ait dépassé un seuil donné peut être aisément calculée, par exemple par échantillonnage de Monte Carlo.

Cependant, si les simulations du processus de dégradation sont effectuées sur l'intégralité de la structure, une campagne d'inspections ne retournera que la mesure de cette dégradation à certains endroits de cette structure. A partir de la Figure 3, nous pouvons donc définir la probabilité d'action calculée à partir des simulations telle que :

$$\mathscr{P}_{act} = \mathscr{P}[D \geq d_c] + \mathscr{P}\left[D >= d_{pm} \mid D < d_c\right],$$

et son estimation résultante des points choisis pour l'inspection $\hat{\mathscr{P}}_{act}$.

Un plan d'expérience adaptatif en deux étapes est proposé pour assurer qu'avec un minimum de points inspectés l'approximation soit suffisamment précise.

La première partie de ce plan utilise l'autocorrélation du champ de dégradation de manière à effectuer des inspections quasi-indépendantes. Connaissant le nombre maximum de points d'inspection autorisés n_{insp_m}, la démarche est la suivante :

- Allouer s_{high} des points d'inspection $\left[x_{insp}^{(i)}, i = 1, \ldots, n_{insp_m}\right]$ dans les zones de fortes dégradations définies par :
$$\underset{x}{\operatorname{argmax}}\, \mathscr{Q}_X(x),$$
avec $\mathscr{Q}_X(x)$ le quantile à 95% de la dégradation au point x dénotée par $P(X(x) \leq \mathscr{Q}_X(x)) = 0.95$;
- Allouer $1 - s_{high}$ des points d'inspection dans les zones faiblement dégradées définies par :
$$\underset{x_{insp}}{\operatorname{argmin}}\, \mathscr{Q}_X(x_{insp}) \text{ ;}$$
- Ajouter les points situées sur les coins du domaine afin de le considérer dans son intégralité ;
- Interpoler les trajectoires entre les points d'inspection pour estimer la distribution de l'indice de dégradation ;

sous contrainte que $\nexists x_{insp}^{(i)}, x_{insp}^{(j)} \diagup R\left(x_{insp}^{(i)}, x_{insp}^{(j)}\right) < 0.3, i \neq j, (i,j) = 1, \ldots n_{insp} \leq n_{insp_m}$, $R(x, x')$ représentant la corrélation linéaire de la dégradation entre les positions d'inspection $x_{insp}^{(i)}$ et $x_{insp}^{(j)}$

La seconde partie de ce plan, la partie *adaptative*, vise à assurer la qualité de l'approximation de la probabilité d'action $\hat{\mathscr{P}}_{act}$.

Soit le critère $I(x)$ qui quantifie la qualité de l'approximation tel que :

$$I(x) = \epsilon_{\mathscr{T}}(x),$$

avec $\epsilon_{\mathscr{T}}(x) = \max\left(\mathscr{T}(x) - \hat{\mathscr{T}}(x)\right) - \min\left(\mathscr{T}(x) - \hat{\mathscr{T}}(x)\right)$ où $\mathscr{T}(x)$ est le vecteur des trajectoires de la dégradation à la position x et $\hat{\mathscr{T}}(x)$ les approximations correspondantes qui résultent du plan d'expérience.

Soit une formulation générique de la précision de l'approximation définie par :

$$\epsilon_{\mathscr{P}} = \frac{\left|\hat{\mathscr{P}} - \mathscr{P}\right|}{\mathscr{P}},$$

où les probabilités $\mathscr{P}$ and $\hat{\mathscr{P}}$ sont respectivement égales à :

- $\mathscr{P}_f$ et $\hat{\mathscr{P}}_f$ pour l'événement de défaillance, la précision étant par conséquent notée $\epsilon_{\mathscr{P}_f}$;
- $\mathscr{P}_{Ma}$ et $\hat{\mathscr{P}}_{Ma}$ pour l'action de maintenance, la précision correspondante étant notée $\epsilon_{\mathscr{P}_{Ma}}$.

En premier lieu, le plan d'expérience adaptatif cherche à améliorer la précision de l'estimation de la probabilité de défaillance en ajoutant aux points d'inspection la solution de :

$$\underset{x}{\operatorname{argmax}}\, I(x),$$

en s'assurant que cette solution permet de diminuer $\epsilon_{\mathscr{P}}$.

De multiples solutions sont trouvées et ajoutées tant que $\epsilon_{\mathscr{P}_f} \geq \epsilon_{\mathscr{P}_{f\,lim}}$ et dans un second temps jusqu'à ce que $\epsilon_{\mathscr{P}_{Ma}} \leq \epsilon_{\mathscr{P}_{Ma_{lim}}}$, tout en vérifiant que $n_{insp} \leq n_{insp_m}$ à la fin de ces deux étapes. L'ordre de ces étapes doit être respecté, étant donné que la probabilité de maintenance est conditionnée par la non-défaillance, une bonne approximation de cette probabilité nécessite une bonne approximation de la probabilité de défaillance.

✓ *La mise en place et l'utilisation de l'IMRM sont décrites dans le Chapitre 2.*

Calibrer le modèle prédictif : le cas du béton armé

Un des objectifs de la thèse est de permettre l'utilisation des données pertinentes pour calibrer le modèle de dégradation utilisé par l'IMRM. Les propriétés du béton, qui sont des entrées de ces modèles, pouvant être connues par :

- Mesure directe ;
- Mesure indirecte ;
- Jugement d'expert ;

La mixité de ces données convient parfaitement au cadre de l'actualisation Bayésienne qui permet de toutes les prendre en compte.

Cependant, il apparaît qu'il est globalement difficile de renseigner les entrées de ces modèles et d'observer leur sortie par des techniques de contrôle non-destructif. A partir de données réelles de carbonatation obtenues par contrôle destructif, il est cependant démontré que la mesure des sorties du modèle de dégradation est plus importante que toute autre mesure. Ce travail permet de mettre en lumière le besoin d'une technique de contrôle non-destructif capable de suivre les dégradations considérées dans un cadre de maintenance préventive.

✓ *Cette partie est détaillée dans le Chapitre 3.*

Optimiser le plan d'inspection

Fonctions objectif

Le coût d'exploitation d'une structure est en général défini par (Frangopol et al. (1997); Sheils et al. (2010a)) :

$$C^{tot} = C^{In} + C^{Ma} + C^{F},$$

avec C^{In}, C^{Ma} and C^{F} les coûts d'inspection, de maintenance et de réparation, respectivement. Dans le contexte probabiliste de cette thèse, chaque coût $C^{\bullet}$ est remplacé par son espérance mathématique $\mathbb{E}[C^{\bullet}]$.

Étant donnés :

- l'IMRM représenté Figure 3 avec m branches, chacune ayant une probabilité $\mathscr{P}_i$ d'être réalisée ;
- l'horizon temporel t_{lim} discrétisé en t_{tot} pas de temps ;
- les dates d'inspection $\boldsymbol{t_{In}}$;
- un taux d'actualisation r ;

Des modèles génériques pour les coûts d'inspection, de maintenance et de défaillance sont définis par :

$$\mathbb{E}\left[C^{In}\right] = \sum_{i=1}^{m} \mathscr{P}_i \sum_{t \in \boldsymbol{t_{In}}} \frac{\boldsymbol{n_I}^{(i,t)} \boldsymbol{C_{In}}^{(t)}}{(1+r)^t},$$

$$\mathbb{E}\left[C^{Ma}\right] = C_{Ma} \sum_{i=1}^{m} \mathscr{P}_i \sum_{t \in \boldsymbol{t_{In}}} \frac{\mathbb{1}_{i,t}^{Ma}}{(1+r)^{t+t_{Ma}}},$$

$$\mathbb{E}\left[C^{F}\right] = C_{F} \sum_{i=1}^{m} \mathscr{P}_i \sum_{t \in \boldsymbol{t_{In}}} \frac{\mathbb{1}_{i,t}^{F}}{(1+r)^{t+t_{R}}},$$

où :

- $n_I^{(i,t)}$ est le nombre de points inspectés à la date t dans la branche i de l'arbre de décision ;
- $\mathbb{1}_{i,t}^{Ma}$ (ou $\mathbb{1}_{i,t}^{F}$) vaut 1 si une maintenance (ou une réparation) est décidée dans la branche i au temps t, 0 sinon ;
- t_{Ma} et t_R sont respectivement les délais de maintenance et de réparation qui peuvent résulter de contraintes techniques ou financières.

Ces formulations génériques dérivées de l'arbre de décision ne font aucune hypothèse sur les coûts associés à une inspection, une maintenance ou une défaillance respectivement notés C_{In}, C_{Ma} and C_F.

Définition du problème d'optimisation

Le problème d'optimisation résolu dans cette thèse est le suivant.

En supposant que :

- L'intervalle de temps entre deux inspections est constant, de façon à mieux représenter les habitudes des gestionnaires d'ouvrages ;
- Une seule technique d'inspection est utilisée lors d'une campagne d'inspection ;

Et étant donnés :

$$\begin{cases} \text{Les techniques d'inspection} & \boldsymbol{T_{In}} = [0, 1, 2, \cdots, n_T] \\ \text{Les coûts d'inspection correspondants} & \boldsymbol{C_{In}} = [C_{In}^{(0)}, C_{In}^{(1)}, \cdots, C_{In}^{(n_T)}] \\ \text{L'horizon temporel} & t_{lim} \\ \text{Le taux d'actualisation} & r \\ \text{Le délai de maintenance} & t_{Ma} \\ \text{Le délai de réparation} & t_R \\ \text{L'indice de dégradation préventif} & D_P \\ \text{L'indice de dégradation curatif} & D_F \\ \text{L'IMRM} & \end{cases}$$

Le problème d'optimisation est de trouver :

$$\begin{cases} \text{L'intervalle de temps entre deux inspections} & \Delta t_{In} \\ \text{Le plan d'inspections} & \boldsymbol{Pl}_{In} \end{cases} = \left[\boldsymbol{T_{In}}^{(0)}, \ldots, \boldsymbol{T_{In}}^{(t_{lim}/\Delta t_{In})} \right]$$

Pour minimiser l'espérance du coût total $\mathbb{E}[(C_{tot})]$ et son intervalle de confiance $CI(\mathbb{E}[(C_{tot})])$ sous certaines contraintes, où

- $i \in \boldsymbol{T_{In}}$ signifie que la technique d'inspection i avec le coût $C_{In}^{(i)}$ est utilisée ;
- $\boldsymbol{Pl_{In}}^{(i)}$ est la technique d'inspection utilisée à la $i-eme$ inspection.

La solution finale est sélectionnée au sein du front de Pareto résultant, à partir de critères donnés par le gestionnaire.

Exploitation du front de Pareto

Un cas simple d'un immeuble comprenant 120 balcons soumis à la carbonatation où 12 d'entre eux sont régulièrement inspectés est considéré. Un exemple de ce type de structure est donné Figure 4. Les coûts d'inspection, de maintenance et de réparation sont fixés à partir d'une analyse de coûts.

Le modèle de carbonatation utilisé est un méta-modèle de type krigeage vectoriel identifié à l'aide de simulations du modèle SCARABET (de Larrard et al. (2014)). Les balcons sont modélisés soit par des poutres de 3 mètres de long, soit des surfaces de 3 mètres de long par 1.2 mètres de large. Les prévisions du modèle de carbonatation ainsi que la structure de corrélation observée sur ces trajectoires sont illustrées Figures 5 et 6, dans le cas unidimensionnel.

Le front de Pareto résultant de l'optimisation du plan d'inspections de ce cas unidimensionnel est donné Figure 7.

Le point $\Delta t_{In} = 12; \mathbf{Pl}_{In} = [0, 2, 0, 1]$ signifie que pour cette solution :

- L'intervalle de temps entre deux inspections est fixé à 12 ans ;
- Sur l'horizon temporel de 60 ans cela amène donc à 4 inspections qui sont successivement réalisées par les techniques d'inspection 0, 2, 0 et 1. L'inspection de type 0 est la plus chère et la plus précise. L'inspection de type 2 est la moins chère et la moins précise.

Ce plan prédit que 2 inspections (avec une probabilité égale à 0.9997) seront utiles :

- La première inspection a 100% de chances d'être inutile ;
- La troisième inspection a 65% de chances d'être effectuée ;

FIGURE 4 – Illustration d'un immeuble à Marseille.

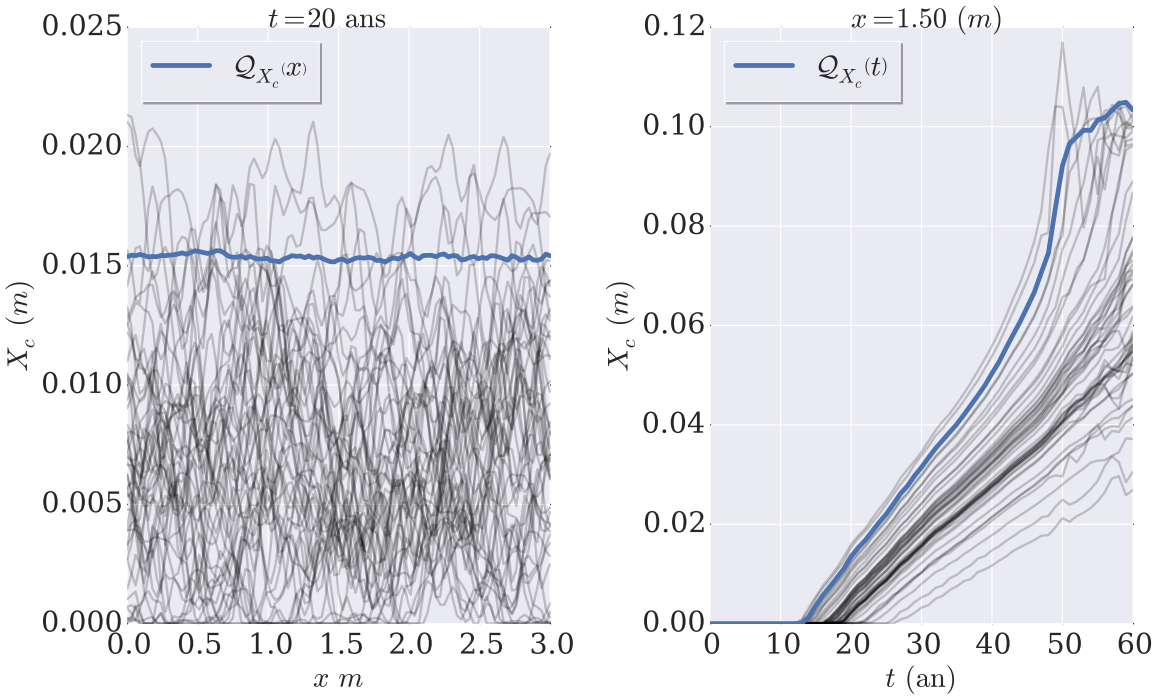

FIGURE 5 – Prévisions du modèle de dégradation.

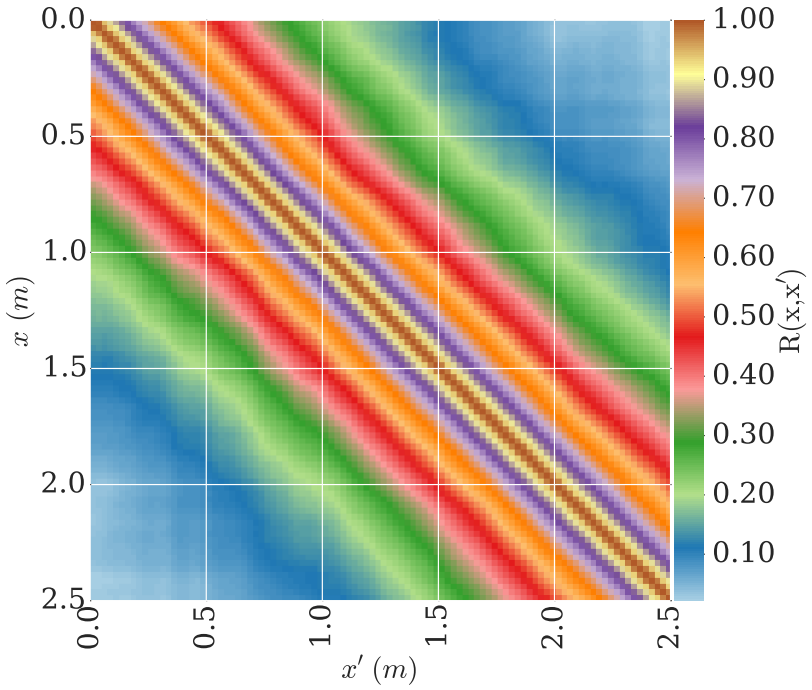

FIGURE 6 – Autocorrélation du processus de carbonatation.

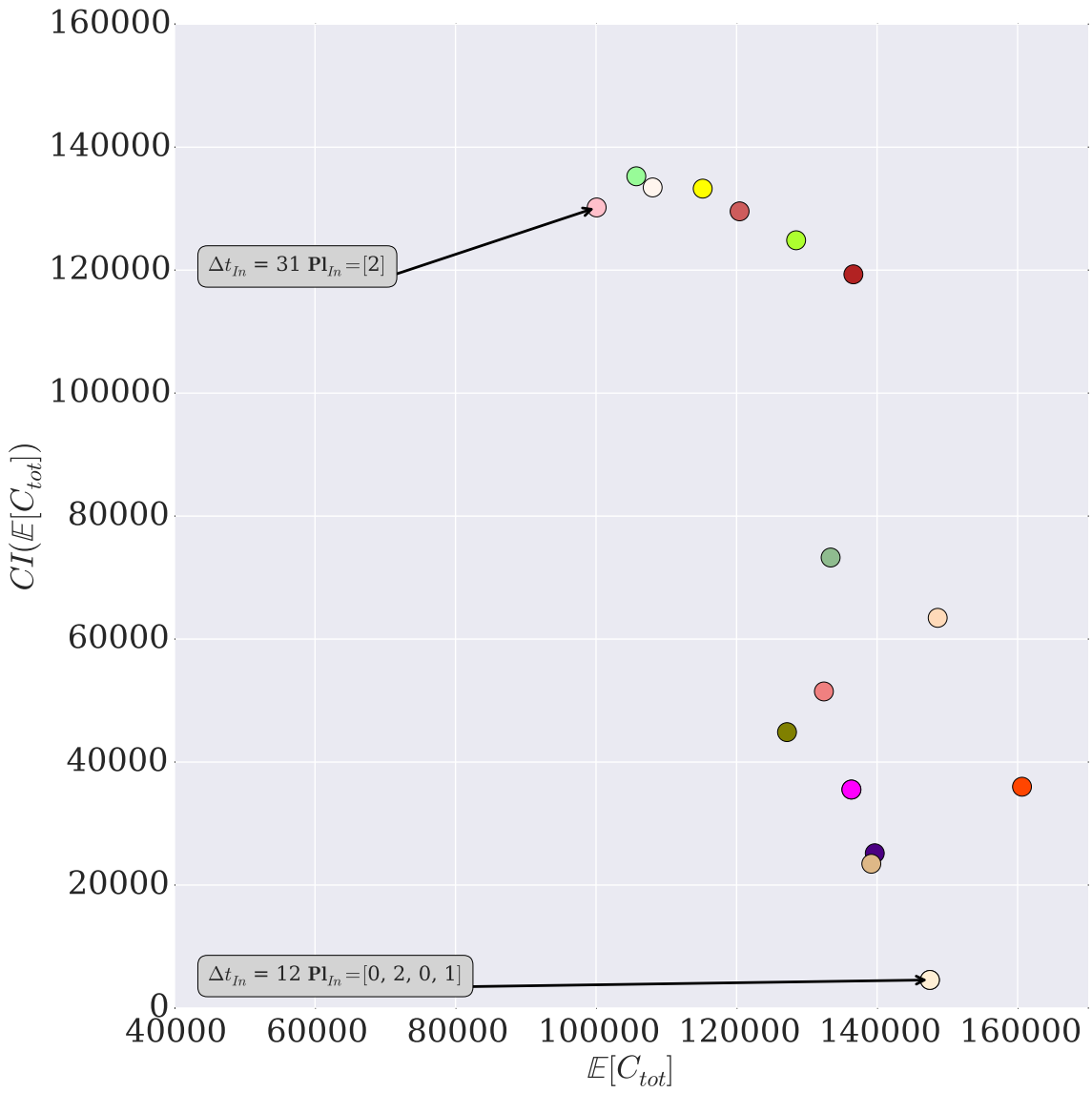

FIGURE 7 – Front de Pareto projeté sur le plan formé par l'espérance du coût total et son intervalle de confiance, uniquement pour les solutions donnant une espérance du temps passé en défaillance inférieure à un an.

- La dernière inspection a 65% de chances d'être inutile.

De nombreux indicateurs peuvent être dérivés de l'arbre de décision, tel que l'espérance et l'intervalle de confiance du nombre de maintenances et de réparations réalisées comme montré dans le Tableau 1. Selon ce plan la probabilité qu'une action de maintenance soit menée est de 77%, celle qu'aucune réparation ne soit nécessaire est de 82%. Les erreurs d'inspections entraînent un risque que deux actions de maintenance soient effectuées avec une probabilité de 24% si la dégradation est suresaDe nmée.

n°	μ_{Ma}	$[CI^-; CI^+]_{Ma}$	μ_F	$[CI^-; CI^+]_F$
0	0.18	$[0.13; 0.09]$	0.82	$[0.87; 0.91]$
1	0.77	$[0.87; 0.67]$	0.18	$[0.13; 0.09]$
2	0.05	$[0; 0.24]$	0	$[0; 0]$
3	0	$[0; 0]$	0	$[0; 0]$
4	0	$[0; 0]$	0	$[0; 0]$

TABLE 1 – Moyenne et intervalle de confiance pour le nombre de maintenances et de réparations avec un intervalle de temps entre deux inspections de 12 ans.

✓ *Cette partie est détaillée dans le Chapitre 4.*

Conclusion

La méthodologie développée dans ce travail répond donc aux objectifs de la thèse. L'utilisation d'un arbre de décision permet de dériver de nombreux indicateurs pour aider le gestionnaire à choisir *sa* solution au sein d'un front de Pareto. Des cas variés ont été traités (modélisation 1D, 2D, système) démontrant les capacités d'adaptation de la méthode à différents choix de modélisation.

Cependant, ce travail, notamment la notion de plan d'expérience adaptatif, n'est pas directement exploitable aux cas où l'action de maintenance dépendrait d'une valeur locale de la dégradation (*e.g.* la présence d'une fissure critique au sein d'une structure en acier). L'extension à d'autres types de dégradation ainsi que l'application sur un cas industriel font partie des principales perspectives de ce travail.

CONTENTS

INTRODUCTION

"O most ingenious Theuth, the parent or inventor of an art is not always the best judge of the utility or inutility of his own inventions to the users of them.

And in this instance, you who are the father of letters, from a paternal love of your own children have been led to attribute to them a quality which they cannot have; for this discovery of yours will create forgetfulness in the learners' souls, because they will not use their memories; they will trust to the external written characters and not remember of themselves.

The specific which you have discovered is an aid not to memory, but to reminiscence, and you give your disciples not truth, but only the semblance of truth; they will be hearers of many things and will have learned nothing; they will appear to be omniscient and will generally know nothing; they will be tiresome company, having the show of wisdom without the reality." Plato

The stakeholder challenge

Since the 19th century, the expansion of developed countries and the fast increase of their population has lead to the build of numerous structures and infrastructures in reinforced concrete in order to answer to the needs in:

- Energy;
- Accomodations;
- Road and railway infrastructures.

In France, the road and railway infrastructures gather:

- 280.000 bridges;
- 50.000 retaining walls;
- 1.000 km of tunnels.

The electricity is produced at 80% by 60 nuclear power plants, 5% by 450 hydraulic dams. 62% of the 4 millions low-cost housing have been built before the eighties. Ensuring

the reliability level of those structures is undoubtedly a major challenge for each developed country considering their economical and social importance.

Due to the economical context, on one side most of the stakeholders plan to extend the original lifespan of their structures to avoid costly reconstructions. Those structures are thus inspected and maintained regularly according to Inspection, Maintenance and Repair (IMR) plans in order to sustain their reliability. Although much lower than reconstruction costs, the costs induced by these IMR plans keep on being significant.

On the other side, the sustainable development has grown as a major subject in the past 10 years which induces to apply the IMR plans in a preventive context of degradation, i.e. to reduce at most the volume of natural material required and the risk of a needed reconstruction.

These aspects call for an optimised procedure to design IMR plans in order to reduce the long run monitoring cost at the same time. Therefore the stakeholders challenge may come down to both:

- *Ensure the maximum safety at a given cost*;
- *Ensure the minimum cost at a given safety level*.

Outline of the thesis

Chapter 1 presents an overview of the concrete degradation processes which can be predicted by empirical, finite-element or statistical models. These processes may lead to a loss of safety and a need of maintenance for the concerned structures. This chapter introduces a literature review of the optimisation methods available for structures management together with the different inspection modellings of non-destructive techniques (NDTs). Finally the objectives of the thesis are derived from an analysis of the latter review.

Chapter 2 is concerned with the prediction of the structure degradation index by a decision tree which includes the effect of inspections and maintenance, i.e. the first step of the methodology proposed in this thesis. In order to account for the spatial variability inherited by the concrete properties and the structures sizes, an adaptive design of experiments based on valuable degradation predictions is proposed to estimate the degradation index of the structure with the minimum number of inspection locations. Low-discrepancy sequences are also introduced and may be used if no reliable degradation predictions are available. A silver thread case study based on balconies management is described and used to demonstrate the usefulness of the decision tree as an *inspection, maintenance and repair* model.

The methodology assumes that a predictive degradation model exists. The purpose of **Chapter 3**, is to give to the stakeholder a tool for calibrating its degradation model. Bayesian statistics are particularly suited to this case since they allow to gather measurement results, expert judgement and structure specifications. The use of such method with the available non-destructive methods for concrete structures is illustrated by real measurements per-

formed on a concrete wall belonging to the French Alternative Energies and Atomic Energy Commission.

Last but not least, **Chapter 4** aims at integrating the life-cycle model designed in Chapter 2 into an optimisation procedure. Genetic algorithms are introduced for their ability to handle multi-objective problems with categorical optimisation variables (e.g. the inspection method). A focus is made on the Non-Sorting Genetic Algorithm (NSGA-II) for its interesting space exploration and *elitism* properties. The optimisation problem is defined such as the expectation of the total cost, its confidence interval and the time spent into the failure state are the three objectives to minimise. The optimisation variables are the time interval between two successive inspection and the inspection method used at each inspection. The optimisation procedure is performed on the silver thread example described in Chapter 2 and demonstrates the ability of the proposed methodology to handle the thesis objectives defined in Chapter 1.

For the sake of clarity, the connections between the different chapters and the overall methodology presented in this thesis are shown in Figure 1.

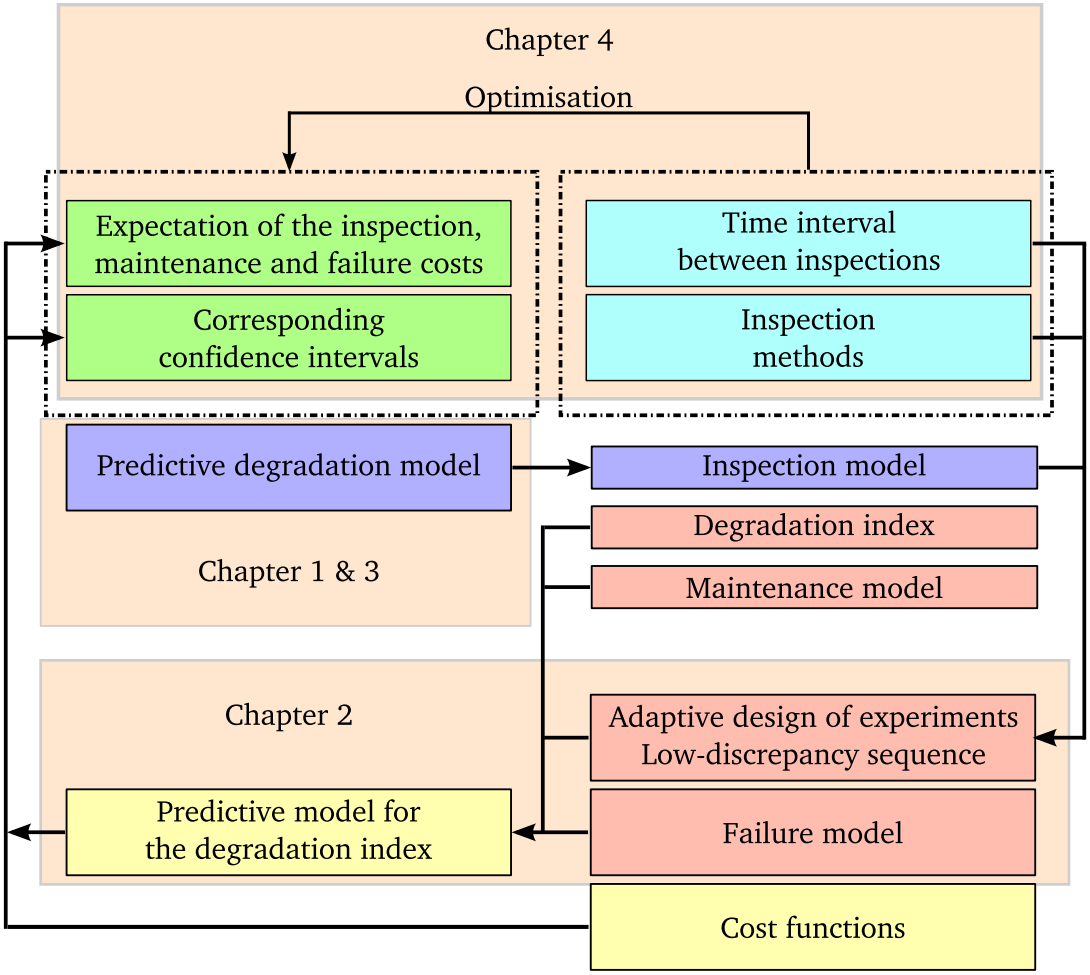

Figure 1 – Outline of the thesis

CHAPTER 1

OVERVIEW ON RC STRUCTURES AND THEIR INSPECTION PLANS

1.1 Introduction

The management of ageing reinforced concrete (RC) structures has been a productive research domain through the past decades. Two complementary views of the optimisation of Inspection, Maintenance and Repair (IMR) plans of structures have emerged from these researches. The first one is based on the degradation predictions of given structures and predicts the potential results of an inspection. The second one uses real observations in order to define the structure state to update the degradation predictions.

This chapter introduces the basics of those management methods. It contains three main sections. Section 1.2 presents the basics of the main degradations affecting RC structures. A focus is made on the statistical models in Section 1.3. Section 1.4 is an overview of the two thinking movements mentioned above, each of them dealing with the optimisation of the management through different methods. Section 1.5 presents the objectives of the thesis which are derived from the inconsistency of the answers those methods give to the stakeholder's challenge.

1.2 Context : RC structures and their degradations

1.2.1 Ageing RC structures

Ensuring the maximum safety is a challenge due to different time-dependent degradation processes of reinforced concrete structures which could lead to structural failure more or less quickly.

1.2.1.1 Physicochemical degradations

The ageing of RC structures finds its origin in physicochemical degradations conditioned by their environmental exposure. Each RC structure placed in atmospheric conditions is at least exposed to the carbon dioxide CO_2 which is the source of the *so-called* carbonation process. As illustrated through Figure 1.1, the carbon dioxide penetrates into the concrete through its porosity. A chemical reaction thus happens between the carbon dioxide and the lime in the cement, forming calcium carbonate. Compared to a normal concrete, a carbonated concrete has:

- a higher compressive strength;
- a lower porosity;
- a lower pH.

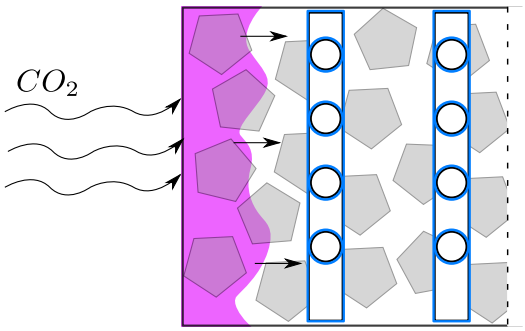

Figure 1.1 – Illustration of the carbonation process of reinforced concrete. The pink area represents the carbonated part.

This degradation process has a slow kinetic which depends mainly on the concrete porosity, the relative humidity and the carbon dioxide concentration in the atmosphere which varies from 0.03% to 0.2% in urban areas.

RC structures close to a marine environment are also exposed to the chloride ingress process. As shown by Figure 1.2 it is similar to the carbonation process since the chlorides progress into the concrete through the porosity, lowering the pH.

The pore solution of the reinforced concrete is *alkaline*, meaning its pH is around 12-13. Under these conditions a passive film (represented in blue in Figures 1.1 and 1.2) is formed on the steel surface of the reinforcement protecting it from the corrosion. If the chloride ingress and the carbonation processes do not damage the concrete by decreasing mechanical properties of the concrete, they still lower the corrosion protection of the rebar by lowering the pH of the pore solution, thus inducing the corrosion when the passive film is broken as illustrated Figure 1.3.

When corrosion occurs, the reinforcements are progressively replaced by the corrosion products which fill the porous zone of the concrete close to the rebar. Since the cross-section area of the reinforcement is reduced and the interface between the concrete and the rebar is weakened, the reinforced concrete load-carrying capacity is drastically decreased.

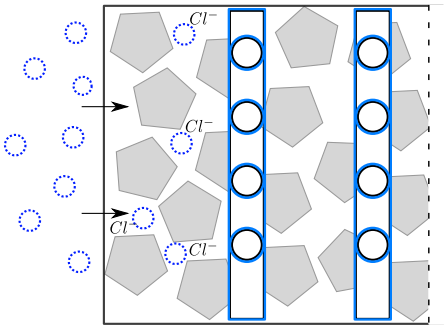

Figure 1.2 – Illustration of the chloride ingress process of reinforced concrete.

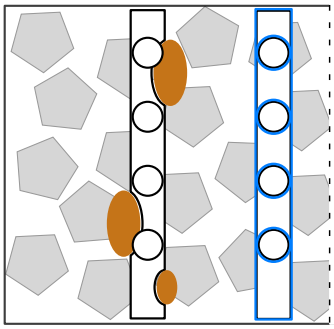

Figure 1.3 – Illustration of the corrosion process of reinforced concrete.

1.2.1.2 Mechanical degradation

When the porous zone close to the reinforcement is filled by the corrosion products, the internal pressure applied to the concrete increases with the corrosion evolution until cracks illustrated in Figure 1.4 appear. From then, the ageing of RC structures is due to both physicochemical degradation and mechanical one which interact between each other. The cracks facilitate the introduction of the oxygen needed by the corrosion process meanwhile the corrosion products keep on creating new cracks.

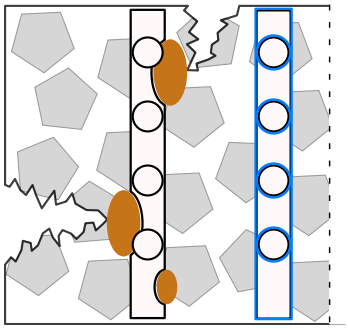

Figure 1.4 – Illustration of the cracking process of reinforced concrete.

The concrete cover is then progressively reduced and thereby increasing the risk of:

- Concrete blocks falls due to spalling;

- Structural failure due to a reduced load-carrying capacity.

1.2.2 Modelling degradation

Since these time-dependent degradation processes lead to an increase of the structural failure probability, their modelling is needed to predict their evolution. Although it appears that a global model able to deal successively with carbonation, chloride ingress, corrosion and cracking does not exist, each step of the ageing process has been modelled by either empirical or physical models.

Many attempts have been made to build empirical models mixing physical knowledge and regression parameters able to predict the evolution of the physicochemical processes. Empirical carbonation models assume that the carbon dioxide pressure evolves linearly from the surface where it equals the environmental pressure to the carbonation depth where it is null due to an assumed instantaneous consumption of the carbon dioxide. The chloride ingress models assume that the chlorides migration into concrete is only due to the concentration gradient observed between the environment and the concrete, independently from the other constituents present in the pore solution. They also mainly assume that the concrete is saturated, i.e. its saturation rate S_r is up to 100%. The corrosion models are either modelling the corrosion rate or the corrosion current which are linked by the Faraday's law, each of them making different assumptions.

The project DuraCrete (2000) proposes a predictive model for each physicochemical degradations mentioned above. They are shortly introduced in the following as an illustration of those models which keep a similar form for a given degradation process.

The carbonation process model (DuraCrete (2000)) reads

$$X_c(t) = \sqrt{\frac{k_e k_c k_t C_s t}{R_{carb}}} * \left(\frac{t_0}{t}\right)^n, \tag{1.1}$$

where $X_c(t)$ is the time-dependent carbonation depth. k_e, k_c, k_t are empirical parameters adjusted with carbonation data obtained through accelerating testings (higher carbon dioxide concentration and optimal rate of humidity) with different types of cement, exposure conditions, curing conditions and concrete composition. C_s is the surface concentration of the carbon dioxide. R_{carb} is a function of both the amount of carbon dioxide required to carbonate a unit volume and the diffusion rate of CO_2. t_0 is a reference time and n is an age-exponent which is a function of both the environment and the degradation of the material properties with time.

For a nearly exhaustive list of the carbonation models, the interested reader is referred to Hyvert (2009).

The proposed model (DuraCrete (2000)) for the chloride ingress reads

$$C(x,t) = C_s erfc\left(\frac{x}{2\sqrt{k_e k_c D_a(t) t}}\right), \tag{1.2}$$

where $C(x,t)$ is the chloride concentration at depth x at time t, C_s is the surface chloride concentration, k_e and k_c factors function of the exposition conditions, the type of cement and the curing conditions. $D_a(t)$ is a time-dependent diffusion coefficient. For a nearly exhaustive list of the chloride ingress models, the interested reader is referred to Deby (2008).

The last model for the corrosion current (DuraCrete (2000)) reads

$$i_{corr} = \frac{k_{corr}}{\rho(t)} F_{Cl} F_{Galv} F_{oxide} F_{Oxy}, \tag{1.3}$$

where k_{corr} is a regression parameter and $\rho(t)$ is the concrete resistivity at time t. F_{Cl}, F_{Galv}, F_{oxide}, F_{Oxy} take into account the impact of chloride content, galvanic effects, continuous formation, ageing of oxides and availability of oxygen respectively. For a nearly exhaustive list of the corrosion models, the interested reader is referred to Otieno et al. (2012); Raupach (2006).

The physical models, mostly based on the resolution of diffusion equations by finite difference or finite elements methods, are not introduced here for the sake of simplicity. However the interested reader is referred to Bary and Sellier (2004); de Larrard et al. (2014); Saetta et al. (1995); Talukdar et al. (2012); Thiery (2005) for physical carbonation model, Bastidas-Arteaga (2010); Deby (2008); Marchand (2001) for chloride ingress models, and Gulikers and Raupach (2006); Redaelli et al. (2006); Warkus et al. (2006b,a) for corrosion models.

Concerning the cracking models, they mainly are a combination of a model predicting the creation of corrosion products, as a function of the corrosion rate, and a mechanical model to compute the pressure applied to the neighbourhood concrete. Experimental studies have been done by Oh Hwan et al. (2009) to identify the critical corrosion amount to cause cracking which is the key parameter for the crack initiation. Either analytical as the model of Bhargava et al. (2006) or numerical as the one of Hansen and Saouma (1999), the crack initiation and propagation is derived from fracture mechanics equations by evaluating the stresses applied on the concrete by the corrosion products, like in Leung (2001). The interested reader is referred to El Maaddway and Soudki (2007); Molina et al. (1993); Pantazopoulou and Papoulia (2001); Val et al. (2009) for more details on the available models for cracking induced by corrosion expansion.

1.2.3 Probabilistic modelling

All the degradation models presented in Section 1.2.2 have some of their inputs dependent on:

- the concrete properties or;
- the environmental exposure.

Due to:

- The concrete realisation process;
- The natural variability of environmental exposure;
- The measurement error relative to both parameters;

both concrete properties and environmental exposure are uncertain and as such be modelled by correlated random variables. The project DuraCrete (2000) proposes probabilistic distributions for the inputs of its carbonation, chloride ingress and corrosion models.

However, considering the structure sizes (for instance a bridge) it may be too strong to assume that a given property (e.g. the concrete porosity) is constant along the structure. In other words modelling the spatial variability of the concrete properties may be needed. To the author's knowledge, few works have been performed to account for the spatial variability of structures' degradation. Correlated random fields may be needed to model the inherent variability of these parameters. A method based on local stationary models is for instance proposed in Straub and Faber (2002).

1.3 Condition states and statistical approaches

1.3.1 Structure rating

Using physical or empirical models to predict the evolution of physicochemical or mechanical degradation in order for a stakeholder to manage his structures is relevant only if the predicted degradation is measured. The fact is that in most cases, the structures are beforehand inspected by visual means and the inspection will not go further until a major defect is noticed. A visual inspection usually results in the classification of the structure in a given condition rate. For instance, Table 1.1 presents the condition rating provided by FHWA (2011) used to determinate the condition state of U.S. bridges and Table 1.2 is the french equivalent provided by the Sétra (1996).

When the only inspections performed on a structure are visual, the only available data to build a predictive model of the condition rate evolution are the condition rate themselves.

1.3.2 Markov chains for condition rate evolution

The markov chains have been widely used as a tool to model the degradation of components and structures. For the sake of clarity, the basics of markov chains are introduced prior to the description of their use.

1.3.2.1 Homogeneous markov chain of the first order

Let E be a discrete state space of size $N \in \mathbb{N}$. A markov process is a stochastic process discrete in time taking its values in E, satisfying a property commonly named the markov

Score	*Description*	*Details*
9	Excellent condition	
8	Very good condition	No problems noted
7	Good condition	Some minor problems
6	Satisfactory condition	Structural elements show some minor deterioration
5	Fair condition	All primary structural elements are sound but may have some minor section loss, cracking, spalling or scour
4	Poor condition	Advanced section loss, deterioration, spalling or scour
3	Serious condition	Loss of section, deterioration, spalling or scour have seriously affected primary structural components. Local failures are possible. Fatigue cracks in steel or shear cracks in concrete may be present.
2	Critical condition	Advanced deterioration of primary structural elements. Fatigue cracks in steel or shear cracks in concrete may be present or scour may have removed substructure support. Unless closely monitored the bridge may have to be closed until corrective action is taken.
1	Imminent failure condition	Major deterioration or section loss present in critical structural components or obvious vertical or horizontal movement affecting structure stability. Bridge is closed to traffic but corrective action may put back in light service.
0	Failed condition	Out of service- beyond corrective action

Table 1.1 – National bridge inventory general condition rating guidance FHWA (2011).

Score	*Description*
1	Good overall state
2	Equipment failures or minor structure damage
2E	Equipment failures or minor structure damage. Urgent maintenance needed
3	Structure deterioration. Non urgent maintenance needed
3E	Serious structure deterioration. Urgent maintenance needed

Table 1.2 – IQOA classification for bridges Sétra (1996)

property which writes

$$\begin{aligned}\mathscr{P}(X_{t+1}=x|X_t=x_t,X_{t-1}=x_{t-1},\dots,X_0=x_0)\\ =\mathscr{P}(X_{t+1}=x|X_t=x_t).\end{aligned} \tag{1.4}$$

This property indicates that the probability of a system being in state $x\in E$, at time $t+1$ is only dependent on its presence in state x_t at time t.

The markov process is therefore called memory-less process. Whatever has happened in the past of the process, its future realisation will only be dependent on its present value. Markov processes have been widely used for management of structures inspections (Baik et al. (2006); Bastidas-Arteaga (2010); Elachachi and Breysse (2007); Kallen (2007); Sheils et al. (2010b,a)). The main idea is that the condition state at time t implicitly contains the history. For smooth and monotonic degradation mechanisms it seems to be an acceptable assumption. In order to prove that a given process is markovian, the interested reader is referred to Bickenbach and Bode (2001) who propose chi-square tests to ensure the Markov property, spatial independence and homogeneity across time of the observed process.

In many civil engineering applications, the structure state is only periodically inspected which is in agreement with the use of a markov chain since it leads to represent the progression of the degradation on a discrete timescale. Moreover, the discretization of the degradation into several states is expected by the managers which aim at handling a limited number of condition states to help them in taking decisions, as suggested by the use of FHWA (2011) and Sétra (1996) recommendations.

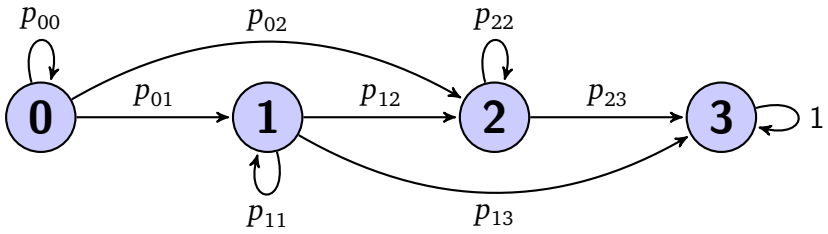

Figure 1.5 – Example of a state diagram

Usually a markov process' behaviour is described with a state diagram as shown in Figure 1.5. A state is defined by a circle, while the arrows represent the transition from one state to another. Each transition from state i at time t to state j at time $t+1$ has a probability p_{ij} to happen defined by a conditional probability

$$p_{ij} = \mathscr{P}(X_{t+1} = j | X_t = i) \quad (i,j) \in E. \tag{1.5}$$

The graph shown on Figure 1.5 has two specific features. First, it is a non-return stage diagram. An element following the markov process modelled by this graph is not able to return to a previous state. Consequently, the last state is called an absorbing state, meaning that once the process reaches this state it will stay within it (for instance, failure after crack propagation, full saturation of a porous material, ...).

The transient probabilities are usually grouped together into a matrix called the markov transition matrix, an example is shown in Eq. (1.6).

$$\mathbf{P} = \begin{bmatrix} p_{00} & p_{01} & p_{02} & p_{03} \\ p_{10} & p_{11} & p_{12} & p_{13} \\ p_{20} & p_{21} & p_{22} & p_{23} \\ p_{30} & p_{31} & p_{32} & p_{33} \end{bmatrix}. \tag{1.6}$$

One has to keep in mind that the matrix components are probabilities, therefore they have to follow probability's rules described by

$$\begin{cases} \sum_{j=1}^{N} p_{ij} = 1, & i \in E \\ 0 \leq p_{ij} \leq 1, & (i,j) \in E \end{cases}. \tag{1.7}$$

Thus in Eq. (1.6) the summation of each matrix line equals one.

Let t_s be a time shift. A markov process is said to be homogeneous if the transition probabilities are not age-dependent, i.e. they are independent from t_s. Consequently

$$p_{ij} = \mathscr{P}(X_{n+t_s} = j | X_n = i) = \mathscr{P}(X_{t_s} = j | X_0 = i), \quad (i,j) \in E. \tag{1.8}$$

Under this assumption, the conditional probability of belonging to a state j at time t knowing that at the initial time it was in state i is then computed by multiplying the probability matrix by itself t times as

$$\mathscr{P}(X_t = j | X_0 = i) = \mathbf{P}^t(i,j), \quad (i,j) \in E. \tag{1.9}$$

Finally the probability of belonging to a state $j \in E$ at time t is computed as follows

$$\mathscr{P}(X_t = j) = \sum_{i \in E} \mathscr{P}(X_0 = i)\mathbf{P}^t(i,j), \quad j \in E, \tag{1.10}$$

and the time dependent states distribution is computed by

$$\boldsymbol{q_t} = \boldsymbol{q_0}\mathbf{P}^t, \tag{1.11}$$

given the initial state distribution $\boldsymbol{q_0}$ as a vector of size n.

Eventually, if the chain is *irreducible, aperiodic* and *reversible*, the state distribution converges q_t toward a stationary distribution π_M when t tends to infinity, independently from the initial state distribution Chung (1967).

1.3.2.2 Transition probabilities estimation

An exhaustive literature review of the existing methods (Bayesian methods, ordered probit methods, ...) to estimate the transition probabilities can be found in Kallen (2007); Kelton and Kelton (1985). This section describes two of them which are mostly used, depending on the available data.

1.3.2.2.1 First case: Transitions observation The most desirable data-set would contain an observation of all the transitions. It means that one knows for any transition from state i to state j the time at which it happened. Let N_{ik} be the number of observed transitions from state i to any other state k, and $N_{ij}, (i,j) \in E$ the number of observed transitions

between states i and j. Then an estimation of the transition probabilities $p_{ij}, (i,j) \in E$ can be assessed by

$$\hat{p}_{ij} = \frac{N_{ij}}{\sum_k N_{ik}} \quad (i,j) \in E. \tag{1.12}$$

As demonstrated by Kelton and Kelton (1985), this method is similar to a likelihood method for which the result of Eq. (1.12) would be the maximum likelihood estimator. Consequently a sufficient number of transitions have to be observed if one wants this estimator to be unbiased. It is indeed a quite easy method to apply, however it has several drawbacks.

The states distribution has to be defined before estimating the transition probabilities, so it may happen that some states are never visited, leading to unnecessary complexity and computational time. In this case, the markov matrix obtained by identification will include a line with all probabilities being equal to 0, which is therefore not acceptable from a probabilistic point of view. Such problem can be managed by aggregating the state never visited with the previous one.

As the probabilities computed by this method are maximum likelihood estimators, some indicators of the quality of the estimation can be derived.

Standard deviation of the probabilities Each computed probability $p_{ij}, (i,j) \in E$ has an associated estimator of its standard deviation BODE (1998) following

$$c_{\hat{p}_{i,j}} = \begin{cases} \sqrt{\frac{1-\hat{p}_{ij}}{N_i \hat{p}_{ij}}} & \text{if } \hat{p}_{ij} \leq 0.5 \quad (i,j) \in E \\ \sqrt{\frac{\hat{p}_{ij}}{N_i(1-\hat{p}_{ij})}} & \text{if } \hat{p}_{ij} > 0.5 \end{cases}, \tag{1.13}$$

where $N_i = \sum_k N_{ik}$. This estimator tends to $+\infty$ when $\hat{p}_{ij}$ tend to 0 or 1.

Stability measurement Berchtold and Ritschard (1997); Berchtold (1998) proposed a method to measure the quality, or the stability, of a discrete probability distribution. The idea of a stability measurement is to measure how the evaluation of a probability distribution is affected by the introduction of an additional data into the used sample for the estimation.

Denoting $(p_1, p_2, \cdots, p_M)$ a discrete probability distribution with $M > 1$ modalities, the stability measure is computed by

$$D = \frac{M}{n+1}(1 - \min_m p_m)); \tag{1.14}$$

where n is the number of data used for the estimation of the distribution. According to Berchtold and Ritschard (1997); Berchtold (1998), the lower the stability measure, the better the estimation. A transition matrix estimation of quality gives a stability measure lower than 5×10^{-3}.

As each line of the transition matrix **P** represents a discrete probability distribution, Mattrand (2011) proposed to apply this criterion to the transition matrix **P**. As a result, for a markov chain with N states, there are N stability measures available.

An estimator of the stability measure for one line of the transition matrix can then be obtained by

$$D_i = \frac{N}{N_i + 1}(1 - \min_j p_{ij}) \quad (i,j) \in E; \tag{1.15}$$

Depending on the use of the markov process, two measures can be proposed (Mattrand (2011)):

- measure of the maximal stability defined by

$$D_M(\mathbf{P}) = \max_i(\frac{N}{N_i + 1}(1 - \min_j p_{ij})), \quad (i,j) \in E; \tag{1.16}$$

  This measure evaluates which distribution, i.e. line, of the transition matrix **P** is the worst evaluated. Then it should be used if one needs to have a proper estimation of all the lines.

- measure of the mean stability defined by

$$D_E(\mathbf{P}) = \frac{1}{N^2}\sum_{i=1}^{N}(\frac{N}{N_i + 1}(1 - \min_j p_{ij})), \quad (i,j) \in E; \tag{1.17}$$

  This measure evaluates the overall quality of the transition matrix estimation. It could be used in cases where it would be admissible to have few poorly estimated distributions.

1.3.2.2.2 Second case: States observation When structures are inspected at a time interval and not monitored, the data-set of observation is less complete. In this case, one will know in which state $i \in E$ was the process at time t_i, but the information about *when* it came into this state is unknown. It is therefore impossible to evaluate the transition probabilities with the maximum likelihood estimator.

However, a markov chain can be used to compute the probability that the process is in a state at a given time using Eq. (1.10). Accordingly, a common method used is to estimate the transient probabilities from a regression over the state expectation. Let $\mathscr{P}_{obs}(X_t = k)$ be the *observed* probability of being in state k at time t and $\mathscr{P}(X_t = j)$ the corresponding probability *computed* with Eq. (1.10). Then the transitions probabilities are computed by a

constrained least-squares optimization

$$\min_{p_{i,j}} \sum_t \sum_k (\mathscr{P}_{obs}(X_t = k) - \mathscr{P}(X_t = j))^2 \quad (i,j) \in E$$

$$\text{under the constraints} \quad \begin{cases} \sum_{j=1}^{N} p_{ij} = 1 \\ 0 \leq p_{ij} \leq 1 \end{cases} . \tag{1.18}$$

This method can obviously be used to estimate a markov model in the case where the transitions are observed.

1.3.2.3 On the use of markov chain

Throughout the literature, the markov chains have been used to predict condition state evolution for structures which are not monitored. Baik et al. (2006) identify a markov chain to predict the conditions of waste-water systems. An ordered probit model which writes

$$z_i = \boldsymbol{\beta_i} \boldsymbol{X} + \epsilon, \quad i \in E \tag{1.19}$$

is used to model the continuous latent deterioration into a discrete state space together with an incremental model reading

$$\begin{aligned} &y_i = j - i, \\ &\quad \text{if } \mu_{i(j-i)} - \boldsymbol{\beta_i} \boldsymbol{X} \leq z_i \leq \mu_{i(j-i+1)} - \boldsymbol{\beta_i} \boldsymbol{X}, \quad (i,j), (j-i) \in E, (0, \cdots, N-1). \end{aligned} \tag{1.20}$$

By assuming that the disturbance term ϵ in Eq. (1.19) is gaussian, the model parameters $\boldsymbol{\beta}, \mu$ can be estimated by a maximum likelihood method. It is then used to identify the transient probabilities of the markov process.

Bocchini et al. (2012) make use of a markov chain with three condition states (service, maintenance and repair state) to predict the lifetime of multiple bridges. Duc Le and Ming Tan (2013) use a continuous-time markov process to model the degradation of a system which, for the sake of simplicity, combines an homogeneous markov chain which determines what will be the next state, and a probabilistic distribution for the time at which the transition will happen. Elachachi and Breysse (2007) use a markov chain with each transition probability computed by a hazard model. Hong (1999) generates new corrosion defects on pipeline systems with a Poisson process and models the effect of these defects size on the pipeline strenght by a markov process. The Kolomogorov forward differential equation is solved to obtain an analytical transition matrix. This equation reads

$$\frac{\partial P_{i,j}(s,t)}{\partial t} = \sum_k P_{i,k}(s,t) A_{k,j}(t), \tag{1.21}$$

where

$$\begin{cases} A_{i,j} = \left[\frac{\partial P_{i,j}(t,u)}{\partial u}\right]_{u=t} \\ A_{j,k}(t) \geq 0 \\ \sum_k Aj,k(t) = 0 \\ t > s. \end{cases}$$

Kallen and van Noortwijk (2006) propose a continuous-time markov process to model the transition between one condition rate to another. The transition intensities are estimated by a maximum likelihood method. Orcesi and Cremona (2010) also propose the use of a markov chain for the evolution of the IQOA score (Sétra (1996)), which is used to derive a maintenance event-tree.

1.3.3 A point on renewal processes

Renewal processes are another type of statistical processes used to estimate the evolution of a condition score index, although it can be identified with any measurable degradation as for instance the carbonation depth. They are lightly introduced for the sake of completeness. The renewal processes are mainly composed of the Brownian motion with drift and the gamma process.

The first is a stochastic process $Y(t), t \geq 0$ with independent increments and decrements according to a normal distribution with mean μt and standard deviation $\sigma\sqrt{t}, \forall t \geq 0$

A gamma random variable has a probability distribution reading

$$Ga(x|v,u) = \frac{u^v}{\Gamma(v)} x^{v-1} exp(-ux)\delta_{(E)}(x) \tag{1.22}$$

where $\delta_E = 1, \forall x \in E$ and $\delta_E = 0, \forall x \notin E$, and $\Gamma(x)$ being the gamma function. A gamma process is monotonic. Once identified, it can be used to derive the distribution of the time to failure for instance.

A review of these processes and on the methods to estimate their parameters is available in van Noortwijk (2009).

1.4 Optimising the management

Although the first step (i.e. predicting the degradation) is reached, modelling the degradation evolution accounting for the effect of inspections, maintenance and repairs which is the so-called *lifetime* of the structure in order to optimise the inspection plan is mandatory. This section first introduces some basics on inspections modelling needed to understand the following literature review.

1.4.1 Inspections modelling

An inspection, visual or resulting from a non-destructive evaluation, may result in two outputs: detection of a default, or non detection. For instance, a default can be the presence of a crack on a plane, or a chloride concentration higher than a critical threshold on a marine concrete structure. A usual mean to quantify the quality of an inspection tool is based on the probability of detection PoD and the probability of a false alarm PFA (detection of a nonexistent default) illustrated through Figure 1.6 (Schoefs and Clément (2004); Schoefs et al. (2009); Straub (2004)).

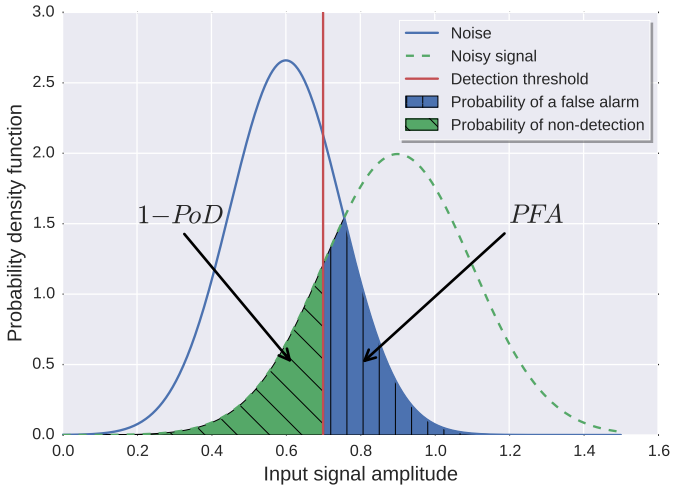

Figure 1.6 – Probabilistic model for PoD and PFA, from Rouhan and Schoefs (2003).

Rouhan and Schoefs (2003) have described measures of probability for events which may happen during an inspection and derived for each of them their probability of occurrence:

- $\mathscr{P}(E_1)$, probability that a default is detected and this default exists;
- $\mathscr{P}(E_2)$, probability that a default is detected and this default does not exist;
- $\mathscr{P}(E_3)$, probability that no default is detected and a default exists;
- $\mathscr{P}(E_4)$, probability that no default is detected and no default exists.

with

$$\mathscr{P}(E_1) = \frac{PoD(a)\gamma(a)}{PoD(a)\gamma(a) + PFA(1-\gamma(a))}, \tag{1.23}$$

$$\mathscr{P}(E_2) = \frac{PFA(1-\gamma(a))}{PoD(a)\gamma(a) + PFA(1-\gamma(a))}, \tag{1.24}$$

$$\mathscr{P}(E_3) = \frac{(1-PoD(a))\gamma(a)}{(1-PoD(a))\gamma(a) + PFA(1-\gamma(a))}, \tag{1.25}$$

$$\mathscr{P}(E_4) = \frac{(1-PFA)(1-\gamma(a))}{(1-PoD(a))\gamma + PFA(1-\gamma(a))}, \tag{1.26}$$

$\gamma(a)$ being the probability that a default of size a exists.

Sahraoui et al. (2013) defined two more outcomes for an inspection than the four presented above:

- $\mathscr{P}(E_5)$, probability that a default is detected, a default exists but no repair is performed due to the acceptable size of the defect;
- $\mathscr{P}(E_6)$, probability that a default is detected, no default exists but no repair is performed due to the acceptable size of the defect.

with

$$\mathscr{P}(E_5) = \frac{PoD(a)\eta(a)}{PoD(a)\eta(a) + PFA(1-\eta(a))}, \tag{1.27}$$

$$\mathscr{P}(E_6) = \frac{PFA(1-\eta(a))}{PoD(a)\gamma(a) + PFA(1-\eta(a))}, \tag{1.28}$$

where $\eta(a)$ being the probability that a default of size a lower than the critical size threshold for repair a_{crit} exists. This definition is, to the author's belief, more adapted to the case of carbonation, chloride ingress or corrosion since the NDTs assess their level, not their presence, and repairing is determined by a critical level of the degradation, not by its presence.

For common inspection tools, the probability of detection $PoD(a) = P(a \geq a_d)$ is considered as dependent on the default's size given a minimal detectable default of size a_d, whenever the probability of false alarm is only dependent on the noise and is therefore constant for a given detection threshold (e.g. Figure 1.6).

Different functions can be used as PoD function. For instance, if the signal represented in Figure 1.6 is normally distributed, then the PoD function writes (Schoefs and Clément (2004))

$$PoD(a) = \int_{a_d}^{+\infty} \frac{1}{\sqrt{2\pi}\sigma(a)} exp\left[-\frac{(a_s-\mu(a))^2}{2\sigma^2(a)}\right] da_s \tag{1.29}$$

For the sake of illustration, probability of detection can also be modelled by exponential functions such as (Nielsen and Sorensen (2011); Straub (2004))

$$PoD(a) = P_0\left[1 - exp(-\frac{a}{\lambda})\right], \tag{1.30}$$

where P_0 is the maximum probability of detection or by log-logistics models (Straub (2004)) writing

$$PoD(a) = \frac{exp\left[\alpha + \beta ln(a)\right]}{1 + exp\left[\alpha + \beta ln(a)\right]}. \tag{1.31}$$

Although the inspections are sometimes assumed as perfect (Barker and Newby (2009); Estes and Frangopol (2001b); Grall et al. (2002)), the probability of detection which models the performance of a non-destructive technique is widely used (Ellingwood and Mori

(1996); Faber and Sorensen (2002); Frangopol et al. (1997); Hong (1997, 1999); Kim and Frangopol (2011); Nielsen and Sorensen (2011); Orcesi and Frangopol (2011b); Soliman et al. (2013)). The probability of false alarm which can lead to wrong maintenance decisions is also usually considered together with the probability of detection (Bastidas-Arteaga (2010); Breysse et al. (2009); Rouhan and Schoefs (2003); Sahraoui et al. (2013); Straub (2004); Sheils et al. (2010a)).

The use of a probability of detection and a probability of false alarm may appear redundant since from a detection one can hardly say if it is a false alarm or not. From this point of view, the so-called *probability of indication PoI* gathers the probability of detection and the probability of false alarm into one indicator of the inspection quality. This probability writes (Straub (2004); Nielsen and Sorensen (2011))

$$PoI(a) = PoD(a) + [1 - PoD(a)]\,PFA. \tag{1.32}$$

1.4.2 Maintenance and optimisation

The previous section has introduced the basics on inspection modelling. A literature review on the optimisation of maintenance and inspection plans is presented below, the latter mostly based on the PoD and PFA definitions.

1.4.2.1 Optimisation

Onoufriou and Frangopol (2002) proposed an interesting review of the reliability-based techniques for the optimisation of inspection plans. The meaning of reliability-based is that the performance criterion which will lead to the decision of performing an inspection (or maintenance) is a reliability index β which has to be higher than a target reliability index, i.e. $\beta \geq \beta_{tar}$, or $p_f \leq p_{f_{tar}}$, the probability of failure p_f being linked to the reliability index β (for linear limit states) by

$$p_f = \Phi(-\beta). \tag{1.33}$$

A generalisation of reliability-based concept leads to the formalisation of the optimisation of inspection (or maintenance) plan such as

$$\min_{x_0,\cdots,x_i} \left\{f_{obj}^{(0)},\cdots,f_{obj}^{(j)}\right\} \text{ such that } \left\{c^{(0)} \geq c_t^{(0)},\cdots,c^{(k)} \geq c_t^{(k)}\right\}, \tag{1.34}$$

where $\{x_0,\cdots,x_i\}$ are the optimisation variables, for instance inspection (or maintenance) time and quality. $\left\{f_{obj}^{(0)},\cdots,f_{obj}^{(j)}\right\}$ are the objective functions which are to be minimised (or maximised), such as the long-term total cost C_{tot} or the redundancy level of a system. Lastly $\left\{c^{(0)} \geq c_t^{(0)},\cdots,c^{(k)} \geq c_t^{(k)}\right\}$ are the different constraints that have to be fulfilled like the previously mentioned target reliability lindex in the reliability-based optimisation.

The following paragraphs introduce a review of the inspection and maintenance plan optimisation. As its title suggests, this thesis is dedicated to inspection plan, yet the presence

of the latter is explained by the link between inspection and maintenance which leads to many similarities between both methodologies.

1.4.2.1.1 Mono-objective optimisation For the sake of clarity, Table 1.3 summarises the inspection models used in the literature review presented below.

Author	*PoD*	*PFA*	*PoI*	*Uniform delay*	*Nonuniform delay*
Barker and Newby (2009)	no	no	no	no	yes
Breysse et al. (2009)	yes	yes	no	yes	no
Ellingwood and Mori (1996)	yes	no	no	yes	no
Estes and Frangopol (2001a)	no	no	no	yes	no
Faber et al. (1996)	yes	no	no	yes	no
Hellevik et al. (1999)	yes	no	no	yes	no
Frangopol et al. (1997)	yes	no	no	yes	yes
Nielsen and Sorensen (2011)	yes	yes	yes	yes	no
Sheils et al. (2010a)	yes	yes	no	yes	no

Table 1.3 – Inspection modelling of the mono-objective optimisation literature review

Barker and Newby (2009) proposed an original minimisation of the expected total cost (inspection and repair costs) for a multivariate Wiener degradation model. The inspections are assumed perfect, and the next inspection date is derived sequentially with the use of a deterministic function of the state of the system x which gives the time until the next inspection. For instance one of these functions writes

$$m(x) = max\left\{1, a - \frac{a-b}{b}x\right\}, \tag{1.35}$$

where a and b are the optimisation parameters of the problem. The minimisation of the expected total cost is then obtained when optimising the function for the time of the next inspection.

Breysse et al. (2009) optimised the delay between two inspections under a reliability constraint with respect to the expected sum of the inspection costs, dependent on the inspection quality, the repair cost growing with the defect size and the failure cost. Each cost is represented as a part of the initial construction cost. *PoD* and *PFA* are accounted for. The measurement error is assumed to follow a centred normal distribution with variance dependent on the quality. The effect of different inspection qualities and different threshold levels for the allowable annual probability of failure on the expected number of false alarm and good assessment is studied.

Ellingwood and Mori (1996) also minimised the total cost composed of the inspection, repair and failure costs to optimise the intervals of inspection under a reliability constraint. The notion of *PoD* is reminded, however the inspections are supposed to have a binary *PoD* function such as

$$PoD(x) = \begin{cases} 0, & x < x_c \\ 1, & x \geq x_c \end{cases}, \tag{1.36}$$

with x_c the detection threshold.

Estes and Frangopol (2001a) proposed an optimisation of maintenance plans. Different repair options are proposed (with their corresponding costs) as for instance replace the deck or replace exterior girders. This is a reliability-based optimisation with $\beta \geq 2$. However serviceability flags are also used as constraints to better model the possible choices of a stakeholder. Namely, a given serviceability flag in this paper is to replace the concrete slab every 28 years even if its strength decay is not a concern, because excessive potholes may have appeared on the deck leading to unacceptable deteriorated driving conditions. Yet the use of serviceability flag is proved to be less efficient in the structural concern problem. In Estes and Frangopol (2001b) a minimisation of the total cost equalling the sum of the inspection cost and of repair cost, by optimising the inspection times, given:

- an inspection technique assumed perfect, defined by the spacing of readings (i.e. the higher the spacing of readings, the lower the number of inspected locations);
- the number of inspections;
- the probability function of repairing depending on the inspection result.

The latter is used to derive a decision tree which is used to estimate the total expected cost. As shown in Figure 1.7, a tree-node splits in two branches after an inspection, one with the probability of repairing, the other with the complementary probability. The cost functions include a discount rate of money in order to derive the real cost of an operation at the application time. For an interesting discussion of this financial aspects, as well as socio-economic point of view, the interested reader is referred to Rackwitz et al. (2005).

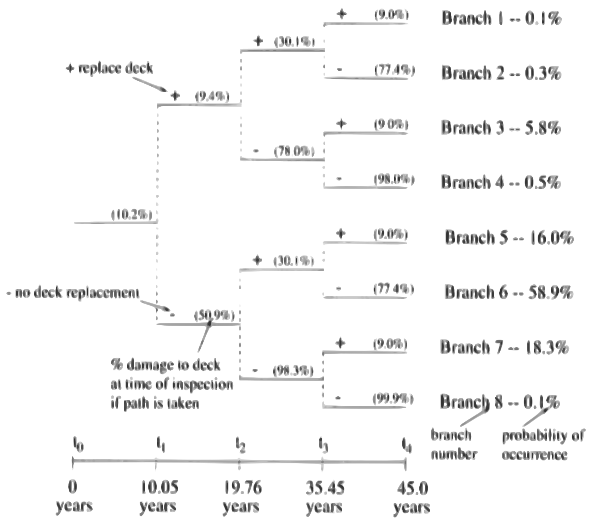

Figure 1.7 – Example of a decision tree from Estes and Frangopol (2001b).

Faber et al. (1996) introduce the maximisation of a utility function

$$u^* = \max_z \max_i \max_d u(z, i, d), \tag{1.37}$$

with z, i and d being respectively the design parameters, the inspection decisions and the repair decisions. This is a generalisation of the optimisation problem similar to Eq. (1.34). The utility function is the minus of the total costs and the optimisation is reliability-based. The probability of detection is accounted for. Hellevik et al. (1999) propose a similar approach for inspection and replacement planning of corroded piping. Both papers consider the cost as being the result of a decision tree shown Figure 1.8.

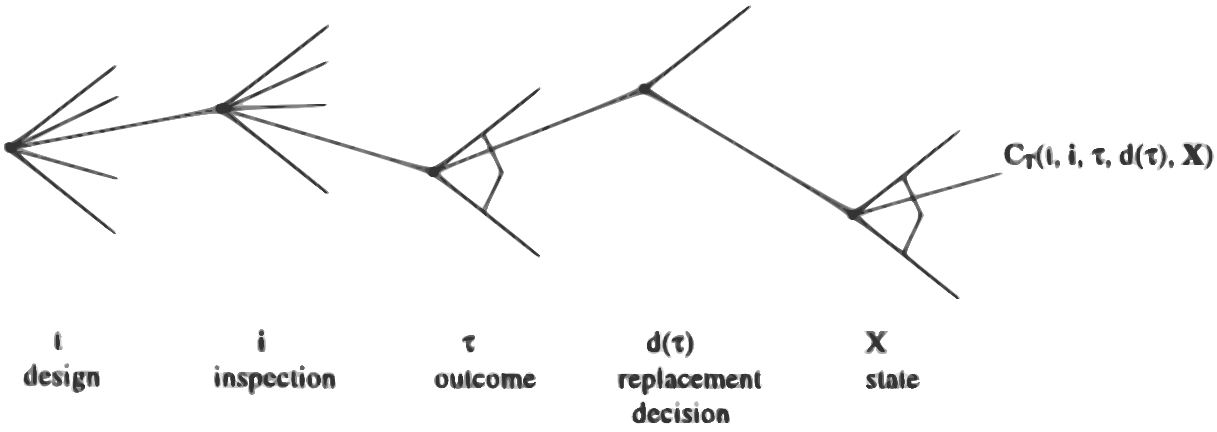

Figure 1.8 – Total cost derived from a decision tree, from Faber et al. (1996).

Frangopol et al. (1997) optimise the inspection plan of a bridge submitted to corrosion. Inspections are modelled by their PoD. The total costs (construction, preventive maintenance, inspection, repair, failure) are minimised under a reliability constraints for both a uniform and a nonuniform delay between inspections. The latter thus writes

$$\begin{aligned} &\min C_{tot} = C_0 + C_{PM} + C_i + C_{rep} + C_f \\ &\text{subject to} \quad \begin{array}{l} \sum_{i=1}^{m} t_i \leq T \\ t_{min} \leq t_i \leq t_{max}, i = (1, \cdots, m) \\ \beta(t) \geq \beta_{tar} \end{array} \end{aligned} , \tag{1.38}$$

where T is the lifetime of the bridge, t_i is the delay between inspection i and $i-1$, t_{min} and t_{max} are respectively the lower and upper constraints of the nonuniform delays. As a conclusion, the nonuniform delay between inspections has been proved *more economic* than the uniform case.

Nielsen and Sorensen (2011), as mentioned in Section 1.4.1, present an optimisation of inspection plan for wind turbine components using the probability of indication PoI (see Eq. (1.32)). A parametric analysis is made to study the effect on the total cost of the degradation threshold for preventive maintenance, the inspection quality, the delay between inspections, the discount rate and the cost related to each operation.

Sheils et al. (2010a) proposed to combine the four probabilities introduced in Section 1.4.1 (see Eq. (1.23) to Eq. (1.26)) to describe the different outcomes of an inspection with the transition matrix of the markov process modelling the degradation to form two

different transition matrices (see Section 1.3.2.1). Considering a uniform delay between two inspections, the first matrix only contains the probabilities linked to the degradation process and the corresponding failure probabilities. At an inspection year, the probabilities corresponding to the inspection outcomes are introduced to obtain the second matrix. When a critical default is detected or when a failure occurs, the structure is immediately repaired to an *as-good-as-new* state.

Transition matrix between two inspections Let p_{f_i} be the failure probability associated with the state i. The different elements of the transition matrix $\mathbf{P}^{(bi)}$ used to predict the process evolution between two inspections write (Bastidas-Arteaga (2010))

$$\begin{cases} p_{i1}^{(bi)} &= p_{ij} + \sum_{k=2}^{N} \left(p_{ik} p_{f_k}\right), & j = 1, i \in E \\ p_{ij}^{(bi)} &= p_{ij}\left(1 - p_{f_j}\right), & j > 1, i \in E \end{cases}, \tag{1.39}$$

with p_{ij} the probabilities of the transition matrix $\mathbf{P}$ of the markov process modelling the degradation.

The Markov chain's predictions at years without inspection being performed thus follow

$$\boldsymbol{q}_t = \boldsymbol{q}_{t-1} \mathbf{P}^{\mathbf{t}(bi)}. \tag{1.40}$$

Transition matrix at inspection years At an inspection year, two events can lead the structure to be repaired: a critical default (existing or not) is detected, or a non-detected default leads to the failure of the structure. Let $\mathscr{P}_i\left(R \bigcup F\right)$ be the joint probability of a return from state i to a *as-good-as-new* state due to a repair R following or not a failure F. The matrix $\mathbf{P}^{(ai)}$ manipulated at inspection years writes (Bastidas-Arteaga (2010))

$$\begin{cases} p_{i,1}^{(ai)} &= p_{i,j} + \sum_{k=2}^{N} \left(p_{i,k} \mathscr{P}_k\left(R \bigcup F\right)\right), & j = 1, i \in E \\ p_{i,j}^{(ai)} &= p_{i,j}\left(1 - \mathscr{P}_j\left(R \bigcup F\right)\right), & j > 1, i \in E \end{cases}, \tag{1.41}$$

with

$$\mathscr{P}_i\left(R \bigcup F\right) = \mathscr{P}_i(\text{Repair}) + \mathscr{P}_i(\text{Failure}|\text{Non-detected}), \quad i \in E, \tag{1.42}$$

in which

$$\mathscr{P}_i(\text{Repair}) = PoD_i \gamma_i + PFA_i(1 - \gamma_i), \quad i \in E, \tag{1.43}$$

and

$$\begin{aligned} \mathscr{P}_i(\text{Failure}|\text{Non-detected}) \;=\; & (1 - PoD_i)\gamma_i \\ & + (1 - PFA_i)(1 - \gamma_i) p_{f_i}, \quad i \in E. \end{aligned} \tag{1.44}$$

In these equations, the PoD and PFA are prescribed for each state, the detection threshold being fixed to the mean degradation of the considered state.

As explained by Sheils et al. (2010a), computing each step of the markov process with Eq. (1.11) is equivalent to simulate the failures and inspections at the end of the period t, e.g. at the end of each year if the temporal discretization is annual. Thus at an inspection year, the degradation and the possible failures *without* inspection have to be simulated before using the inspection matrix $\mathbf{P}^{(ai)}$. The prediction therefore writes

$$\boldsymbol{q}_t = \left(\boldsymbol{q}_{t-1}\mathbf{P}^{\mathrm{t}(bi)}\right)\mathbf{P}^{\mathrm{t}(ai)}. \tag{1.45}$$

The predictions using Eq. (1.40) and Eq. (1.45) are not computed from the initial state of the process. Indeed, with the change of transition matrix, the markov process loses its homogeneity. It is consequently not possible to predict the process state only from the initial state and the time spent as described by Eq. (1.11).

1.4.2.1.2 Multi-objective optimisation The main goal achieved by the use of multi-objective optimisations is to replace the constraints of the mono-objective problem into objective functions, such that the choice of the stakeholder will result from a compromise between the different objectives.

Bocchini and Frangopol (2011) minimise the cost and maximise the network performance of a group of bridges to find the optimal times of preventive maintenance. A constraint on the maximum cost is considered. The originality of this work is that a correlation between each bridges is accounted for as a function of the distance separating them, their characteristics and structural similarities. This correlation is proved to have a great impact on the network performance indicators such as the distance covered by all the users of the network in a unit time, and the times spent by them to reach their destination.

Barone and Frangopol (2014) consider the cost to be minimised and the reliability or the system hazard to be respectively maximised or minimised. The structure considered is a bridge for which either a girder or the deck may be repaired. Kim and Frangopol (2011) use as objective functions to minimise the inspection cost and the delay prior to damage detection for a ship hull structure in order to optimise the inspection date and the inspection quality (i.e. a parameter of the PoD function used for the inspections). Okasha and Frangopol (2009, 2010) propose to minimise the cost, to maximise the redundancy and to minimise the probability of failure or the unavailability to optimise the preventive maintenance plans of structures. The first is applied to a truss while the latter uses a Colorado bridge as an application example. Orcesi and Cremona (2010) optimise the maintenance plan of a bridge network to minimise the users and owners costs, the first being expressed as a function of the travel distance, the latter being the maintenance costs.

Orcesi and Frangopol (2011a) optimise the management of a bridge to minimise the maintenance costs, the failure costs, and the error in the decisions taken at a given performance assessment date. The optimisation is constrained by the reliability of the bridge and considers on one side the available budget of the stakeholder for maintenance operation and on the other side the delay existing between a performance assessment and a maintenance operation. All the publications mentioned in this paragraph use the Non-Sorted Genetic Algorithm-II (NSGA-II) proposed by Deb et al. (2000) to solve the multi-objective optimisation.

1.5 Objectives of the thesis

The overview of Faber and Stewart (2003) on the generalisation of risk-based inspection makes interesting conclusions as the two following:

- Engineers may not be fully convinced by the use of risk-based inspection methods, as they judge it “too difficult”, “too mathematical” to assess the risk of an event never observed;
- A general tendency and a long experience lead to restrain the risk analysis methods to the well-known and standardised ones which may not be fully appropriate for all cases.

The author is fully according with these points which have driven the thesis objectives.

The literature review has more or less revealed that nearly each case study has its optimisation methodology. For instance the methodology developed by Sheils et al. (2010a) makes two strong assumptions:

- Maintenance actions are performed immediately and instantaneously when a default is detected;
- The structure is back in a *as-good-as-new* state after any maintenance action;

and is completely dependent with the PoD definition, as many methodologies. From the author point of view, the main drawback here is that these methods cannot be generalised. Therefore they do not answer the conclusions of Faber and Stewart (2003) cited above.

Based on these observations, the thesis objectives are:

1. To propose a methodology for the optimisation of inspection plans:
   - Not driven by a unique objective to be reached;
   - As independent as possible with the different assumptions that could be made to model inspection, failure and maintenance;
   - Able to deal with structures of different sizes, submitted to spatially correlated degradation process or not;
   - Independent from the degradation process and the corresponding degradation indexes;
   - As simple as possible with an affordable computational cost.
2. To allow the use of any existing data which would be relevant in order to calibrate the degradation model or to update the inspection plan computed with the methodology mentioned above.

1.6 Conclusion

This introductory chapter has presented the basics concerning the degradation modes of RC structures (carbonation, chloride ingress, corrosion and crack propagation). Although modelling the physical of degradation processes is not the subject of this thesis, the author wants to point out the difficulties to predict the sequential appearance and propagation of each degradation process since the transitions between them and their interactions are still on-going subjects of research.

The same thing can be said about the optimisation of inspection plans. Many methodologies have been presented, each of them having different assumptions and different objectives, but few of them are insensitive to a change in these assumptions and objectives. Considering this together with the conclusions drawn by Faber and Stewart (2003), this thesis should result in a methodology to optimise the inspection plan:

- adjustable to the different assumptions a stakeholder may make;
- efficient with any degradation process, should it be spatially correlated;
- simple to understand, fast to be computed.

The author assumes that at least the first predicted inspection will be performed, consequently this thesis also contains tools to help the stakeholder using the results of this inspection to take a decision.

The first step of this methodology is to build a predictive model of the condition evolution of a structure including the degradation, the inspections and the maintenance actions. This degradation index predictive model is described in the following chapter. As mentioned in Section 1.2.3, the spatial variability of the degradation may be accounted for therefore being able to simulate and handle such degradation predictions is another challenge which is addressed in this chapter.

Although the methodology developed herein is independent of the degradation process and the corresponding degradation indexes, this thesis was conducted in a preventive maintenance context. As such and for the sake of simplicity the carbonation and chloride ingress processes are the only ones considered in the following chapters.

CHAPTER 2

PREDICTING THE EVOLUTION OF A DEGRADATION INDEX

2.1 Introduction

As described in the previous chapter, the first part of any methodology aiming at optimising the inspection plan of a structure is to derive a predictive model for the *life cycle* of this structure. This chapter presents in a first part some basics on the probability theory prior to the theory of the random fields in a second section. Since this thesis aims at considering the spatial variability of the degradation processes, it appears important to be able to simulate physically representative random fields. The third section is dedicated to the construction of the life-cyle model. Based on a decision tree, it combines the degradation predictions, potentially spatially correlated, the inspection models as well as the maintenance and failure ones in order to predict the long-run evolution of a given degradation index.

2.2 Basics of probability theory

2.2.1 Probability space

In probability theory, $(\Omega, \mathscr{F}, \mathscr{P})$ is the probability space where

- Ω is the event space, the set of all possible outcomes;
- $\mathscr{F}$ is the σ-algebra defining the events as combinations of the elements in Ω;
- $\mathscr{P}$ is the probability measure of any event in $\mathscr{F}$, defined in $[0,1]$.

2.2.2 Random variable

A real-valued random variable X is an application of the probability space $(\Omega, \mathscr{F}, \mathscr{P})$ which return a real value $X(\omega) \in D_X$ for any event ω with the probability $\mathbb{P}[X = X(\omega)] \in [0,1]$, where $D_X \subset \mathbb{R}$ is the support of X.

This application is totally defined by the so-called *cumulative distribution function* (CDF) reading

$$F_X(x) = \mathscr{P}[Y \leq y]. \tag{2.1}$$

The CDF also reads

$$F_X(x) = \int_{-\infty}^{x} f_X(x)dx \tag{2.2}$$

where $f_X(x)$ is the *probability density function*.

2.2.2.1 Moments of a random variable

Provided all the integrals in this section exist, the mathematical expectation of a random variable X (i.e. its mean value) writes

$$\mu_X = \mathbb{E}[X] = \int_{D_X} x f_X(x)dx. \tag{2.3}$$

The moments of order $k > 1$ are given by

$$\mathbb{E}\left[X^k\right] = \int_{D_X} x^k f_X(x)dx. \tag{2.4}$$

The centred moments read

$$\mathbb{E}\left[(X-\mu_X)^k\right] = \int_{D_x} (x-\mu_X)^k f_X(x)dx. \tag{2.5}$$

Special attention is given for the centred moments of order 2 which is called the *variance* of the random variable and denoted by $\sigma_X^2 = \mathrm{Var}[X]$, its square root σ_X being the so-called *standard deviation*.

2.2.3 Random vector

Given n real-valued random variables $X_1, \ldots, X_n$, the random vector $\boldsymbol{X} = \{X_1, \ldots, X_n\}$ is an application of Ω such as

$$\boldsymbol{X} = \left\{ \begin{array}{ccc} \Omega & \rightarrow & \mathbb{R}^n \\ \omega & \mapsto & \{X_1(\omega), \ldots, X_n(\omega)\} \end{array} \right. \tag{2.6}$$

2.2.3.1 Joint probability distribution

Just as random variables, continuous random vectors are defined by their joint CDF $F_{\boldsymbol{X}}(\boldsymbol{x})$

$$F_{\boldsymbol{X}}(\boldsymbol{x}) = \mathscr{P}(X_1 \leq x_1 \cap \cdots \cap X_n \leq x_n), \tag{2.7}$$

which can also be expressed as a function of the joint probability distribution

$$F_{\boldsymbol{X}}(\boldsymbol{x}) = \int \cdots \int_{\mathbb{R}^n} f_{\boldsymbol{X}}(\boldsymbol{x}) dx_1 \cdots dx_n \tag{2.8}$$

2.2.3.2 Marginal distribution

The marginal distribution of any $X_i, i \leq n$ reads

$$f_{X_i}(x_i) = \int \cdots \int_{\mathbb{R}^{n-1}} f_{\boldsymbol{X}}(\boldsymbol{x}) dx_1 \cdots dx_{i-1} dx_{i+1} \cdots dx_n. \tag{2.9}$$

2.2.3.3 Moments of a random vector

The mathematical expectation $\boldsymbol{\mu_X}$ of a random vector gathers the mean of each random variable of the random vector such as

$$\boldsymbol{\mu_X} = \left\{\mu_{X_1}, \ldots, \mu_{X_n}\right\} \tag{2.10}$$

The centred moment of order two for a random vector is called the *covariance* and is derived for each pair of random variables by

$$\mathrm{Cov}\left[X_i, X_j\right] = \mathbb{E}\left[(X_i - \mu_{X_i})(X_j - \mu_{X_j})\right], \quad \forall i, j = (1, \ldots, n). \tag{2.11}$$

The covariances of a random vector are usually gathered in a symmetric and positive definite matrix denoted **C** where the components read

$$C_{ij} = \mathrm{Cov}\left[X_i, X_j\right]. \tag{2.12}$$

The diagonal of the covariance matrix is thus the variance of each component of the random vector X. The covariance represents both the combined variance of two components and their dependency. The pearson correlation matrix **R** can therefore be derived as

$$R_{ij} = \frac{\mathrm{Cov}\left[X_i, X_j\right]}{\sigma_{X_i}\sigma_{X_j}}. \tag{2.13}$$

2.3 Random fields

2.3.1 Definition

A random field $X(\boldsymbol{x},\omega), \boldsymbol{x} \in D_X \subset \mathbb{R}^n$ is composed of an infinite set of random variables indexed by $\mathbb{R}^n$ and taking its values in $\mathbb{R}^n$. It reads

$$X = \left\{ \begin{array}{ccc} \Omega & \rightarrow & \mathbb{R}^n \\ \omega & \mapsto & X(\boldsymbol{x},\omega) \in \mathbb{R}, x \in \mathbb{R}^n \end{array} \right. \tag{2.14}$$

Therefore at any position $\boldsymbol{x_0} \in D_X$, $X(\boldsymbol{x_0},\omega)$ is a random variable, and over the domain D_X, $X(\boldsymbol{x},\omega_0)$ is called a *trajectory* of the random field.

A random field defined on $\mathbb{R}$ such as

$$X = \left\{ \begin{array}{ccc} \Omega & \rightarrow & \mathbb{R}^n \\ \omega & \mapsto & X(\boldsymbol{x},\omega) \in \mathbb{R}, x \in \mathbb{R} \end{array} \right. \tag{2.15}$$

is usually denoted as *random process*.

2.3.2 Properties

The mean of a random field $X(\boldsymbol{x},\omega)$ is a function of $\boldsymbol{x}$ denoted $\mu_X(x)$. The corresponding centred moment of order 2 is called the covariance function $\mathrm{Cov}(\boldsymbol{x},\boldsymbol{x'})$.

A random field is said to be *stationary* of the first order if its mean is independent of $\boldsymbol{x}$ such as

$$\mu_X(\boldsymbol{x}) = \mu_X, \quad \forall \boldsymbol{x} \in \mathbb{R}^n. \tag{2.16}$$

The stationarity of the second order implies that the variance is constant and the covariance function of the random field is only dependent of the distance between two points and is therefore writing

$$\mathrm{Cov}\left(\boldsymbol{x},\boldsymbol{x'}\right) = \sigma_X^2 * \mathrm{R}(x - x'), \tag{2.17}$$

With the pearson autocorrelation function $\mathrm{R}(x - x')$.

Finally, a random field is said to be *ergodic* if the mean and variance of a trajectory are respectively equal to the mean and variance of the random field, therefore denoting

$$\mathbb{E}\left[(X(\boldsymbol{x},\omega_0)\right] = \mu_X; \tag{2.18}$$

$$\mathrm{Var}\left[X(\boldsymbol{x},\omega_0)\right] = \sigma_X^2. \tag{2.19}$$

Consequently, the ergodicity of a random field implies the stationarity of the second order.

2.3.3 Simulation of random fields

As it could have been expected, dealing with an infinite set of random variables is not trivial. This section presents the basics of the random fields simulation.

2.3.3.1 The different methodologies

To simulate a random field, it is usually discretized with a finite set of random variables $\{\chi_i, i = 1, \ldots, n\}$ and then the random field approximate reads (Sudret and Der Kiureghian (2000))

$$\hat{X}(\boldsymbol{x}) = \mathscr{F}[\boldsymbol{x}, \boldsymbol{\chi}] \tag{2.20}$$

The discretization methods can be separated into two groups:

- *Local discretization methods*, where the random vector $\boldsymbol{\chi}$ is identified from selected values or local averages of $X(\boldsymbol{x}, \omega)$;
- *Series expansion methods*, where the random field is *exactly* represented as a series of given random variables and spatial functions.

Among all the methods presented in Sudret and Der Kiureghian (2000), the author selected the Karhunen-Loève expansion described in the following, for reasons exposed latter on.

2.3.3.2 Karhunen-Loève

2.3.3.2.1 Definition The *Karhunen-Loève* (KL) (Loève (1977); Ghanem and Spanos (2003)) denotes

$$X(\boldsymbol{x}, \omega) = \mu(\boldsymbol{x}) + \sum_{i=1}^{+\infty} \sqrt{\lambda_i} \xi_i(\omega) \phi_i(\boldsymbol{x}), \quad x \in D_x, \omega \in \Omega, \tag{2.21}$$

where $\xi_i, i \in \mathbb{N}^{+*}$ are centred and uncorrelated random variables. In the case of a gaussian random field, these random variables are also normally distributed.

The covariance function of the random being bounded, symmetric and positive definite admits the following decomposition:

$$\mathrm{Cov}\left(x,x'\right)=\sum_{i=1}^{+\infty}\lambda_i\phi_i(x)\phi_i(x'), \tag{2.22}$$

where the pairs $\{(\lambda_i,\phi_i), i\in\mathbb{N}^{+*}\}$ are respectively the eigenvalues rearranged in the descending order and the corresponding eigenvectors, solutions of the Fredholm integral of the second kind reading

$$\int_{D_X} C(\boldsymbol{x},\boldsymbol{x}')\phi_i(\boldsymbol{x})d\boldsymbol{x}=\lambda_i\phi_i(\boldsymbol{x}'). \tag{2.23}$$

In practice, the decomposition is truncated after M terms (the so-called *truncation order*) in order to obtain an approximate of the random field writing

$$\hat{X}(\boldsymbol{x},\omega)=\mu(\boldsymbol{x})+\sum_{i=1}^{M}\sqrt{\lambda_i}\xi_i(\omega)\phi_i(\boldsymbol{x}),\quad x\in D_x,\omega\in\Omega. \tag{2.24}$$

Truncating the expansion indeed implies that the Karhunen-Loève expansion tends to underestimate the true variance of the random field $X(\boldsymbol{x},\omega)$.

2.3.3.2.2 Solving the Fredholm integral Except for specific cases of domains and covariance function (Ghanem and Spanos (2003)), there is no analytic solution to this problem.

The basic idea proposed by Ghanem and Spanos (2003) is to use a Galerkin-type method to solve Eq. (2.23).

By decomposing the eigenfunctions $\{\phi_i(\boldsymbol{x}), i\in\mathbb{N}^{+*}\}$ onto a complete set of functions $\left\{h_j(\boldsymbol{x}), j=1,\ldots,N\right\}$ such as

$$\phi_i(\boldsymbol{x})=\sum_{j=1}^{N}d_j^{(i)}h_j(\boldsymbol{x}), \tag{2.25}$$

and substituting Eq. (2.25) into Eq. (2.23), the error made by the truncation therefore reads

$$\epsilon_N=\sum_{j=1}^{N}d_j^{(i)}\left[\int_{D_X}C(\boldsymbol{x},\boldsymbol{x}')\phi_i(\boldsymbol{x})d\boldsymbol{x}-\lambda_i\phi_i(\boldsymbol{x}')\right]. \tag{2.26}$$

By imposing the error ϵ_N to be orthogonal with the set of functions $\{h_k(\boldsymbol{x}), k=1,\ldots,N\}$ it comes

$$\sum_{j=1}^{N}d_j^{(i)}\left[\int_{D_X}\left[\int_{D_X}C(\boldsymbol{x},\boldsymbol{x}')h_j(\boldsymbol{x})d\boldsymbol{x}\right]h_k(\boldsymbol{x}')d\boldsymbol{x}'-\lambda_i\int_{D_X}h_j(\boldsymbol{x})h_k(\boldsymbol{x})d\boldsymbol{x}\right]=0. \tag{2.27}$$

Rewriting the matrix **C** as

$$C_{ij} = \int_{D_X} \int_{D_X} C(\boldsymbol{x}, \boldsymbol{x}') h_j(\boldsymbol{x}) h_k(\boldsymbol{x}') d\boldsymbol{x} d\boldsymbol{x}', \tag{2.28}$$

denoting the matrix **B**

$$B_{ij} = \int_{D_X} h_j(\boldsymbol{x}) h_k(\boldsymbol{x}) d\boldsymbol{x}, \tag{2.29}$$

the matrix **D**

$$D_{ij} = d_i^{(j)}, \tag{2.30}$$

and finally the matrix $\boldsymbol{\Lambda}$

$$\Lambda_{ij} = \delta_{ij} \lambda_i, \tag{2.31}$$

with δ_{ij} being the Kronecker delta, Eq. (2.27) becomes

$$\mathbf{CD} = \boldsymbol{\Lambda}\mathbf{BD}. \tag{2.32}$$

Classical sets of orthogonal functions of size N are:

- Legendre polynomials (Phoon et al. (2002a)) reading

$$\Pi_0 = 1, \quad \Pi_1 = x, \ldots, \Pi_i = \frac{2i-1}{i} x \Pi_{i-1} - \frac{i-1}{i} \Pi_{i-2}, \quad i = 2, \ldots, P \tag{2.33}$$

  where $P = (N-1)$ is the highest polynomial degree. They are defined on the interval $[-1, 1]$ and thus needs to be scaled. It gives access to a maximum $M = P - 1$ eigenvalues;

- Haar wavelets (Phoon et al. (2002a)). They are generated by the Haar mother wavelet function denoted by

$$\Psi(x) = \begin{cases} 1 & x \in [0, 1/2[\,; \\ -1 & x \in [1/2, 1[\,; \\ 0 & \text{otherwise.} \end{cases} \tag{2.34}$$

  By shifting and scaling the Haar wavelets such as

$$\Psi_{j,k}(x) = \alpha_j \Psi(2^j x - k), \quad j, k \in \mathbb{Z}, \tag{2.35}$$

  the set of Haar wavelets is defined by

$$\Psi_0(x) = 1, \quad \Psi_i(x) = \Psi_{j,k}(x) \tag{2.36}$$

with $i = 2^j + k$; $k = 0, \ldots, 2^j - 1$; $j = 0, \ldots, m-1$ where m is the maximum wavelet level. The number of eigenvalues achievable is $M = (2^m)^{\text{card}(D_X)} - 1$. With $\alpha_j = 2^{j/2}$ the corresponding set of Haar wavelets are orthonormal.

- Finite elements basis (Ghanem and Spanos (2003); Recek et al. (2005)) where the set of orthogonal functions is composed by the shape functions of the mesh, the number of eigenvalues computed being equal to the number of elements.

2.3.3.2.3 Choice of the basis In order to test the different bases, let us consider a gaussian non-stationary random field with its mean and covariance matrix shown in Figure 2.1. It is defined over a domain $D_X \subset \mathbb{R}$ of size 500. This random field presents a non-derivable point on the middle of the domain. The correlation function of the field is an exponential function reading

$$R(x, x') = exp(\frac{-\|x - x'\|}{l}) \tag{2.37}$$

where l is called the correlation length and is equal to 10. The variance of the field is defined with a constant coefficient of variation $c_v = 0.05\mu_X(x)$. In other words, as illustrated in Figure 2.1, the correlation length is pretty small in front of the domain width.

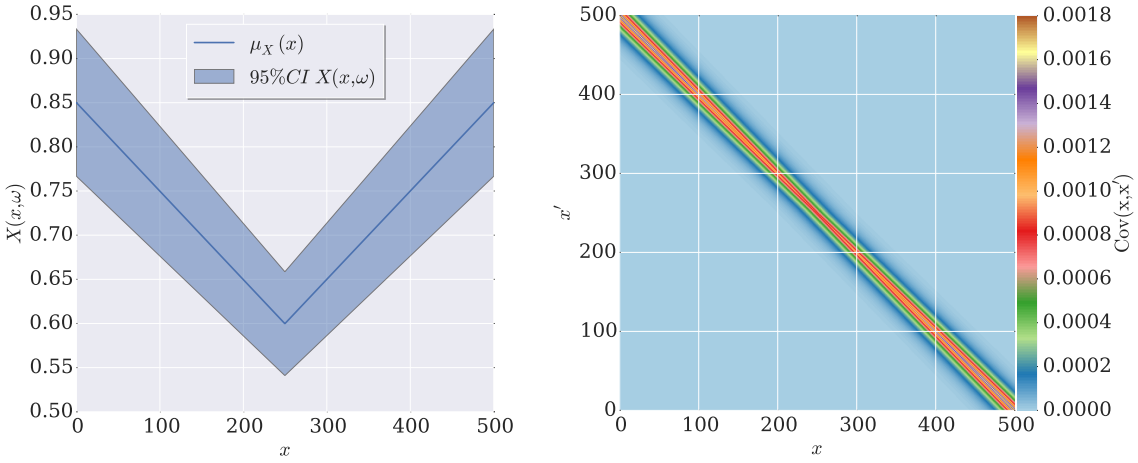

Figure 2.1 – On the left, the mean of the random field with its confidence interval derived from the covariance on the right.

Legendre polynomial basis The Legendre polynomials basis in this case is up to 51, which should give access to 50 eigenvalues solutions of Eq. (2.32). Figure 2.2 presents the covariance resulting from the simulations with truncation orders M equal to 20 and 50 with Legendre polynomials order up to order 21 and 51.

Figure 2.2 clearly shows that the Legendre polynomials basis is quite sensitive to its parameters. On one hand, the increase of the polynomials order does not improve the approximation of the covariance function for a given truncation order. On the other hand,

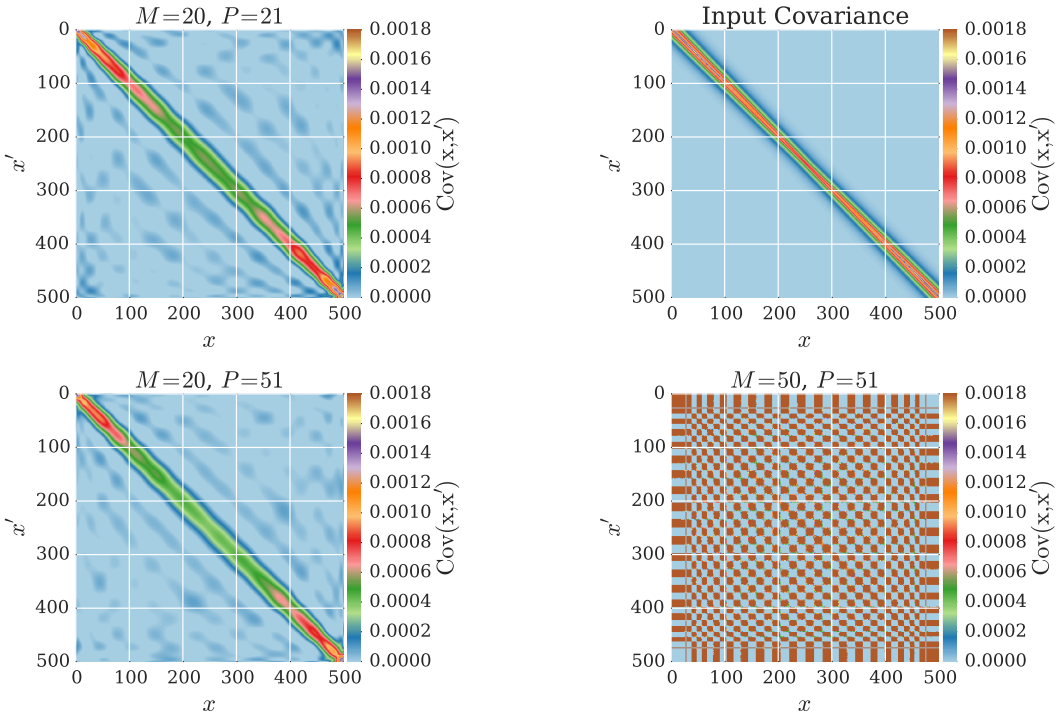

Figure 2.2 – Autocovariance matrix of the simulated field for different Legendre polynomials orders and truncation orders. On the upper right is the real covariance which was used as an input.

increasing the truncation order up to the maximum possible (deduced from the polynomials order) leads to a diverging estimate.

These results are somehow intuitive since high polynomial orders are known to be oscillating with high amplitudes. An example given in Figure 2.3 confirm this to be the cause of the bad approximation of the eigenfunctions. For a domain large in front of the correlation length, the smaller polynomial orders appears unable to approximate well the covariance function.

Haar wavelet basis On the same principle, the wavelet basis has a maximum wavelet level ranging from 5 to 10 with a truncation order equal to 20 and 1000.

Through Figure 2.4 it is clear that an increase of the wavelet level gives a smoother approximation of the covariance. With a wavelet level equal to 10, the decomposition seems sensitive to the boundary of the domain where it returns a covariance higher than the real one.

When extending the decomposition up to 1000 eigenvalues, the global covariance is reproduced with a pretty high accuracy. A focus on the sub-domain $[0, 20] \subset D_X$ (see Figure 2.5) proves that the local accuracy in this case also tends to be pretty good. On the opposite the lower truncation order shows the border effect which return a completely biased estimate of the covariance while with a small wavelet level it is clear that the wavelets are

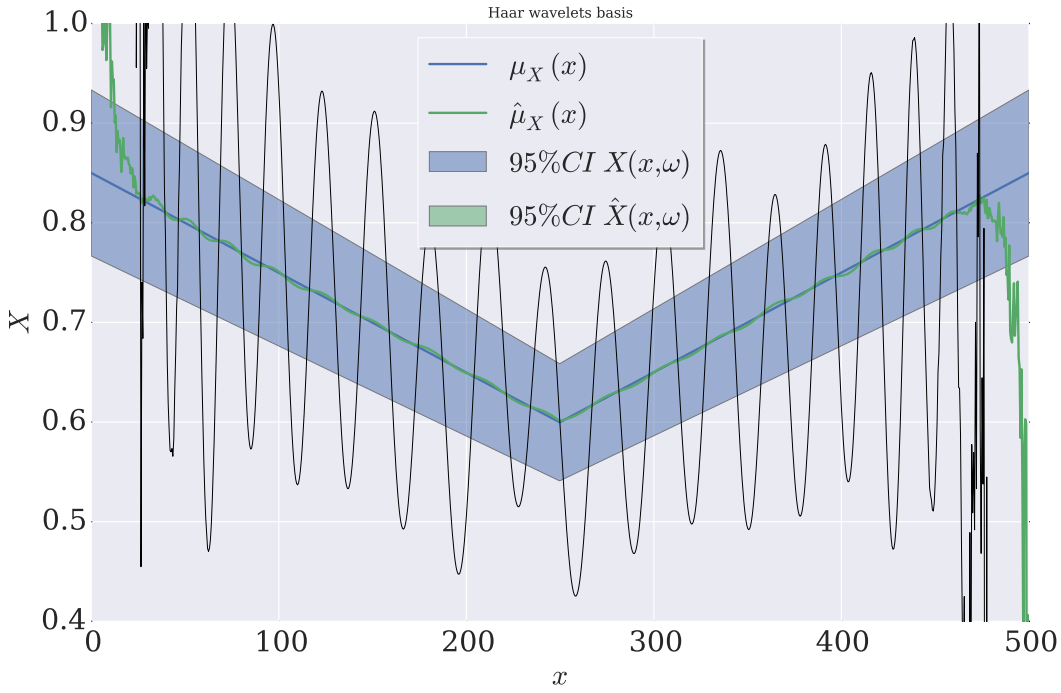

Figure 2.3 – Mean, confidence interval and an example of trajectory resulting from the KL decomposition on a Legendre polynomials basis with order 51 and truncation order equal to 50.

way too large which creates visible discontinuities.

Finite elements basis Finally the finite elements basis contains on one hand 100 elements and 1000 on the other hand, the truncation order ranging from 20 to 1000. The elements have linear shape functions and are equally subdividing the domain.

The finite elements help in decomposing the eigenfunctions solutions of the Fredholm integral Eq. (2.23) into local shape functions. In Figure 2.6, the covariance evolution appears to be smooth enough for the linear shape functions of the finite elements, since the increase in the number of elements with a constant truncation order does not have much effect.

However increasing the truncation order, thus adding information on the covariance into the KL decomposition, helps pretty much to fit the input covariance of the simulated field $X(x, \omega)$.

A focus on the sub-domain $[0, 20] \subset D_X$ made in Figure 2.7 confirms the above observations.

Conclusion Apart from the Legendre polynomials basis, the choice of the basis cannot be easily driven by the approximation accuracy. With the wavelet and the finite element

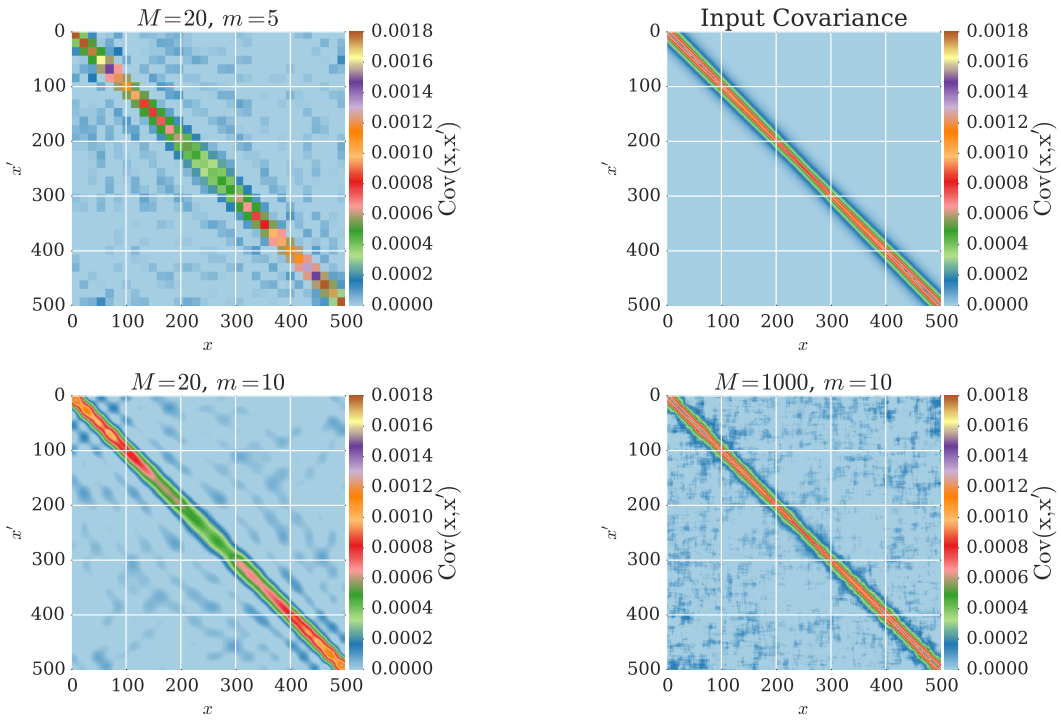

Figure 2.4 – Autocovariance matrix of the simulated field for different Haar wavelets levels and truncation orders. On the upper right is the real covariance which was used as an input.

bases, in this configuration the results are equivalent given than the wavelet order, the number of elements and the number of eigenvalues kept in the decomposition are enough.

The decomposition made with Legendre polynomials is less efficient for large domain and building a basis of polynomials of order 1001 (i.e. to compute 1000 eigenvalues) is impossible due to the numerical instability of high order polynomials.

Such an order may seem unnecessary, yet computational cost is not impacted enough for the wavelet and the finite element basis to justify any choice of truncation, provided that the evaluated eigenvalues keep on being positive.

The choice of the basis therefore results from the major difference between the Haar wavelets and the finite elements: the first derives a global basis while the latter creates a local one.

In the context of this thesis, which aims at proposing a methodology able to deal with large structures, it is evident that the finite elements have two great advantages over the Haar wavelets:

- it is not limited to rectangular domain;
- if needed, in case of strong local non-stationarity, the mesh can be refined in the zone of interest without having to increase the precision over the whole domain.

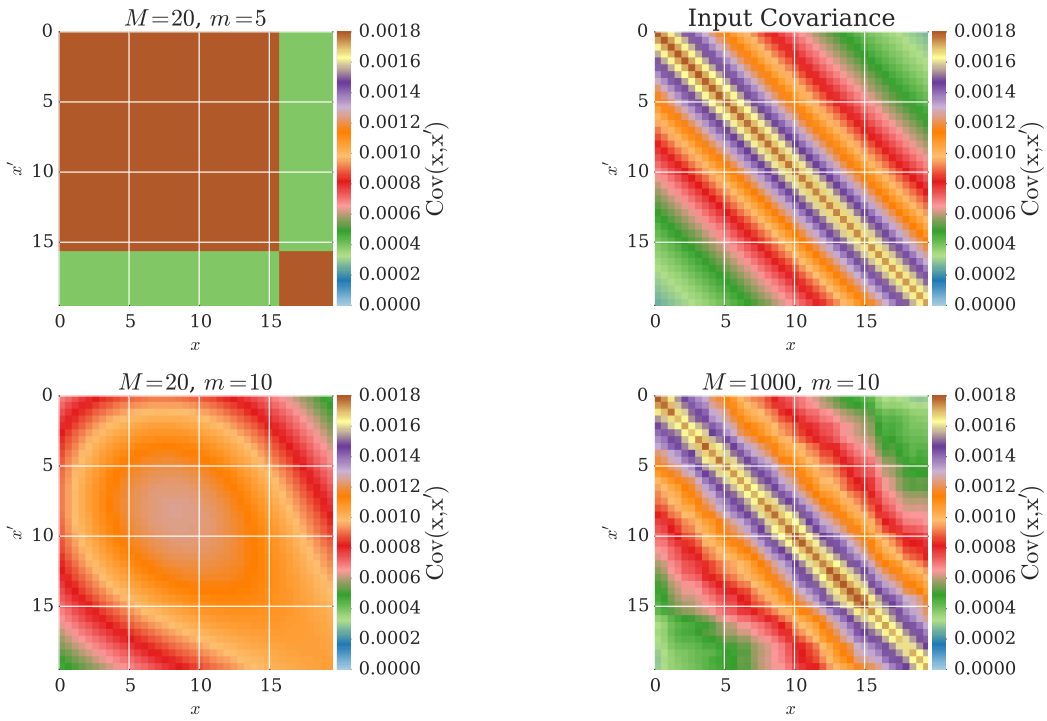

Figure 2.5 – Autocovariance matrix of the simulated field for different Haar wavelets levels and truncation orders. On the upper right is the real covariance which was used as an input. Focus on the domain $[0, 20]$.

Considering these advantages, the following simulation of random fields will be made with the help of a finite element basis.

2.3.3.3 Why the Karhunen-Loève expansion ?

The previous section has made it clear that this thesis uses the Karhunen-Loève expansion, but it has never said why.

The first point is that it answers perfectly one of the objectives of this thesis: it is completely versatile. The Karhunen-Loève expansion is the only decomposition which does not need any assumption to be made on the simulated field (Sudret and Der Kiureghian (2000)).

In Eq. (2.21), it is obvious that both the mean and the covariance can be non-stationary as it has been shown in Section 2.3.3.2.3. The marginal distribution of the field is defined by the distributions of the random variables $\xi_i, i \in \mathbb{N}^{+*}$. In case of a gaussian random field, the law of these random variables is also gaussian, but for other cases it is unknown.

Let $\hat{X}(\boldsymbol{x}, \omega)$ being observed trajectories of the random field $X(\boldsymbol{x}, \omega)$, $\hat{\mu}(\boldsymbol{x})$ and $\hat{\mathrm{Cov}}(x, x')$ respectively the empirical mean and covariance estimated from the observed trajectories, thus the random variables $\xi_i, i \in \mathbb{N}^{+*}$ read

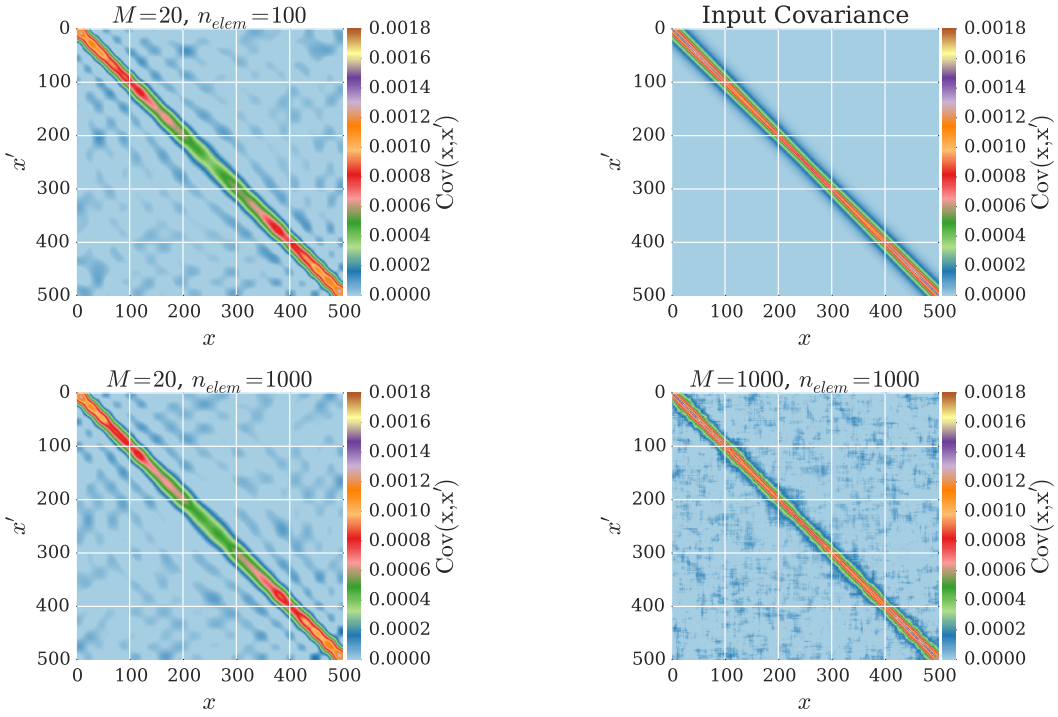

Figure 2.6 – Autocovariance matrix of the simulated field with a finite elements basis for different number of elements and truncation orders. On the upper right is the real covariance which was used as an input.

$$\xi_i(\omega) = \frac{1}{\sqrt{\lambda_i}} \int_{D_X} \left[\hat{X}(\boldsymbol{x},\omega) - \hat{\mu}(\boldsymbol{x})\right] \phi_i(\boldsymbol{x}) d\boldsymbol{x}. \tag{2.38}$$

It means that with enough observed trajectories, the laws of the random variables $\xi_i, i \in \mathbb{N}^{+*}$ can be estimated without making any assumption.

These appealing properties together with the use of a finite element basis consequently encouraged the author to prefer this methodology.

2.3.4 Simulation of non-gaussian fields

In case of a random field with not enough observation to estimate the probability distributions of the random variables $\xi_i, i \in \mathbb{N}^{+*}$, it is still possible to simulate a non-gaussian random field by the so-called *translation field* transformation (also called the *Nataf* transformation for random variables and random vectors) defined as:

$$Y(\boldsymbol{x},\boldsymbol{\omega}) = F_Y^{-1}\left[F_U(U(\boldsymbol{x},\omega)\right], \tag{2.39}$$

where $Y(\boldsymbol{x},\omega)$ is random field with the marginal CDF F_Y and $U(\boldsymbol{x},\omega)$ being a stationary gaussian random field with 0 mean and unit variance. This method is the Nataf transformation for random variables applied to random fields, yet it has the major drawback that such

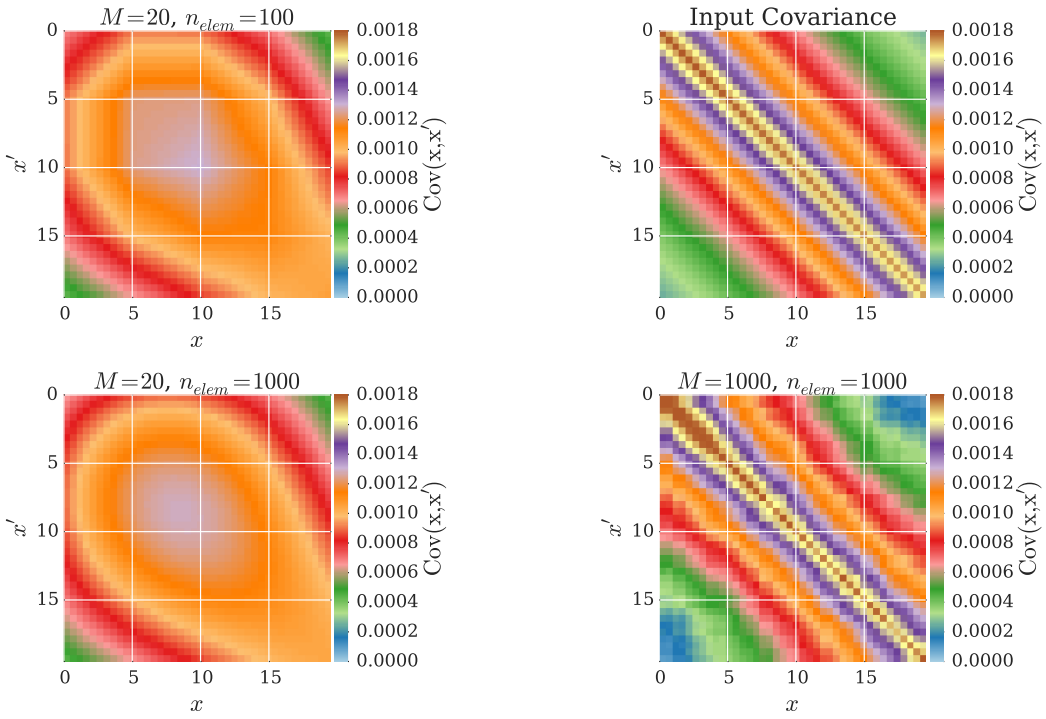

Figure 2.7 – Autocovariance matrix of the simulated field with a finite elements basis for different number of elements and truncation orders. On the upper right is the real covariance which was used as an input. Focus on the domain $[0, 20]$.

non-linear transformation does not conserve the autocorrelation of the underlying gaussian random field.

To the author's knowledge, two methods exist to simulate non-gaussian random fields.

2.3.4.1 Covariance and marginal fitting methods

The covariance fitting methods aim at identifying the underlying gaussian random fields autocorrelation which will result in non gaussian random fields with the desired autocorrelation.

Puig (2003) and Puig and Akian (2004) proposed to decompose the transformation $F_Y^{-1}(F_U(x))$ on a hermite polynomials basis such as:

$$f_n = (n!)^{-1} \int_{\mathbb{R}} F_Y^{-1}(F_U(x)) H_n(x) \frac{e^{\frac{-x^2}{2}}}{\sqrt{2\pi}} dx, \tag{2.40}$$

where $H_n(x)$ are the hermite polynomials reading

$$H_0(x) = 1, \quad H_n(x) = (-1)^n e^{x^2/2} \frac{d^n}{dx^n} e^{-x^2/2}, \quad n \in \mathbb{N}^*. \tag{2.41}$$

From this point the resulting correlation function of the transformation writes

$$\hat{\mathrm{R}}_Y(x,x') = \sum_{n=1}^{M} n! f_n^2 (\mathrm{R}_U(x,x'))^n, \tag{2.42}$$

where $R_U(x,x')$ is the autocorrelation function of the underlying stationary gaussian process.

The objective is thus to minimise the residual defined by

$$\|\mathrm{R}_Y(x,x') - \sum_{n=1}^{M} n! f_n^2 (\mathrm{R}_U(x,x'))^n\|. \tag{2.43}$$

The main difficulty is to constrain the autocorrelation function of the underlying gaussian process to stay positive definite.

Most of the methods available aim at estimating the autocorrelation function of the underlying process in similar ways (Gioffré et al. (2000); Gurley (1997); Sakamoto and Ghanem (2002)).

Alternatively, a procedure proposed by Phoon et al. (2002b) and Phoon et al. (2004), based on the KL decomposition iterates over the random variables $\xi_i, i \in \mathbb{N}^{+*}$ in order to fit the marginal distribution of the random field. The target covariance being an input of the decomposition, as soon as the random variables $\xi_i, i \in \mathbb{N}^{+*}$ are zero-mean, unit variance and non-correlated, Eq. (2.21) ensures that the covariance is kept unmodified. The main difficulty concerns the non-stationary random fields for which the marginal distribution is also indexed by the random field domain.

2.3.4.2 Fractile correlation

An interesting idea proposed in Phoon et al. (2004) consists in using a gaussian copula (Caniou (2012)) to define the autocorrelation of the underlying gaussian random field $U(x,\omega)$.

Indeed, the idea is to target a rank correlation function $R_S(x,x')$, or fractile correlation, for the non-gaussian random fields. From Eq. (2.39) the transformation being based on cumulative density functions is monotonic. From the definition of a rank correlation it is evident that it is invariant with monotonic transformations.

Similarly to the gaussian copula relationships, the pearson correlation function then denotes

$$R(\boldsymbol{x},\boldsymbol{x}') = 2\sin\left(\frac{\pi}{6} R_S(\boldsymbol{x},\boldsymbol{x}')\right). \tag{2.44}$$

2.3.5 Simulation of cross-correlated random fields

As inputs of a degradation model, multiple variables may be considered as random fields, and analogically with the random variables, a correlation between two or more random fields may be considered. To the author's knowledge, three methods exist to cross-correlate several random fields.

2.3.5.1 Translation field

The Nataf transformation of random vectors aims at making every component of a random vector independent with a standard gaussian distribution. The invert Nataf transformation goes back into the space of non-gaussian and *correlated* random variables, so does the *translation field*.

Let $\mathbf{R}_{cross}$ be the cross-correlation matrix between the components of a vector-valued random field $\boldsymbol{X}(\boldsymbol{x},\omega)$ with $\boldsymbol{x} \in D_{\boldsymbol{X}} \subset \mathbb{R}^n$. Let $\boldsymbol{U}(\boldsymbol{x},\omega)$ be a gaussian vector-valued random process with each component being an independent standard gaussian random field.

The Cholesky decomposition of the cross-correlation reads

$$\mathbf{R}_{cross} = \mathbf{L}\mathbf{L}^T, \tag{2.45}$$

with $\mathbf{L}$ being a lower triangular matrix, then the random field $\boldsymbol{X}(\boldsymbol{x},\omega)$ writes

$$\boldsymbol{X}(\boldsymbol{x},\omega) = \boldsymbol{F}_{\boldsymbol{X}}{}^{-1}\left[\boldsymbol{F}_{\boldsymbol{U}}(\mathbf{L}\boldsymbol{U}(\boldsymbol{x},\omega)\right]. \tag{2.46}$$

The advantage of this simple method is that all the autocorrelation functions defined for the components of the gaussian random field $\boldsymbol{U}(\boldsymbol{x},\omega)$ are conserved in the random field $\boldsymbol{X}(\boldsymbol{x},\omega)$ if they have been defined as fractile correlation (see Section 2.3.4.2)

Example 2.3.1. *Let $\boldsymbol{U}(x,\omega) = U_1(x,\omega), U_2(x,\omega)$ be a gaussian standard random field with each component's correlation function denoting*

$$R(x,x') = 2sin\left[\frac{\pi}{6}exp\left((x-x')^2\right)\right]. \tag{2.47}$$

Let $\boldsymbol{X}(x,\omega) = X_1(x,\omega), X_2(x,\omega)$ be the lognormal stationary random field with $F_{X_1} \sim LN(\mu = 5, \sigma = 1)$ and $F_{X_2} \sim LN(\mu = 15, \sigma = 3)$ and the cross-correlation coefficient $\rho_{X_1X_2} = -0.8$

Using the translation field *method to cross-correlate the components of the random field $\boldsymbol{X}(x,\omega)$ gives satisfactory results as shown in Figure 2.8 since the input autocorrelation function is conserved.*

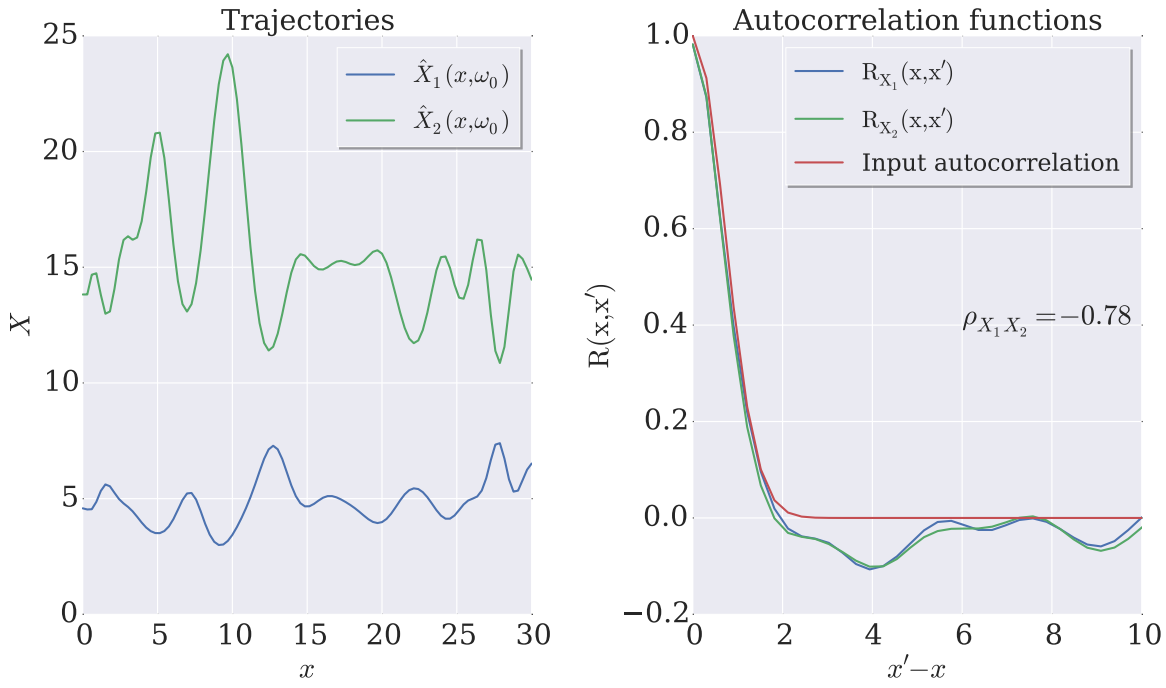

Figure 2.8 – On the left, two trajectories of random fields cross-correlated with the translation field methodology. On the right the resulting marginal autocorrelation functions.

2.3.5.2 Vorechovsky method

The method proposed by Vorechovsky (2008) aims at cross-correlating the components of a vector-valued random field $\boldsymbol{X}(x,\omega)$ with $\boldsymbol{x} \in D_X \subset \mathbb{R}^n$ using the KL decomposition of each component.

Indeed, while the covariance is represented by the eigenvalues and eigenfunctions of the fredholm integral in the KL decomposition (see Eq. (2.21), the randomness is represented by the random variables $\xi_i, i \in \mathbb{N}^{+*}$.

The idea of Vorechovsky (2008) is to correlate each components of $\boldsymbol{X}(x,\omega)$ by correlating the random variables of the decomposition.

Let us define $\left\{\xi^j, j=(1,\dots,n)\right\}$ the vector gathering the random variables $\left\{\xi_i^j, i=(1,\cdots,M), j=(1,\dots,N)\right\}$, M being the truncation order of the KL decomposition, identical for all the components of the vector-valued random field, and $\xi = \left\{\left[\xi^j\right]^T, j=(1,\dots,n)\right\}$ the random vector gathering all the random variables.

Finally let $\mathbf{R}_{(n\times n)}$ be the cross correlation matrix of the vector-valued random field.

The cross-correlation matrix of the random vector ξ therefore writes

$$\mathbf{D} = \begin{bmatrix} \mathbf{I}_{(M\times M)} & R_{1,2}\mathbf{I}_{(M\times M)} & R_{1,3}\mathbf{I}_{(M\times M)} & \dots & R_{1,N}\mathbf{I}_{(M\times M)} \\ \vdots & \mathbf{I}_{(M\times M)} & R_{2,3}\mathbf{I}_{(M\times M)} & \dots & R_{2,N}\mathbf{I}_{(M\times M)} \\ \vdots & \vdots & \mathbf{I}_{(M\times M)} & \dots & R_{3,N}\mathbf{I}_{(M\times M)} \\ \vdots & sym. & \vdots & \ddots & \vdots \\ \dots & \dots & \dots & \dots & \mathbf{I}_{(M\times M)} \end{bmatrix}. \tag{2.48}$$

The spectral decomposition of $\mathbf{D}$ writes

$$\mathbf{D} = \mathbf{\Phi}\mathbf{\Lambda}\mathbf{\Phi}^T. \tag{2.49}$$

Consequently, the correlated random variables of the vector-valued random field KL decomposition are denoted by:

$$\xi^c = \mathbf{\Phi}(\mathbf{\Lambda})^{1/2}\xi. \tag{2.50}$$

The major drawback of this methodology is that it requires to truncate all the KL decomposition at the same order, which could be problematic in case of very heterogeneous covariance functions among the components of the vector-valued random field. On the other hand, the advantage is that the marginal covariance function of each random field is not modified, even if the autocorrelations are not derived from the fractile correlation.

Example 2.3.2. *Starting from Example 2.3.1, the random fields $U_1(x,\omega)$ and $U_2(x,\omega)$ are simulated with a KL decomposition on a Legendre polynomials basis up to order 41 with 38 eigenvalues kept, the 39th and 40th eigenvalues available being negative due to approximation errors.*

These fields are correlated with the Vorechovsky method beforehand and then transformed into the target random fields $X_1(x,\omega)$ and $X_2(x,\omega)$ with Eq. (2.39).

As expected, the Vorechovsky correlation method is equivalent to the translation field method as demonstrated in Figure 2.9.

2.3.5.3 Vector valued random fields

Provided by Perrin et al. (2013), the main idea is to directly extend the Karhunen-Loève decomposition to the vector-valued random field $\boldsymbol{X}(\boldsymbol{x},\omega)$ with $\boldsymbol{x} \in D_X \subset \mathbb{R}^n$. This way, the cross-correlations are to be contained in the eigenfunctions solutions of the Fredholm integral as written in Eq. (2.23).

In this case the covariance becomes a matrix-valued function reading

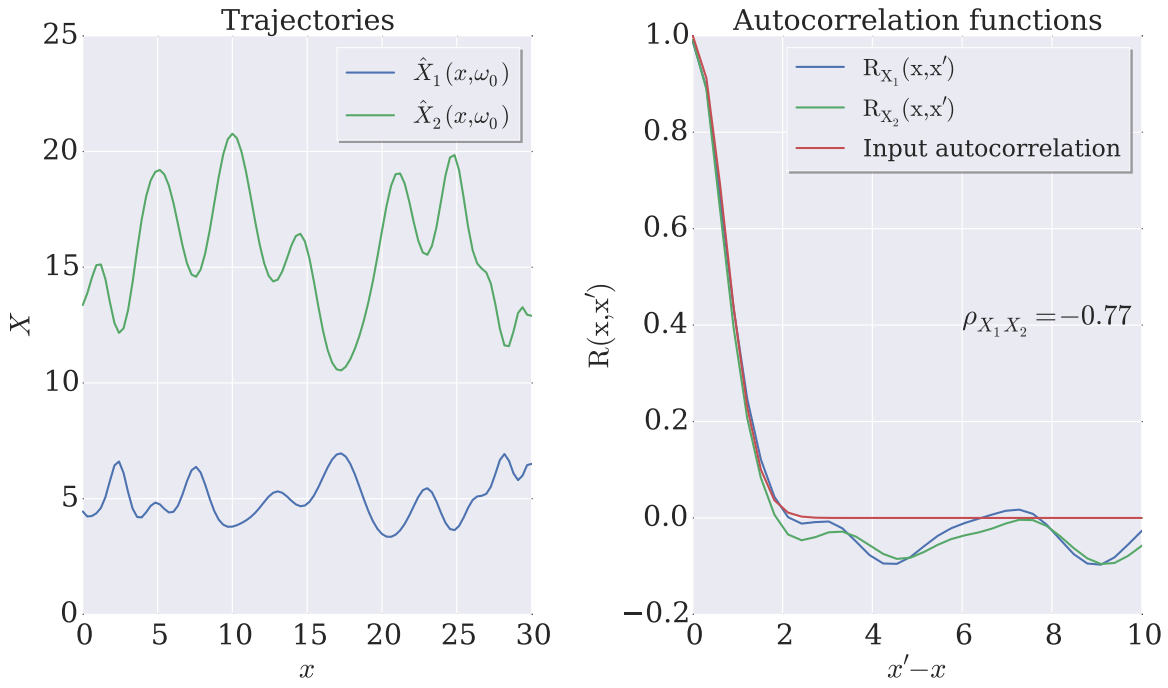

Figure 2.9 – On the left, two trajectories of random fields cross-correlated with the Vorechovsky methodology. On the right the resulting marginal autocorrelation functions.

$$\mathbf{Cov}(\boldsymbol{x},\boldsymbol{x}') = \begin{bmatrix} \mathrm{Cov}_{11}(\boldsymbol{x},\boldsymbol{x}') & \cdots & \mathrm{Cov}_{1n}(\boldsymbol{x},\boldsymbol{x}') \\ & \ddots & \\ \vdots & \mathrm{Cov}_{ij}(\boldsymbol{x},\boldsymbol{x}') & \vdots \\ & & \ddots \\ \mathrm{Cov}_{n1}(\boldsymbol{x},\boldsymbol{x}') & \cdots & \mathrm{Cov}_{nn}(\boldsymbol{x},\boldsymbol{x}') \end{bmatrix}, \quad i,j = 1,\ldots,n. \tag{2.51}$$

The KL decomposition minimises the square error committed on the variance approximation. It seems logical that on a vector-valued random fields the components with higher variance will tend to be better estimated than the other components. To solve this issue, Perrin et al. (2013) proposed to project the KL decomposition on different basis in order to distribute the approximation error among the components of the vector-valued random field to the user's will.

Despite the fact that it has not been used in this thesis because of the complexity induced by the estimation of a cross-covariance function, to the author's opinion this method is to be preferred when possible (i.e. the cross-covariances are known or estimable).

2.3.6 Conclusion

This section has presented the basics concerning the simulation of random fields, should they be Gaussian or not, cross-correlated or not. The purpose is now to describe how to build an inspection, maintenance and repair model for the degradation index, denoted as *IMRM* in the following, according to the thesis objectives and being able to consider the spatial variability of reinforced concrete degradation phenomena using the methods presented in this section.

2.4 Evolution of the degradation index

The objective of an IMRM is to gather the degradation predictions, the inspection, maintenance and failure models in order to predict the long-run evolution of a given degradation index. It is evident that proposing a methodology able to deal with any problems represents a dream. Having this point in mind, the present section is organised as follows.

The first section presents the global concept of the IMRM based on a decision tree used in this thesis. The following section is dedicated to the construction of the degradation indexes and of their estimators. The last exhibits two examples which will be the silver threads in the following chapters.

2.4.1 Inspection, maintenance and repair model for the degradation index

As explained in Section 1.4, many methodologies based on markov chains or decision trees have been developed as models for the evolution of a condition index. Markov chains methods are well-suited with the *PoD* definition, however the probability of detection is defined for *one* mesure at *one* point. In case of spatial variability, it becomes much more tricky to define a *PoD* since:

- It seems difficult to interpret the *PoD* of a degradation index defined for a large scale, the maximum of the carbonation depth for instance, when only parts of the structure are inspected (e.g. in Schoefs et al. (2009) where polynomial chaos decomposition of the degradation and the measurement noise are used to derive spatial PoD);
- With a fully inspected structure, the definition of the overall *PoD* would be difficult to write, considering that two measurements being close may not be independent.

Moreover, the *PoD* may not be always defined for a given measurement technique.

In order to propose a methodology:

- As independent as possible of the different assumptions that could be made on the inspection, failure and maintenance models;

- Independent of the degradation process;
- Independent of the considered structure;

the choice of decision trees for the IMRM appears more appropriate. Indeed, a simple tree like in Figure 2.10 may answer to the objectives since:

- The inspection node resulting in two probability estimates which depend on a degradation index D:
  - The probability of repairing (i.e. the probability of failure) reading

$$\tilde{\mathscr{P}}_f = \tilde{\mathscr{P}}\left[D >= d_c\right], \tag{2.52}$$

    where d_c is the failure threshold corresponding to index D;
  - The probability of maintenance reading

$$\tilde{\mathscr{P}}_{Ma} = \tilde{\mathscr{P}}\left[D >= d_{pm} \mid D < d_c\right], \tag{2.53}$$

    with d_{pm} the maintenance threshold corresponding to index D. The probability of maintenance is conditioned by the index not violating the failure threshold.

  The inspection method leading to the estimate of these probabilities of repairing has no special requirements;
- Repairing and maintaining only lead to the next inspection, without any assumptions on the repairing process (perfect or not, modifying the degradation kinetic, ...).

2.4.2 Estimating the degradation index

In the methodology developed herein, predicting the degradation of RC structures aims at predicting the evolution of a degradation index.

This index shall be seen as one decision variable of the stakeholder, the variable saying *it is time to repair* or not. Beware, this may not be the only decision variable and the maintenance could thus be postponed considering the others. For instance, the degradation index could be *no crack length is higher than the threshold* and its evaluation may indicate the necessity of a maintenance while at the same time other decision variables of the stakeholders could be *repair the most degraded structure* and *choose among the structures to be repaired the ones with predicted maintenance costs affordable considering the annual budget*.

Since both carbonation and chloride ingress processes lead to the depassivation of the reinforcements in concrete (see Section 1.2.1.1), this thesis uses a unique degradation index reading

$$D = \frac{|L_d - L_t|}{L_t}, \tag{2.54}$$

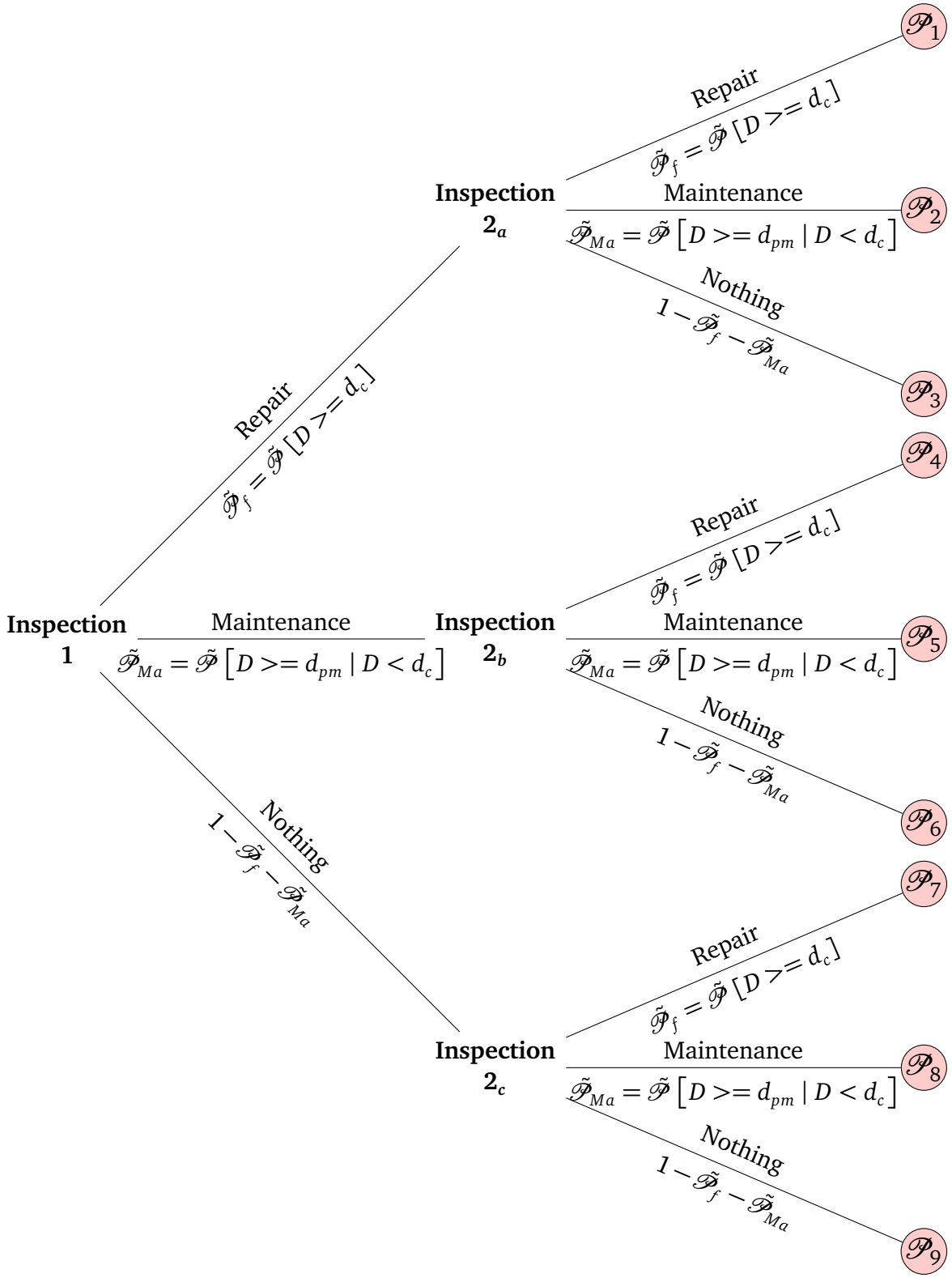

Figure 2.10 – Decision tree with two inspections. $\mathscr{P}_\circ$ is probability of the branch $\circ$.

with L_d being the length of a reinforced concrete zone with a carbonation depth higher than a given threshold (maintenance of failure) and L_t the total length of the considered structure. From the simulations of the prediction model for the considered degradation (carbonation in this thesis), the probability for the degradation index violating a given threshold $\mathscr{P}[D \geq d]$ can easily be computed through Crude Monte Carlo simulations or more advanced reliability methods (the interested reader is referred to Dubourg (2011, Chapter 3) for a complete review of those methods).

Yet this probability will be computed considering the whole domain of the degradation random field, provided that the discretisation of the random field is fine enough. One can note, no stakeholder will perform an inspection campaign on the entire structure, but only on a limited number of locations mostly driven by budget considerations. Referring to the decision tree presented in Figure 2.10, the probability of acting, which has to be returned from the simulation of inspections, is indeed an approximate of the predicted probability

$$\mathscr{P}_{act} = \mathscr{P}[D \geq d_c] + \mathscr{P}\left[D >= d_{pm} \mid D < d_c\right], \tag{2.55}$$

which is denoted $\hat{\mathscr{P}}_{act}$.

Consequently, the question is: *Given an inspection budget and considering the spatial variability of the degradation process, in which locations should the structure be inspected in order to ensure a good estimate of* $\mathscr{P}_{act}$ *?*

Two situations may occur:

- No information available to predict accurately the degradation process (e.g. no idea of the autocorrelation structure or no confidence in the model predictions, ...). In this case, the probability $\mathscr{P}_{act}$ is assumed as being intractable;
- An efficient way to predict the degradation process exists.

The two following sections propose different solutions to position the inspection depending on the above cases.

2.4.2.1 Classical Design of Experiments

If no reliable data are available for the prediction, or not enough information on the spatial variability to predict anything more than homogeneous degradation over the structure, the best way to investigate is evident. The inspections points shall fill the space the best as they could considering the number of measurements that can be afforded.

The so-called *space filling* sequences are perfectly adapted for this case.

2.4.2.1.1 Discrepancy Let define $\mathscr{B}$ as the subset family of $\mathbb{I}_n = [0,1]^n$ Lebesgue measurable and the domain $\mathbb{B} \subset \mathbb{I}_n$ where n is the space dimension, the measure of discrepancy of an ensemble of variables $\{X_i, i = 1, \ldots, N\}$ is defined by:

$$\mathscr{D}(\mathscr{B},\boldsymbol{X}_N) \triangleq \sup_{\mathbb{B}\in\mathscr{B}} \left| \frac{1}{N} A(\mathbb{B},\boldsymbol{X}_n) - \lambda(\mathbb{B}) \right|, \tag{2.56}$$

with $A(\mathbb{B},\boldsymbol{X}_N)$ being the number of elements of X_N in $\mathbb{B}$ and $\lambda(\bullet)$ the Lebesgue measure.

If $\mathscr{B}$ gathers all the subsets of the form $\prod_{i=1}^{n}[0,u_i[$,the star discrepancy is denoted by:

$$\mathscr{D}_N^*(\boldsymbol{X}_N) = \mathscr{D}(\mathscr{B},\boldsymbol{X}_N) \triangleq \sup_{u\in[0,1]^n} |F_N(u) - F_U(u)|, \tag{2.57}$$

where $F_N(u)$ is the empirical cumulative density function and $F_U(u) = \prod_{i=1}^{n} u_i$ the uniform CDF.

We also define the extreme-discrepancy as $\mathscr{D}_N(\boldsymbol{X}_N) = \mathscr{D}(\mathscr{B},\boldsymbol{X}_N)$ if $\mathscr{B}$ aggregates all the subsets of the form $\prod_{i=1}^{n}[u_i,v_i[$.

It is harsh to derive analytical expressions of the discrepancies except for the case of uni-dimensional space. In this case the star discrepancy is defined by:

$$\mathscr{D}_N^*(X_N) = \frac{1}{2N} + \max_{1\le i\le N} \left| X_i - \frac{2i-1}{2N} \right|, \tag{2.58}$$

which is the Kolmogorov-smirnov goodness-of-fit test applied for a uniform distribution over $[0,1]$.

The extreme-discrepancy is denoted by:

$$\mathscr{D}_N(X_N) = \frac{1}{N} + \max_{1\le i\le N} \left(\frac{i}{N} - X_i \right) - \min_{1\le i\le N} \left(\frac{i}{N} - X_i \right). \tag{2.59}$$

The discrepancy measures the dispersion of the sequence $\boldsymbol{X}_N$ over the space. The smaller the discrepancy, the better the space filling. Based on this metric, it has been proved (Franco (2008)) that the easiest way to fill the space is to use the low-discrepancy sequences introduced hereafter.

2.4.2.1.2 Low-discrepancy sequences Among the low-discrepancy sequences, the most famous one is the Van der Corput (VDC) sequence defined by (Van der Corput (1935)):

$$x_k \triangleq \phi_b(k) = \sum_{i=0}^{m-1} a_i b^{-(i+1)}, \tag{2.60}$$

where b is the chosen base and a_i is the i-th digit of k written in basis b. For instance, $[50]_{10}$ in base 10 writes $[1212]_3$ in base 3, thus $m=4$, $a_0=1$, $a_1=2$, $a_2=1$ and $a_3=2$. The discrepancy of the VDC sequence is bounded by:

$$N\mathscr{D}_N^*(X_\infty) = N\mathscr{D}_N(X_\infty) \le 1 + \frac{\log(N)}{\log(8)} \tag{2.61}$$

For dimension $n \geq 1$, Halton (Halton (1960)), Hammersley (Hammersley (1960)) and Sobol (Sobol' (1967)) sequences are generalisations of the uni-dimensional VDC sequence.

The Halton sequence is defined by:

$$\boldsymbol{x_k} \triangleq \left(\phi_{b_1}(k), \ldots, \phi_{b_{n-1}}(k), \phi_{b_n}(k)\right)^T, \tag{2.62}$$

where $\phi_{b_i}(k)$ is the VDC sequence in base $\{b_i \in \mathbb{N}, i = 0, \ldots, n\}$. They are chosen such as $\text{GCD}\left(b_i, b_j\right) = 1, \forall i \neq j$. In practice they are the n-th firsts prime numbers $\{q, q = 2, 3, 5, 7, 11, 13, 17, 19, 23, \ldots\}$.

The Hammersley sequence is a Halton sequence completed by a term dependent on the sequence length. It writes

$$\boldsymbol{x_k} \triangleq \left(\frac{k}{N}, \phi_{b_1}(k), \ldots, \phi_{b_{n-1}}(k)\right)^T. \tag{2.63}$$

On the opposite of the VDC and the Halton sequences, since the Hammersley sequence is dependent on the number of points in the sequence, it cannot be augmented.

The star discrepancies of the Halton and Hammersley sequences are respectively bounded by:

$$\mathscr{D}_N^*(\boldsymbol{X}_\infty) \leq A_n \frac{[\log(N)]^n}{N} + \mathscr{O}\left(\frac{[\log(N)]^{n-1}}{N}\right) \tag{2.64}$$

$$\mathscr{D}_N^*(\boldsymbol{X}_\infty) \leq A_{n-1} \frac{[\log(N)]^{n-1}}{N} + \mathscr{O}\left(\frac{[\log(N)]^{n-2}}{N}\right) \tag{2.65}$$

with $\lim_{n\to\infty} \dfrac{\log(A_n)}{n\log(n)} = 1$, meaning that A_n, thus the star discrepancy, exponentially increases with the dimension n.

The Sobol sequence construction is not developed in this thesis for the sake of simplicity. The interested reader is referred to Franco (2008) which gathers an extended set of low-discrepancy sequences along with the classical design of experiments methods (e.g. factorial experiments design, ...).

When dealing with space-filling methods, the so-called *curse of dimensionality* is one of the major problems encountered. However distributing the inspection locations will be done at most in a 3-dimensional space thus the *curse of dimensionality* is out of concern in this thesis.

However the number of locations, i.e. the size of the sequence, indeed tends to be pretty small ($N \leq 20$) in this context. Since the discrepancy of the sequence is decreasing with the number of points N (e.g. Eq. (2.64)), the optimal space-filling becomes out of reach.

Examples are given in Figure 2.11 and Figure 2.12 for the 20 and 100 first points of the Halton and Sobol sequences. It appears that the space-filling tendency of the Sobol and

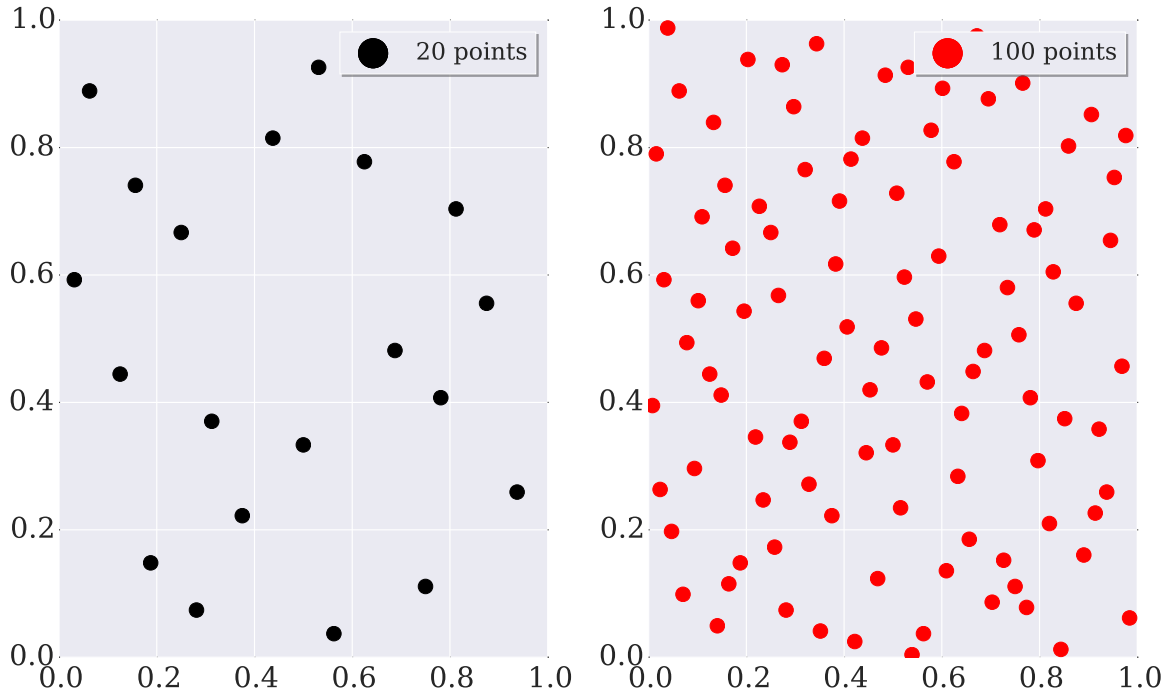

Figure 2.11 – Halton sequence realisations in two dimensions.

Halton sequences with 100 points is better but also creates useless point concentrations. For both sequences, with the first 20 points the point's distribution is far from being uniform.

2.4.2.1.3 K-means clustering An efficient way to circumvent this issue is to make use of the K-means clustering method described herein. Let us define $\mathscr{C}$ a set of clusters $\{C_i, i = 1, \ldots, n_c\}$ and the so-called metric *inertia* derived by:

$$\mathscr{I}(\boldsymbol{X}, \mathscr{C}) = \sum_{i=1}^{n_c} \sum_{X \in C_i} \|\boldsymbol{x} - \mu_i\|_2^2, \tag{2.66}$$

where μ_i is the centre of cluster C_i. Inertia is a measure of the points concentration around the centre of the cluster they belong to.

Consequently, in order to define the best cluster, i.e. to minimise the distance between a point and the centre of its cluster, the following optimisation problem is solved:

$$\underset{\mathscr{C}}{\operatorname{argmin}} \sum_{i=1}^{n_c} \sum_{X \in C_i} \|\boldsymbol{x} - \mu_i\|_2^2. \tag{2.67}$$

Given a number of clusters n_c, the steps to solve this optimisation problem are:

1. Initialise the centres of the clusters $[\mu_i, i = 1, \ldots, n_c]$;

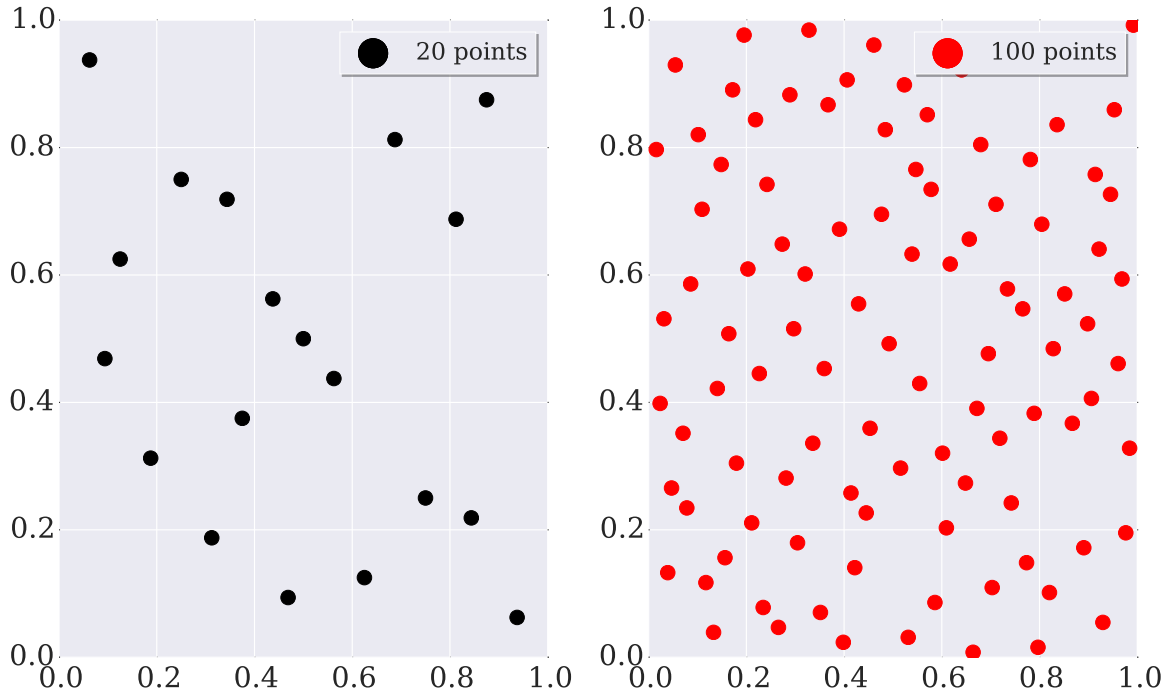

Figure 2.12 – Sobol sequence realisations in two dimensions.

2. Attribute each point corresponding to the closest cluster such that

$$\left\{l : \|\boldsymbol{x}_l - \mu_i\| < \|\boldsymbol{x}_l - \mu_j\| \forall i \neq j, l = 1, \ldots, N\right\}; \tag{2.68}$$

3. Compute the mean of each cluster as the mean of all the points belonging to it:

$$\mu_i = \frac{1}{\text{Card}\,(C_i)} \sum_{j \in C_i} \boldsymbol{x}_j, \quad i = 1, \ldots, n_c; \tag{2.69}$$

4. Repeat step 2 and 3 until convergence. The convergence criterion could be fixed by a limited iteration number or/and by a threshold for a minimum increase of the inertia.

The optimisation problem may have multiple local solutions, consequently the k-means algorithm shall be run with multiple seeds for the clusters' centres.

An example of a K-mean clustering with 20 clusters identified from a Sobol sequence with 1000 points is given Figure 2.13. The distribution of the inspection points appears to be much more appropriate compared to the Halton and Sobol sequences with the same number of measurement locations as Figure 2.14 illustrates. The maximum of the minimum distance between each point of the sequences shown in Table 2.1 confirms this point since the maxi-min criterion of the K-means is 24% lower than the same criterion computed for the Halton sequence.

However like the Hammerslay sequence, a set of points obtained through the K-means algorithm cannot be augmented (i.e. increasing the number of clusters) without running again the K-means algorithm.

Sequence	*maxi-min distance*
Halton	1.31
Sobol	1.59
K-means	0.99

Table 2.1 – Maximum of the minimum distance between each point of the sequence

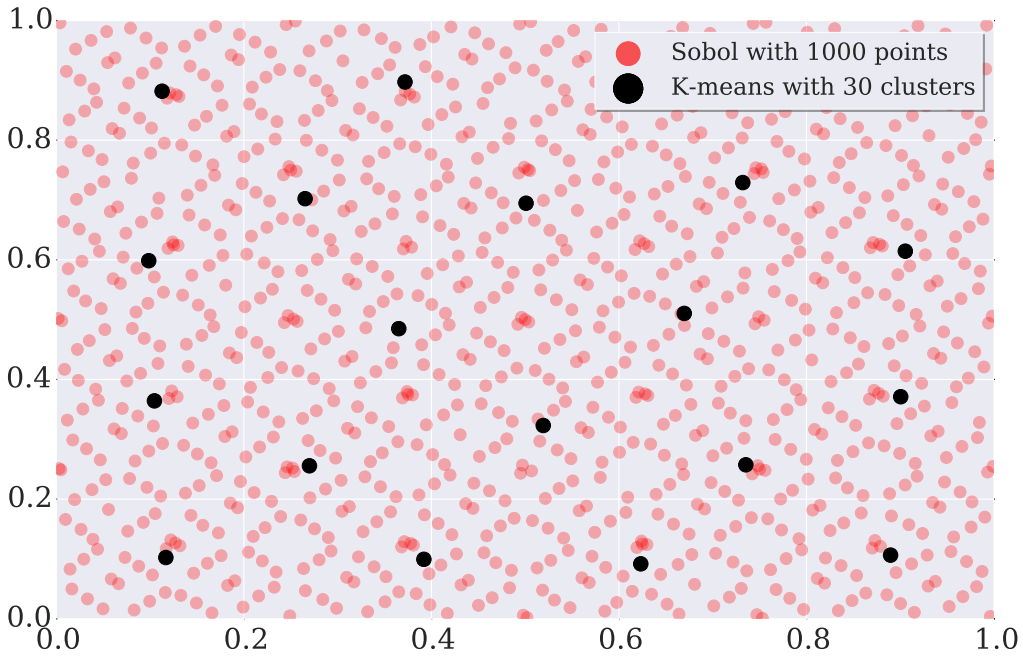

Figure 2.13 – Space-filling with K-means algorithm used on a Sobol sequence.

2.4.2.2 Adaptive Design of Experiment

If an efficient way to predict the degradation is available, it would seem evident to head for the area *where* the degradation predictions are high. In this case the space-filling properties of the low-discrepancy sequences would lose their attractiveness.

However, only considering degraded area would put the stakeholder at risk to:

- Miss an area of interest due to a bias of the predictive model;
- Overestimate the degradation index by missing a poorly degraded area when interpolating the process between two maximums.

In addition, combining this information with the autocorrelation structure of the degradation random field gives another tip on the minimum distance to put between two inspected points. Intuitively if two points of a structure appear to be very correlated, there will not be

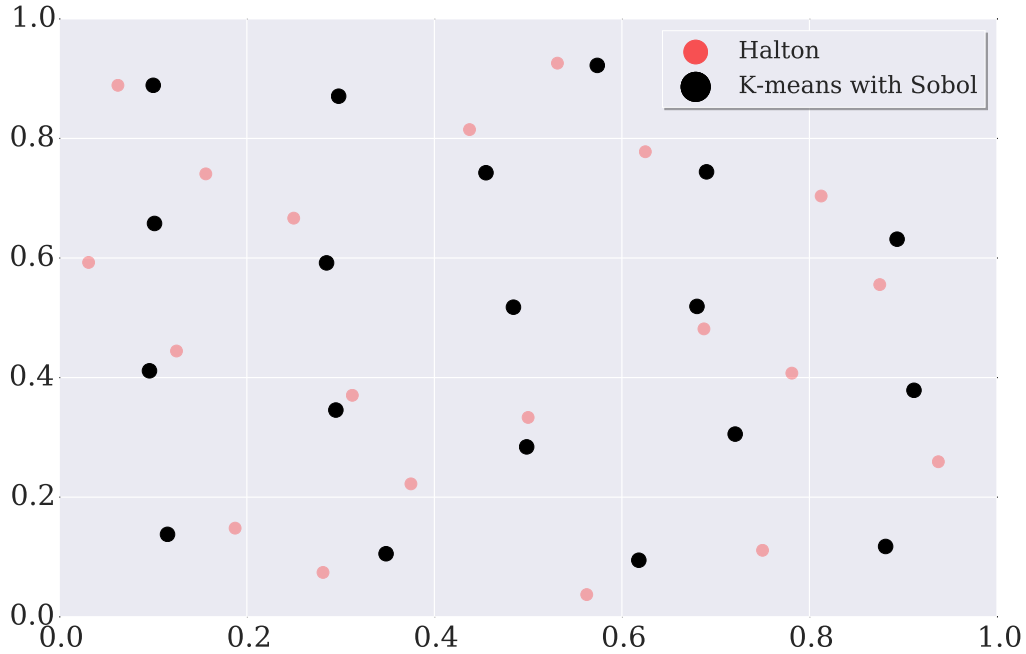

(a)

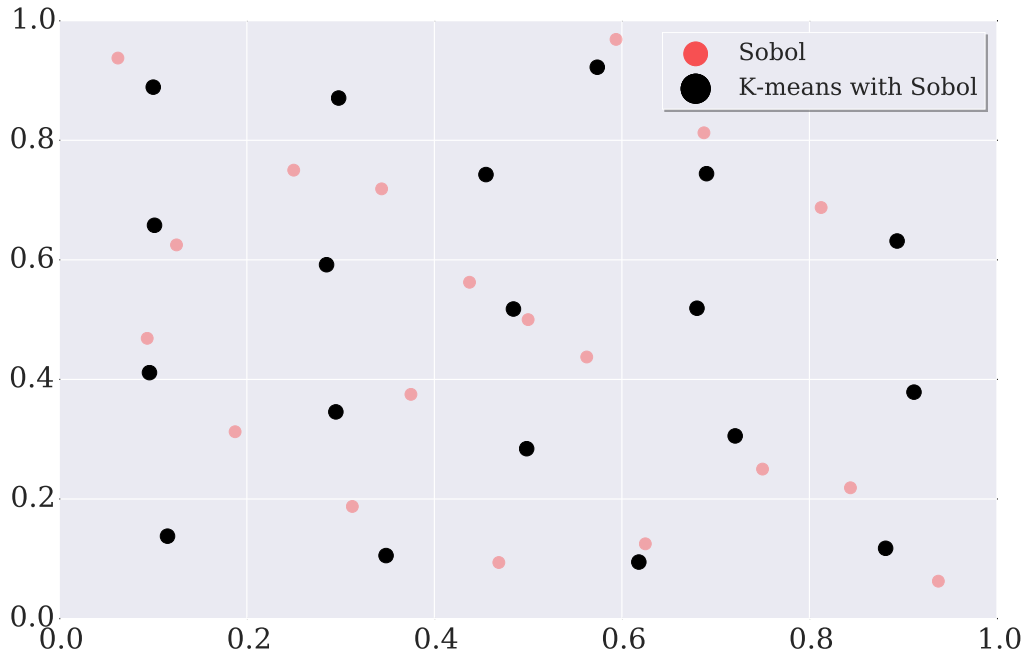

(b)

Figure 2.14 – Space-filling wih K-menas algorithm used on a Sobol sequence compared to the Halton (a) and Sobol (b). All sequences have 30 points.

any advantage to inspect both points. On the opposite, to improve the statistical knowledge on the degradation process the inspections should be as independent as possible.

On this purpose, Schoefs et al. (2015) have studied the effect of the inspection distance threshold on the estimate of the two first moments (namely the mean and the standard deviation, see Section 2.3.2) of a stationary random process, and they concluded that for $R(x,x') \leq 0.3$ the inspection points can be assumed independent.

Consequently, given a degradation random field $X(x,\omega)$, $x \in D_X \subset \mathbb{R}^n$ the design of experiments (DoE) described herein proposes to:

- Allocate s_{high} of the inspected points $\left[x_{insp}^{(i)}, i = 1,\ldots,n_{insp_m}\right]$ in the highly degraded locations reading
$$\underset{x}{\text{argmax}}\, \mathscr{Q}_X(x), \tag{2.70}$$
with $\mathscr{Q}_X(x)$ being the 95% quantile of the degradation at location x denoted by $P\left(X(x) \leq \mathscr{Q}_X(x)\right) = 0.95$;
- Distribute the $1-s_{high}$ of allowed inspected points in the poorly degraded parts of the structures defined by:
$$\underset{x_{insp}}{\text{argmin}}\, \mathscr{Q}_X(x_{insp}); \tag{2.71}$$
- Add the points located on the corners of the domain to ensure that the whole domain is being considered;
- Interpolate the trajectories between the inspected points to estimate the degradation index (see Eq. (2.54)).

provided that $\nexists x_{insp}^{(i)}, x_{insp}^{(j)} \diagup R\left(x_{insp}^{(i)}, x_{insp}^{(j)}\right) < 0.3, i \neq j, (i,j) = 1,\ldots n_{insp} \leq n_{insp_m}$. It is clear that a number of points $n_{insp} \leq n_{insp_m}$ could verify this constraint and thus the DoE may contain less inspected points than the maximum affordable.

Example 2.4.1. *Let us consider a RC beam 5 metres long being submitted to a non-stationary carbonation random field derived with the DuraCrete model (see Eq. (1.1)). The autocorrelation of the process, the quantile $\mathscr{Q}_{X_c}(x)$ of the carbonation and a subset of the 10,000 simulated trajectories are given in Figures 2.15 and 2.16, respectively.*

In Figure 2.15, a pearson correlation lower than 0.3 corresponds approximately to the points in the green and blue areas on the horizontal or vertical axes. The corresponding length is approximately ranging from 1 metre to 1.5 metres. Considering that 20 measures can be done, with $s_{high} = 0.5$, the corresponding DoE is represented with red dots on Figure 2.16. In this case, the number of inspected points is much lower than the maximum allowed (7 for 20).

Considering the percentage of concrete carbonated up to the reinforcements as the degradation index given in Eq. (2.54) together with a concrete cover of 2 centimetres (i.e. failure is not considered) the effect of the DoE is illustrated in Figure 2.17. The coloured area corresponds with the length of carbonation depth higher than the threshold, the degradation index being the proportion of this area's width in front of the domain size. On the left, this degradation

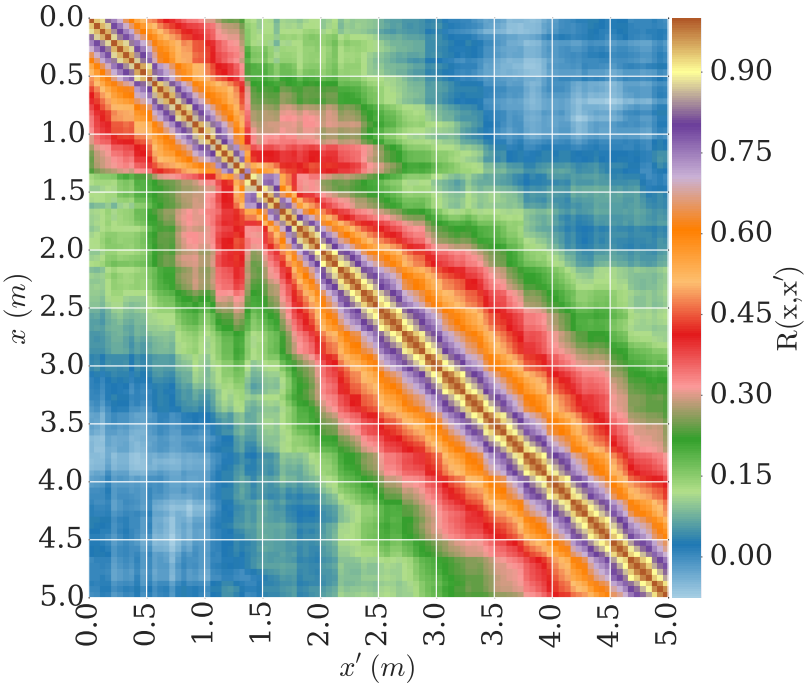

Figure 2.15 – Non-stationary autocorrelation matrix

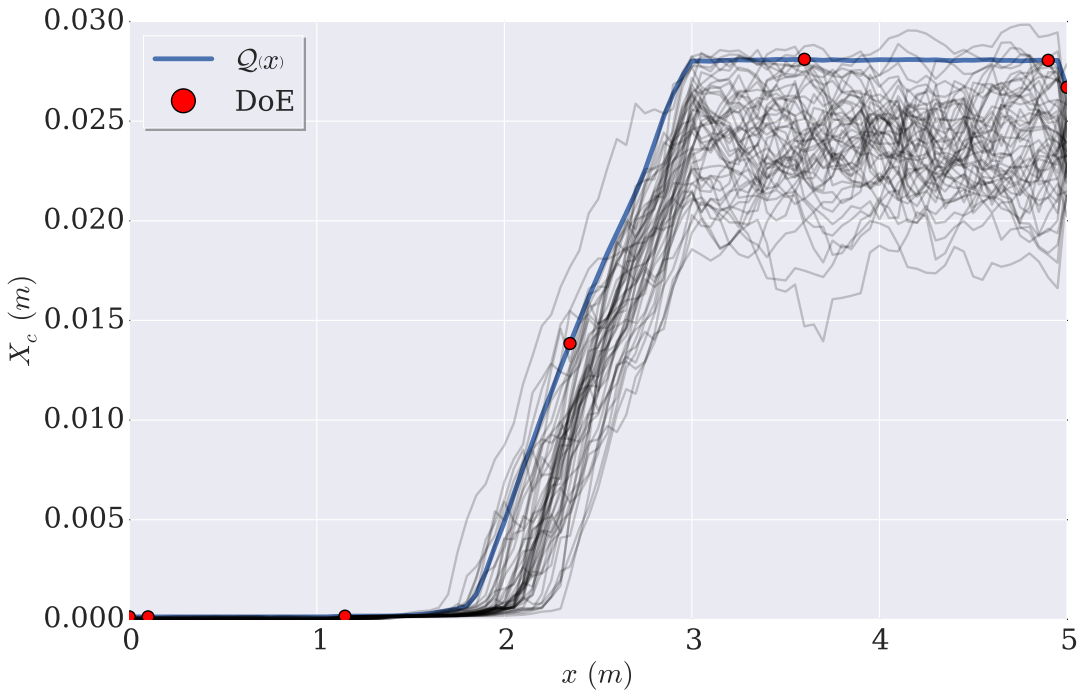

Figure 2.16 – $\mathcal{Q}_{X_c}(x)$ in blue, the red dots are the points identified by the DoE. Grey lines are examples of trajectories.

index is estimated using the trajectory while on the right, it is derived from the approximate of the process. The benefice in looking into the poorly degraded area is evident, without the second, third and fourth points (starting from the left), the approximate would not grasp the sudden increase of the trajectory therefore the degradation index could be quite overestimated. The probability $\hat{\mathscr{P}}_{act}$ is finally estimated considering all the trajectories one by one.

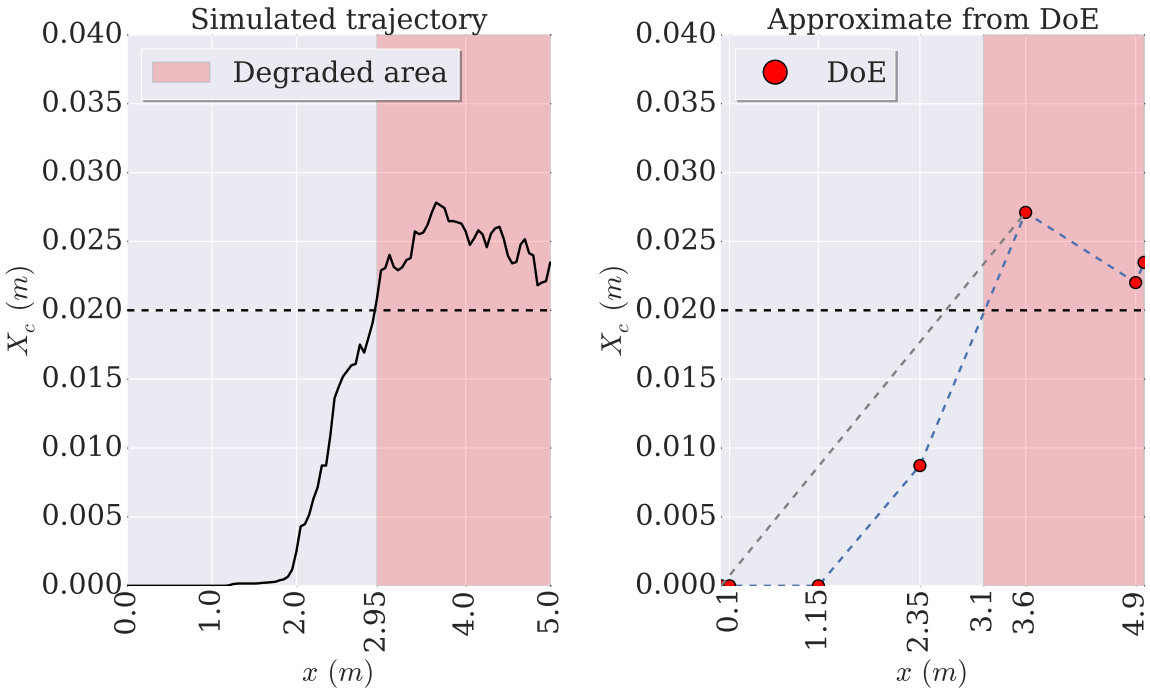

Figure 2.17 – Illustration of the approximation resulting from the DoE on one trajectory.

As pointed out in Section 2.4.2, the DoE shall allow to derive a good approximate $\hat{\mathscr{P}}_{act}$ of the probability for the degradation index to be higher than the corresponding threshold, identified with the degradation predictions. Until now, the proposed methodology to build the DoE does not ensure that this approximate will be efficient. For instance, the DoE shown in Figure 2.17 tends to underestimate the degradation index on the illustrative trajectory. This is the purpose of the forthcoming *adaptive design of experiments* (ADoE).

Referring to Eq. (2.55), to derive a good approximate of the action probability means that good approximates of the probability of failure and the probability of maintenance have to be derived at the same time.

Let us define the criterion $I(x)$ which quantifies the quality of the approximation such as

$$I(x) = \epsilon_{\mathscr{T}}(x), \tag{2.72}$$

with $\epsilon_{\mathscr{T}}(x) = \max\left(\mathscr{T}(x) - \hat{\mathscr{T}}(x)\right) - \min\left(\mathscr{T}(x) - \hat{\mathscr{T}}(x)\right)$ where $\mathscr{T}(x)$ is the vector of the

degradation trajectories at location x and $\hat{\mathscr{T}}(x)$ the corresponding approximate resulting from the DoE. Let define the generic accuracy $\epsilon_{\mathscr{P}}$ reading

$$\epsilon_{\mathscr{P}} = \frac{\left|\hat{\mathscr{P}} - \mathscr{P}\right|}{\mathscr{P}}, \tag{2.73}$$

where the probabilities $\mathscr{P}$ and $\hat{\mathscr{P}}$ are respectively set to

- $\mathscr{P}_f$ and $\hat{\mathscr{P}}_f$ for the failure event, the accuracy thus being denoted by $\epsilon_{\mathscr{P}_f}$;
- $\mathscr{P}_{Ma}$ and $\hat{\mathscr{P}}_{Ma}$ for the maintenance event, the corresponding accuracy reading $\epsilon_{\mathscr{P}_{Ma}}$.

The ADoE first helps to improve the estimate of the failure probability by adding to the inspected points the solution of:

$$\underset{x}{\operatorname{argmax}}\, I(x), \tag{2.74}$$

given that this point helps in decreasing $\epsilon_{\mathscr{P}}$.

Solutions of Eq. (2.74) are found and added to the inspected points until $\epsilon_{\mathscr{P}_f} \leq \epsilon_{\mathscr{P}_{f\,lim}}$, and in a second step until $\epsilon_{\mathscr{P}_{Ma}} \leq \epsilon_{\mathscr{P}_{Malim}}$ and verifying that $n_{insp} \leq n_{insp_m}$ at the end of the two steps.

The ordering of the steps indeed has an importance. Referring to Eq. (2.53) the probability of maintenance is conditioned by the complementary of the failure probability and as such requires a good approximate of the failure probability.

Example 2.4.2. *Resuming Example 2.4.1, let denote* $\epsilon_{\mathscr{P}_{Malim}} = 0.05$ *and the threshold for the degraded proportion of the beam* $d_c = 0.5$ *(i.e. half of the beam is violating the degradation threshold). The error* $\epsilon_{\mathscr{P}_{Ma}}$ *on the probability of repairing due to the approximation made by the DoE is up to* 91% *(see Table 2.2).*

The DoE alone largely underestimates the probability $\mathscr{P}_{Ma}$ *as it could have been expected (see Figure 2.17). Indeed Figure 2.18 shows that the simulated trajectories tends to be underestimated from 2.5 metres to the top of the RC beam, where the degradation predictions are the highest according to Figure 2.16.*

Using the ADoE methodology described above, this error comes down to 3% *with three locations added to the inspected points shown in Figure 2.19. All of them are located in the area where the degradation predictions are high. Indeed, further increasing the accuracy in the poorly degraded area obviously does not help to improve the accuracy of the probability estimate as the probability of maintenance is underestimated. Finally, one may notice that the highest point of the criterion* $I(x)$ *is not the first one to be added. Again, through Figure 2.18 the first most needed point appears to be in the region where nearly all the trajectories are underestimated.*

It proves the usefulness of completing the DoE with the criterion $I(x)$ *(see Eq. (2.74)) given that it helps in decreasing* $\epsilon_{\mathscr{P}_{Ma}}$.

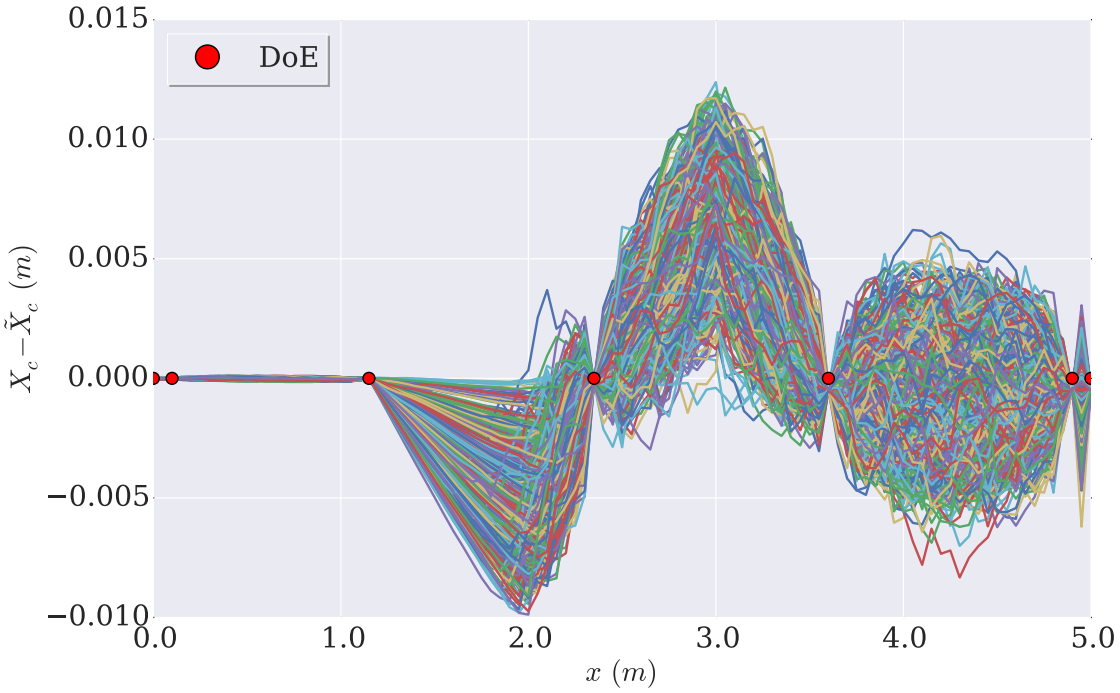

Figure 2.18 – Approximate error made by the DoE on each trajectory.

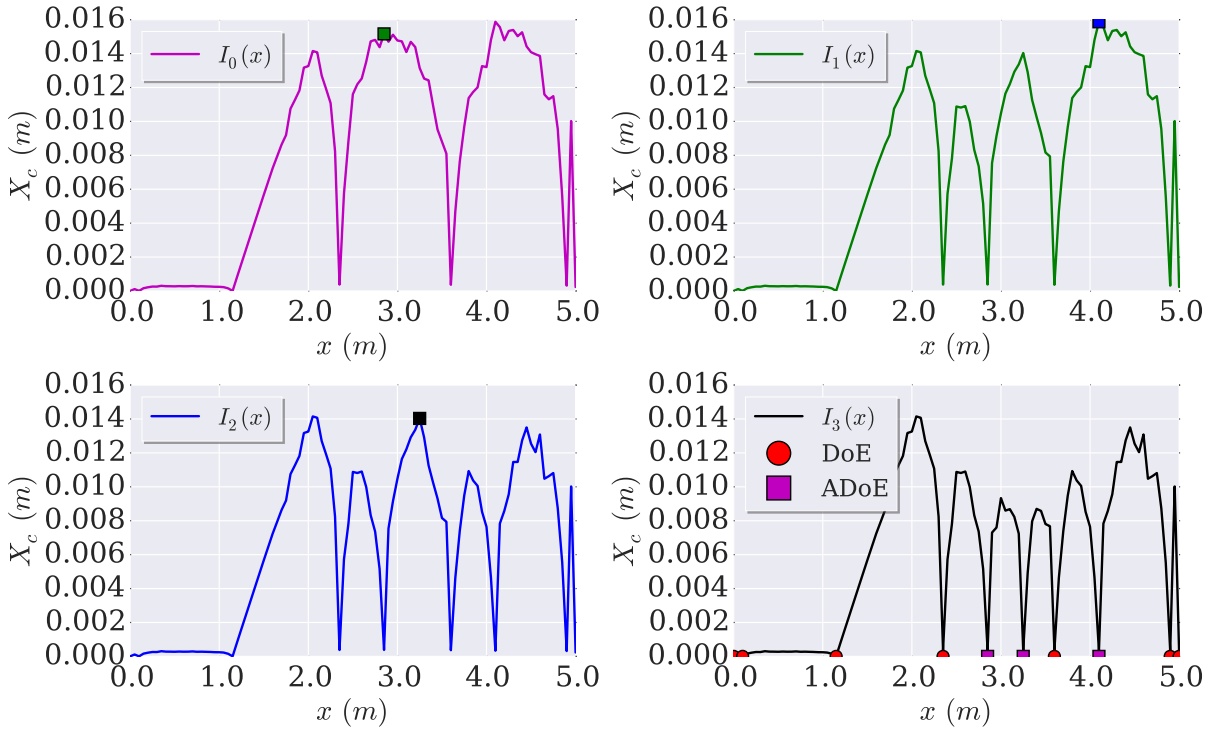

Figure 2.19 – Illustration of the criterion $I(x)$, and the position of the points successively added by the ADoE to the inspected locations with respect to Eq. (2.74).

	DoE	*ADoE*
$\mathscr{P}_{Ma}$	6.3×10^{-1}	6.3×10^{-1}
$\hat{\mathscr{P}}_{Ma}$	0.51×10^{-1}	6.2×10^{-1}
$\epsilon_{\mathscr{P}_{Ma}}$	91%	3%
n_{insp}	7	10

Table 2.2 – Evolution of $\epsilon_{\mathscr{P}}$ with the ADoE which adds three points to achieve $\epsilon_{\mathscr{P}} \leq \epsilon_{\mathscr{P}_{lim}}$.

Up to now, the ADoE has assumed that if the predicted trajectory was real, an inspection would return the real value of this trajectory at the point considered. In other words, inspection is assumed to be perfect. Reminding that:

- The probability of detection function PoD may not have been derived for every inspection method;
- Even though, assuming that the inspections are independent in order to combine the PoD of different inspected points would be hard to prove;
- The most basic information of the inspection error is the standard deviation of the measure resulting from its repetition;

The author chose to model the inspection error with a confidence interval around the observed value. Let define $\left\{y_{obs}^{(i)}, i = 1, \ldots, n_{insp}\right\}$ the observations vector of the variable of interest y. With the standard deviations $\left\{\sigma_{y_{obs}^{(i)}}, i = 1, \ldots, n_{insp}\right\}$ known, one can compute a confidence interval at 95% by

$$CI_{95\%}\left(\boldsymbol{y}_{obs}\right) = \left\{\boldsymbol{y}_{obs} \pm 1.96 * \boldsymbol{\sigma}_{y_{obs}}\right\}, \tag{2.75}$$

assuming the measurement error is unbiased and normally distributed. This confidence interval could be computed knowing the bias, or either the distribution of the measurement error. In other words, approximately all the inspection models for the measurement error can be reduced to confidence intervals, this way the methodology becomes nearly independent of the inspection method.

By successively considering the upper and lower bounds of $CI_{95\%}\left(\boldsymbol{y}_{obs}\right)$ as the result of the inspections (i.e. all the measurements overestimate the degradation, respectively underestimate), two bounds of the corresponding approximate $\hat{\mathscr{P}}_{act}$ can be derived. Consequently, the greater the inspection error, the greater the uncertainties on $\hat{\mathscr{P}}_{act}$, thus on the probabilities of maintenance and failure.

The notion of confidence interval *may seem improper. Indeed, the* mean *probability of a branch may be outside the bounds defined as a confidence interval. Overestimating the degradation may lead from maintenance action to repair, while in the same time underestimating may lead to no action being performed. Both probabilities of going into a maintenance branch would be decreased, thus leading the* mean *probability to be outside these bounds. In the following, the bound denoted* $95\%CI^{+}$*, resp.* $95\%CI^{-}$*, refers to the bound obtained while overestimating, resp. underestimating, the degradation process.*

Example 2.4.3. *To conclude Example 2.4.1 and Example 2.4.2, let us consider that the inspection method has an error normally distributed with 0 mean and a standard deviation of 2.5 millimetres.*

Figure 2.20 presents both the modification of the approximate which includes the inspection points added by the adaptive part of the methodology and the confidence interval resulting from the standard deviation of the inspection technique.

Finally Table 2.3 contains the confidence interval of $\hat{\mathscr{P}}_{Ma}$ *which clearly denotes the impact of the measurement error, despite its standard deviation could have seemed insignificant at first.*

$\hat{\mathscr{P}}_{Ma}$	$CI_{95\%}\left(\hat{\mathscr{P}}_{Ma}\right)$
6.3×10^{-1}	$\left[0.2 \times 10^{-1}; 9.9 \times 10^{-1}\right]$

Table 2.3 – Confidence interval for the probability of maintenance.

The following section presents the two silver thread examples which are used throughout this manuscript, the IMRM described in Section 2.4.1 applied on them in this chapter.

The maintenance and failure models have not been described here since they are both very specific to the stakeholder habits and to the considered structure. Consequently they will be introduced straight after together with each example.

2.5 Illustrations : balconies of a building

2.5.1 Description

The example is inspired from the management of balconies in a housing in Marseille (France) exposed in Figure 2.21.

2.5.1.1 Different cases

On purpose of demonstrating the capabilities of the ADoE, and latter in this manuscript of the optimisation methodology, three cases are considered:

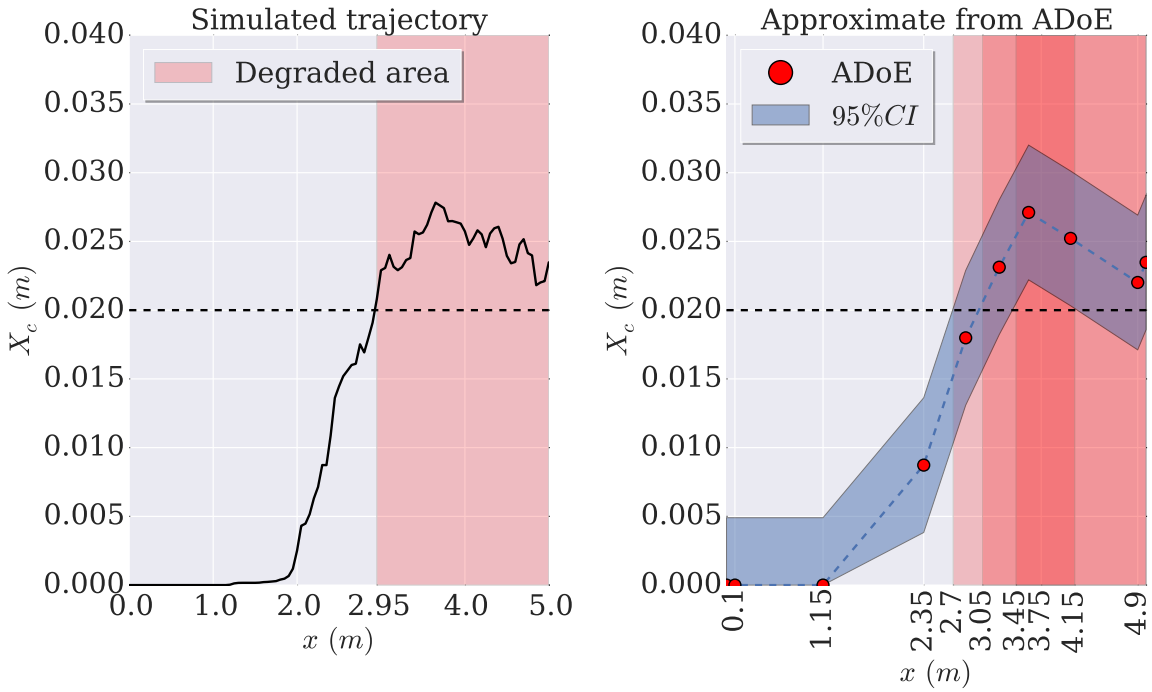

Figure 2.20 – Illustration of the approximation resulting from the ADoE on one trajectory. The blue area corresponds with the confidence interval resulting from the measurement errors. Three superimposed degraded areas result from this consideration.

1. One-dimensional case : A balcony is approximated by a simple line which means that its width is neglected. In this example we will consider a building with 120 balconies and 10 percents of them are inspected;

2. Bi-dimensional case : A balcony is modelled as a rectangle, in order to take into account the variation of concrete cover thickness along the width of a balcony, for water evacuation purpose. Again, a building with 120 balconies and 12 balconies inspected is considered;

3. System bi-dimensional case : in this illustration the balcony modelling is the same as in the bi-dimensional case. However it considers 12 buildings, each of them with 120 balconies, where only 1 balcony per building is inspected.

These three examples shall demonstrate the capacity of the developed methodology to deal with:

- Stationary and non-stationary processes;
- One and Bi-dimensional models;
- Components and system approaches.

2.5.1.2 Degradation modelling

A surrogate vectorial gaussian process has been identified from 149 independent simulations of a carbonation finite elements model modelling a 10cm concrete cover (de Larrard et al. (2014)) with the random variables listed in Table 2.4 and with humidity and temperature official measurements made over the last 50 years in Marseille. For more details on the surrogate modelling procedure, the interested reader is referred to Dubourg (2011, Chapter 1).

Random variable	*Designation*	*Probabilistic distribution*
CH_0	Initial portlandite quantity (mol/m^3)	$LN(\mu = 2519, \frac{\sigma}{\mu} = 10\%)$
ϕ	Concrete porosity (%)	$LN(\mu = 11.8, \frac{\sigma}{\mu} = 15\%)$
K_0	Inherent permeability (m^2)	$LN(\mu = 2.45 \times 10^{-17}, \frac{\sigma}{\mu} = 25\%)$

Table 2.4 – Random variables used as input for the finite elements model of carbonation (de Larrard et al. (2014)). $LN(\bullet)$ denotes the log-normal probabilistic distribution.

Using the fractile autocorrelation function based on the Matérn function reading

$$R(\boldsymbol{x},\boldsymbol{x}') = 2\sin\left[\frac{\pi}{6}\prod_{i=1}^{n}\frac{1}{2^{\nu-1}\Gamma(\nu)}\left(2\sqrt{\nu}\frac{|\boldsymbol{x}'-\boldsymbol{x}|}{0.9}\right)^{\nu}\mathscr{K}\left(\nu,2\sqrt{\nu}\frac{|\boldsymbol{x}'-\boldsymbol{x}|}{0.9}\right)\right], \tag{2.76}$$

with $\mathscr{K}(\nu,x)$ being the modified Bessel function of the second kind and n the spatial dimension, let us define three cross-correlated stationary random fields $CH_0(x,\omega)$, $\phi(x,\omega)$ and

Figure 2.21 – Capture of a housing in Marseille, France.

$K_0(x,\omega)$ with the same marginal probabilistic distributions as the corresponding random variables listed in Table 2.4. The cross-correlation matrix of the random fields writes

$$\mathbf{R}_{cross} = \begin{bmatrix} 1 & -0.85 & -0.70 \\ -0.85 & 1 & 0.70 \\ -0.70 & 0.70 & 1 \end{bmatrix} \begin{matrix} CH_0(x,\omega) \\ \phi(x,\omega) \\ K_0(x,\omega) \end{matrix} \tag{2.77}$$

This correlation matrix has been also used to correlate the inputs of the carbonation finite elements model.

The cross-correlated random fields are simulated with the translation field method (see Section 2.3.5.1) and a KL decomposition with a finite element basis.

In the end, the carbonation random field is computed with the surrogate model of the finite elements model for one balcony with the three random fields previously defined $CH_0(x,\omega)$, $\phi(x,\omega)$ and $K_0(x,\omega)$ as inputs assuming that each balcony is identically exposed to the carbonation process (which implies indentical solar radiation, rain exposition, ...).

2.5.1.2.1 One-dimensional model Each balcony is approximated by a mesh of 100 linear elements, the length L_t of a balcony assumed equal to 3 meters.

Some trajectories of the inputs of the degradation model are provided in Figure 2.22 with the evaluation of their autocorrelation function which perfectly matches the input function given in Eq. (2.76). The cross correlations derived with the translation field are also given in Eq. (2.78).

$$\hat{\mathbf{R}}^{(1D)}_{cross} = \begin{bmatrix} 1 & -0.83 & -0.68 \\ -0.83 & 1 & 0.69 \\ -0.68 & 0.69 & 1 \end{bmatrix} \begin{matrix} \hat{CH}_0(x,\omega) \\ \hat{\phi}(x,\omega) \\ \hat{K}_0(x,\omega) \end{matrix} \tag{2.78}$$

The conclusions made in Section 2.3.5.1 on the use of the fractile correlation together with the translation field method for cross-correlated random fields are confirmed by this example.

The predictions resulting from these inputs are illustrated in Figure 2.23. On the right panel, the process appears to be non-monotonous. The carbonation depth is close to 10cm which is the boundary of the finite elements model used to evaluate the surrogate model. This behaviour indeed is unrealistic however since it appears far from any realistic concrete cover thickness of balconies, it is out of concern.

The correlation structure of the simulated carbonation process is given Figure 2.24. The stationarity is conserved and the distance between two points being correlated at most at 0.3 indicates that the DoE will propose inspection locations distanced by more than 1 metre.

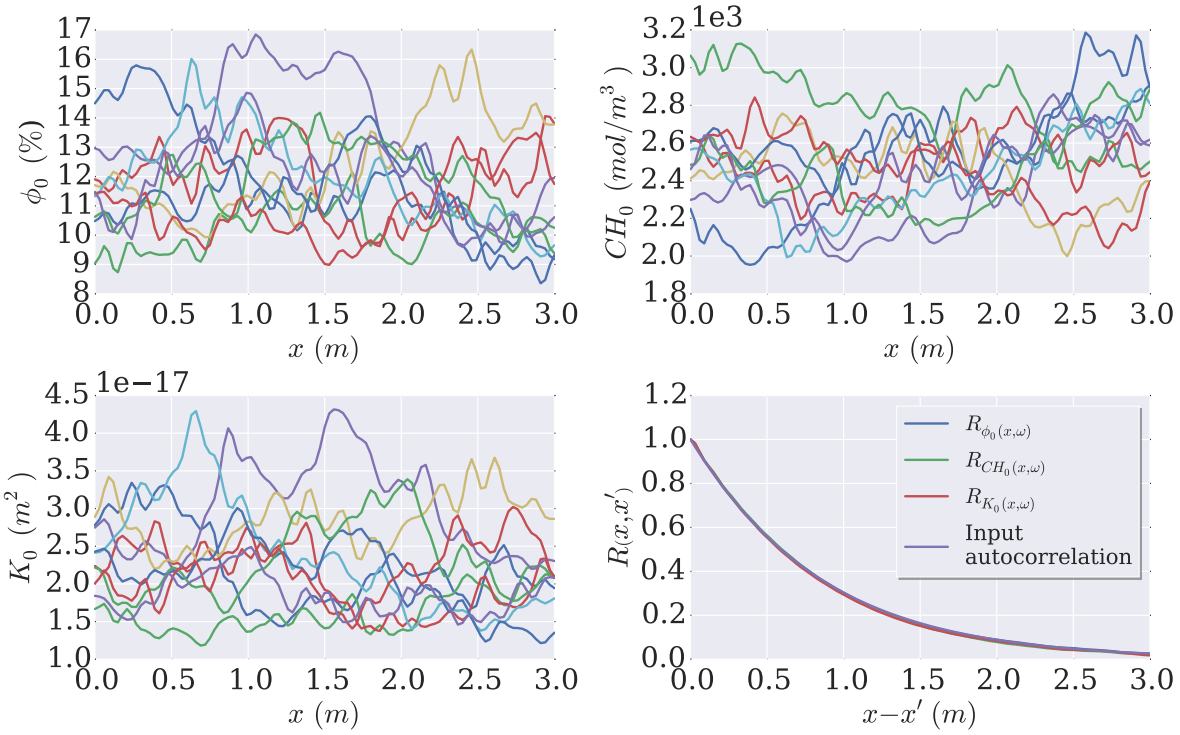

Figure 2.22 – Trajectories of the inputs for the degradation model together with their empirical auto-correlation functions - one dimensional case.

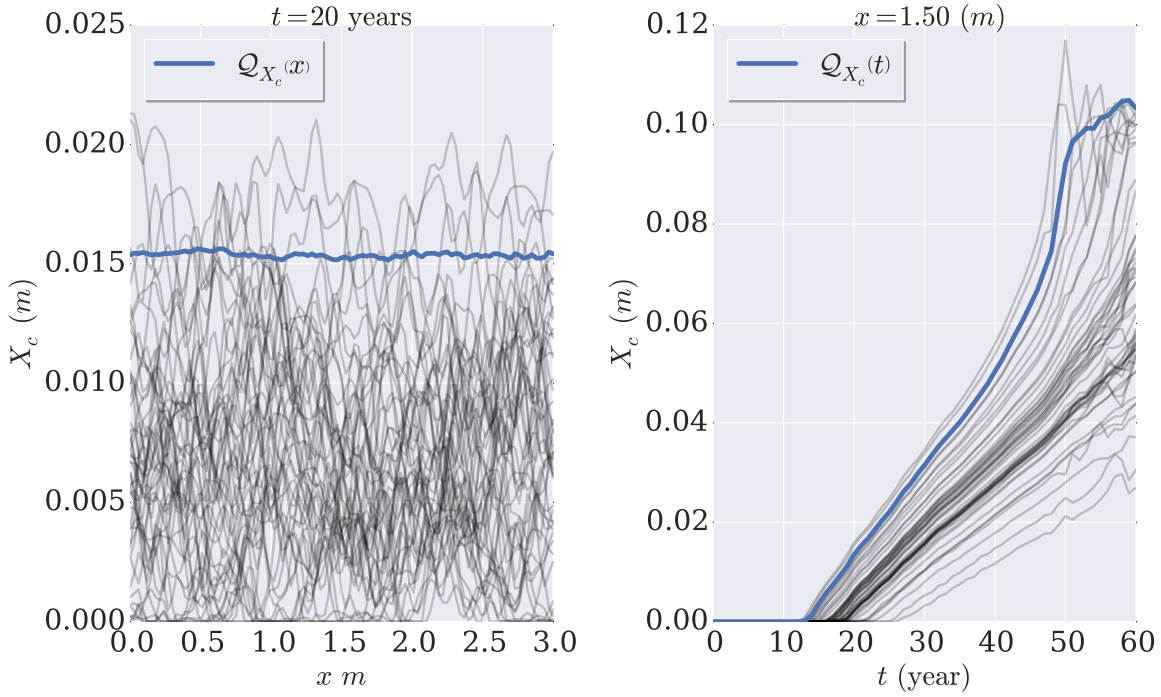

Figure 2.23 – Predictions of the degradation model.

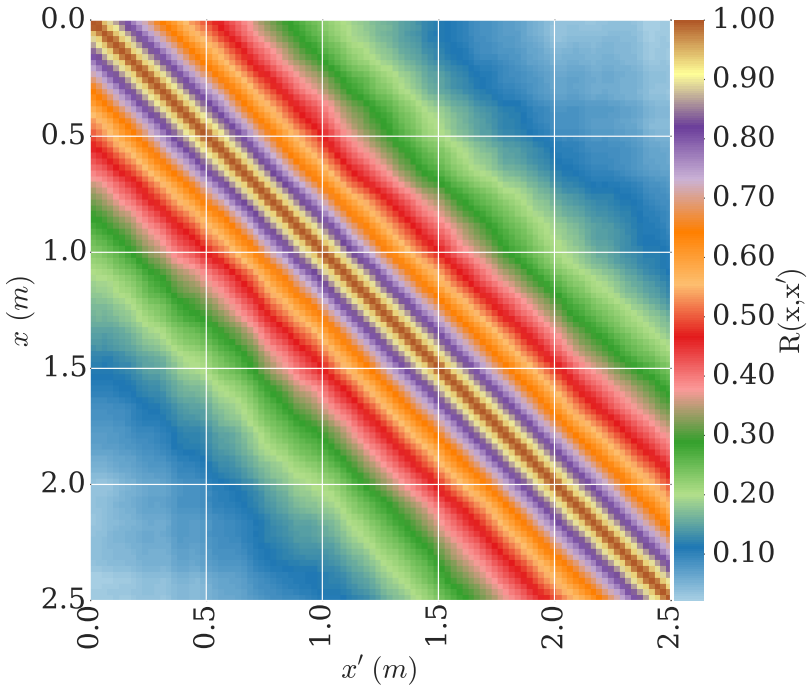

Figure 2.24 – Predictions of the degradation model.

2.5.1.2.2 Bi-dimensional model The mesh of a balcony is composed by 320 triangular elements, the length L_t of a balcony assumed equal to 3 metres and its width l_t equal to 1.2 metres. Assuming that the mesh of the reinforcement is equal to 15cm, each of them is decomposed into two elements.

The classical inspection methods assume the homogeneity of the concrete parameters inside a reinforcement mesh. According to this point, an element value is computed as the mean of its nodel values. A mesh of reinforcement being composed of two elements, the mean of their value is set to be the mesh value.

One trajectory for each input is given in Figure 2.25. For the sake of simplicity, instead of comparing the correlation matrices for multiple inputs by plotting them, e.g. Figure 2.6, Figure 2.26 presents their adequation with the input correlation function (see Eq. (2.76)), i.e. each term of the input matrix is plotted in front of the corresponding estimated term for each input. As such a perfect match is represented by the dashed-line. From Figure 2.26, the adequations therefore appear to be.

$$\hat{\mathbf{R}}_{cross}^{(2D)} = \begin{bmatrix} 1 & -0.83 & -0.68 \\ -0.83 & 1 & 0.70 \\ -0.68 & 0.70 & 1 \end{bmatrix} \begin{matrix} \hat{CH}_0(x,\omega) \\ \hat{\phi}(x,\omega) \\ \hat{K}_0(x,\omega) \end{matrix} \tag{2.79}$$

The conclusions made in Section 2.3.5.1 on the use of the fractile correlation together with the translation field method for cross-correlated random fields are confirmed by this

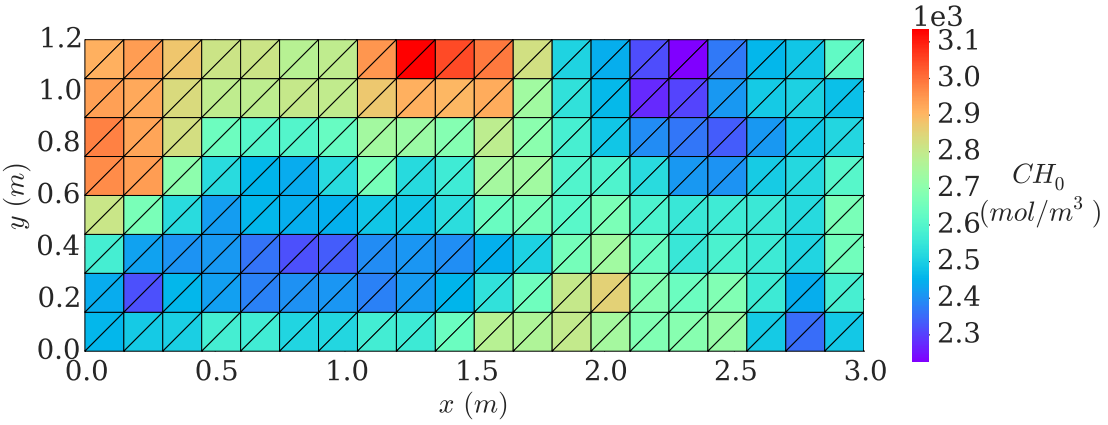

(a) Instance of a trajectory for CH_0.

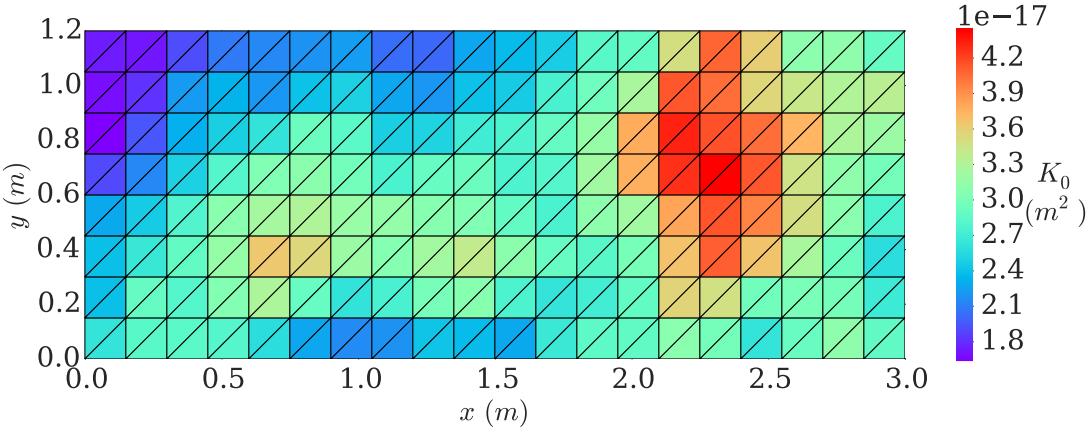

(b) Instance of a trajectory for K_0.

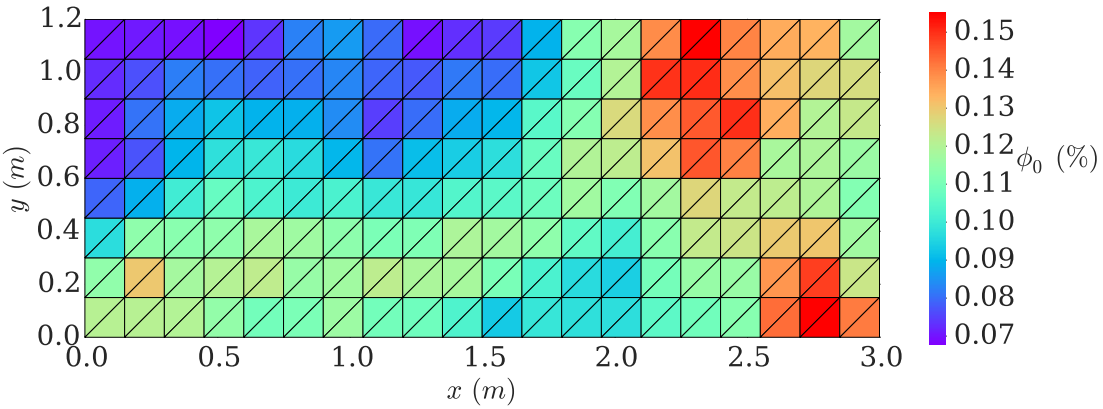

(c) Instance of a trajectory for ϕ_0.

Figure 2.25 – One trajectory for each input of the degradation model. The correlation between the variables is visible.

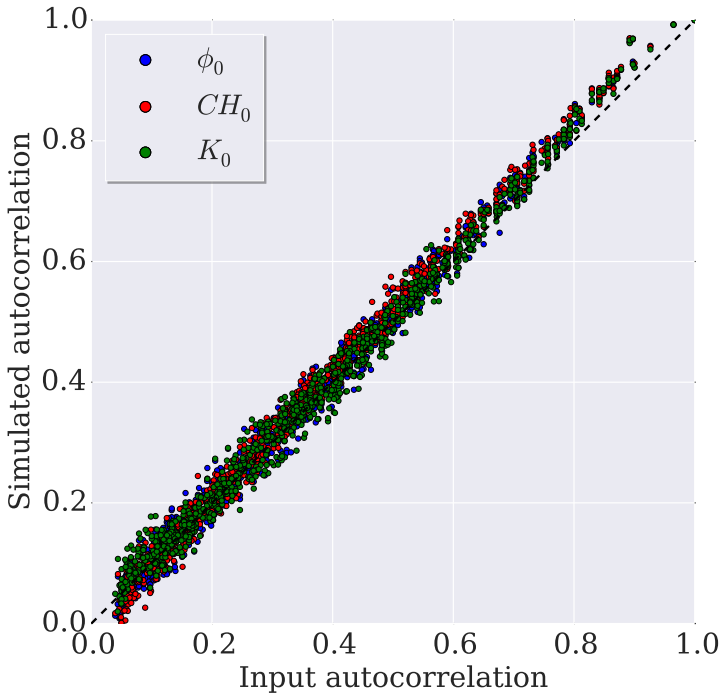

Figure 2.26 – Adequation between the simulated autocorrelation matrices for K_0, CH_0 and ϕ_0 and the input desired autocorrelation.

example.

The resulting predictions of the degradation model are shown in Figure 2.27 after 20 years of carbonation. The quantile indeed has a similar order of magnitude than in the one-dimensional case (see Figure 2.23), around 1.5 centimetres. The representation of the concrete cover thickness is also plotted on Figure 2.27. It is deterministic and decreases linearly from 3 centimetres to 2 centimetres.

2.5.1.3 Inspection, maintenance and failure modelling

2.5.1.3.1 Inspection modelling The inspection error of the method used in this example is denoted by $\epsilon_{insp} \sim N(\mu = 0, \frac{\sigma}{\mu} = 10\%)$, meaning that it is unbiased. The maximum number of inspected points is set to $n_{insp_m} = 20$. Two cases are distinguished:

- The inspected locations are derived with the ADoE. The accuracy bound for the probabilistic degradation index estimate is set to $\epsilon_{\mathscr{P}} = 10\%$ (see Eq. (2.73)) ;
- The inspected locations are derived with a Sobol low-discrepancy sequence, with a length equal to n_{insp_m}.

The time interval between two inspections is successively set to 10 and 20 years. The time horizon being equal to 60 years, consequently 2 and 5 inspections will be performed (i.e. the inspection at the end of the lifetime is not considered).

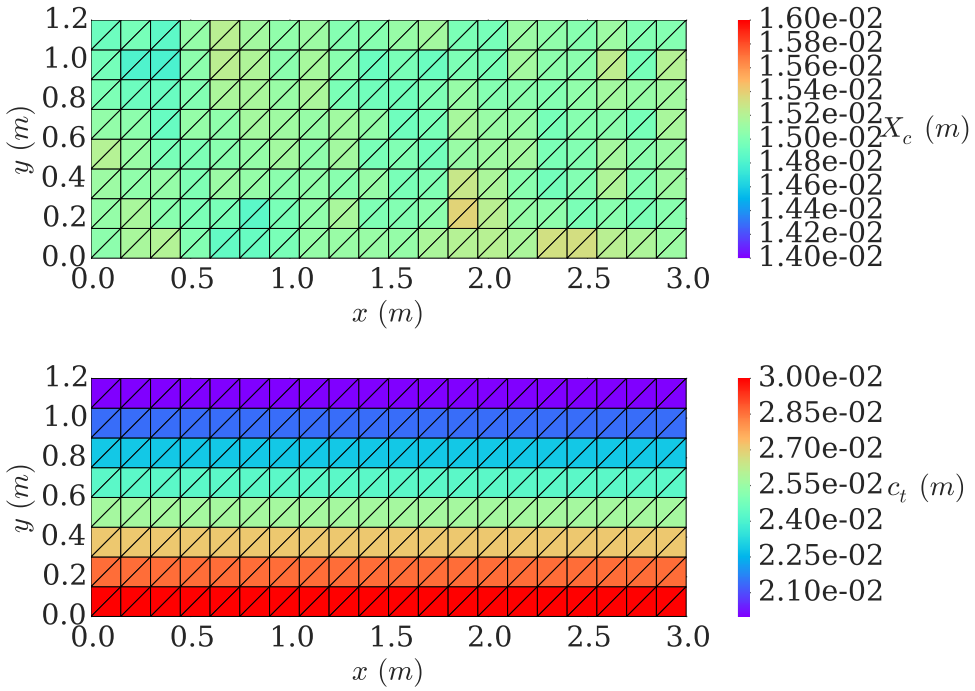

Figure 2.27 – On top, quantile of the degradation model predictions at 20 years. Below is the representation of the concrete cover thickness.

If at an inspection, the probability of action $\mathscr{P}_{act}$ equals 0, which means that neither maintenance nor repair actions are expected, we will consider two cases:

- The inspection is performed
- The inspection is judged useless and thus avoided.

2.5.1.3.2 Failure modelling The failure state assumes that the reinforcements are depassivated. With respect to the considered degradation process (see Section 1.2.1.1), the corresponding degradation index writes

$$D_F = \frac{\left| L_{X_c > c_t} - L_t \right|}{L_t} \tag{2.80}$$

where c_t is the curative threshold.

Due to the local heterogeneity of the concrete (e.g. presence of aggregates) which are not modelled by the degradation processes shown in Section 1.2.1.1, the carbonation depth may be varying around the predicted value. In an attempt to account for this heterogeneity the curative threshold c_t threshold is equal to the concrete cover thickness increased by 0.5 centimetre.

The repair action is triggered if the carbonation depth has reached the reinforcements over $d_c = 25\%$ of a balcony.

2.5.1.3.3 Maintenance modelling For the uni-dimensional case, the maintenance action is triggered if the carbonation depth has been found higher than the preventive threshold $p_t = 1.5cm$ (i.e. half of the concrete cover) over $d_{pm} = 25\%$ of a balcony. It is assumed that after repair the balcony is always back to an *as-good-as-new* state. From Eq. (2.54) we thus derive a preventive degradation index:

$$D_P = \frac{\left| L_{X_c > p_t} - L_t \right|}{L_t} \tag{2.81}$$

Concerning the bi-dimensional case, the maintenance action is triggered if any of the 12 inspected balconies presents a carbonation depth violating the preventive threshold over d_{pm} of a balcony.

However for the system bi-dimensional case (where only one balcony is inspected per building), only 25% of the buildings (i.e. 3 of them) may be repaired at the same time, between two inspections. Moreover, a building cannot be maintained two successive times. In this case, it means that for each IMRM (one per building), the probability of maintenance $\mathscr{P}_{Ma}$ for a given building at a given inspection is rewritten by:

$$\mathscr{P}_{Ma} = \mathscr{P}\left[D >= d_{pm} \mid D < d_c, n_{maint} \leq 3\right], \tag{2.82}$$

where n_{maint} is the number of other building to be maintained.

This conditional probability is hard to evaluate without simulation. Thus to compute the probability of realisation of a IMRM branch (see Figure 2.10), simulations of the IMRM are run in a sufficient number for every building, with the constraint that only one building at a time is able to get in a maintenance branch. At the end, the new probabilities for each branches are re-estimated. An instance of such simulation is given in Figure 2.28 where 3 buildings are considered, each of them being simulated one time, and without allowing more than one maintenance action between two inspection. The simulation gives the third balcony as being maintained, yet the second one is already in such state thus nothing is done on the third balcony. The probabilities of each branch are computed again on the right. Indeed one sample is not enough to correctly estimate these probabilities. On this purpose and throughout this illustration, the tree is simulated 100,000 times.

2.5.2 Evaluation of the life-cyle model

2.5.2.1 One-dimensional problem

Figure 2.29 and Figure 2.30 present the probabilistic distributions of the number of maintenances and inspections for a time interval between two inspections equal to 10 and 20 years, respectively.

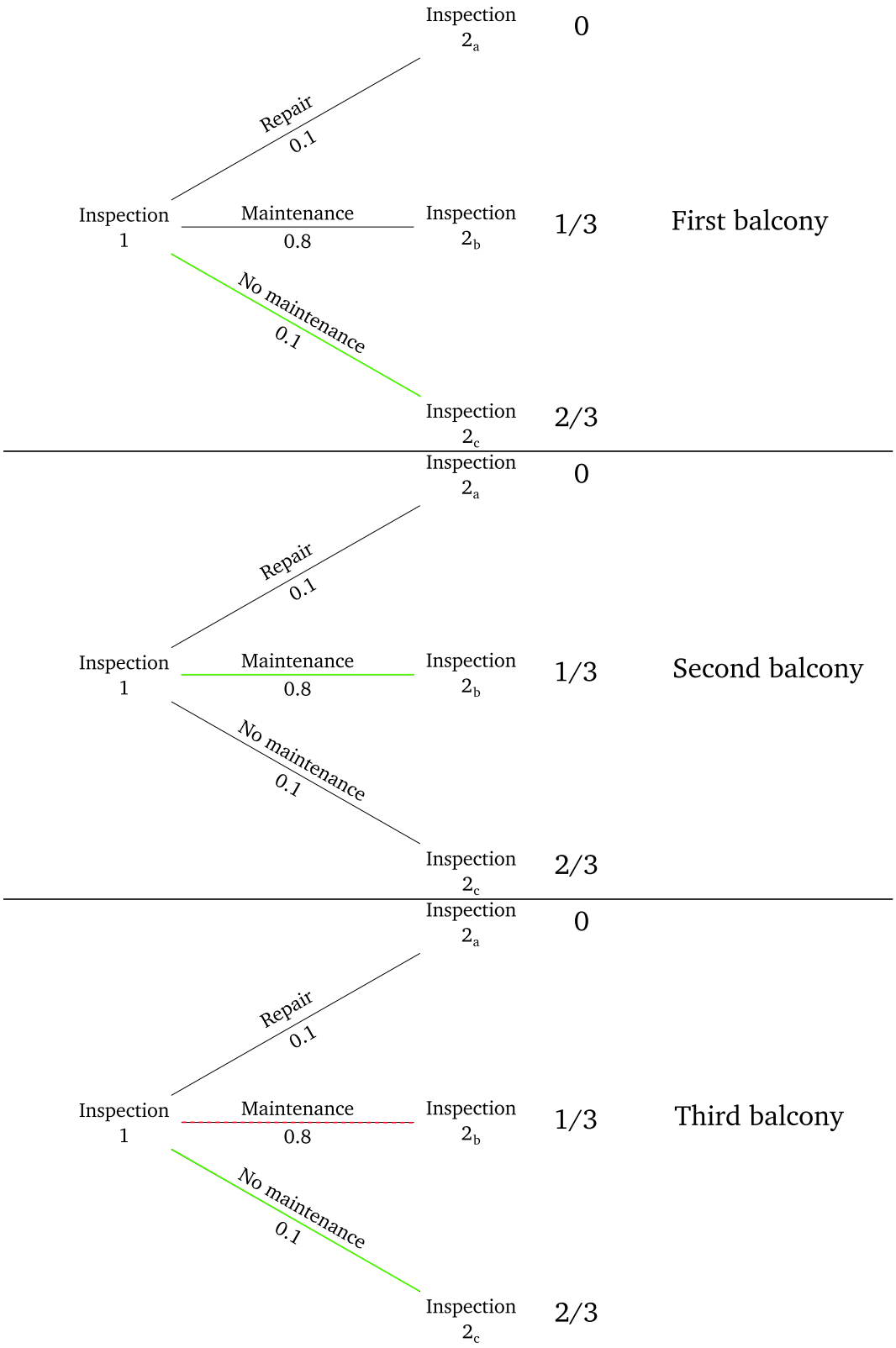

Figure 2.28 – Illustration of the tree simulation with a constraint on the number of simultaneous maintenance. A green line represents the followed path. A dotted red line denotes the effect of the constraint.

The first observation is that the results are equivalent, shall the inspected points be defined with the ADoE or the Sobol low-discrepancy sequence. This point is discussed later on in this section.

When inspecting every 10 years, after 60 years the probability is very high that only one maintenance action is going to be performed. In this case, if the inspections judged as useless are always performed, 5 inspections are made. The probability of repairing 3, 4 or 5 times being null, it means that inspecting 5 times is useless. If the useless inspections are not performed, it is more likely that only 3 inspections will be made, confirming the previous intuition. According to the degradation trajectories shown in Figure 2.23, in 10 years the carbonation process has not been initiated which explains why an inspection every 10 years is useless if the structure has been repaired.

The dispersions presented in Table 2.5 are not significant in this case.

n°	μ_{Ma}	$[CI^-; CI^+]_{Ma}$	μ_F	$[CI^-; CI^+]_F$	*Type*
0	0.04	$[0.05; 0.10]$	0.96	$[0.96; 0.89]$	ADoE
0	0.03	$[0.04; 0.11]$	0.97	$[0.96; 0.88]$	Sobol'
1	0.94	$[0.95; 0.82]$	0.04	$[0.04; 0.11]$	ADoE
1	0.95	$[0.96; 0.80]$	0.03	$[0.04; 0.12]$	Sobol'
2	0.02	$[0; 0.08]$	0	$[0; 0]$	ADoE
2	0.02	$[0; 0.09]$	0	$[0; 0]$	Sobol'
3	0	$[0; 0]$	0	$[0; 0]$	ADoE
3	0	$[0; 0]$	0	$[0; 0]$	Sobol'
4	0	$[0; 0]$	0	$[0; 0]$	ADoE
4	0	$[0; 0]$	0	$[0; 0]$	Sobol'
5	0	$[0; 0]$	0	$[0; 0]$	ADoE
5	0	$[0; 0]$	0	$[0; 0]$	Sobol'

Table 2.5 – Mean and confidence interval of the number of maintenances and repairs with an inspection interval of 10 years.

n°	μ_{Ma}	$[CI^-; CI^+]_{Ma}$	μ_F	$[CI^-; CI^+]_F$	*Type*
0	0.63	$[0.21; 0.84]$	0.37	$[0.79; 0.16]$	ADoE
0	0.65	$[0.21; 0.84]$	0.35	$[0.79; 0.16]$	Sobol'
1	0.37	$[0.79; 0.16]$	0.63	$[0.21; 0.84]$	ADoE
1	0.35	$[0.79; 0.16]$	0.65	$[0.21; 0.84]$	Sobol'
2	0	$[0; 0]$	0	$[0; 0]$	

Table 2.6 – Mean and confidence interval of the number of maintenances and repairs with an inspection interval of 20 years.

When the interval between inspections is set to 20 years, Figure 2.30 shows that the 2 inspections will be made. On these two inspections, it is likely that none of them will lead to a maintenance action. Yet the mean probability and the probability resulting from an underestimation of the degradation process for 1 maintenance performed are not negligible (respectively equal to 0.37 and 0.79, see Table 2.6).

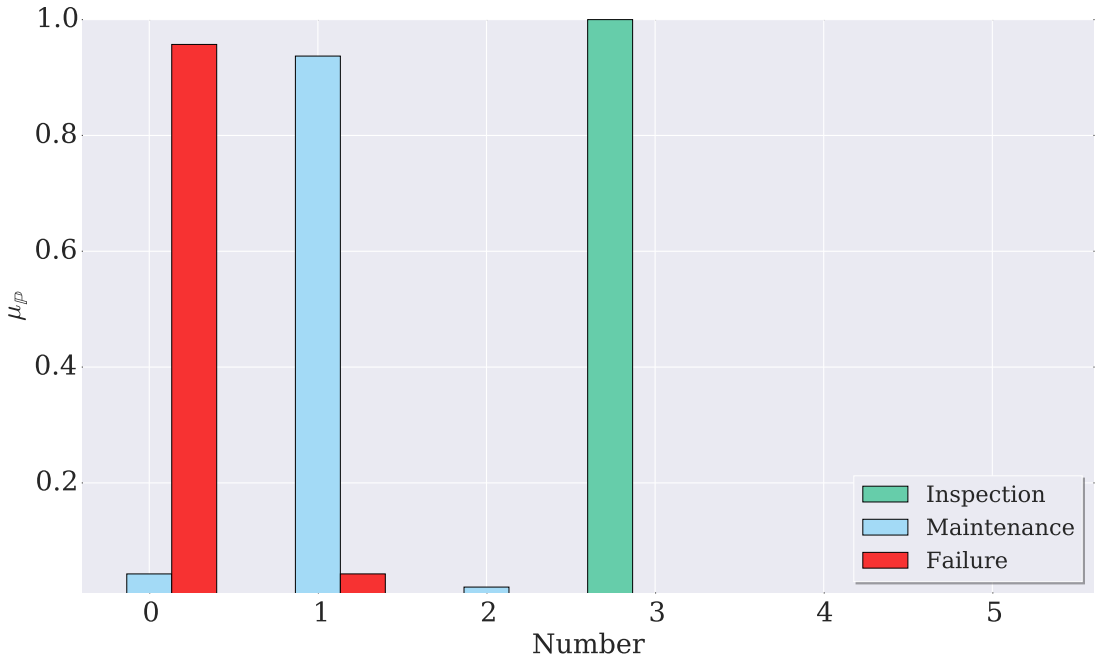

(a) Inspected points designed according to ADoE.

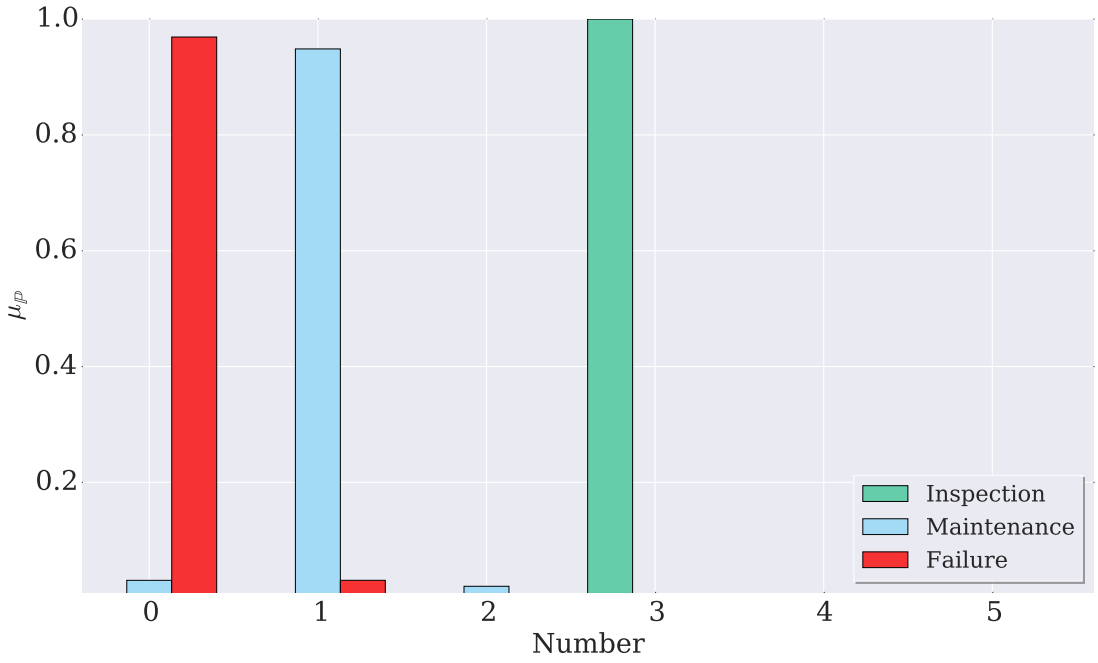

(b) Inspected points designed with a Sobol low-discrepancy sequence.

Figure 2.29 – Probabilistic distributions for the number of maintenances, inspections and repairs with an inspection interval of 10 years.

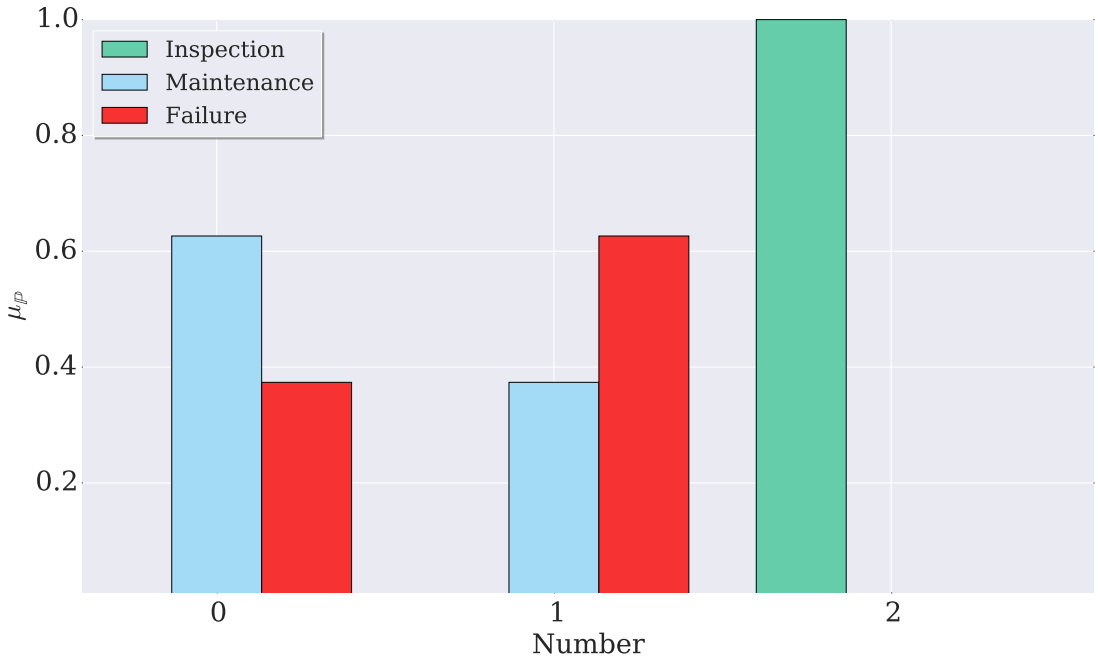

(a) Inspected points designed according to ADoE.

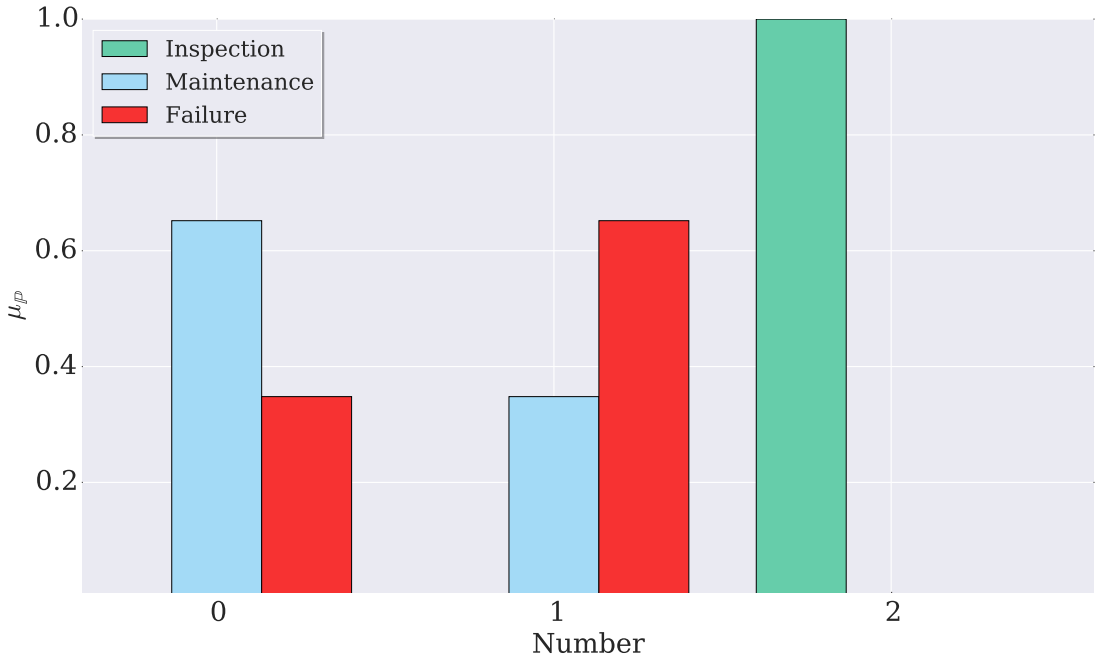

(b) Inspected points designed with a Sobol low-discrepancy sequence.

Figure 2.30 – Probabilistic distributions for the number of maintenances, inspections and repairs with an inspection interval of 20 years.

With the same degradation process, the interval between inspections may lead to no maintenance action being performed. In a sense, it could be interpreted as a better chance to lower the costs. However regarding Figure 2.29 and Figure 2.30 the chances of failure occurring (i.e. corrosion occurs) are indeed higher (from 4 percents with a 10 years interval to 62 percents with the 20 years interval), which may not be an advantage. Moreover in case of an overestimation of the degradation, this probability is increased to 84% (see Table 2.6).

The last point of this illustration of a one-dimensional case is related to the use of the ADoE or a low-discrepancy sequence. We have seen that it has no effect on the estimates presented above. In order to point out the main difference, Figure 2.31 illustrates the Sobol sequence and the ADoE resulting from the first inspection with a time interval between inspections of 20 years. The approximate resulting from these design of experiments is shown on two trajectories extracted from the sample of the degradation predictions at 20 years. As expected, given the stability of the quantile of the carbonation depth (see Figure 2.24) the ADoE only proposes 4 points against 22 for the Sobol sequence (as for the ADoE, the borders have been added to the sequence). For the trajectories shown on the two panels of Figure 2.31, the approximate resulting from the ADoE happens to miss all the pikes of the trajectory, which does not happen with the Sobol sequence. It was to be expected, this is one tricky point of the so-called *stationarity*. Given a lot of trajectories, the predictions are uniform. Yet for one trajectory this is not the case, unfortunately the DoE takes into consideration where the degradation shall be the highest, which is not an information given to this modelling when considering stationary random processes. Moreover, the relatively high correlation length considering the structure's size limits the number of acceptable points. Finally, in this case approximating the trajectories by a few points is enough to get a correct evaluation of the probability of action $\mathscr{P}_{act}$ such that the adaptive part does not add any point.

In other words, in case of stationary random process, the use of a low-discrepancy sequence is to be preferred. Obviously, this is strongly dependent with the maximum number of inspections n_{insp_m}.

2.5.2.2 Two-dimensional problem

For the sake of simplicity, in the following only the results obtained through the ADoE are exposed. The two-dimensional problem uses the same concrete specifications for the predictions of carbonation as the one-dimensional one, the major difference being the concrete cover thickness. This case assumes that it decreases linearly from 3 to 2 cm, for water evacuation purpose. In other words, the degradation is the same, but the cover thickness tends to be lower than in the one-dimensional case.

The results with an inspection interval of 10 years on Figure 2.32 do not show any significant tendency comparing to the similar one-dimensional case shown on Figure 2.29. Indeed, the risk of failure tends to be small and the threshold for the maintenance action is constant over the balcony, therefore the effect of the second dimension does not appear. Except for the number of inspections which would be more likely equal to 2. This denotes that the degradation index increases slower than in the one dimensional case due to the

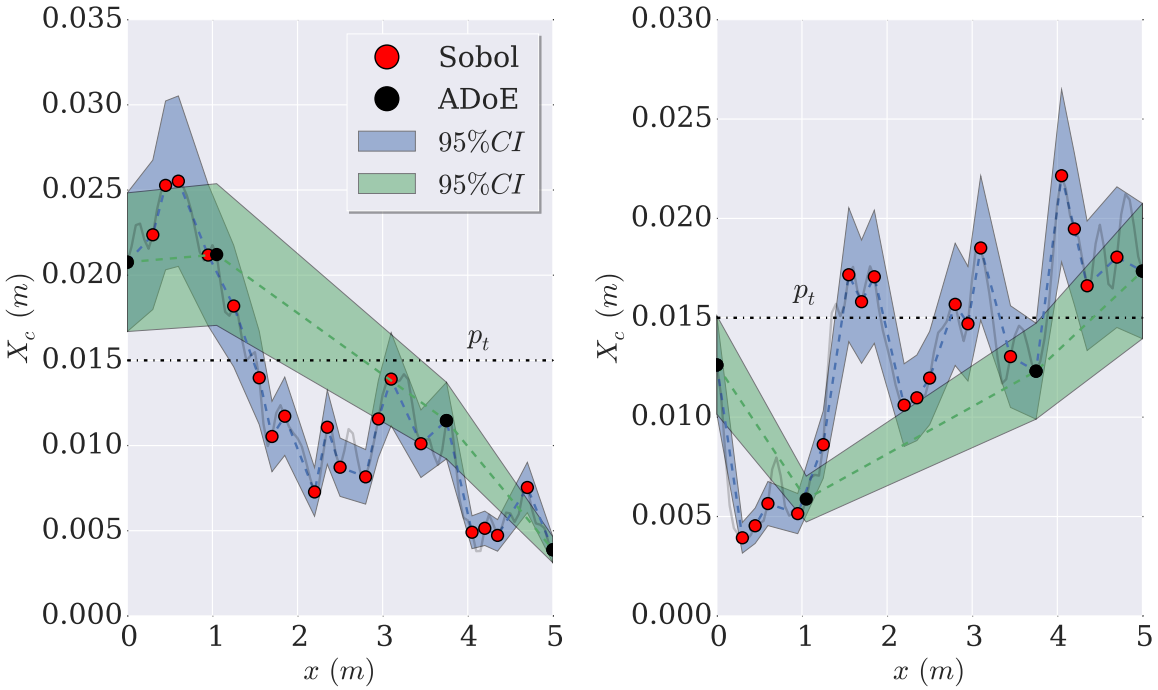

Figure 2.31 – Comparison of the approximated made by the ADoE and the Sobol sequence at 20 years for two trajectories of the simulation sample. The overestimation (resp. underestimation) on the left (resp. right) panel of the

increase of the reinforcement total length. However concerning the confidence intervals shown in Table 2.7 an overestimation may lead to a repair action with 34% of chances against 11% in the one-dimensional case (see Table 2.5).

n°	μ_{Ma}	$[CI^-;CI^+]_{Ma}$	μ_F	$[CI^-;CI^+]_F$
0	0.10	$[0.09;0.33]$	0.90	$[0.91;0.66]$
1	0.89	$[0.91;0.63]$	0.10	$[0.09;0.34]$
2	0.01	$[0;0.04]$	0	$[0;0]$
3	0	$[0;0]$	0	$[0;0]$
4	0	$[0;0]$	0	$[0;0]$
5	0	$[0;0]$	0	$[0;0]$

Table 2.7 – Mean and confidence interval of the number of maintenances and repairs with an inspection interval of 10 years.

n°	μ_{Ma}	$[CI^-;CI^+]_{Ma}$	μ_F	$[CI^-;CI^+]_F$
0	0.92	$[0.75;0.96]$	0.08	$[0.45;0.04]$
1	0.08	$[0.25;0.04]$	0.92	$[0.55;0.96]$
2	0	$[0;0]$	0	$[0;0]$

Table 2.8 – Mean and confidence interval of the number of maintenances and repairs with an inspection interval of 20 years.

However a clear tendency is detectable with an inspection interval of 20 years. Figure 2.32 shows that the number of maintenances is highly decreased, from 65% (see Table 2.6) that one maintenance is to be made to less than 8% (see Table 2.8), while the probability of one repair action increases by nearly 29%. The confidence interval evolves in the same way since:

- An underestimation of the degradation results in a probability of repairing equal to 55% (instead of 21% in the one-dimensional case, see Table 2.8);
- The degradation being overestimated increases the probability of repairing up to 96% (instead of 84% in the one-dimensional case).

There is the effect of a mean cover thickness lower than the one-dimensional case, where the failure state intuitively becomes easier to reach.

2.5.2.3 System approach for the two-dimensional problem

Last but not least, Figure 2.33 presents the results obtained with the system of two-dimensional balconies.

The main difference remains in the constraint set on the maintenance action since only three buildings may be repaired after an inspection. Through Figure 2.32, the consequence of a system approach is clear: the constraint on the maintenance actions reduces the chances

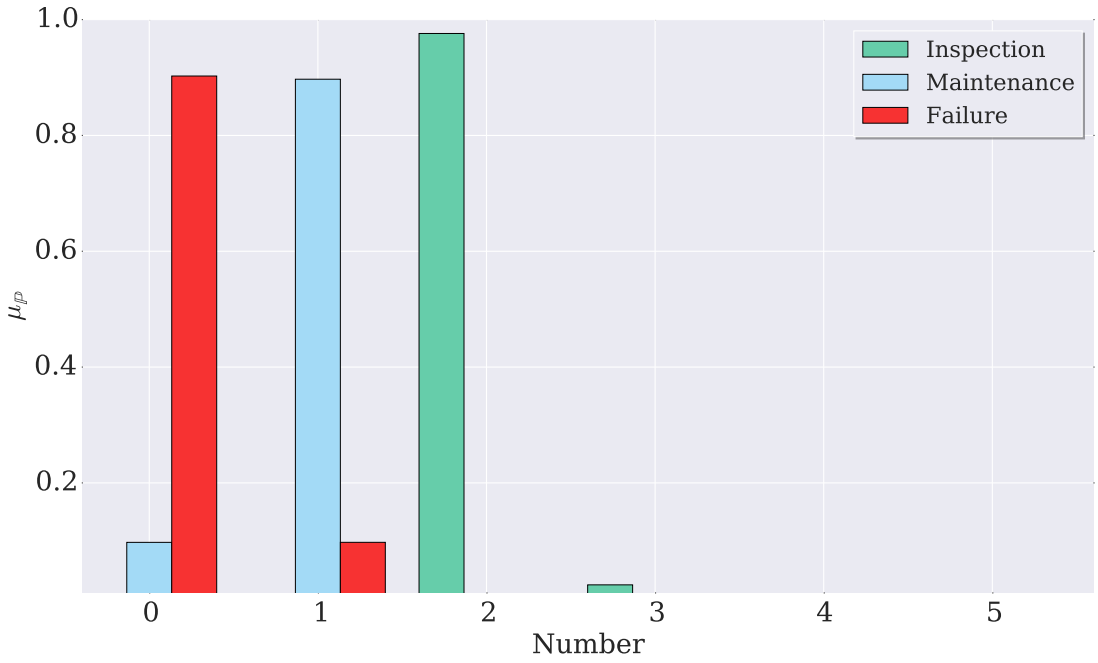

(a) Inspection interval of 10 years.

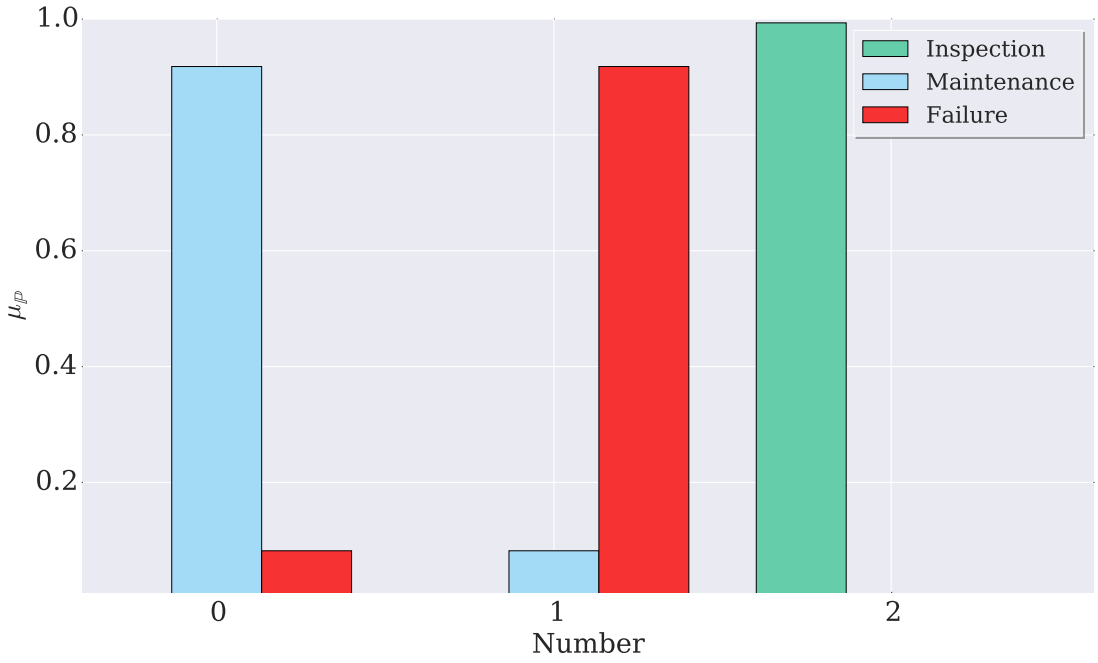

(b) Inspection interval of 20 years.

Figure 2.32 – Probabilistic distributions for the number of maintenances, inspections and repairs for two inspection intervals.

for a balcony to be maintained before failure when maintenance actions were predicted (i.e. with a 10 years interval), while it has no effect when the chances of maintenance being performed were already low (i.e. with 20 years between two successive inspections).

Regarding Table 2.9 and Table 2.10, the measurement uncertainties increase the probability of maintenance with an inspection interval of 10 years yet it means that maintenance decision may be taken instead of repairing ones which is not an advantage either. With a delay between two inspections of 20 years, both underestimation and overestimation keep the probability of repairing above the probability of maintenance.

$n°$	μ_{Ma}	$[CI^-; CI^+]_{Ma}$	μ_F	$[CI^-; CI^+]_F$
0	0.69	[0.52; 0.71]	0.31	[0.87; 0.91]
1	0.30	[0.48; 0.26]	0.69	[0.13; 0.09]
2	0.01	[0; 0.03]	0	[0; 0]
3	0	[0; 0]	0	[0; 0]
4	0	[0; 0]	0	[0; 0]
5	0	[0; 0]	0	[0; 0]

Table 2.9 – Mean and confidence interval of the number of maintenances and repairs with an inspection interval of 10 years.

$n°$	μ_{Ma}	$[CI^-; CI^+]_{Ma}$	μ_F	$[CI^-; CI^+]_F$
0	0.92	[0.75; 0.96]	0.08	[0.45; 0.04]
1	0.08	[0.25; 0.04]	0.92	[0.55; 0.96]
2	0	[0; 0]	0	[0; 0]

Table 2.10 – Mean and confidence interval of the number of maintenances and repairs with an inspection interval of 20 years.

2.5.2.3.1 Conclusions In order to prove the ability of the methodology to handle various cases, three different ones have been developed:

- an uni-dimensional case;
- a bi-dimensional case;
- a bi-dimensional case for several buildings linked by a maintenance constraint.

At this point, this illustration demonstrates the capability of the decision tree as an IMRM. It gives valuable information on the number of maintenances, the number of inspections and the probability of failure which are expected, which allow to study the impact of a given inspection plan. These examples have pointed out that the predictions may be used to determine if a planned inspection can be avoided or not. Since the degradation is supposed to be stationary with a high correlation length regarding the length of a balcony, the information given on the degradation distribution over a balcony is not discriminating enough for the ADoE to be efficient. In this case a low-discrepancy sequence would be a better choice.

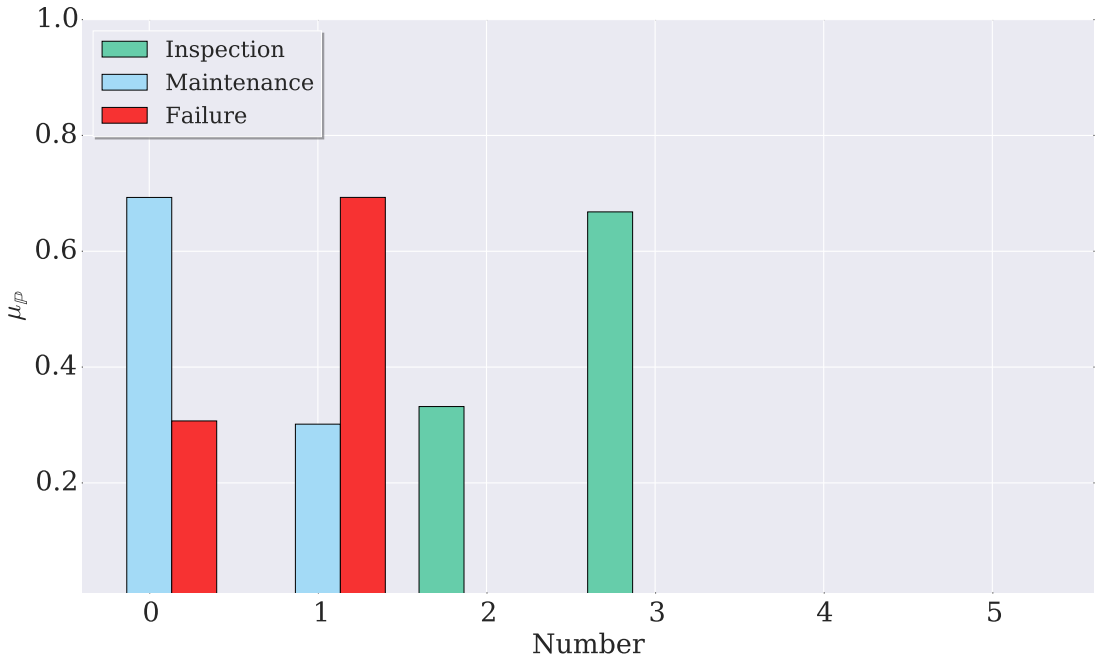

(a) Inspection interval of 10 years.

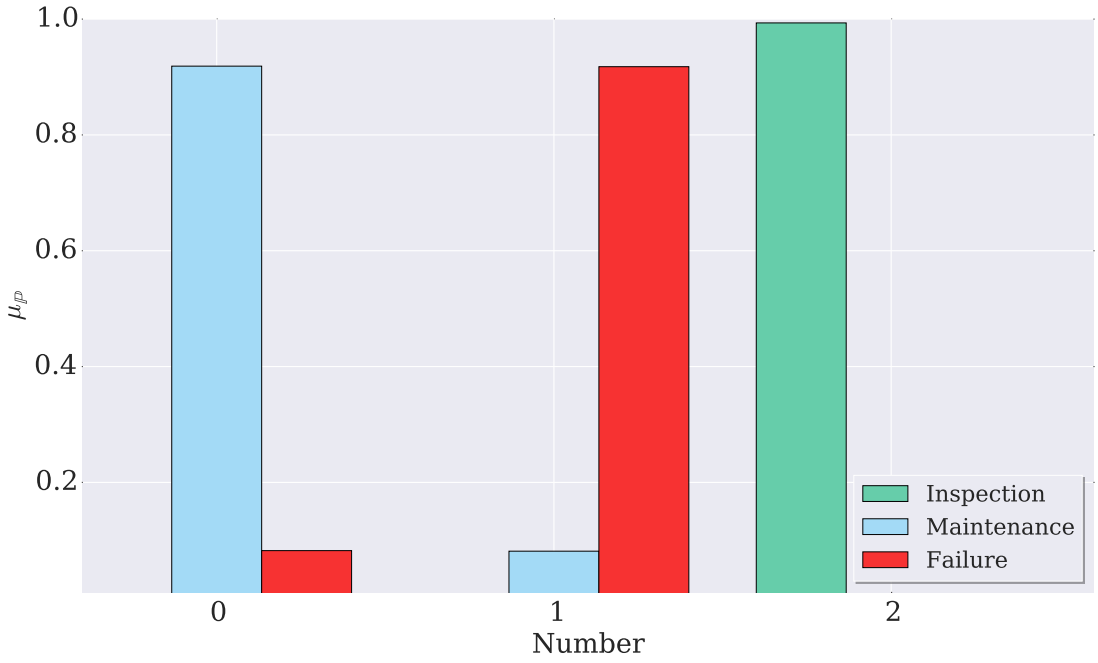

(b) Inspection interval of 20 years.

Figure 2.33 – Probabilistic distributions for the number of maintenances, inspections and repairs for two inspection intervals.

2.6 Conclusion

This chapter introduces the basics of the probability theory prior to the basics of the random fields. In order to account for the spatial variability of any degradation process, it appears important to present the methodologies available to simulate spatially correlated processes.

Among the methodologies available, the Karhunen-Loève has been chosen since it is the most versatile one and it does not need any assumption on the random field to be simulated. In order to simulate non-gaussian random fields which have not been observed, the KL decomposition is to be used for simulating a standard gaussian random field on which the translation field method is applied to transform the field into a non-gaussian one. The inconvenience here is that the correlation structure of the field is to be given to the underlying gaussian process and is then modified by the translation field method. It can be circumvent by optimisation methods or by the use of the fractile correlation function. The latter being the simplest, it is prescribed by the author. The same goes for the simulation of cross-correlated random fields, since it is simpler than the presented Vorechovsky method, although the method proposed by Perrin et al. (2013) has the author's preference.

The second part of the chapter presents the IMRM used in this thesis which is based on a simple decision tree. This sort of model is nearly assumption-independent which is the best fit regarding the thesis objectives. The inspection node of the decision tree is introduced by the classical low-discrepancy sequences and the adaptive design of experiments developed in this thesis. Both aims at obtaining the better statistical knowledge of the degradation random field from a limited number of inspected points. The first is, to the author's advice, to be used in case of stationary random process and any case where the degradation predictions cannot be reliable.

The maintenance node and the failure consideration are presented in the first example of the thesis which studies the case of multiple balconies of french housings. Submitted to a stationary carbonation process, the predictions are made using a surrogate model identified with simulations of a finite element model. The inputs of the model are cross-correlated, non-Gaussian, thus defined with the fractile autocorrelation function and simulated with the translation method. Applying the IMRM for two time steps between inspections, it has shown that:

- Avoiding inspections if the estimated probability of maintenance equals 0 can be useful in case of a short time step between inspections since increasing the time interval may lead to a higher expectation of the probability of failure encountered in the decision tree;
- Although the ADoE and the low-discrepancy sequence give similar results for the probabilities derived by the IMRM, regarding the approximate done by each of them on a unique trajectory shows that the low-discrepancy sequence is to be preferred in the case of stationary random process;
- Confidence intervals are available for all the quantities derived from the decision tree since it propagates the measurement error.

However the use of this IMRM needs a predictive degradation model. The following chapter is dedicated to the calibration by a bayesian framework of such model based on inspection results or structure specifications.

CHAPTER 3

UPDATING THE PREDICTIVE MODEL

3.1 Introduction

The previous chapter introduced a methodology based on a decision tree in order to predict the evolution of a given structure submitted to any inspection plan.

Two things are worth to be pointed out on this methodology:

- It assumes that a predictive degradation model exists. If it does, it may however not be calibrated really well for young structures;
- Its output is an inspection plan likely to be applied, at least for the first inspection.

These considerations drove another objective of this thesis: *To allow the use of any existing data which would be relevant in order to improve the inspection plan computed with the methodology*. Indeed relevant measure coming from an inspection may be used to improve the accuracy of the predictive model in order to derive a better inspection plan.

This situation is particularly suited to Bayesian statistics. This chapter presents in a first section the Bayesian framework prior to a discussion on its potential.

3.2 Bayesian framework

3.2.1 Bayesian updating in structures management

The Bayesian methodology is well known for its ability to mix data coming from measurements and from expert judgement.

Estes and Frangopol (2001b) adopted this methodology. Their life-cycle model is based on an event tree applied to a deteriorating bridge. They update the predictions through a Bayesian context and rerun the optimisation process. The expected exploitation cost is reduced by 97%, since the update drastically decreases the probability that a maintenance will be performed during the lifetime of the bridge.

Faber et al. (1996) use the Bayes theorem in order to update the probability of failure of a structure or the probability density function of an observed random variable. Faber and Sorensen (2002) derive the update of a Bayesian indicator. Applied on a structure submitted to localised and distributed corrosion, the corrosion measurements help to refine the knowledge on the indicator first defined with an expert judgement (presence or not of corrosion deduced from a given threshold of half-cell measurement).

Hellevik et al. (1999) optimise the inspection and replacement planning for piping subjected to carbonation-induced corrosion. The probability of maintenance and the probability of failure are updated based on inspection results of the degradation. It results in an increase of the reliability index of the structure by a factor two after a first inspection after 7 years.

Ma et al. (2013) use Bayesian statistics to update the model of corrosion-induced strength degradation, using data of flexural bearing capacity testing. It greatly reduces the uncertainties of the model predictions.

Perrin (2008) uses Bayesian technique to update the knowledge of the material properties of a concrete by indirect measurements of concrete creep, through a creep model. He developes a methodology able to take into consideration the errors coming from the inspection technique and from the model approximations.

Zhang and Mahadevan (2000) update the predictions of a fatigue model based on non-destructive measure. Each observation (e.g. crack detected) is linked with the PoD definition of the inspection technique (see Section 1.4.1).

3.2.2 Bayes theorem

Bayesian updating relies on the Bayes theorem. Let $\boldsymbol{X} = [X_1, \ldots, X_n]$ be a random vector such as

$$\boldsymbol{X} = \left\{ \begin{array}{ccc} \Omega & \rightarrow & \mathbb{R}^n \\ \omega & \mapsto & \{X_1(\omega), \ldots, X_n(\omega)\} \end{array} \right. \tag{3.1}$$

$\pi_X(\boldsymbol{x})$ its *prior* probability density function, estimated from test data or from expert judgement (for instance, machining production follows a normal distribution centred on the nominal value, the distribution of temperature along the time is uniformly distributed between two bounds, ...).

Let $\boldsymbol{X}^{obs}$ be a set of observations such as

$$\begin{aligned}\boldsymbol{X}^{obs} = \big\{&\boldsymbol{x}^{(z_i,t_j)},\\ &\forall i = (1,\cdots,P); \forall j = (1\cdots,Q)\big\},\end{aligned} \tag{3.2}$$

with each component $\{x^{(z_i,t_j)}\}$ indexed by its location z_i and the observation date t_j.

Since these observations are realisations of the random vector $\boldsymbol{X}$, the *posterior* probability density function of the random vector $\boldsymbol{X}$ is given by the Bayes theorem:

$$f_X(\boldsymbol{x}|\boldsymbol{X}^{obs}) = \frac{1}{c}\pi_X(\boldsymbol{x})\mathscr{L}(\boldsymbol{x},\boldsymbol{X}^{obs}), \tag{3.3}$$

where $\mathscr{L}(\boldsymbol{x},\boldsymbol{X}^{obs})$ is the likelihood of the observations with respect to the probabilistic distribution of the random vector $\boldsymbol{X}$, and c is a normalisation constant which reads

$$c = \int_{\mathscr{D}_X} \pi_X(\boldsymbol{x})\mathscr{L}(\boldsymbol{x},\boldsymbol{X}^{obs})d\boldsymbol{x}. \tag{3.4}$$

The equation 3.3 is unfortunately not easy to solve as this integral only has an analytic solution in a few academic examples.

3.2.3 Estimation of the posterior distribution

Several methods help in estimating the posterior distribution given in Eq. (3.3). As pointed out in the previous section the main issue comes with the evaluation of the normalisation constant (see Eq. (3.4)). A historical way to circumvent this problem was to make use of conjugate distributions but the development of numerical simulation permitted to develop more complex methods such as the *Markov chain Monte Carlo* (Metropolis and Ulam (1949); Metropolis (1987)), introduced in the following together with the conjugate distributions, or method based on polynomial chaos expansion of the likelihood function (Nagel and Sudret (2015) which is the most recent method to the author's knowledge).

3.2.3.1 Conjugate prior distributions

Conjugate distributions are specific combinations of prior distribution and likelihood which return known form of the posterior distribution. This section present a brief overview of conjugate prior distributions. The reader is refereed to Fink (1997); Ntzoufras (2009); Perrin (2008) for a nearly exhaustive list of the conjugate prior distributions.

3.2.3.1.1 Binomial likelihood The binomial likelihood with success probability θ reads

$$\mathscr{L}(\theta, k) = \binom{n}{k} \theta^k (1-\theta)^{n-k}, \tag{3.5}$$

n and k being the number of trials and the number of desired successes, respectively.

One prior conjugate distribution for the parameter θ is the gamma distribution

$$\pi_\theta(\theta) = \frac{\Gamma(a+b)}{\Gamma(a)\Gamma(b)} \theta^{a-1} (1-\theta)^{b-1}, \tag{3.6}$$

with parameters a and b, which combines with the likelihood so that the posterior distribution yields

$$f_\theta(\theta | x^{obs}) \propto \theta^{k+a-1} (1-\theta)^{n-k+b-1}. \tag{3.7}$$

3.2.3.1.2 Normal distribution with unknown mean A Gaussian likelihood with unknown mean θ and known variance σ^2 writes

$$\mathscr{L}(\theta, x^{obs}) \propto \exp\left[-\frac{1}{2} \frac{\left(x^{obs} - \theta\right)}{\sigma^2} \right]. \tag{3.8}$$

Combined with a Gaussian prior for θ with mean θ_0 and variance τ_0^2, thus reading

$$\pi_\theta(\theta) \propto \exp\left[-\frac{1}{2} \frac{(\theta - \theta_0)}{\tau_0^2} \right], \tag{3.9}$$

after some basic algebra the posterior distribution of θ writes

$$f_\theta(\theta | x^{obs}) \propto \exp\left[-\frac{1}{2} \frac{(\theta - \theta_1)^2}{\tau_1^2} \right], \tag{3.10}$$

where

$$\begin{cases} \theta_1 = & \frac{\frac{1}{\tau_0}\theta_0 + \frac{1}{\sigma^2} x^{obs}}{\frac{1}{\tau_0} + \frac{1}{\sigma^2}}; \\ \tau_1^2 = & \frac{1}{\frac{1}{\tau_0} + \frac{1}{\sigma^2}} \end{cases}. \tag{3.11}$$

3.2.3.1.3 Normal distribution with unknown variance For a sample $\boldsymbol{X}^{obs} = \left\{ x^i, \forall i \in (1, \ldots, n) \right\}$, each experiment being exchangeable, with known mean μ and unknown variance θ, a Gaussian likelihood reads

$$\mathscr{L}(\theta, x^{obs}) \propto \prod_{i=1}^{n} \theta^{-\frac{1}{2}} \exp\left[-\frac{1}{2}\frac{\left(x^{(i)}-\mu\right)^2}{\theta}\right]. \tag{3.12}$$

Combined with an inverted-gamma prior such as

$$\pi_\theta(\theta) \propto \theta^{-(a_0+1)} \exp\left[-\frac{b_0}{\theta}\right], \tag{3.13}$$

the posterior distribution of θ is also an inverted-gamma yielding

$$f_\theta(\theta|\boldsymbol{X}^{obs}) \propto \theta^{-(a_1+1)} \exp\left[-\frac{b_1}{\theta}\right], \tag{3.14}$$

where

$$\begin{cases} a_1 = & \frac{n+2a}{2}; \\ b_1 = & b + \frac{1}{2}\sum_{i=1}^{n}\left(x^{(i)}-\mu\right)^2 \end{cases}. \tag{3.15}$$

3.2.3.2 Markov Chain Monte Carlo

Markov Chain Monte Carlo (MCMC) method, introduced by Metropolis and Ulam (1949), is used to sample directly into the posterior distribution (see Eq. (3.3)).

If a Markov chain is *irreducible, aperiodic* and *reversible* (see Section 1.3.2.1) and its stationary distribution is the posterior distribution $f_X(\boldsymbol{x}|\boldsymbol{X}^{obs})$ thus sampling this chain will return the posterior distribution.

Two issues are to be addressed, which are illustrated in Figure 3.1:

- Indeed the chain shall start from an initial point, the so-called *seed*. Depending on this point the convergence towards the stationary distribution will need a different initial sample size. The *burn-in* period removes this sample from the overall chain in order to only keep the points which belong to the stationary distribution.
- Despite the memoryless property of the Markov chain, the sample points may be correlated between each other. This autocorrelation is to be avoided in order to get independent experiments thus the sample is *thinned* (e.g. only one point every 4 points is stored).

Finally the major remaining issue is to sample *from* a Markov chain with $f_X(\boldsymbol{x}|\boldsymbol{X}^{obs})$. For this purpose, Hastings (1970) improved a proposition of Metropolis et al. (1953) called the *Metropolis-Hasting* algorithm. They found out that any Markov chain with transition probabilities being a ratio of the stationary distribution and the proposal distribution both evaluated on the proposed point and the last accepted one will converge asymptotically to

Algorithm 3.1 MCMC with Single-component Metropolis-Hastings sampler

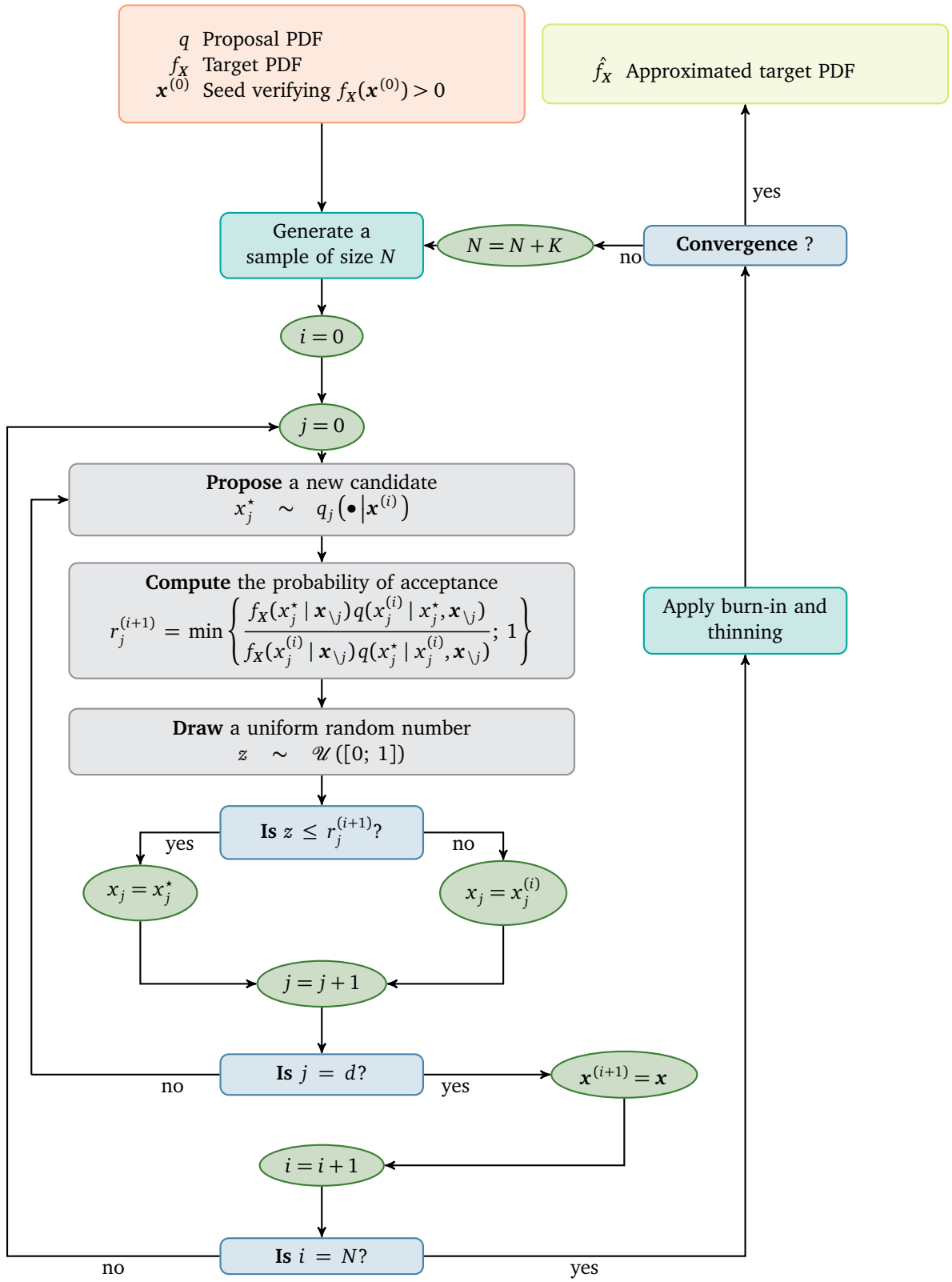

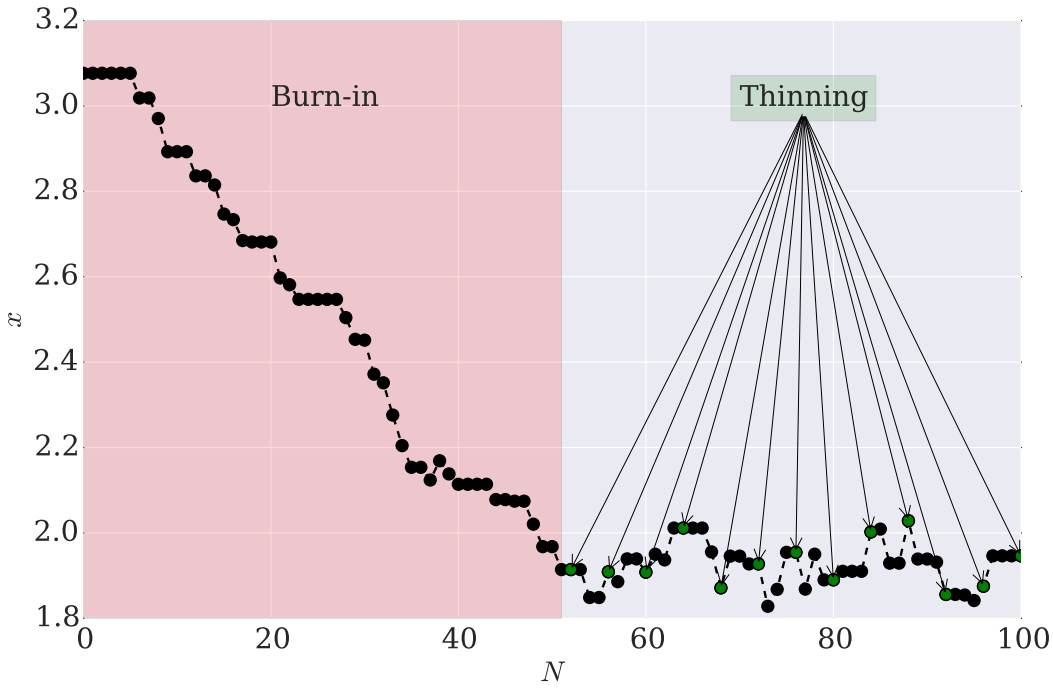

Figure 3.1 – Illustration of Burn-in and Thinning of Markov Chain.

the stationary distribution (i.e. the posterior distribution). Many variant of this algorithm have been proposed, such as the single-component Metropolis-Hastings sampler illustrated in Algorithm 3.1, the Gibbs sampler, the slice sampler, etc ... (Perrin (2008))

3.2.4 Model calibration

The Bayesian statistics are known for their efficiency in model calibration Perrin (2008); Nagel and Sudret (2015) since unlike classical methods such as the least-square problem, they:

- allow to calibrate a model with a small number of points if the prior distributions are relevant;
- return a distribution of possible values for the model parameters, i.e. probability distributions.

Given a model $\mathscr{M}$ which tries to predict an outcome $\boldsymbol{y} \in \mathscr{D}_Y \subset \mathbb{R}^{d_y}$ given some inputs $\boldsymbol{x} \in \mathscr{D}_X \subset \mathbb{R}^{d_x}$, any observation of the output denoted $\boldsymbol{y}^{obs}$ could be written as Perrin (2008):

$$\boldsymbol{y}^{obs} = \mathscr{M}(\boldsymbol{x}) + \boldsymbol{\epsilon}, \tag{3.16}$$

where $\boldsymbol{\epsilon}$ represents the model approximations and output observations uncertainties assumed to be independent of each other.

From this point, three situations may occur:

- First case: an inspection returns measurements of some model outputs. In this case the purpose is to calibrate the model parameters in order to fit the observations;
- Second case: an inspection returns measurements of some model inputs. This is not a calibration problem. Each observed inputs are to be updated and the corresponding posterior distributions propagated through the model $\mathscr{M}$;
- Third case: Both measurements could be made, which would lead to a calibration of the unobserved model inputs.

3.2.4.1 Model outputs observation

From Eq. (3.16), we could write each observation $\left\{\boldsymbol{y}^{\boldsymbol{obs}^{(i)}}, i = 1, \ldots, N_{obs}\right\}$ as being a realisation of the model/measurement uncertainties:

$$\boldsymbol{\epsilon}^{(i)} = \boldsymbol{y}^{\boldsymbol{obs}^{(i)}} - \mathscr{M}(\boldsymbol{x}), \quad i = (1, \ldots, N_{obs}). \tag{3.17}$$

Let assume that the model/measurement error random vector is normally distributed with 0 mean such as

$$\boldsymbol{\epsilon} \sim \mathscr{N}(\mathbf{0}, \boldsymbol{\sigma}_{\boldsymbol{\epsilon}} \times \mathbf{I}), \tag{3.18}$$

where $\mathbf{0}$ is a vector of zeros with size d_y, $\boldsymbol{\sigma}_{\boldsymbol{\epsilon}}$ the corresponding vector of standard deviations and $\mathbf{I}$ the identity matrix of shape $d_y \times d_y$ (i.e. the components of the error random vector are independent).

Given that each observation is independent, the likelihood of the observations with respect to the model predictions reads

$$\mathscr{L}\left(\boldsymbol{x}, \boldsymbol{\sigma}_{\boldsymbol{\epsilon}}, \boldsymbol{Y}^{\boldsymbol{obs}}\right) = \prod_{i=1}^{N_{obs}} \prod_{j=1}^{d_y} \varphi\left(\frac{\mathscr{M}(\boldsymbol{x}) - y_{i,j}^{obs}}{\sigma}\right), \tag{3.19}$$

where φ is the probability density function of the standard normal distribution.

The *posterior* distribution of the input parameters of the model $\mathscr{M}$ is thus defined by

$$f_{X,\boldsymbol{\sigma}_{\boldsymbol{\epsilon}}}\left(\boldsymbol{x}, \boldsymbol{\sigma}_{\boldsymbol{\epsilon}} \mid \mathbf{Y}^{\mathbf{obs}}\right) \propto \pi_X(\boldsymbol{x}) \pi_{\boldsymbol{\sigma}_{\boldsymbol{\epsilon}}}(\boldsymbol{\sigma}_{\boldsymbol{\epsilon}}) \mathscr{L}\left(\boldsymbol{x}, \boldsymbol{\sigma}_{\boldsymbol{\epsilon}}, \boldsymbol{Y}^{\boldsymbol{obs}}\right). \tag{3.20}$$

3.2.4.2 Combined observations of the model outputs and inputs

Due to the capacity of the measurement techniques, some outputs of the model $\mathscr{M}$ can be measured together with some components of the input random vector $\boldsymbol{X}$. The proposition made to deal with this particular case is to split up the random vector $\boldsymbol{X}$ into two sub-vectors.

Let define the random vector $\boldsymbol{X}^{obs}$ which gathers the inputs of the model $\mathscr{M}$ which have been measured, and $\boldsymbol{X}^{\overline{obs}}$ the random vector of the inputs not observed.

Following the assumptions made in Section 3.2.4.1, the likelihood writes

$$\mathscr{L}\left(\boldsymbol{x}^{\overline{obs}}, \boldsymbol{\sigma}_{\epsilon}, \boldsymbol{Y}^{obs}, \boldsymbol{x}^{obs}\right) = \prod_{i=1}^{N_{obs}} \prod_{j=1}^{d_y} \varphi\left(\frac{\mathscr{M}\left(\boldsymbol{x}^{\overline{obs}}, \boldsymbol{x}^{obs\,(i)}\right) - y_{i,j}^{obs}}{\sigma_{\epsilon}^{(j)}}\right), \tag{3.21}$$

and the posterior distribution of the non-observed input parameters denotes

$$f_{\boldsymbol{X}^{\overline{obs}}, \boldsymbol{\sigma}_{\epsilon}}\left(\boldsymbol{x}^{\overline{obs}}, \boldsymbol{\sigma}_{\epsilon} \mid \mathbf{Y}^{\mathbf{obs}}, \mathbf{X}^{\mathbf{obs}}\right) \propto \pi_{\boldsymbol{X}^{\overline{obs}}}(\boldsymbol{x}^{\overline{obs}}) \pi_{\boldsymbol{\sigma}_{\epsilon}}(\boldsymbol{\sigma}_{\epsilon}) \mathscr{L}\left(\boldsymbol{x}^{\overline{obs}}, \boldsymbol{\sigma}_{\epsilon}, \boldsymbol{Y}^{obs}, \boldsymbol{x}^{obs}\right). \tag{3.22}$$

Above equations however assume that the observations of the input parameters are perfect still there is no reason for them to be perfect while the measurements of the output are not. Knowing the error made on this measurement, for instance $\boldsymbol{\epsilon}_{\boldsymbol{x}^{obs}} \sim \mathscr{N}\left(\mathbf{0}, \boldsymbol{\sigma}_{\epsilon_{\boldsymbol{x}^{obs}}} \times \mathbf{I}\right)$, the idea to circumvent this problem is to get from the distribution of the error $\boldsymbol{\epsilon}_{\boldsymbol{x}^{obs}}$ centred on the observed value (i.e. $\mathscr{N}\left(\boldsymbol{x}^{obs}, \boldsymbol{\sigma}_{\epsilon_{\boldsymbol{x}^{obs}}} \times \mathbf{I}\right)$) a sample $\tilde{\boldsymbol{x}}^{obs}$ of size d_y and rewrite the likelihood Eq. (3.21) as:

$$\mathscr{L}\left(\boldsymbol{x}^{\overline{obs}}, \boldsymbol{\sigma}_{\epsilon}, \boldsymbol{Y}^{obs}, \boldsymbol{x}_{\boldsymbol{s}}^{obs}\right) = \prod_{i=1}^{N_{obs}} \prod_{j=1}^{d_y} \varphi\left(\frac{\mathscr{M}\left(\boldsymbol{x}^{\overline{obs}}, \boldsymbol{x}_{\boldsymbol{s}}^{obs\,(i)}\right) - y_{i,j}^{obs}}{\sigma_{\epsilon}^{(j)}}\right). \tag{3.23}$$

Drawing such a sample at each step of the MCMC shall take into account the measurement error. The corresponding single-component Metropolis-Hastings sampler is given in Algorithm 3.2.

Algorithm 3.2 MCMC with Single-component Metropolis-Hastings sampler

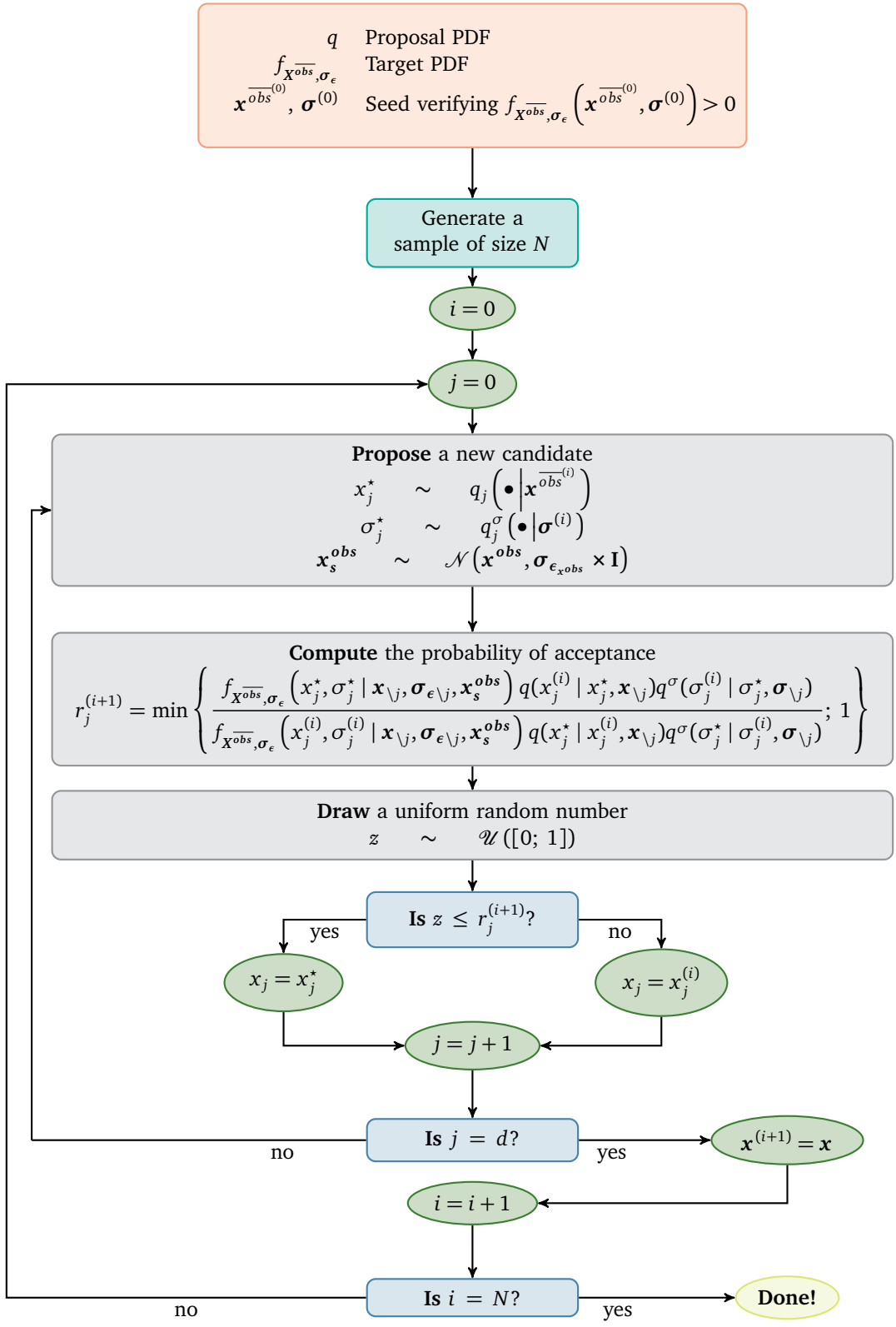

3.3 Discussion on the use of Bayesian statistics for concrete structures

3.3.1 Problem statement

Although for steel structures the non-destructive techniques have been used for a long time, concerning concrete structures it remains an active research subject with promising results Garnier et al. (2014). The french national project SENSO (2009) which aimed at designing non-destructive inspection protocols for concrete structures resulted in the ability to measure:

- The saturation rate (i.e. the water content) S_r;
- The concrete porosity ϕ;
- The Young modulus E_c;
- The compressive strength R_c.

The models presented in Section 1.2.2 helps to predict:

- A carbonation depth (e.g. Eq. (1.1));
- A chloride concentration (e.g. Eq. (1.2));
- A corrosion current (e.g. Eq. (1.3)).

In order for them to compute accurate predictions, they need specific inputs such as:

- The exposure conditions of the concrete;
- The type of concrete;
- The curing conditions;
- The diffusion coefficient associated with the penetration agent.

Basically, it means that at the instant of this manuscript writing, none of the non-destructive inspection techniques may be of any help to improve the predictions of the carbonation, the chloride concentration and the corrosion degradation processes.

However:

- The exposure conditions of the concrete may be given by meteorological records;
- The type of concrete and the curing conditions may be found in the construction specifications of the building, with respect to the trust one may have in the concordance between the specifications and the resulting concrete;
- The diffusion coefficient may be estimated by empirical formulations introduced below for the carbonation process.

3.3.2 Empirical formulations for the carbonation process

In order to use non-destructive testing results to estimate the evolution of the carbonation depth, the research project EVADEOS funded by the French National Research Agency experienced the use of the following empirical formulations.

Let define both the concrete degree of hydration denoted by (Taylor (2004))

$$\alpha_H = 1 - \exp[-3.3w/c], \tag{3.24}$$

where w/c is the water-cement ratio (available in the construction specifications) and the volume fraction of cement writing (m^3/m^3) (Taylor (2004))

$$V_c = \frac{c}{1000(1-\phi_{air})}\left(\frac{1}{\rho_c} + w/c\right), \tag{3.25}$$

with c the cement quantity (kg/m^3), ϕ_{air} the air content and ρ_c the concrete relative density.

Then, the initial porosity of concrete may be estimated by (Taylor (2004))

$$\phi = \left[\frac{w/c}{w/c+0.32} - 0.53\alpha_H\left(1 - \frac{w/c}{w/c+0.32}\right)\right]V_c. \tag{3.26}$$

As a reminder, the DuraCrete carbonation model (DuraCrete (2000)) presented in Chapter 1 reads

$$X_c(t) = \sqrt{\frac{k_e k_c k_t C_s t}{R_{carb}}} * \left(\frac{t_0}{t}\right)^n. \tag{1.1}$$

R_{carb} can be derived by

$$R_{carb} = 1000\frac{C_1 M_{CaO}}{D_{CO_2}}V_c \tag{3.27}$$

where C_1 is given by (Hyvert (2009)):

$$\begin{cases} C_1 &= \left[\alpha_H \frac{1-\phi_{air}}{\frac{1}{\rho_c}+w/c}\frac{CaOC_k}{M_{CaO}}\right] - C_2 \\ C_2 &= 1.65\alpha_H \frac{1-\phi_{air}}{\frac{1}{\rho_c}+w/c}\frac{SiO_2C_k}{M_{SiO_2}} \end{cases} \tag{3.28}$$

CaO and SiO_2 are respectively the amount of calcium oxide and silicone dioxide, with M_{CaO} and M_{SiO_2} their molar mass, respectively.

Finally D_{CO_2} is the coefficient of diffusion which writes (Thiery (2005))

$$D_{CO_2} = D_{CO_2}^{air}\phi^{2.74}(1-S_r)^{4.2}, \tag{3.29}$$

with $D_{CO_2}^{atm}$ the diffusion coefficient for the carbon dioxide in the air.

With these empirical models, the DuraCrete model is thus dependant on the concrete porosity and saturation rate, two of the measurable concrete properties by NTDs.

3.3.3 Case study

Through the research project EVADEOS, destructive (DT) and non-destructive testings have been performed on an area delimiting wall belonging to French Alternative Energies and Atomic Energy Commission (CEA), built 35 years ago. The output of this testing campaign were measurements of:

- Carbonation depth (DT);
- Saturation rate (DT and NDT);
- Concrete porosity (DT and NDT);
- Compressive strength (DT and NDT).

The NDTs were performed with the methodology described in Garnier et al. (2014) which basically combines the results of different non-destructive techniques which are sensitive to the quantity of interest one wants to measure. An illustrative plan of the measurement site is shown in Figure 3.2 together with a picture of the inspection team in Figure 3.3. Some of the results extracted from this inspection campaign are gathered in Table 3.1. Together with these results, the cement quantity c has been estimated to 350 kg/m^3 by destructive testing.

X_c *(DT) (mm)*	19, 19, 20, 22, 20, 17, 19, 17, 22 16, 21, 19, 17, 18, 17, 23, 25, 28
S_r *(NDT) (%)*	73.3, 70, 66.1, 61.1, 54.7, 51.4, 57, 59, 62.7 53.4, 58.9, 56.1, 64.8, 62.2, 61.4, 56.8, 56.4, 57.4
ϕ *(NDT) (%)*	17, 17, 17.2, 17.6, 17.9, 19.2, 18.7, 18.2, 17.4 18.7, 18.9, 18.6, 17.5, 19.2, 18.8, 19.3, 18.4, 16.8

Table 3.1 – Results of the inspection campaign. Each couple of X_c, S_r and ϕ have been measured at the same location. DT, resp. NDT, means that the values have been obtained through destructive testing, resp. non-destructive testing.

3.3.3.1 Material parameters

Since this wall does not have any structural utility, it is assumed that the concrete is a C25. According to DuraCrete (2000) and expert knowledge (since no structure specifications were available), the DuraCrete model parameters have been considered as random variables described in Table 3.2.

3.3.3.2 Updating cases

Before any update, the prior distributions of the carbonation model inputs (see Table 3.2) are used to predict the carbonation depth evolution of the wall during 35 years, i.e. until the

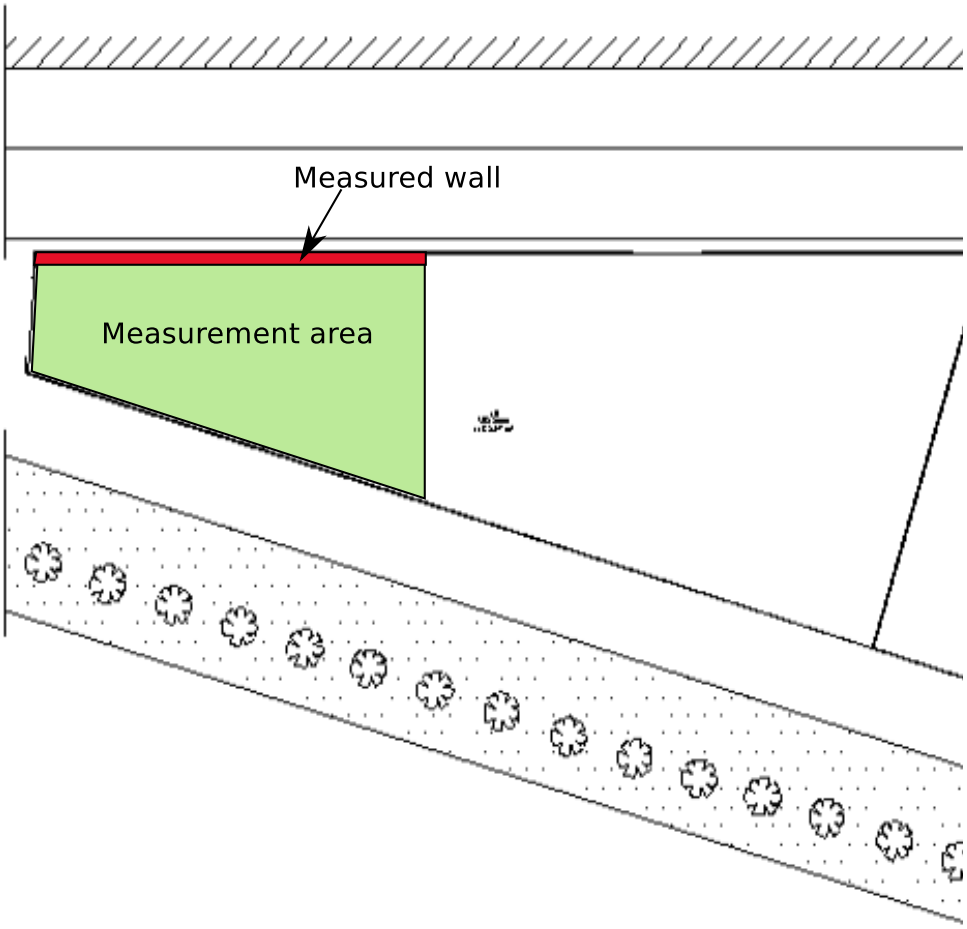

Figure 3.2 – Plan of the measurement site

inspection date. Then in order to highlight the data needed to perform an efficient update, three cases are considered:

Case 1: The first case uses the measurements of the carbonation depth together with the measurements of S_r and ϕ. (see Section 3.2.4.2);

Case 2: Since this work shall use NDT results, the update of S_r and ϕ is performed and the carbonation depth predictions are made with the identified posterior distributions;

Case 3: The last case uses the measurements of the carbonation depth only, although they have been obtained by destructive testing (see Section 3.2.4.1). In this case the concrete porosity is not updated through the model but identified by Eq. (3.26).

In order to reduce the number of random variables, a sensitivity analysis has been performed on the DuraCrete model by computing the total order Sobol' indices Sobol' (1993) which are easy to interpret (e.g. an indice of 10% for an input means that the total variance of this input is responsible for 10% of the output variance). Yet they do not account for the correlation which may exists between the variables but which is not modelled since it

Figure 3.3 – Picture of the inspection team on the CEA measurement site

Item	*Distribution*	*Description*
k_e	$LN\,(mu_{LN} = 0.82, \sigma_{LN} = 0.27)$	
k_c	$Beta\,(r = 1.86, t = 2.96, a = 0.35, b = 1)$	
k_t	$N\,(\mu = 0.983, \sigma = 0.023)$	
n	$Beta\,(r = 0.802, t = 2.102, a = 0, b = 0.5)$	$Beta$: Beta distribution
$c\,\left(kg/m^3\right)$	$U\,(a = 320, b = 370)$	U : Uniform distribution
C_k (%)	$U\,(a = 95, b = 100)$	N : Normal distribution
w/c (%)	$U\,(a = 40, b = 70)$	LN : Lognormal distribution
CaO (%)	$U\,(a = 64, b = 66)$	Tr : Triangular distribution
SiO_2 (%)	$U\,(a = 20, b = 21)$	
S_r (%)	$Tr\,(a = 50, b = 100, c = 70)$	
ϕ (%)	$U\,(a = 1, b = 30)$	

Table 3.2 – Distribution of the DuraCrete model inputs

is completely unknown. If the correlation was introduced, indices based on the covariance decomposition (Caniou (2012)) may be efficient.

The sensitivity analysis has been performed two times:

- The first analysis considers S_r and ϕ as known parameters;
- The second analysis does not.

A classic interpretation of Figure 3.4 would be that without considering the measurements on the concrete porosity and saturation rate, n, S_r, k_e, k_c and CaO should be kept. However to the author's experience with the DuraCrete model, n and S_r indices are way too important (i.e. around 10 times higher) to update them with k_e, k_c and CaO. Indeed n and S_r are coefficients of power laws while k_e, k_c and CaO are only multiplying factors. The mean sensitivity to n and S_r is then expected to be much higher. When S_r and ϕ measurements are considered, following this principle only n shall be updated. Thus for the three cases mentioned above, two different updates are done:

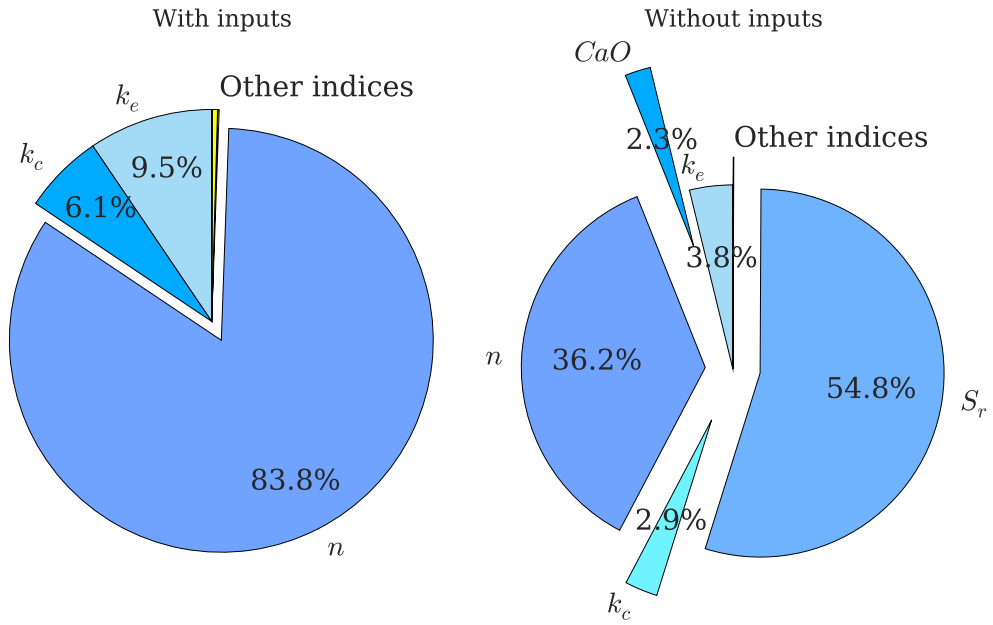

Figure 3.4 – Sobol total indices for the DuraCrete model. On the left S_r and ϕ have been considered as known, on the right no input is measured.

Case a: If the input measurements are considered, only n is modelled as a random variable. If not, n and S_r are modelled as random variables. For both cases, all the other parameters are set equal to their mean.

Case b: If the input measurements are considered, n, k_e and k_c are modelled by random variables, but k_e and k_c are not updated (i.e. always accepted in Algorithm 3.2. If not, n, S_r, k_e, k_c and CaO are considered as random variables yet only n and S_r are updated Algorithm 3.1.

The measurement/model error standard deviation ϵ is modelled by a uniform random variable between 0 and 1.6. In all cases, the MCMC algorithm is used with a burning period of 5,000 points and a thinning of 5 (see Figure 3.1) in order to get 2,000 experiments of the posterior distribution.

3.3.3.3 Results and analysis

3.3.3.3.1 Case a

Case a-1 The posterior distributions shown in Figure 3.5 have converged towards unimodal distributions. The concrete porosity mean is around 18%, which is different from the porosity predicted by Eq. (3.26) which gives a porosity of 14.6%.

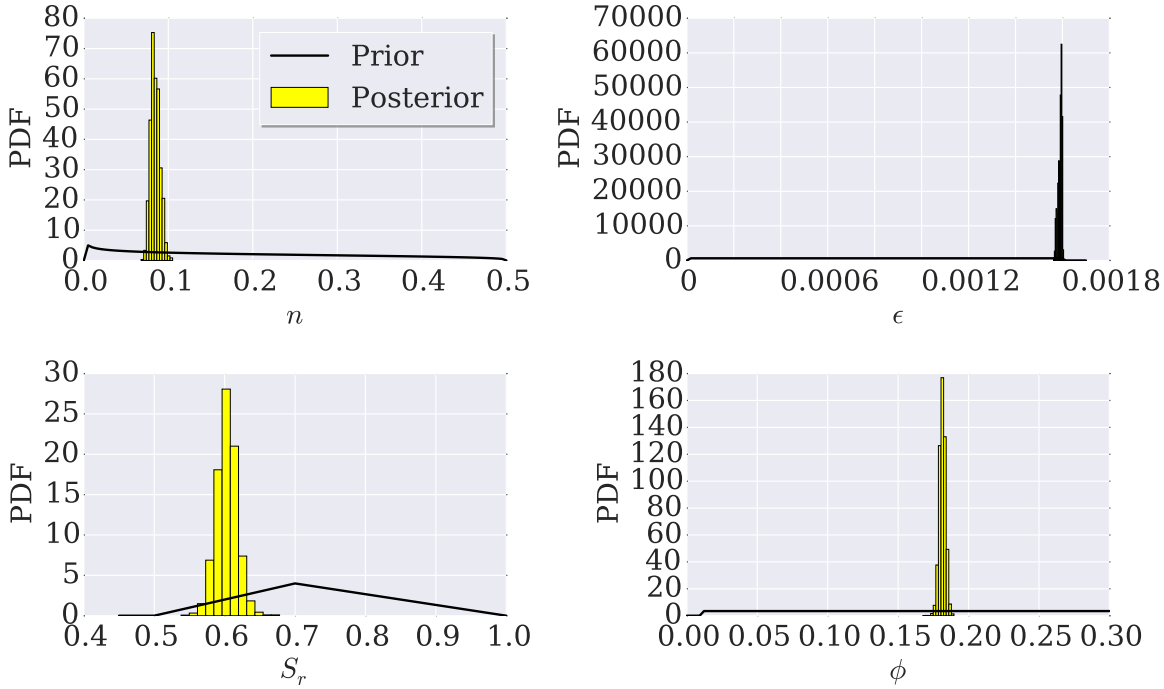

Figure 3.5 – Prior and posterior distributions of the updated random variable in the Case a-1.

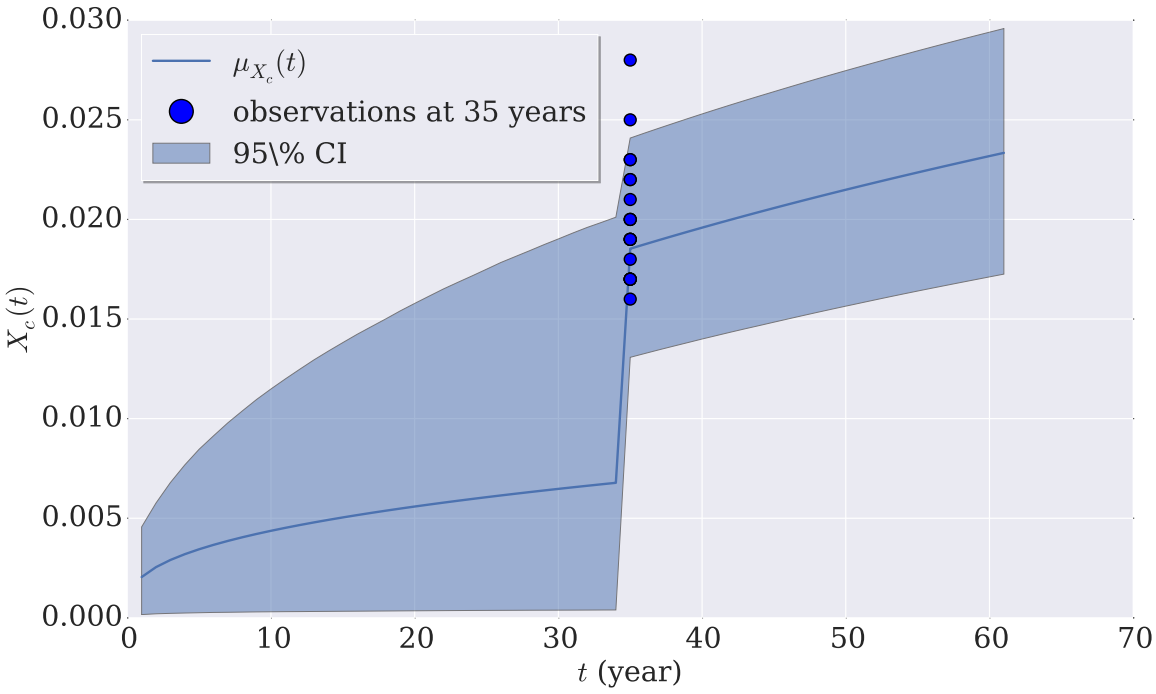

Figure 3.6 – Prior and posterior degradation predictions in the Case a-1.

The analysis of the predictions shown in Figure 3.6 demonstrates the usefulness of the Bayesian updating. The prediction mean which was quite underestimating the real degradation evolution is corrected, and the confidence interval around this mean is reduced at the same time.

Case a-2 However, if only the updates of the saturation rate and the porosity are considered (see Figure 3.5), although the confidence interval of the updated prediction in Figure 3.7 contains most of the observed carbonation depth, the mean is below all of them. At 35 years it is equal to 1.5cm while the lowest carbonation depth equal 1.7cm, the observed mean being near 2cm (i.e. a plausible value for the concrete cover). Such prediction could thus lead to a false conclusion concerning the reinforcement depassivation.

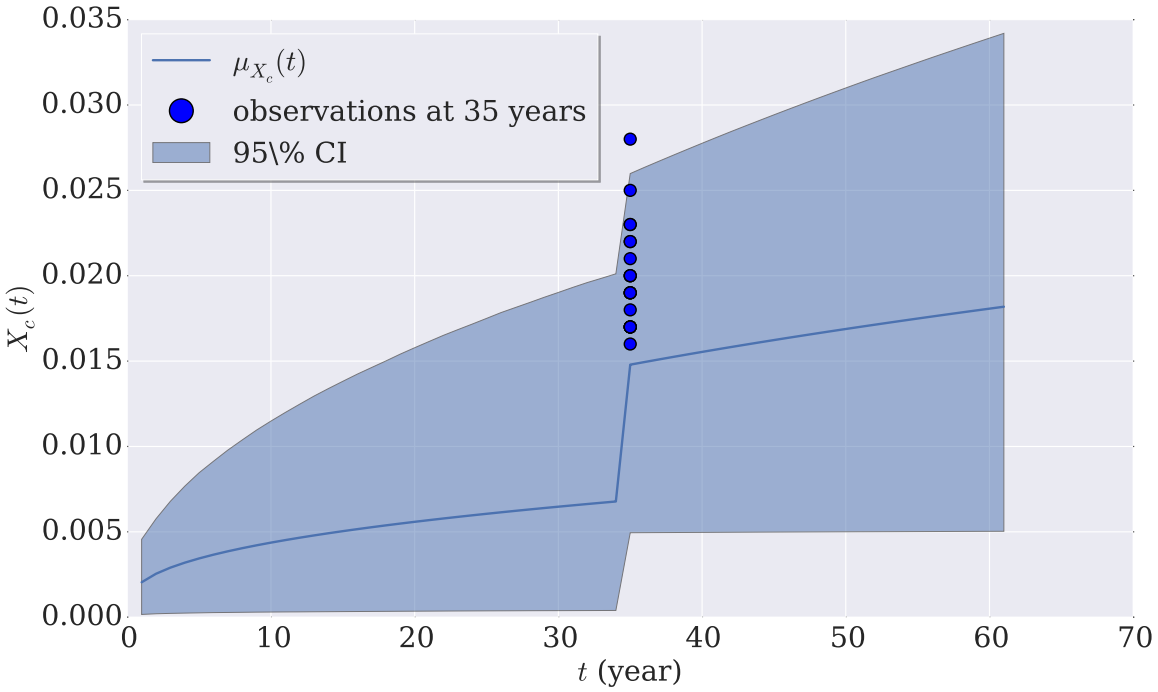

Figure 3.7 – Prior and posterior degradation predictions in the Case a-2.

Case 3 When the measures of the saturation rate and the concrete porosity are not considered, the posterior distribution of the saturation performed through the degradation model shown in Figure 3.8 is similar with the posterior obtained with direct measurements (see Figure 3.5). The posterior distribution of n is however slightly different, yet as already mentioned the porosity predicted by the empirical formulation in Eq. (3.26) is lower than the observed one.

Finally, the updated degradation predictions in Figure 3.9 appear quite similar compared to Figure 3.6 which indicates that the most useful measurements are the measurements of the output itself in this case.

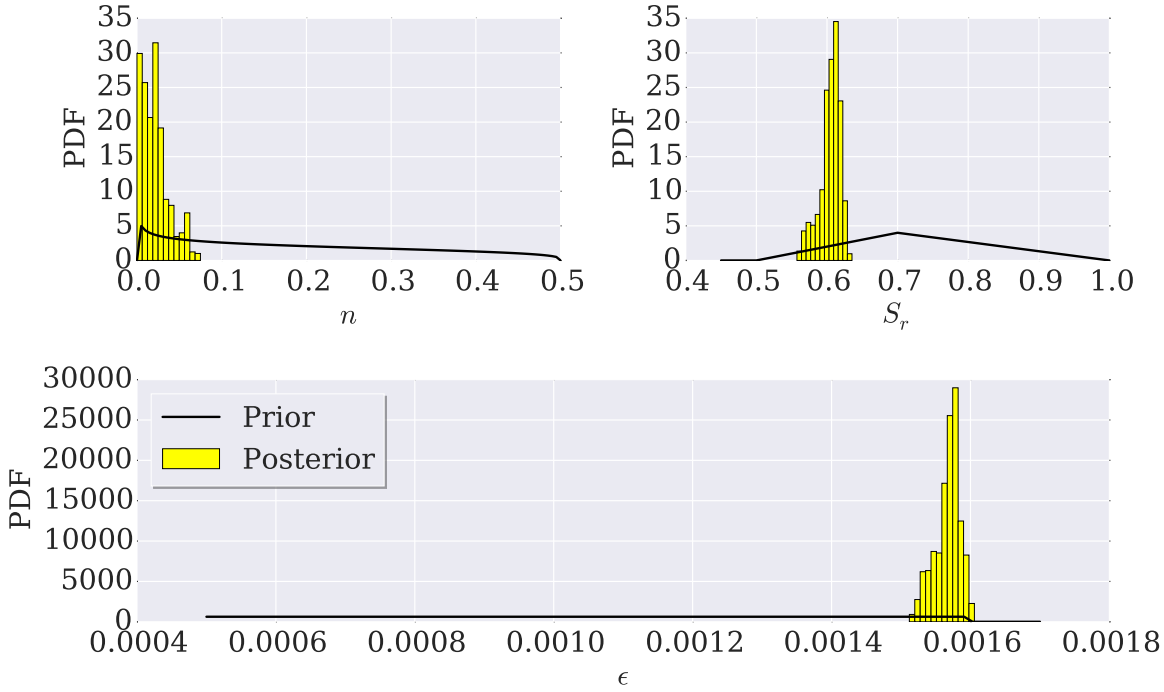

Figure 3.8 – Prior and posterior distributions of the updated random variable in the Case a-3.

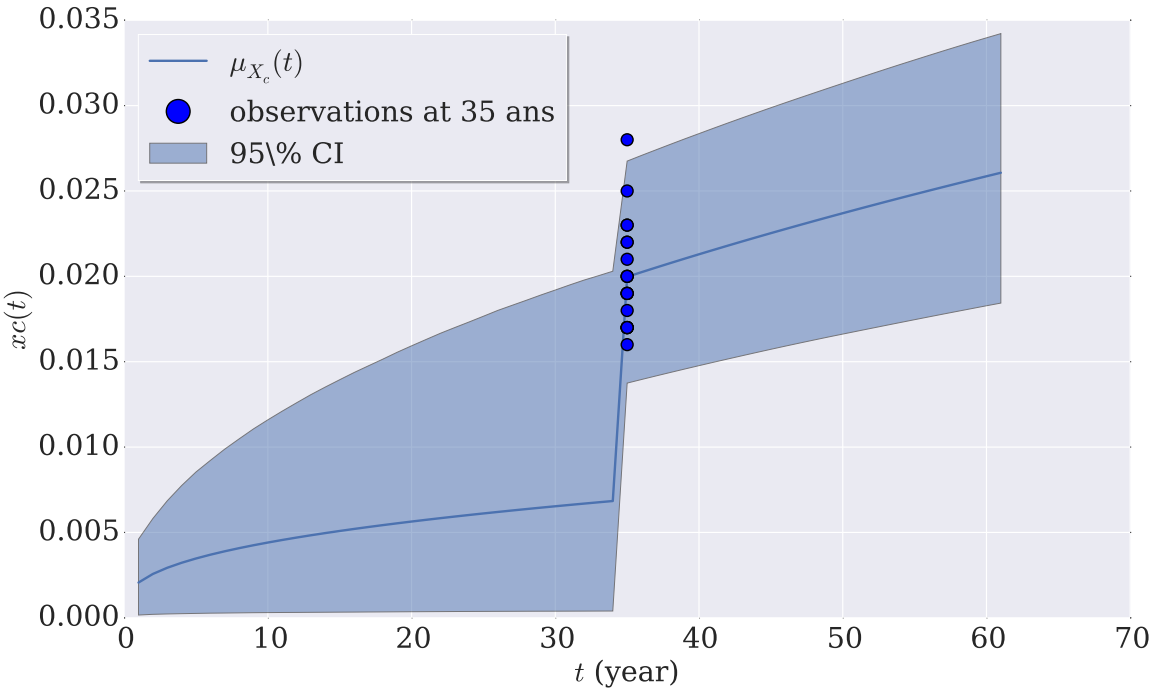

Figure 3.9 – Prior and posterior degradation predictions in the Case a-3.

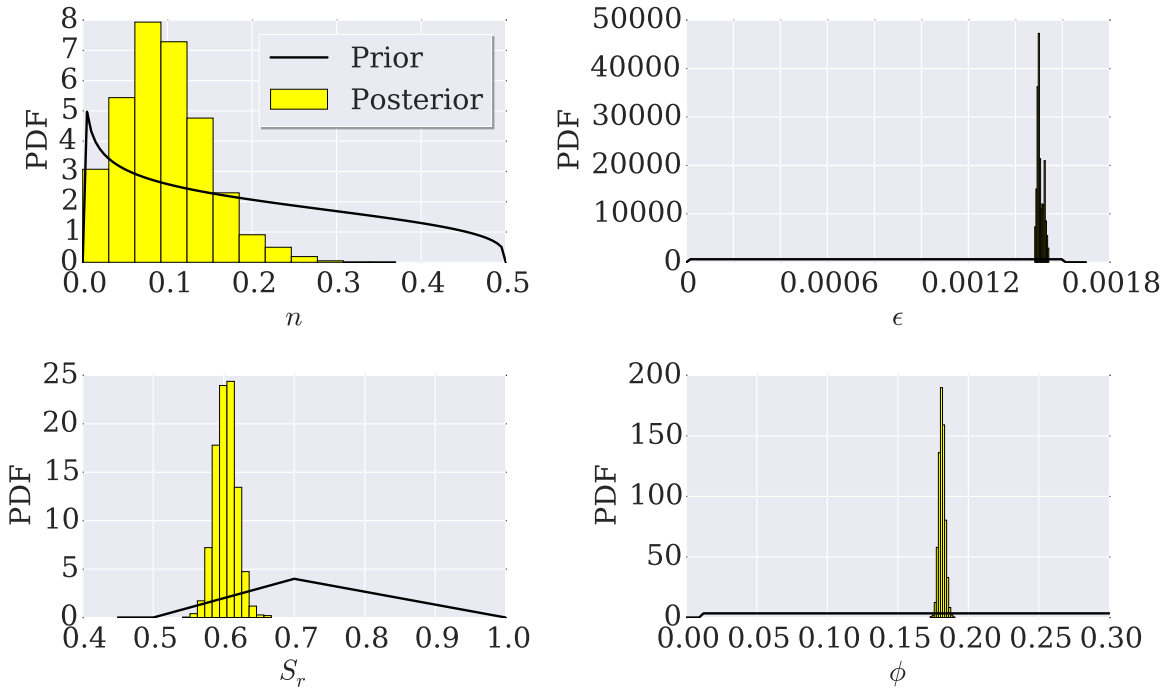

Figure 3.10 – Prior and posterior distributions of the updated random variable in the Case b-1.

3.3.3.3.2 Case b, cases 1 and 3 When considering k_e and k_c as random variables, the posterior PDF of n in Figure 3.10 appears larger than in the case a-1 (see Figure 3.5), so does the confidence interval of the DuraCrete model predictions shown in Figure 3.11. Yet compared to the case a-1 in Figure 3.6, the posterior means of the predictions are pretty similar. In the end, considering k_e and k_c as random variables only enlarge the confidence interval (which ios normal considering their Sobol' indices up to 6 and 9.5 % as it was expected due to their role in the DuraCrete model.

Regarding Figures 3.12 and 3.13, for the case where only the carbonation depth values are used to update n and S_r and with S_r, k_e, k_c and CaO modelled as random variables, the results of the Bayesian update lead to the same conclusions.

3.3.4 Conclusions

This case study, based on real on-site measurement, basically shows that:

- To improve the predictions of a simple degradation model, the best way is to update them with observations of the degradation itself. Indeed only updating the material parameters which are made inputs of the predictive model through the use of several empirical formulations is not efficient. Yet it is hard to say if this inefficiency is due to wrong prior distributions chosen, inaccuracy of the degradation model or of the combined empirical equations;

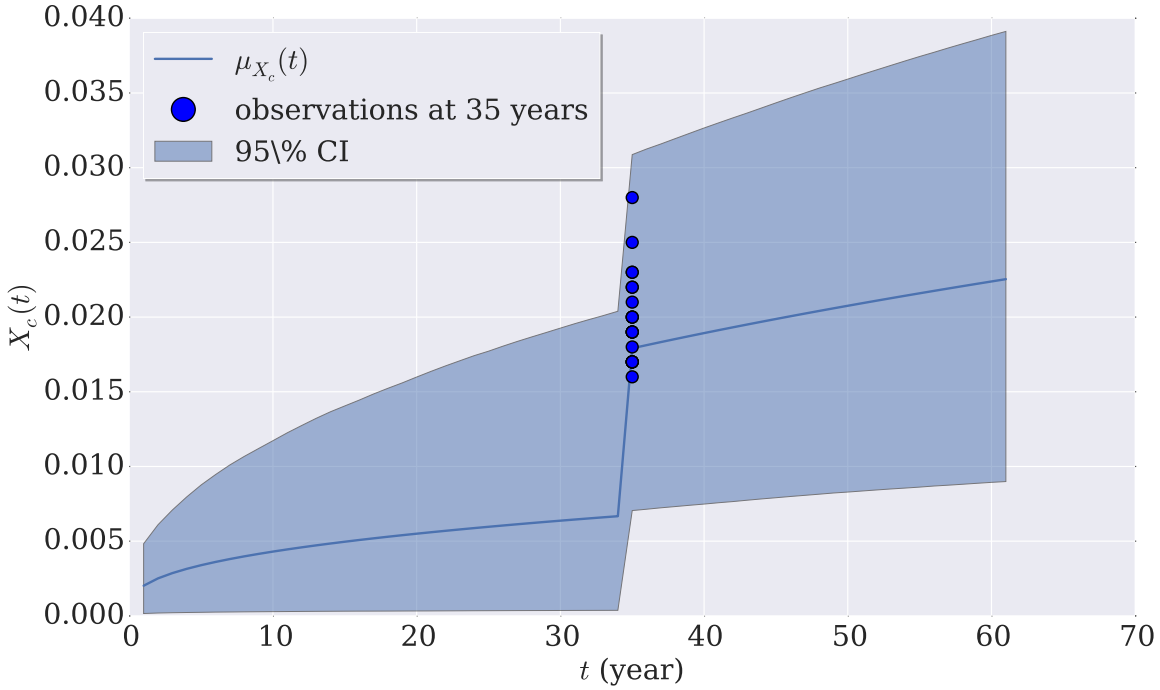

Figure 3.11 – Prior and posterior degradation predictions in the Case b-1.

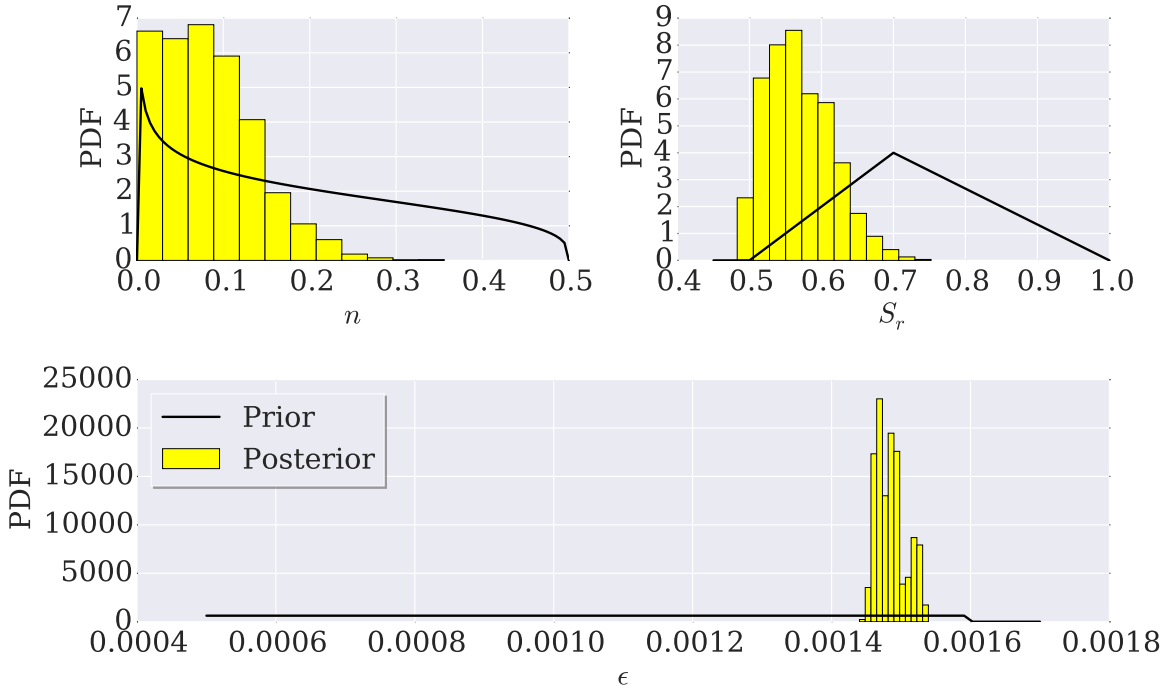

Figure 3.12 – Prior and posterior distributions of the updated random variable in the Case b-3.

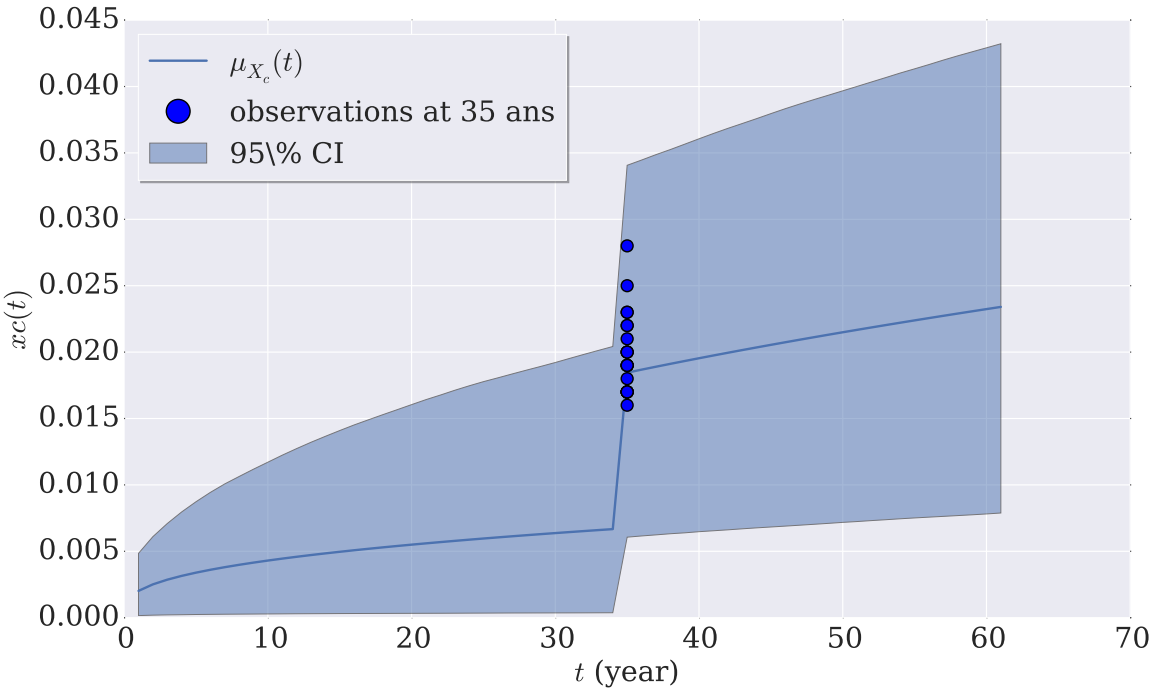

Figure 3.13 – Prior and posterior degradation predictions in the Case b-3.

- Using both some observed inputs and the output of the degradation model to update its prediction does not give results different enough compared to the use of the output alone.

Such conclusions somehow seem logical since all the degradation models (even the finite element ones) gather some physical (or not) parameters which are impossible to measure. Measurements of the model output are then necessary to identify these parameters.

In the case of non-destructive testings, it therefore calls for the development of non-destructive methods able to measure the degradation itself in order to be able to improve the predictions.

3.4 Conclusions

When dealing with degradation predictions, the situation which often occurs is that the inputs of the degradation model are known but with large uncertainties. In order to define an optimal inspection plan, the predictions have to be as accurate as possible. Mixing the data coming from various sources such as:

- Structure specifications;
- Destructive or non-destructive testings;

with the prior knowledge available on the predictive model inputs is made possible by the use of Bayesian statistics.

In a first part this chapter presents the basics on Bayesian statistics in order to calibrate/update the knowledge of given parameters through the use of conjugate distributions or Monte Carlo Markov Chains. The latter is used in the purpose of model calibration based either on:

- Output measurements of the model;
- Combined measurements of some inputs and the output of the model, considering the possible measurements error made on the inputs.

Despite the appealing properties of the Bayesian statistics, the second part the chapter discusses on their possible application in case of concrete structures. A case study which uses on-site measurements demonstrates that the most important data to obtain in order to efficiently update the degradation predictions are measurements of the degradation itself. Unfortunately non-destructive techniques are not yet able to measure the considered degradation (carbonation depth or chloride ingress). This thesis being dedicated to the use of NDT's to perform an inspection, the Bayesian statistics cannot be wisely used in the scope of this manuscript. Fortunately, the assessment of carbonation depth and chloride ingress profiles is an on-going subject of research with promising perspectives.

The next chapter is dedicated to the optimisation of the inspection plan in order to answer to the last objectives of this thesis: *When and how shall the structure be inspected ?*

CHAPTER 4

OPTIMISATION OF THE INSPECTION PLAN

4.1 Introduction

Chapter 1 has presented the basics of the stakeholders' concerns for the management of their structures. It has resulted in the overall question: *Where, when and how should the structure be inspected ?* That is the focus of risk based inspection that links an action with its cost and allows to formulate an optimisation problem (Rouhan and Schoefs (2003); Straub and Faber (2005)). The answer shall be given by an optimisation methodology as simple as possible with an affordable computational cost, independent of the structure and its degradation process, the inspection techniques, the maintenance and the failure modes.

In order for the optimisation problem to keep an affordable computational cost, the inspection locations may not take part in any optimisation problem. Indeed, it would lead to an infinite set of solutions. The purpose of Chapter 2 was thus to propose a modelling based either on an adaptive design of experiments or a low-discrepancy sequence in order to position the minimum inspection points needed to ensure a good approximate of the structure degradation state.

When and *How*, these terms have not been answered yet even if Chapter 2 briefly demonstrates their impact. The ambition of the present chapter is consequently to determine which is the best time interval between two inspections and which are the inspection methods to be used at each inspection.

The present chapter is thus decomposed in two parts. The first one presents the basics on the genetic algorithms, especially the non-dominated sorting genetic algorithm (NSGA-II), since their abilities to deal with discrete variables (i.e. the inspection dates, the capability of the inspection methods) with multiple objectives answer completely the optimisation problem of this manuscript. The second section is dedicated to the formalisation of this optimisation problem and to the application of the overall optimisation methodology on the two silver threaded examples.

4.2 Genetic algorithms

4.2.1 Description

Genetic algorithms (GAs), as the name suggests, were originally designed in order to simulate the evolution of natural ecological systems driven by genetic modifications (Fraser (1957); Holland (1975)). Basically any living being possesses a mix of the genetic patrimony of its parents. Throughout multiple generations, mutations may occur in this patrimony which will be persistent (i.e. the individual will survive) if the mutations help the concerned species to adapt itself to its environment, the so-called *natural selection* illustrated in Figure 4.1.

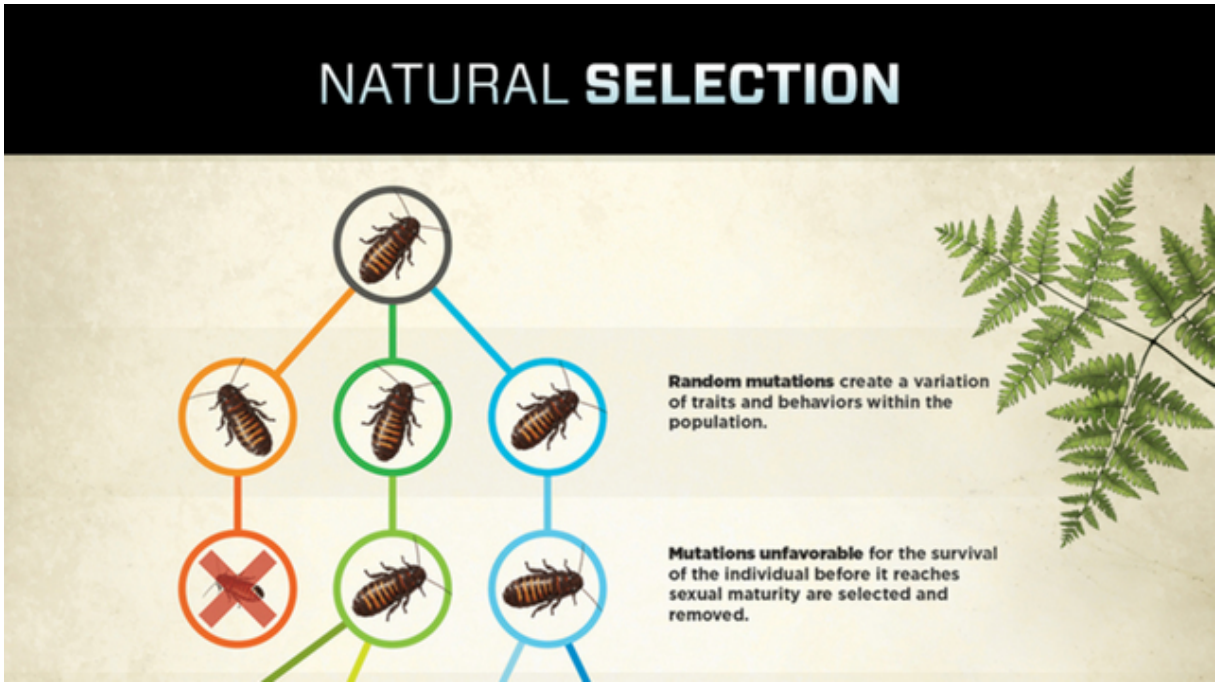

Figure 4.1 – Illustration of the natural selection. Credits: radio canada, sedna IV project.

Concerning the use of GA to find the optimal solution of a search problem like the one given in Eq. (1.34), the optimisation variables $\{x_0, \cdots, x_i\}$ are encoded into strings of alphabets with a given cardinality. Each string is a candidate solution for the optimisation problem, so-called *chromosome*, i.e. a combination of candidate values for each optimisation variables (Forrest (1993)). Each alphabet, or optimisation variable, is referred to as *gene* with their value being called *allele*. Any set of chromosomes is called a *population*.

In order to determine an order in a population, each chromosome is associated with the so-called *fitness* value, which would be for instance the objective function value for this candidate solution in the case of a mono-objective optimisation.

According to the natural evolution of ecological systems, the first set of candidate solutions results into new candidate solutions, i.e. a new population, through the process of *evolution*:

- Selection of candidates through the population;
- Recombination of the candidates;
- Mutation of the candidates;
- Replacement of the population.

Each step is lightly described in the following sections.

4.2.1.1 Main steps

4.2.1.1.1 Selection The basic idea behind the selection step is to define which chromosomes among the population are going to be used in order to create an offspring which will be used to define a new population of candidate solutions. The selection methods could be separated into two classes:

- Fitness-dependant methods;
- Ordinal methods.

One of the most famous fitness-dependant methods is the so-called *roulette-wheel* method (Goldberg (1989)). A probability is attributed to each candidate proportionally to its fitness contribution with respect to the fitness of the population (i.e. the sum of each individual fitness) such as

$$\mathscr{P}[S = c] = \frac{f_c}{\sum_{i \in \mathscr{C}} f_i}, \tag{4.1}$$

$\mathscr{C}$ being the set of chromosomes (i.e. the population), $f_i, i \in \mathscr{C}$ the fitness of chromosome i and S the selected candidate.

Candidates are selected with respect to these probabilities until the desired number of candidates is reached. Let us highlight that this selection process may select the same chromosomes multiple times, thus creating *copies* of them into the maiden pool.

Among the ordinal methods, first we could cite the tournament selection described in Goldberg (1989) which consists in selecting the best chromosome in a randomly created subset of the population. As in the previous method, the tournament is to be run until the desired number of candidates is reached, with or without replacement of the subsets which would again create copies into the maiden pool. Another famous ordinal method is the truncation selection introduced by Mühlenbein and Schlierkamp-Vooser (1993). The population is simply ordered by descending chromosome fitness and truncated up to the number of desired candidates.

4.2.1.1.2 Cross-over Recombination, or *cross-over*, as the name suggests combines chromosomes of the maiden pool called the *parents* in order to create offspring chromosomes with hopefully better fitness.

Figure 4.2 illustrates one of the numerous available methods to recombinate two chromosomes, the *k-point* cross-over method. Basically, *k* cross-over points are randomly located and the alleles of the chromosome between two points are swapped.

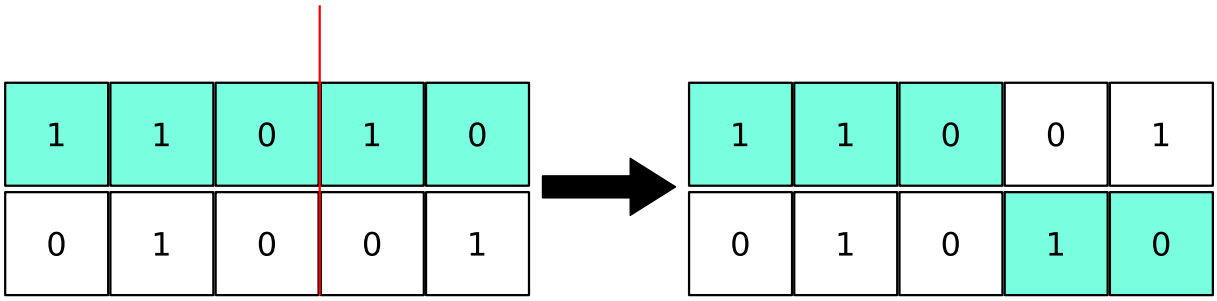

(a) One point recombination.

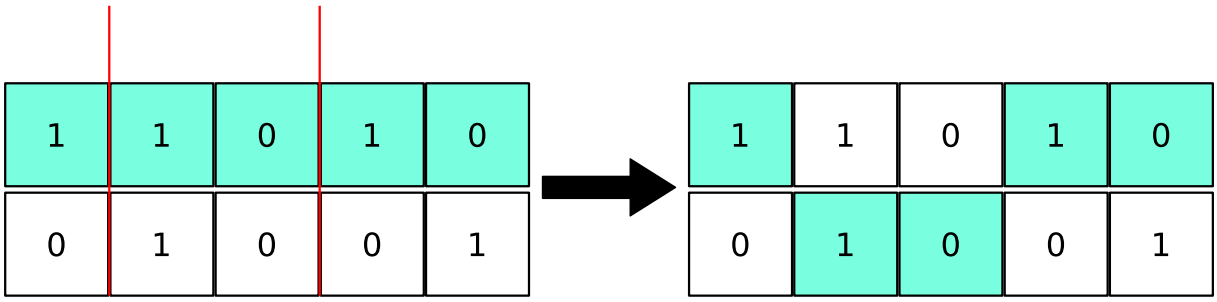

(b) Two points recombination.

Figure 4.2 – Illustration of k-point cross-over method.

Many methods could be cited, such as the uniform crossover which randomly swaps each allele. The interested reader is referred to Goldberg (1989) for more details.

As illustrated through Figure 4.2(b), unfortunately such recombination methods could result in no change. Moreover if the two parent chromosomes are identical, the cross-over may never give new chromosomes, thus the population would not evolve anymore. Mutation is applied to circumvent this issue.

4.2.1.1.3 Mutation Similarly to natural systems, the introduction of diversity into a population is the result of genetic mutations. They are usually performed after the cross-over step in GAs, with a low probability. The most simple mutation is the bit-flip mutation which consists in reverting a binary allele (i.e. from 0 to 1 or the opposite).

4.2.1.1.4 Replacement Once an offspring of new chromosomes has been created, they are to be used in order to form the new population. Two basic strategies of replacement are:

- Replace the parent population by the offspring;

- Replace some chromosomes of the parent population by some of the offspring. The number of replacement as well as the choice of the chromosomes replaced are parameters to be chosen.

More advanced replacement strategies have been derived in order to ensure that the best points of the population and the offspring are selected, such as the NSGA-II algorithm presented below.

4.2.2 NSGA-II

Proposed by Deb et al. (2000), the Non-dominated Sorting Genetic Algorithm (NSGA-II) is a genetic algorithm following the global steps presented in Section 4.2.1.1 where selection, cross-over and mutation methods are not prescribed. The NSGA-II specificity relies on the replacement step.

4.2.2.1 Non-dominated selection

The first step of the replacement is the detection of the non-dominated individuals considering both the maiden pool generated by the selection and the offspring resulting from recombination and mutation. Given a number of objectives to optimise n_{obj} and the set of chromosomes (i.e. the population and the offspring) $\mathscr{C}$, any candidate solution $p \in \mathscr{C}$ is dominating any other candidate solution $q \in \mathscr{C}$, i.e. $p \prec q$, if it follows:

$$\text{if } \begin{cases} f_i(p) & \leq & f_i(q) \\ \exists f_i(p) & < & f_i(q) \end{cases} \begin{matrix} p \prec q \\ , \quad i = 1, \ldots, n_{obj} \\ p, q \in \mathscr{C}, p \neq q \end{matrix} \tag{4.2}$$

Finding all the non-dominated chromosomes results in a first front, which is namely the Pareto front. These candidates are removed from $\mathscr{C}$, all the new non-dominated solutions detected are gathered in a second front, and this process is repeated until every front has been identified.

Figure 4.3 presents an example with two objectives functions $f_1(x)$ and $f_2(x)$ with the first three fronts identified. By using the initial population and the resulting offspring to detect the best solutions, it clearly appears that if any parent chromosome has resulted in a worse child, the latter will at least not be selected without its parent. It thus ensures that the replacement will not result in a new population worse than the previous one. This property in GAs is called *elitism* and has been proved to increase the GAs efficiency (Rudolph (1999); Zitzler et al. (2000)).

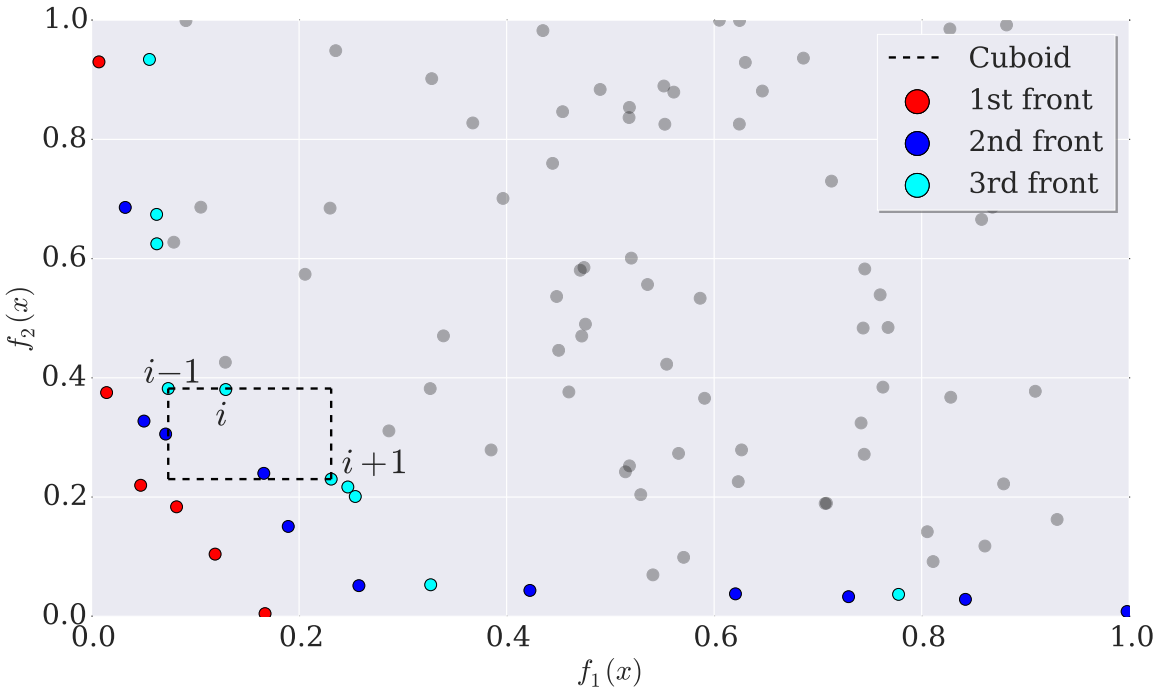

Figure 4.3 – Illustration of the three first non-dominated fronts identified

4.2.2.2 Replacement

The new population is then filled by the candidates in the successive fronts.

Considering a front construction, each candidate in a given front is equivalently efficient. If a front cannot be fully included in the new population (i.e. the population size would become too large), in order to select which candidates of this front are to be included in the new population another criterion has been introduced by Deb et al. (2000) called the *crowding distance*. The crowding distance is defined as the average side-length of the largest cuboid wrapping a candidate without including any other chromosome. An example of such cuboid is given for the third non-dominated front in Figure 4.3.

Consequently, if candidates of the same front have to be selected the NSGA-II will select the points associated with the greatest crowding distance (i.e. the more isolated ones) in an attempt to increase the space exploration.

4.2.3 Conclusion

This section has seen the presentation of the general framework for genetic algorithms. Among them, the NSGA-II has been chosen mainly due to its *elitist* property and space-search filling attempts. The following section is dedicated to the definition of the optimisation problem which points out the need of a genetic algorithm.

4.3 Optimisation problem

4.3.1 Definitions

Referring to Chapter 1, the general form of an optimisation problem reads

$$\min_{x_0,\cdots,x_i} \left\{ f_{obj}^{(0)}, \cdots, f_{obj}^{(j)} \right\} \text{ such that } \left\{ c^{(0)} \geq c_t^{(0)}, \cdots, c^{(k)} \geq c_t^{(k)} \right\}, \tag{1.34}$$

where $\{x_0, \cdots, x_i\}$ are the optimisation variables, for instance inspection (or maintenance) time and quality; $\left\{ f_{obj}^{(0)}, \cdots, f_{obj}^{(j)} \right\}$ are the objective functions which are to be minimised (or maximised), such as the long-term total cost C_{tot} or the redundancy level of a system; lastly $\left\{ c^{(0)} \geq c_t^{(0)}, \cdots, c^{(k)} \geq c_t^{(k)} \right\}$ are the different constraints that have to be fulfilled.

4.3.2 Objective functions

As mentioned in Chapter 1, the objective of this thesis is to propose a methodology to minimise the exploitation cost of reinforced concrete structures. This cost generally writes (Frangopol et al. (1997); Sheils et al. (2010a))

$$C^{tot} = C^{In} + C^{Ma} + C^{F}, \tag{4.3}$$

with C^{In}, C^{Ma} and C^{F} are the inspection, maintenance and failure costs respectively. In a probabilistic framework, each cost $C^{\bullet}$ is substituted by its mathematical expectation $\mathbb{E}[C^{\bullet}]$.

4.3.2.1 Cost functions

Given:

- the IMRM represented in Figure 2.10 with m branches, each one having a probability $\mathscr{P}_i$ to be realised ;
- the time horizon t_{lim} discretised into t_{tot} time steps;
- the inspection dates $\boldsymbol{t_{In}}$;
- a discount rate r;

General models for the inspection, maintenance and failure expected costs respectively write

$$\mathbb{E}\left[C^{In}\right] = \sum_{i=1}^{m} \mathscr{P}_i \sum_{t \in \boldsymbol{t_{In}}} \frac{\boldsymbol{n_I}^{(i,t)} \boldsymbol{C_{In}}^{(t)}}{(1+r)^t}, \tag{4.4}$$

$$\mathbb{E}\left[C^{Ma}\right] = C_{Ma} \sum_{i=1}^{m} \mathscr{P}_i \sum_{t \in \boldsymbol{t_{In}}} \frac{\mathbb{1}_{i,t}^{Ma}}{(1+r)^{t+t_{Ma}}}, \tag{4.5}$$

$$\mathbb{E}\left[C^{F}\right] = C_{F} \sum_{i=1}^{m} \mathscr{P}_i \sum_{t \in \boldsymbol{t_{In}}} \frac{\mathbb{1}_{i,t}^{F}}{(1+r)^{t+t_{R}}}, \tag{4.6}$$

where:

- n_I^t is the number of points inspected at time t in the branch i;
- $\mathbb{1}_{i,t}^{Ma}$ (or $\mathbb{1}_{i,t}^{F}$) are equal to 1 if a maintenance (or repair) action is decided on branch i at time t, 0 otherwise;
- t_{Ma} and t_R are respectively the maintenance and repair delays, which could be due to financial or technical consideration;

These are generic formulations based on the decision tree. They do not make any assumption on the costs of an inspection, a maintenance and a failure written respectively as C_{In}, C_{Ma} and C_F. For instance, the inspection cost could be dependant on the installation cost, the post-treatment cost, the inspection technique, etc... The failure cost could include direct and indirect costs such as the repair cost and the impact of a loss of reputation due to the failure.

4.3.2.2 Mono-objective optimisation

The objective could basically be to minimise the exploitation cost alone. The optimisation problem is therefore defined as follows.

Assuming that:

- The time between two inspections shall be constant in order to best represent the stakeholders habits;
- Only one inspection technique may be used at an inspection date;

And given:

$$\begin{cases} \text{The inspection types} & \boldsymbol{T_{In}} = [0, 1, 2, \cdots, n_T] \\ \text{The corresponding inspection costs} & \boldsymbol{C_{In}} = [C_{In}^{(0)}, C_{In}^{(1)}, \cdots, C_{In}^{(n_T)}] \\ \text{The time horizon} & t_{lim} \\ \text{The discount rate} & r \\ \text{The maintenance delay} & t_{Ma} \\ \text{The repair delay} & t_R \\ \text{The preventive degradation index} & D_P \\ \text{The curative degradation index} & D_F \\ \text{The IMRM} & \end{cases} \tag{4.7}$$

The optimisation problem is to find:

$$\left\{ \text{The time between two inspections} \quad \Delta t_{In} \right. \tag{4.8}$$

In order to minimise the total expected cost $\mathbb{E}\left[(C_{tot})\right]$, under given constraints, where

- $i \in \boldsymbol{T_{In}}$ means inspection i with cost $C_{In}^{(i)}$ is performed;
- $\boldsymbol{Pl_{In}}^{(i)}$ is the inspection method used for the $i-th$ inspection.

4.3.3 Multi-objective optimisation

Any objective could be added to the minimisation of the exploitation cost. Considering the IMRM which provides confidence interval for its outputs related to the inspection errors (see Section 2.4.2.2), we shall consider the confidence interval of the expected exploitation cost as an objective to be minimised.

4.3.3.1 Pareto front

Intuitively, an accurate inspection is likely to be more expensive than an inaccurate one. Thus by reducing the confidence interval of the expected cost (i.e. using an accurate inspection technique) the expected cost will increase.

These two objectives are therefore called *competing* objectives. In this context, no global solution exists but only a set of optimal solutions, the so-called *Pareto front*, all of them being a compromise between the two competing objectives.

The Pareto front is mathematically composed by all the solutions which are not dominated (see Eq. (4.2)), in other words the Pareto front is the first front derived by the NSGA-II algorithm, as illustrated in Figure 4.3.

With this set of optimal solutions, the question is: *Which solution is to be preferred ?* Here comes the so-called *multi-criteria* methodology which consists in the selection among these solutions the one which best answers to quantitative or qualitative criterion of the stakeholder. It could be for instance the solution which:

- Minimises the highest probability of failure encountered during the life-cycle;
- Minimises the risk of exceeding an annual budget;
- Leads to the smaller number of inspections.

4.3.3.2 Problem definition

In this multi-objective context, the optimisation problem is thus defined as follows.

Assuming that:

- The time between two inspections shall be constant in order to best represent the stakeholders habits;
- Only one inspection technique may be used at an inspection date;

And given:

$$\begin{cases} \text{The inspection types} & \boldsymbol{T_{In}} = [0,1,2,\cdots,n_T] \\ \text{The corresponding inspection costs} & \boldsymbol{C_{In}} = [C_{In}^{(0)}, C_{In}^{(1)}, \cdots, C_{In}^{(n_T)}] \\ \text{The time horizon} & t_{lim} \\ \text{The discount rate} & r \\ \text{The maintenance delay} & t_{Ma} \\ \text{The repair delay} & t_R \\ \text{The preventive degradation index} & D_P \\ \text{The curative degradation index} & D_F \\ \text{The IMRM} & \end{cases} \tag{4.9}$$

The optimisation problem is to find:

$$\begin{cases} \text{The time between two inspections} & \Delta t_{In} \\ \text{The inspection plan} & \boldsymbol{Pl}_{In} = \left[\boldsymbol{T_{In}}^{(0)}, \ldots, \boldsymbol{T_{In}}^{(t_{lim}/\Delta t_{In})}\right] \end{cases} \tag{4.10}$$

In order to minimise the total expected cost $\mathbb{E}[(C_{tot})]$ and its confidence interval $CI(\mathbb{E}[(C_{tot})])$ under given constraints, where

- $i \in \boldsymbol{T_{In}}$ means inspection i with cost $C_{In}^{(i)}$ is performed;
- $\boldsymbol{Pl_{In}}^{(i)}$ is the inspection method used for the $i-th$ inspection.

The final solution is selected among the Pareto front by considering the given criteria.

4.4 Study case

4.4.1 Presentation of the study case

Based on the degradation modelling of the balconies proposed in Section 2.5, the present illustration thus makes use of the IMRM (i.e. the decision tree shown in Figure 2.10) and the ADoE in order to optimise the inspection plan of the balconies. Prior to the optimisation the different cost functions mentioned in Section 4.3.2.1 are introduced in the following.

4.4.1.1 Inspection costs

The inspection cost $\boldsymbol{C_{In}}$ (see Eq. (4.4)) is composed of the unit cost for each inspection method used in the inspection plan. This illustration considers that inspections are performed by non-destructive testing, according to the methodology described in Garnier et al. (2014).

For the sake of completeness, the basic idea is to combine the results of different non-destructive techniques (NDT's) which are sensitive to the quantity of interest one wants to measure. According to the results of the research project EVADEOS funded by the French National Research Agency, the chosen combination uses 4 NDT's: impact echo, capacity, ultrasounds and radar. Including, per point:

- The cost of a qualified technician;
- The cost of a qualified engineer;
- The cost of the material (including amortisation);
- The cost of the measure (i.e. multiple points are performed to get one measure);
- The transport cost of the needed material;
- The rental cost of an aerial lift;

the cost of this combination has been estimated around 400 euros per point. It indeed seems high, yet one has to remind that such combinations are not yet industrialised and we could thus expect this cost to decrease in the future.

Unfortunately, this combination only helps to measure both the concrete porosity and saturation rate. No combination able to measure a carbonation depth actually exists. Moreover the knowledge on the accuracy of such combination is leaking.

This illustration thus extrapolates on the future developments which are on-going and proposes three different levels of costs and accuracy for the inspection methods, presented in Table 4.1.

Inspection Technique	0	1	2
Cost per point (euro)	500	300	100
Coefficient of variation	5%	10%	25%

Table 4.1 – Inspection costs and accuracy for each technique.

4.4.1.2 Maintenance costs

Bastidas-Arteaga et al. (2010) proposed a summary of different maintenance technique costs for RC concrete structures. The solution retained in this illustration is to replace the concrete

cover with wet shotcrete (projected concrete). The costs associated with such technique are gathered in Table 4.2.

Item	*Cost (Euro / m^3)*
Hydrodemolition	1500
Waste management	172
Materials	1309
Labor	685
Equipments	183

Table 4.2 – Maintenance costs

A balcony is assumed to be 3 metres long, 1.2 metres wide and 6 centimetres high (twice the concrete cover thickness then). It leads to a rounded cost of 800 euros for maintaining a balcony.

Local maintenance actions are not considered due to the actual ignorance of any positive effect of such maintenance technique. Indeed creating a composite material has a known worsening effect on the corrosion initiation and corrosion rate since it creates difference of potentials.

4.4.1.3 Failure costs

Finally, the failure implies that corrosion may have occurred. In this case the reinforcement is to be exchanged. Bastidas-Arteaga and Schoefs (2012) for instance proposed to use a factor 2 between the maintenance costs and the repair costs (which also implies the replacement of the concrete cover). Following this idea, the failure of a balcony is expected to cost 1,600 euros.

4.4.1.4 Summary

Table 4.3 presents a summary of the different costs introduced above. As a reminder, for the three cases considered, all of them with a time horizon of 60 years:

- One and bi-dimensional cases: 12 balconies are inspected at the same time, repair or maintenance actions are applied to 120 balconies simultaneously;
- System bi-dimensional cases: 12 balconies are inspected at the same time, repair or maintenance actions may be applied to multiple buildings, each of them composed of 120 balconies.

The discount rate r is set to 0, according to the inflation perspectives in force at the writing time of the present manuscript.

All the thresholds and delays are given in Section 2.5. Last but not least, the maintenance/repair delay is set equal to 3 years. It includes:

- 2 years to raise funds and select the company;

- 1 year to perform the maintenance/repair action.

The maximum number of inspected point depends on the inspection technique. The budget allowed for an inspection is set to 6,000 euros per balcony, with a minimum delay between two inspections equal to 10 years: that was suggested by the stakeholders to preserve the life quality of inhabitants and due to the expectation of inhabitants turn over in the apartments.

Item	*Cost (Euro)*
Inspection type 0	500 (per point and balcony)
Inspection type 1	300 (per point and balcony)
Inspection type 2	100 (per point and balcony)
Maintenance action	800 (per balcony)
Repair action	1600 (per balcony)

Table 4.3 – Summary of the different costs

4.4.2 One-dimensional problem

4.4.2.1 Mono-objective optimisation

The first approach used is a mono-objective optimisation. According to the problem definition in Section 4.3.2.2, the optimisation variable is the time step between two inspections Δt_{In}.

Considering that the inspection method 1 (see Table 4.1) is used, the predicted inspection, maintenance and failure costs for Δt_{In} ranging from 10 to 60 years are shown in Figure 4.4 and Figure 4.5. The first considers that unnecessary inspections are performed, not the latter. The main difference between these two cases is the inspection costs for $\Delta t_{In} \leq 20$ years. An inspection interval of 10, 15 of 30 years may be chosen thanks to this. In the following, this manuscript thus only considers that unnecessary inspections can be avoided.

In both cases, the first point to highlight is the presence of several local solutions, including at 15 and 30 years for instance, due to the change of the number of inspections performed with a given lifetime ($\Delta t_{In} = 29$ years gives two inspections, with 30 years only one). Together with the use of discrete optimisation variables, these aspects give credits to the use of genetic-algorithms which are less sensitive to local solutions than gradient-based methods.

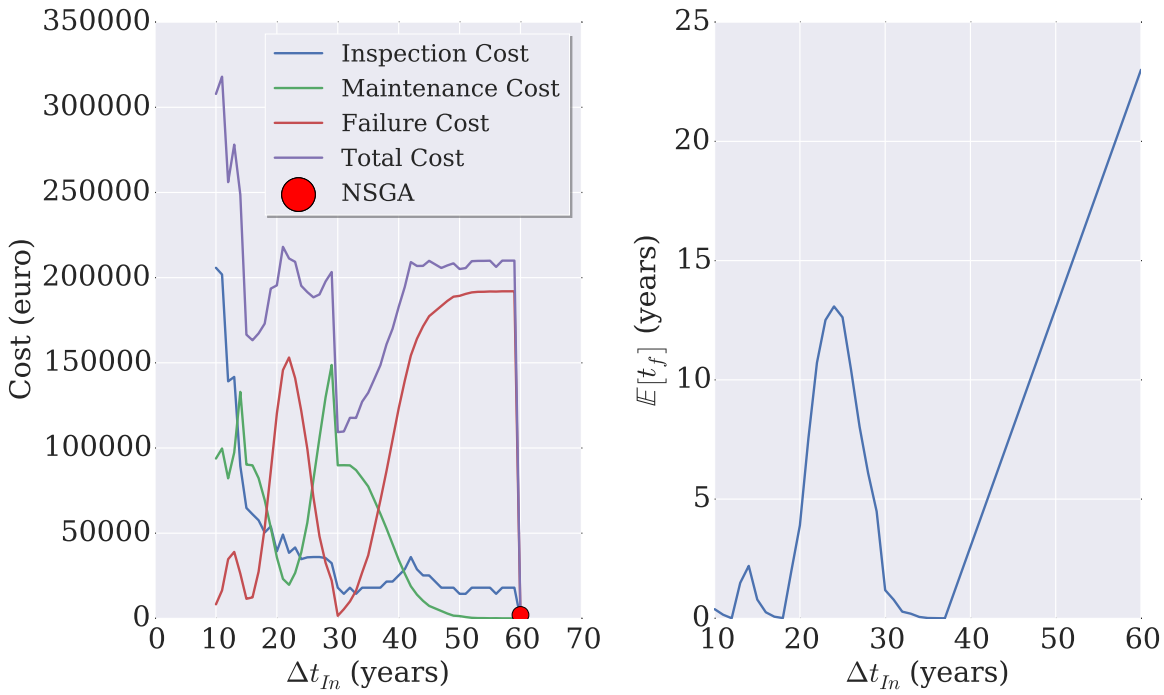

Figure 4.4 – Optimisation of the total expected cost without avoiding useless inspections. The red dot corresponds to the solution found by the NSGA-II algorithm.

The global solution in both cases is found by the NSGA algorithm. The optimal Δt_{In} is equal to the time horizon: no inspection shall be performed. Indeed, regarding the IMRM in Figure 2.10 and considering the degradation process which does not lead to the limit state of service, no maintenance or repair action can be performed without an inspection. Thus the optimum cost is obtained with no inspection being performed. Let define the time during which there is more than 50% of chances that the balcony is in the failure state as the time spent in the failure state t_f.

On the right panels of Figures 4.4 and 4.5 the expectation of the time spent by a balcony in the failure state $\mathbb{E}\left[t_f\right]$ clearly indicates that with no inspection, the reinforcement is expected to be depassivated during 23 years. Obviously such situation is unacceptable and calls for either a constrained optimisation problem or a multi-objective one. The last solution has been chosen in this manuscript since it also aims at optimising a second objective (i.e. the confidence interval of the total cost expectation) according to the problem defined in Section 4.3.3. A third objective is thus added: minimising the expectation of the time spent in the failure state $\mathbb{E}\left[t_f\right]$. This is the purpose of the following section.

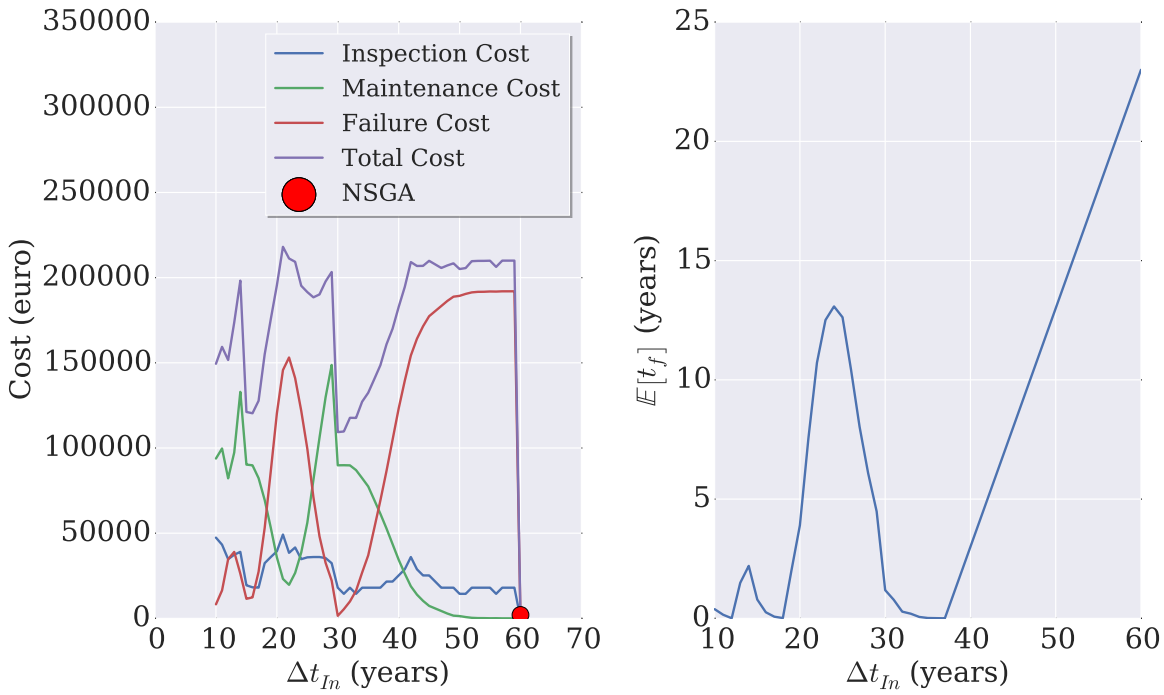

Figure 4.5 – Optimisation of the total expected cost with useless inspections being avoided. The red dot corresponds to the solution found by the NSGA-II algorithm.

4.4.2.2 Multi-objective optimisation

Basically, the problem with multi-objective optimisation comes with competing objective functions which lead to a Pareto front of optimal solutions. The present optimisation problem deals with 3 objectives:

- The expected total cost, competing with its confidence interval since an increase of the latter implies the use of a cheaper inspection method;
- The expected time spent in the failure state, not competing with any objective as shown through Figures 4.4 and 4.5. A focus is made on several points to point out the corresponding values of the optimisation variables defined in Eq. (4.10), i.e. the time interval between two inspections $\Delta t_i In$ and the vector gathering the method used at each inspection $\boldsymbol{Pl}_{In}$.

Figure 4.6 presents the Pareto front obtained after 10 generations of 50 chromosomes, projected on the plan shaped by $\mathbb{E}[C_{tot}]$ and its confidence interval $CI(\mathbb{E}[C_{tot}])$. Figure 4.7 and Figure 4.8 present the Pareto front projected on the two other plans formed by the objective functions, $\mathbb{E}[C_{tot}]$ and $\mathbb{E}\left[t_f\right]$ for the first,$CI(\mathbb{E}[C_{tot}])$ and $\mathbb{E}\left[t_f\right]$ for the latter.

It clearly appears that the minimisation of $\mathbb{E}\left[t_f\right]$ is not competing with the other two objectives.

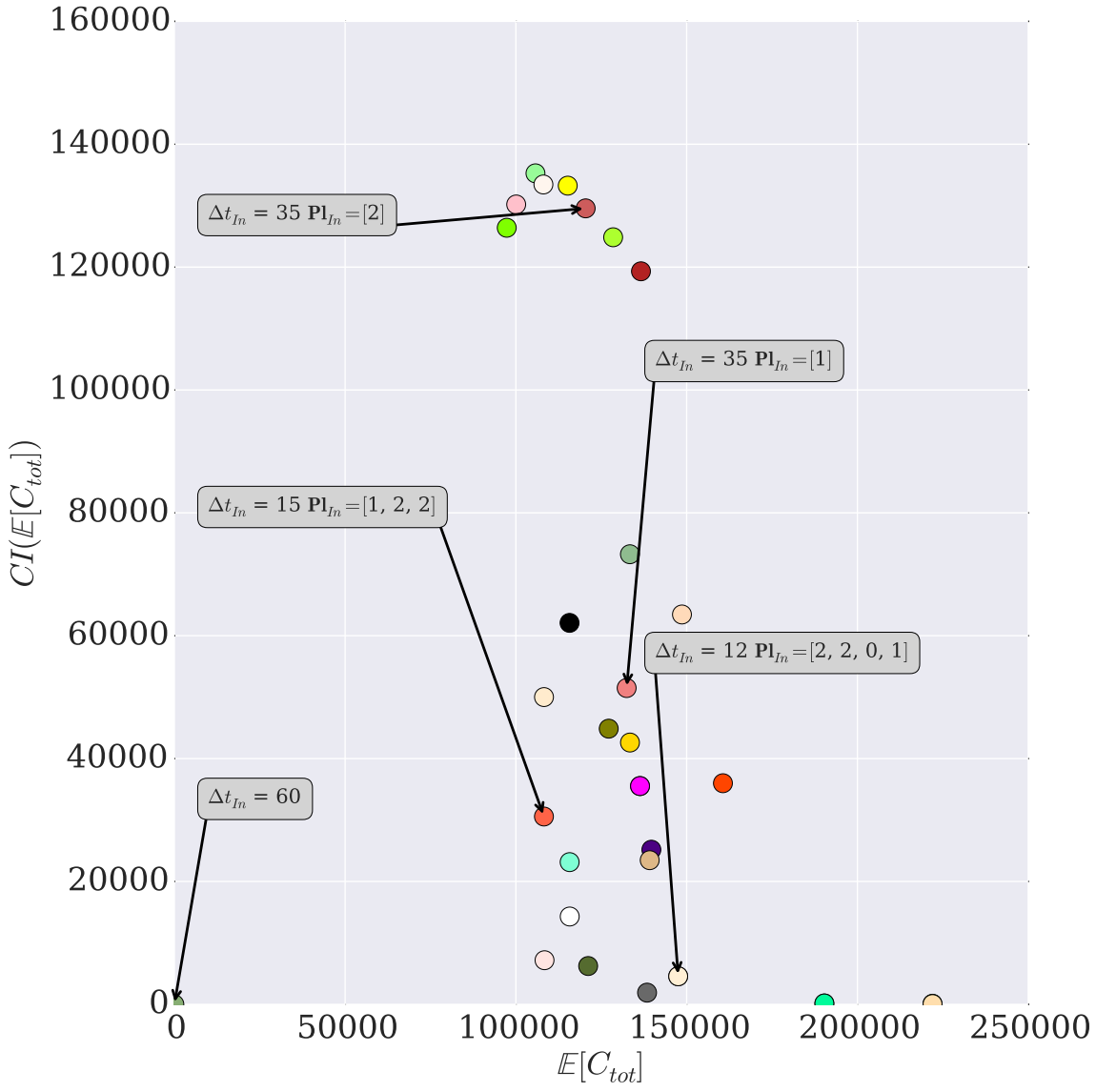

Figure 4.6 – Pareto front projected on the plan made by the expected total cost and its confidence interval.

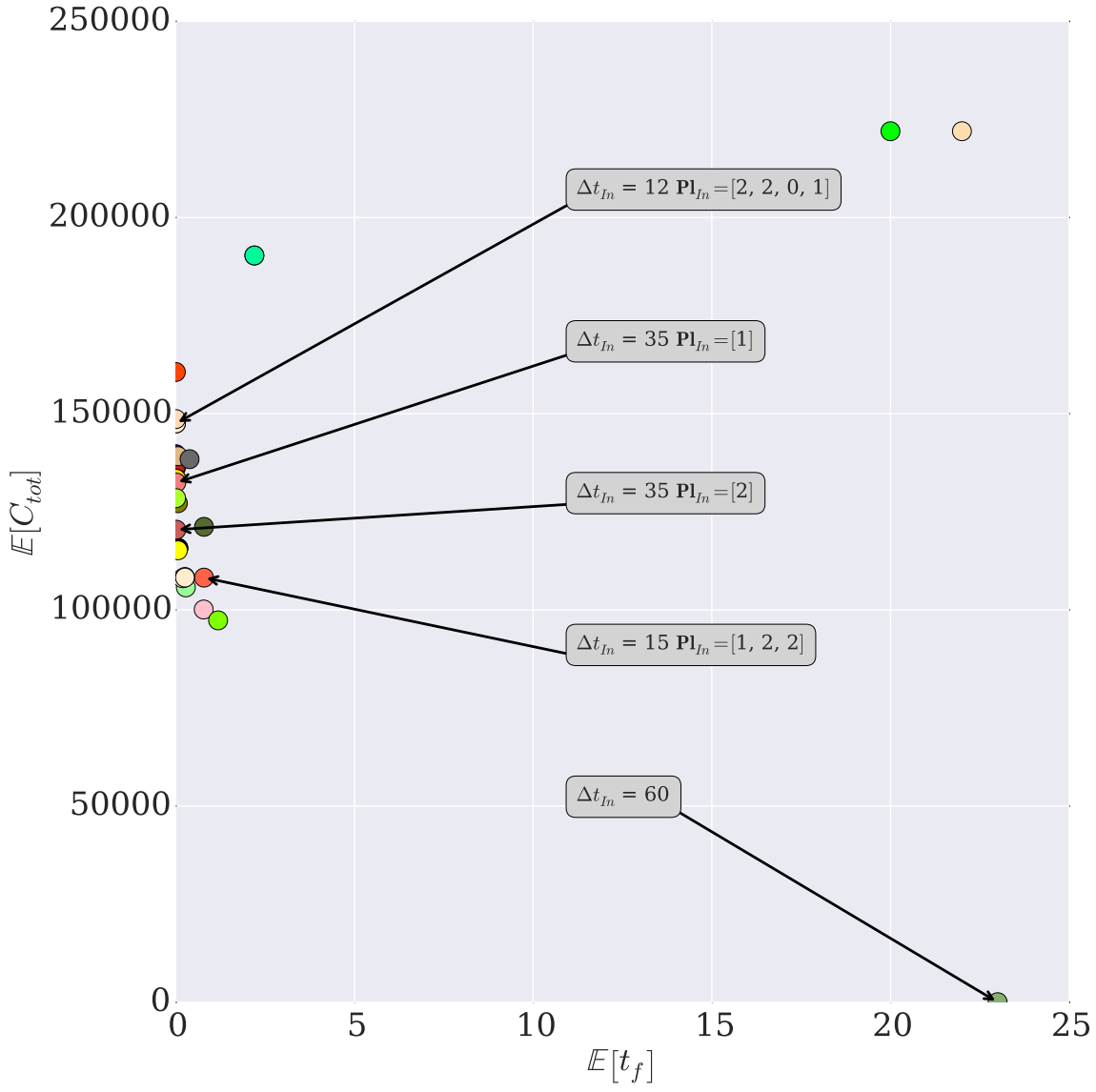

Figure 4.7 – Pareto front projected on the plan made by the expected total cost and the expected total time spent in the failure state.

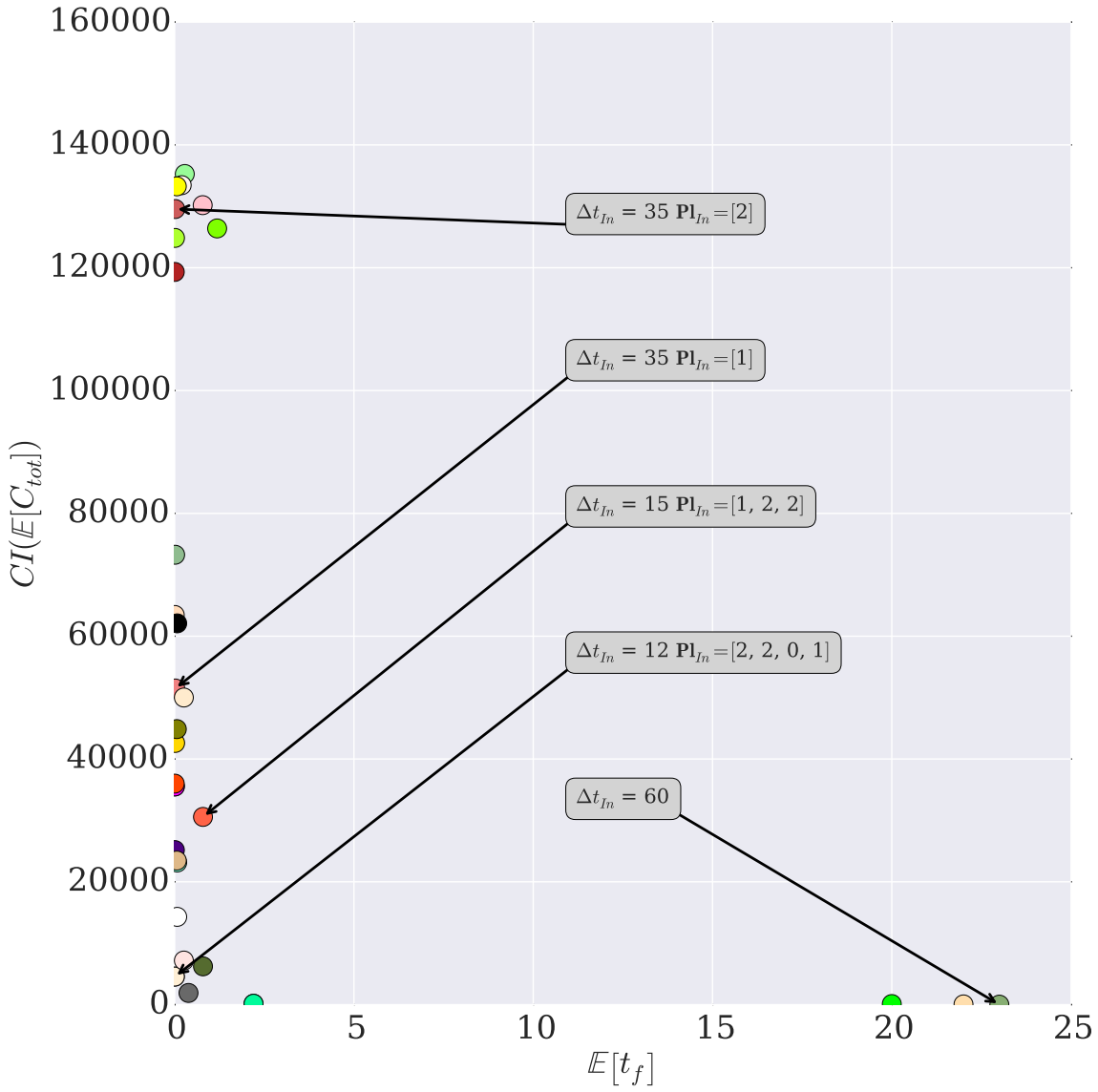

Figure 4.8 – Pareto front projected on the plan made by the confidence interval of the expected total cost and the expected total time spent in the failure state.

Indeed the problem with such set of solutions is to select one of them. For this purpose, a first criterion is applied: *an expected time spent in the failure state higher than 1 year is unacceptable*. Figure 4.9 presents the candidate solutions extracted from the Pareto front according to this criterion. Basically from this reduced number of solutions, three points are extracted.

4.4.2.2.1 First candidate solution An inspection plan with a time interval between two inspections Δt_{In} equals to 31 years (i.e. one inspection during the lifetime of the building), where the inspection number 2 is used (see Table 4.1). This solution presents the lowest

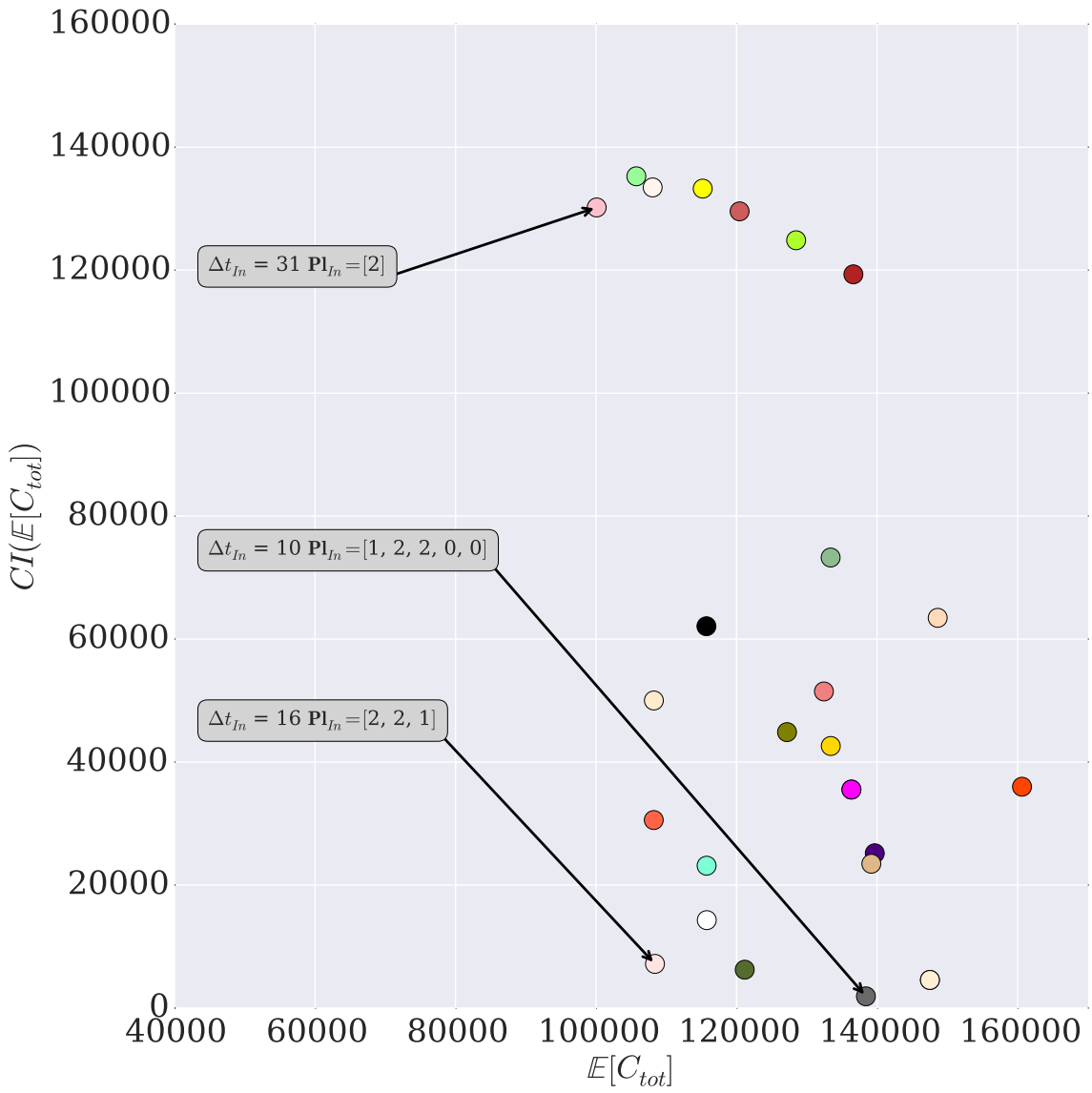

Figure 4.9 – Pareto front projected on the plan made by the expected total cost and its confidence interval, without the solutions giving an expected total time spent in the failure state higher than one year.

$\mathbb{E}[C_{tot}]$, 100,000 euros, but one of the largest confidence intervals (due to the inspection method) equal to $[20,000; 150,470]$ euros.

$n°$	μ_{Ma}	$[CI^-; CI^+]_{Ma}$	μ_F	$[CI^-; CI^+]_F$
0	0.04	[0.81; 0.61]	0.97	[1; 0.38]
1	0.96	[0.19; 0.38]	0.03	[0; 0.62]

Table 4.4 – Mean and confidence interval of the number of maintenances and repairs with an inspection interval of 31 years.

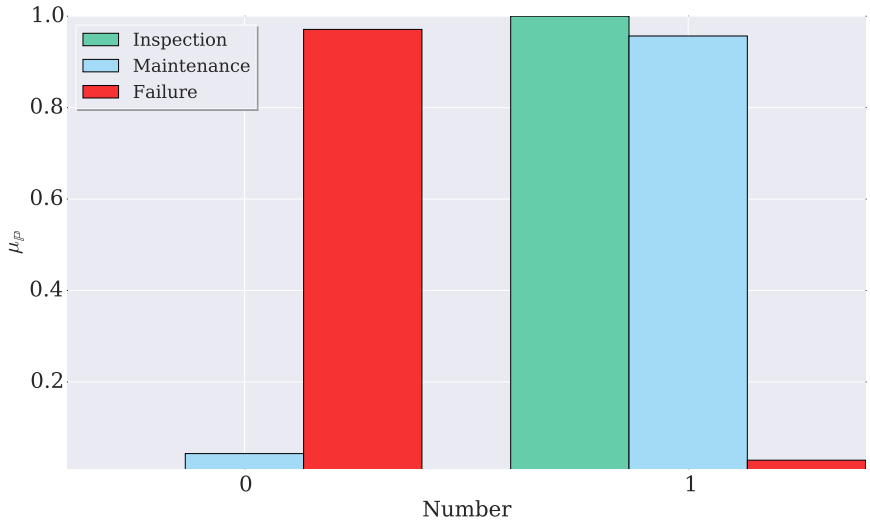

Figure 4.10 – Probabilistic distributions for the number of maintenances, repairs and inspections with an inspection interval of 31 years.

Figure 4.10 illustrates the corresponding probabilistic distributions of the number of maintenances, inspections and repairs. With this candidate solution, the unique inspection is not judged as useless and it seems nearly certain that one maintenance action will be performed. However due to the use of the less accurate inspection method, there exists a significant probability (with respect to the 95% confidence interval of the inspection method) that a repair action may be decided instead of a maintenance one as written in Table 4.4. On one hand, overestimating the degradation process may lead to a repair with a probability of 62%. On the other hand an underestimation may result in neither repair nor maintenance during the time horizon.

4.4.2.2.2 Second candidate solution An inspection plan with $\Delta t_{In} = 10$ years leads to 5 inspections respectively performed with inspection techniques 1, 2, 2, 0 and 0 (see Table 4.1). The expectation of the total costs is the highest of the three selected points (138,000 euros) yet the width of its confidence interval equal to 1900 euros is the lowest of the Pareto front. However, as mentioned in Section 2.4.2.2, the term *confidence interval* may not be really fitted in this case. The lower bound is up to 183,000 euros, the higher bound to 185,000 euros. Indeed these are not any more bounds for the expected total cost.

Figure 4.11 shows that the mean tendency (i.e. with perfect inspections) results in a pretty high probability of maintenance with 3 inspections really needed instead of 5.

$n°$	μ_{Ma}	$[CI^-; CI^+]_{Ma}$	μ_F	$[CI^-; CI^+]_F$
0	0.03	$[0.39; 0.36]$	0.97	$[0.61; 0.63]$
1	0.95	$[0.61; 0.41]$	0.03	$[0.39; 0.37]$
2	0.02	$\left[10^{-5}; 0.23\right]$	0	$[0; 0]$
3	0	$[0; 0]$	0	$[0; 0]$
4	0	$[0; 0]$	0	$[0; 0]$
5	0	$[0; 0]$	0	$[0; 0]$

Table 4.5 – Mean and confidence interval of the number of maintenances and repairs with an inspection interval of 10 years.

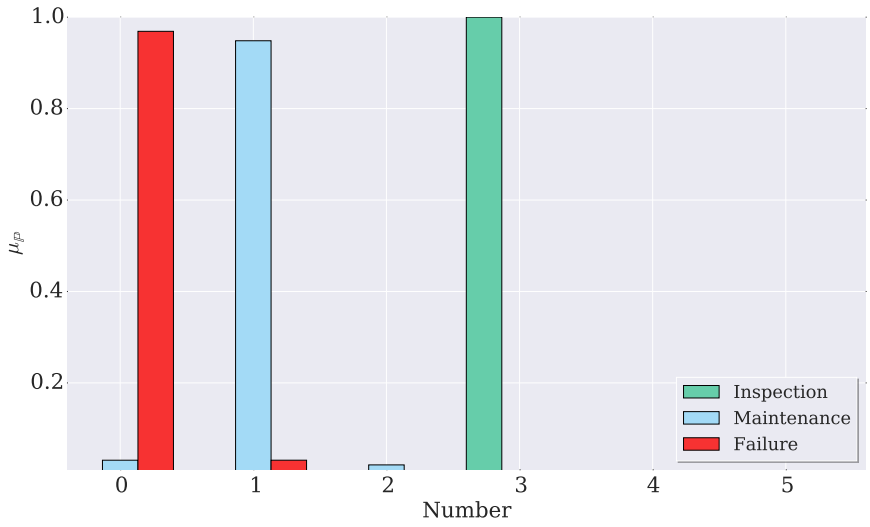

Figure 4.11 – Probabilistic distributions for the number of maintenances, repairs and inspections with an inspection interval of 10 years.

Table 4.5 illustrates the phenomenon. In both cases, underestimating and overestimating the degradation leads to an increase of the probability of repairing, from 3% to respectively 39% and 37%. In one case, a maintenance action is avoided thus leading to a repair one at the following inspection. In the other case, instead of a maintenance action, the overestimate leads to a repair decision.

4.4.2.2.3 Third candidate solution An inspection plan with $\Delta t_{In} = 16$ years which leads to 3 inspections, the firsts two performed with inspections number 2, the last one with inspection number 1 (see Table 4.1). $\mathbb{E}[C_{tot}]$ is equal to 108,000 euros, and $CI(\mathbb{E}[C_{tot}])$ to 7,179 euros. Again, the expected total cost is outside of the bounds ranging from 164,832 euros to 172.011 euros. The confidence bounds of the inspection results once more lead to an increase of the failure probability, as shown in Table 4.6. Like the second candidate

solution, the mean prediction illustrated in Figure 4.12 leads to a significant probability of one maintenance action being performed during the time horizon of 60 years.

$n°$	μ_{Ma}	$[CI^-; CI^+]_{Ma}$	μ_F	$[CI^-; CI^+]_F$
0	0.07	$[0.58; 0.72]$	0.93	$[0.42; 0.28]$
1	0.93	$[0.42; 0.27]$	0.07	$[0.58; 0.72]$
2	0	$[0; 0]$	0	$[0; 0]$
3	0	$[0; 0]$	0	$[0; 0]$

Table 4.6 – Mean and confidence interval of the number of maintenances and repairs with an inspection interval of 16 years.

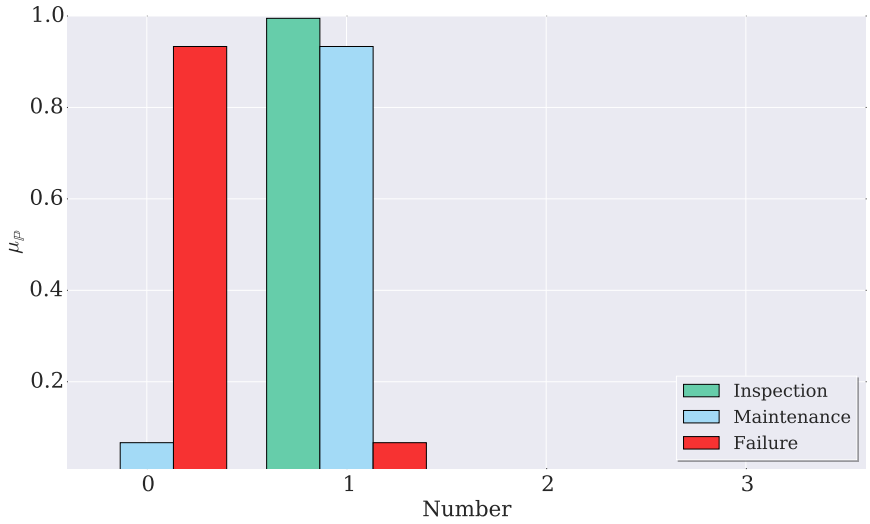

Figure 4.12 – Probabilistic distributions for the number of maintenances, repairs and inspections with an inspection interval of 16 years.

4.4.2.3 Multi-objective optimisation with a supplementary criterion

Consequently to the precedent results, another criterion is to be applied on the Pareto front. In order to avoid really bad measurement error effects which could lead to an increase of the failure probability, the Pareto front presented in Figure 4.13 is now reduced by two criteria:

$$\begin{cases} \mathbb{E}\left[t_f\right] & \leq & 1 \text{ year} \\ \mathbb{E}\left[C_{tot}\right] & \in & \left[CI\left(\mathbb{E}\left[C_{tot}\right]\right)^-; CI\left(\mathbb{E}\left[C_{tot}\right]\right)^+\right] \end{cases} \tag{4.11}$$

where $CI\left(\mathbb{E}\left[C_{tot}\right]\right)^-$, resp. $CI\left(\mathbb{E}\left[C_{tot}\right]\right)^+$, is the bound of $\mathbb{E}\left[C_{tot}\right]$ resulting from the complete underestimation, resp. overestimation, of the true degradation approximated by the inspections.

Mainly candidate solutions with both a low expected total cost and confidence interval were removed. From this front, the best points for each objective are selected. The first one

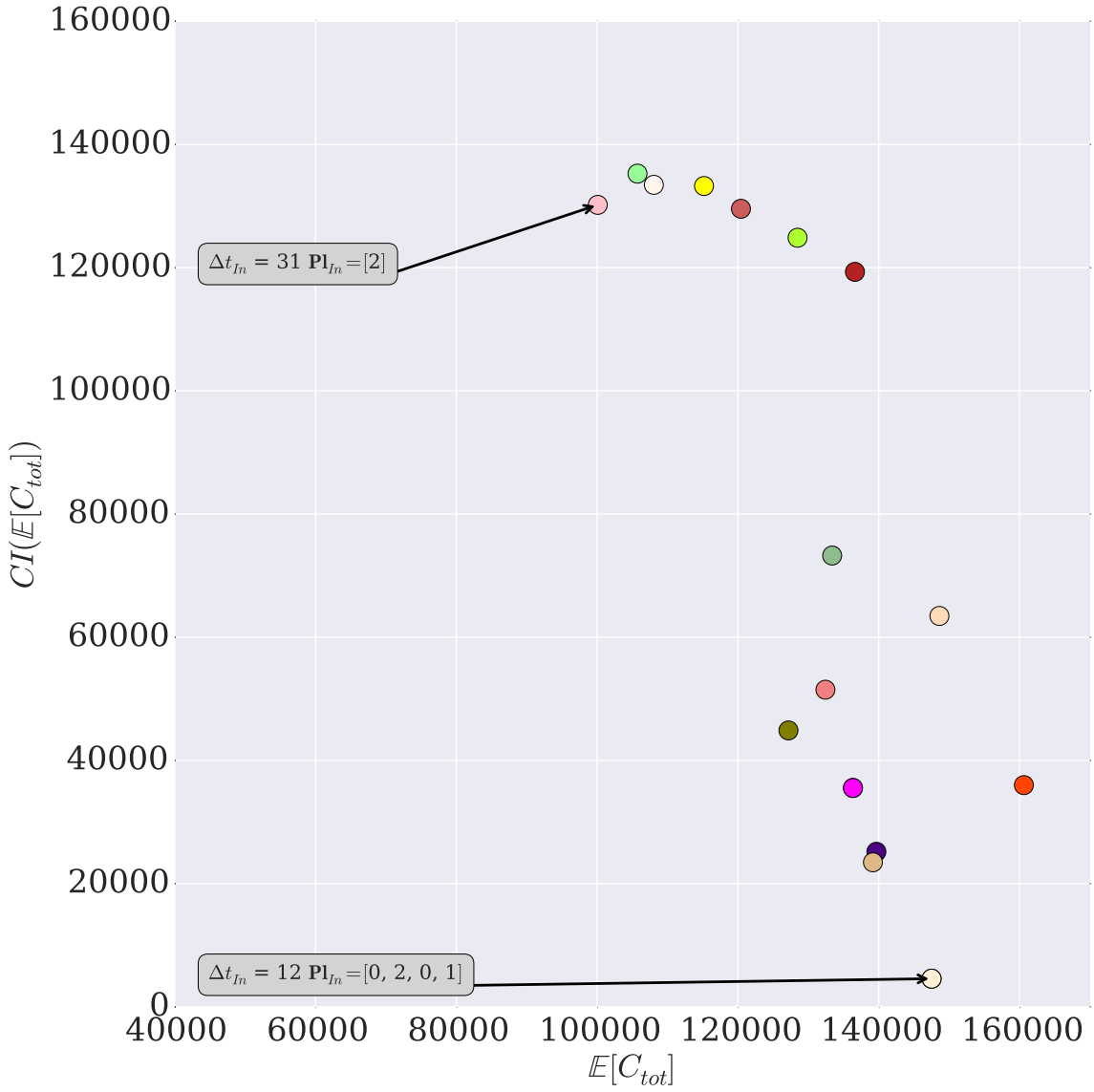

Figure 4.13 – Pareto front projected on the plan made by the expected total cost and its confidence interval, without the solutions giving an expected total time spent in the failure state higher than one year and an expected total cost outside of the bounds formed by its confidence interval.

was already studied in Section 4.4.2.2.1. The second one has an inspection interval of 12 years.

The corresponding probabilistic distributions for the number of maintenances, repairs and inspections are shown Figure 4.14. Consequently to the use of a second criterion, this inspection plan *worsens* false estimates of the degradation process due to inspection errors lead to a decrease of the probability for the number of repairs from 18% to 13% and 9% (see Table 4.7).

$n°$	μ_{Ma}	$[CI^-; CI^+]_{Ma}$	μ_F	$[CI^-; CI^+]_F$
0	0.18	[0.13; 0.09]	0.82	[0.87; 0.91]
1	0.77	[0.87; 0.67]	0.18	[0.13; 0.09]
2	0.05	[0; 0.24]	0	[0; 0]
3	0	[0; 0]	0.03	[0; 0]
4	0	[0; 0]	0.03	[0; 0]

Table 4.7 – Mean and confidence interval of the number of maintenances and repairs with an inspection interval of 12 years.

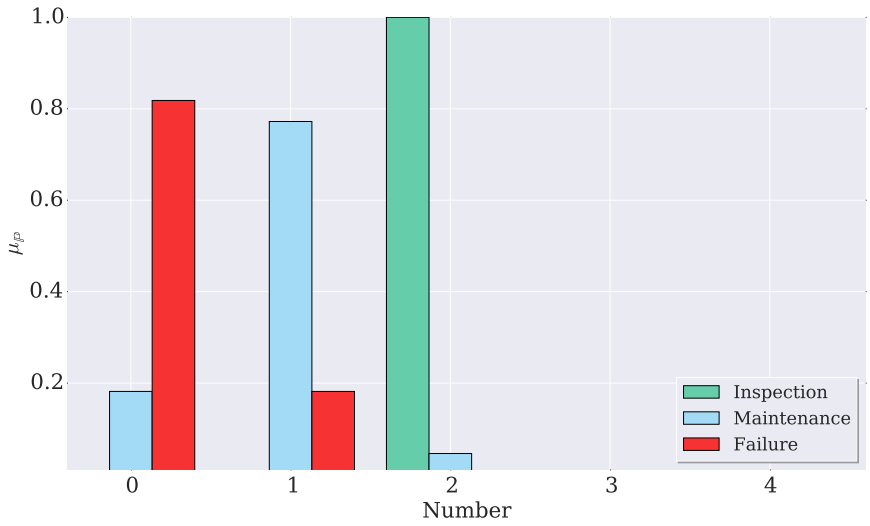

Figure 4.14 – Probabilistic distributions for the number of maintenances, repairs and inspections with an inspection interval of 12 years.

This plan predicts that only 2 inspections (with a probability equal to 0.9997) will be useful:

- The first inspection has 100% of chances to be useless;
- The third inspection has 65% of chances to be performed;
- The last inspection has 65% of chances to be useless.

n°	Δt_{In} (year)	$\mathbb{E}[C_{tot}]$ (€)	$CI(\mathbb{E}[C_{tot}])$ (€)	μ_{t_f} (year)	σ_{t_f} (year)
1	31	100,089	130, 0195 [20,275; 150,470]	0.78	4
2	12	147,519	4,568 [143,893; 148,461]	5×10^{-3}	0.32.

Table 4.8 – Summary of the two selected inspection plans

4.4.2.3.1 Synthesis Table 4.8 summarises the results obtained for the two selected candidate inspection plans. Considering that:

- The second inspection plan leads to a first inspection performed at 24 years, thus reducing the possible error due to a bias of the predictive degradation model;
- The first inspection due to the inspection method used (the less accurate) could lead to a highest expected total cost of both plans;
- The second inspection plan predicts an expected time spent in the failure state pretty small with less than 4 months of standard deviation, instead of the 4 years of standard deviation predicted by the first plan;

If the expected total cost of the second plan fits within the stakeholders budget constraints, this inspection plan would be recommended.

4.4.3 Two-dimensional problem

Using the same criteria as for the one-dimensional problem, the resulting Pareto front is given Figure 4.15. The total expected cost of each candidate solution tends to be higher than the average obtained in the one-dimensional case (150,000 euros against 120,000 euros). Since the two-dimensional model presents a mean concrete cover depth lower than the one-dimensional case, failure is easier to achieve thus an increase of $\mathbb{E}[C_{tot}]$ is not surprising.

Moreover, the two selected points (like all the points of the Pareto front) propose an inspection interval higher than 30 years. As pointed out in Section 2.5.2.2, the maintenance threshold is on the opposite harder to reach (due to the increase of the reinforcement length), thus an increase of Δt_{In} seems logical as well.

Unlike the one-dimensional case, the difference between the two selected points is the inspection technique used to perform the only inspection predicted at 31 years.

4.4.3.1 First candidate solution

The first candidate solution proposes to use the less accurate method for the inspection and thus returns the largest confidence interval equal to 165,331 euros, higher than $\mathbb{E}[C_{tot}]$ which is equal to 155,000.

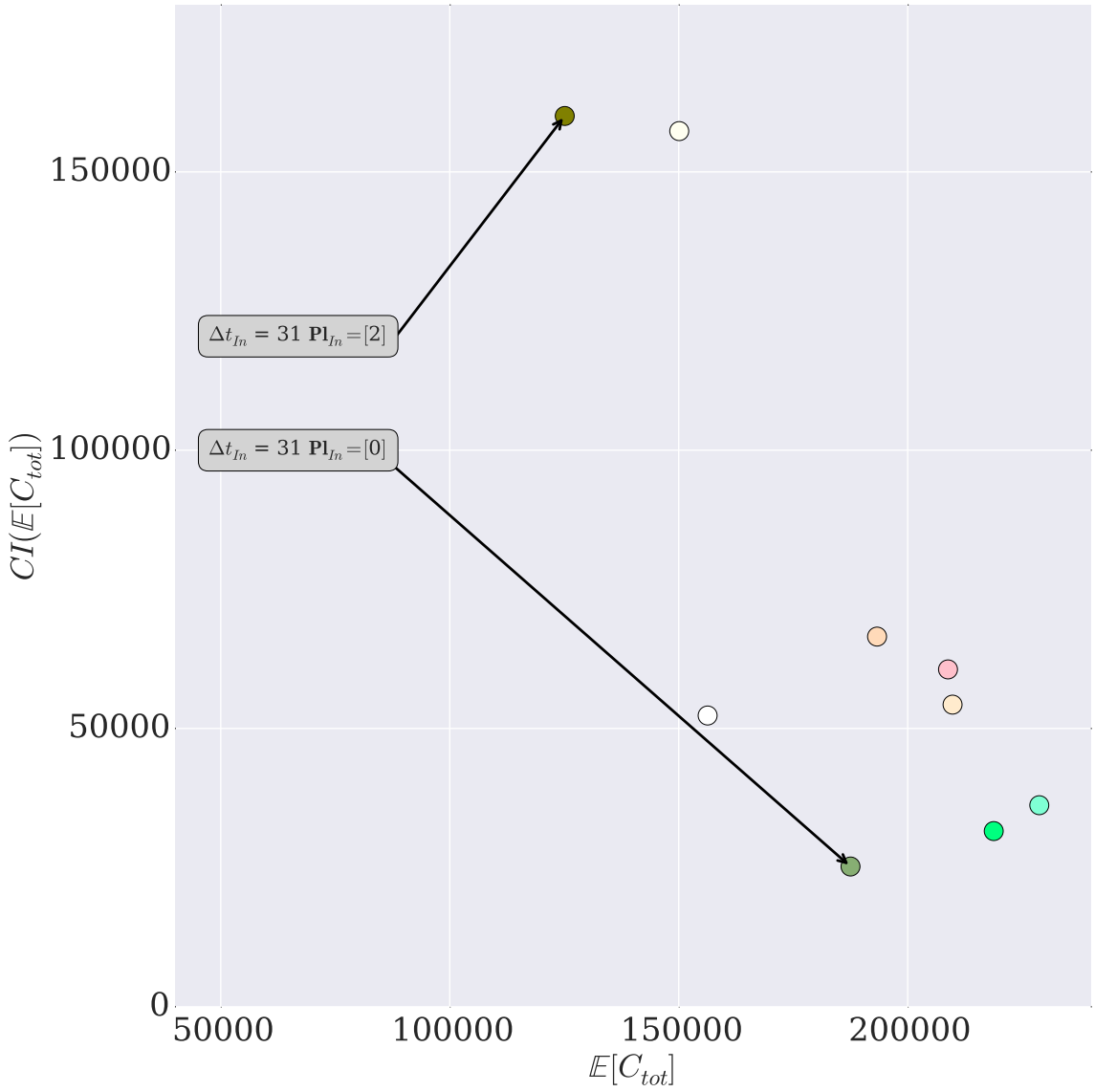

Figure 4.15 – Pareto front projected on the plan made by the expected total cost and its confidence interval, without the solutions giving an expected total time spent in the failure state higher than one year and an expected total cost outside of the bounds formed by its confidence interval.

As seen in Figure 4.16, the perfect inspection predicts 83% of chances that the building will be maintained at the inspection, against 18% that failure will be observed. The measurement error leads to a confidence interval for the total expected cost between 48,796 and 214,128 euros. In the first case, the degradation is underestimated and since there is only one inspection through the lifetime of the structure with this plan, Table 4.9 shows that there is a probability of 85% that nothing will be done to the building. On the opposite, overestimating nearly ensure (with a probability of 87%, see Table 4.9) that a repair action will be performed instead of the needed maintenance action.

$n°$	μ_{Ma}	$[CI^-; CI^+]_{Ma}$	μ_F	$[CI^-; CI^+]_F$
0	0.16	[0.85; 0.87]	0.84	[1; 0.13]
1	0.84	[0.15; 0.13]	0.16	[0; 0.87]

Table 4.9 – Mean and confidence interval of the number of maintenances and repairs with an inspection interval of 31 years resulting in one inspection performed with the inspection technique 2.

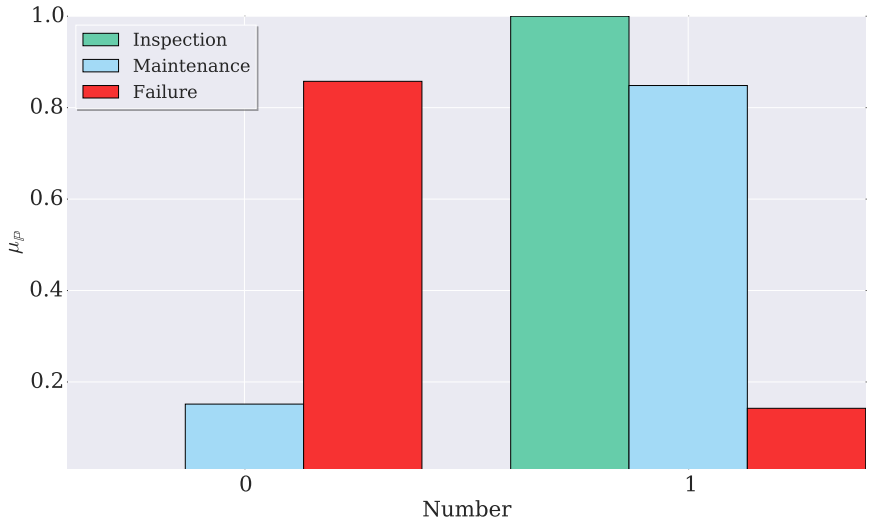

Figure 4.16 – Probabilistic distributions for the number of maintenances, repairs and inspections with an inspection interval of 31 years resulting in one inspection performed with the inspection technique 2.

4.4.3.2 Second candidate solution

The second candidate solution uses the most accurate inspection technique. In this case the expected total cost reaches 210,000 euros and is included within the interval $[199,411; 226,608]$ euros. The mean tendency is equivalent with the first inspection plan. In fact, it should indeed be the same. Yet the ADoE being dependent on the inspection cost (through the maximum number of inspected points), the resulting approximate may

be slightly different thus returning equivalent (due to the control of the approximate error) but not identical.

The major difference comes with the confidence intervals. From Table 4.10, with this technique the probability of repairing is increased by only 17% if the degradation is repeatedly overestimated. The probability of maintaining is higher in case of underestimation, from 85% to 93% which means that such measurement errors are more likely to lead from a repair decision to a maintenance one and not from a maintenance decision to nothing being done.

$n°$	μ_{Ma}	$[CI^-; CI^+]_{Ma}$	μ_F	$[CI^-; CI^+]_F$
0	0.15	$[0.07; 0.30]$	0.87	$[0.96; 0.70]$
1	0.85	$[0.93; 0.70]$	0.13	$[0.04; 0.30]$

Table 4.10 – Mean and confidence interval of the number of maintenances and repairs with an inspection interval of 31 years resulting in one inspection performed with the inspection technique 0.

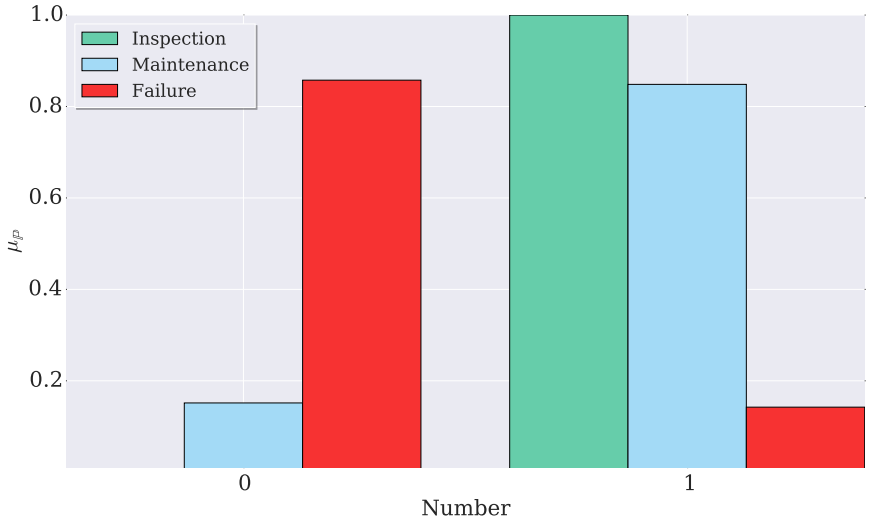

Figure 4.17 – Probabilistic distributions for the number of maintenances, repairs and inspections with an inspection interval of 31 years resulting in one inspection performed with the inspection technique 0.

4.4.3.3 Synthesis

Table 4.11 presents the overall results of the two selected points. Considering the risk that neither maintenance nor repair action may be decided due to the inaccuracy of the inspection method, the use of the second inspection plan may be preferred.

n°	Δt_{In} (year)	$\mathbb{E}[C_{tot}]$ (€)	$CI(\mathbb{E}[C_{tot}])$ (€)	μ_{t_f} (year)	σ_{t_f} (year)
1	31	155,000	165,331 [48,796; 214,128]	0.24	2.48
2	31	210,787	27,196 [199,411; 226,608]	0.22	2.40.

Table 4.11 – Summary of the two selected inspection plans

4.4.4 System approach for the two-dimensional problem

The system approach for the two-dimensional problem adds a constraint on the number of buildings which can be maintained between two inspections (3 over 12 buildings), with no constraint on the repair action.

The Pareto front resulting from the optimisation is shown in Figure 4.18, projected on the plan $\left(\mathbb{E}\left[t_f\right], \mathbb{E}[C_{tot}]\right)$. It unfortunately appears that due to the constraint applied on the maintenance action no inspection plan leads to a time spent in the failure state lower than 5 years, which is far from the first criterion applied on the two previous cases.

This criterion is thus modified in the following: no expected time spent in the failure state higher than 6 years will be accepted. The produced set of candidate solutions is shown in Figure 4.19.

Basically, the optimisation tends to increase the delay between two inspection Δt_{In}. Indeed it tries to minimise both the total expected cost and the time spent in the failure state. In this context, the optimal solution is not to maintain 3 buildings earlier, and then repair the 9 buildings left at another inspection, but to wait until all the buildings are to be repaired, so that they will not go back in the failure state after repair before the end of the lifetime.

The two candidate solution results shown in Figure 4.20 and Figure 4.21 illustrate this point, since for both cases the probability of a building to be repaired is around 80%.

From the dispersion shown in Table 4.12 and Table 4.13, it is clear that using the less accurate inspection technique as the first candidate may lead to repair action performed with probability one if the degradation is overestimated. On the other side with the most accurate technique the probability of repairing is only increased by 10%. In case of underestimation, it may become more problematic since the less accurate technique returns a 0 probability of repairing and only a probability of 25% that a maintenance action is to be made. Since only one inspection is to be performed in this inspection plan, a significant probability exists for the building to stay in the failure state during more than 20 years (see Figure 4.5).

n°	μ_{Ma}	$[CI^-; CI^+]_{Ma}$	μ_F	$[CI^-; CI^+]_F$
0	0.80	[0.75; 1]	0.25	[1; 0]
1	0.20	[0.25; 0]	0.75	[0; 1]

Table 4.12 – Mean and confidence interval of the number of maintenances and repairs with an inspection interval of 37 years.

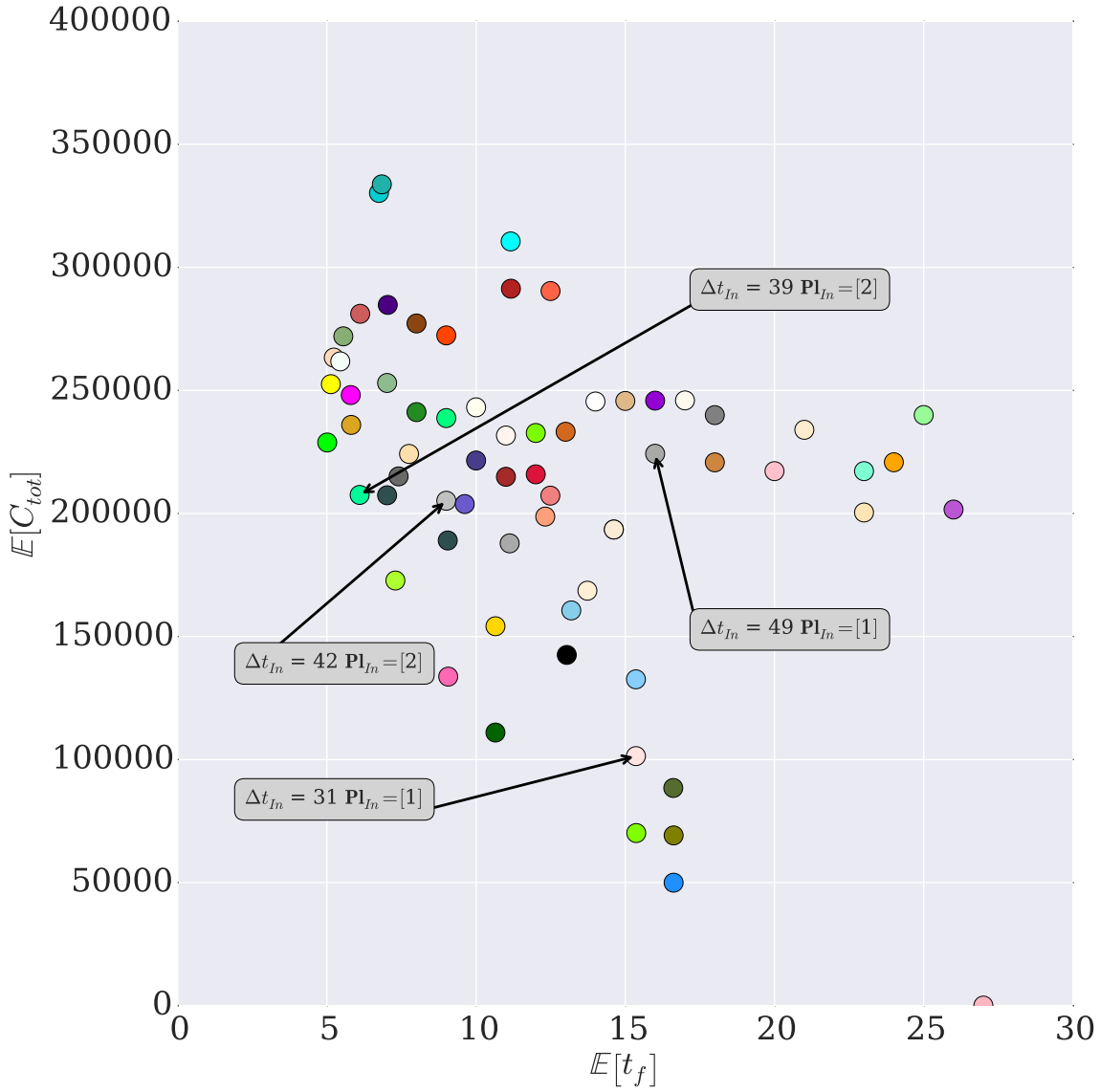

Figure 4.18 – Pareto front projected on the plan made by the expected total cost and the expected time spent in the failure state.

$n°$	μ_{Ma}	$[CI^-; CI^+]_{Ma}$	μ_F	$[CI^-; CI^+]_F$
0	0.84	[0.76; 0.93]	0.17	[0.38; 0.07]
1	0.16	[0.24; 0.07]	0.83	[0.60; 0.93]

Table 4.13 – Mean and confidence interval of the number of maintenances and repairs with an inspection interval of 38 years.

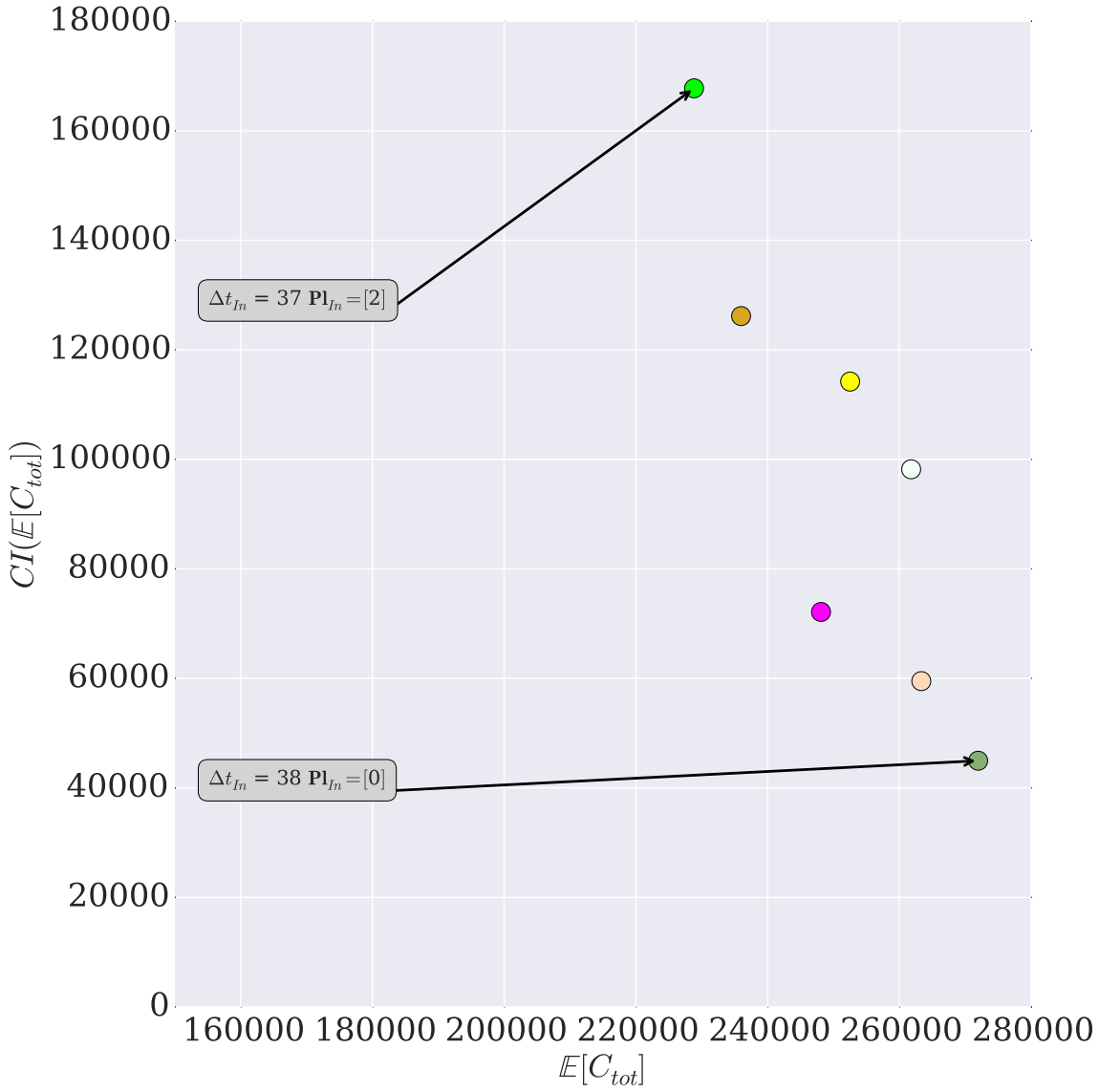

Figure 4.19 – Pareto front projected on the plan made by the expected total cost and its confidence interval, without the solutions giving an expected total time spent in the failure state higher than six years and an expected total cost outside of the bounds formed by its confidence interval.

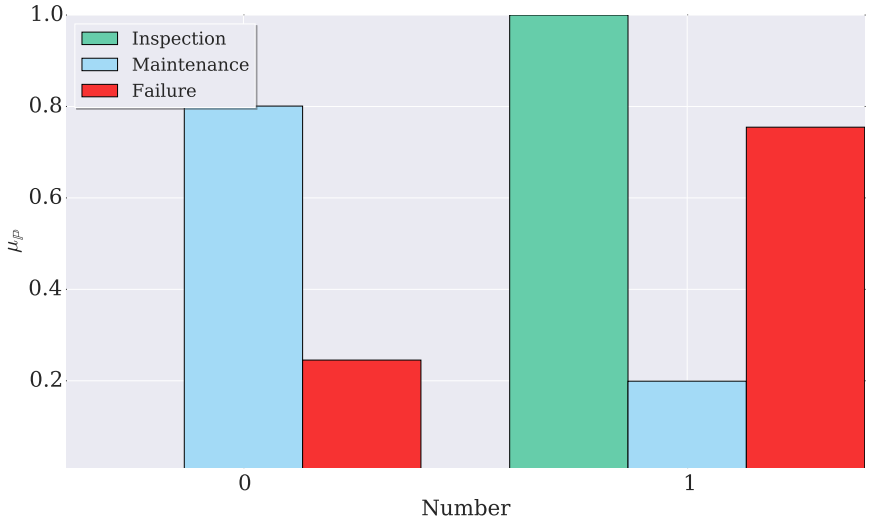

Figure 4.20 – Probabilistic distributions for the number of maintenances, repairs and inspections with an inspection interval of 37 years.

4.4.4.1 Synthesis

Table 4.14 summarises the properties of the two selected inspection plans. The second one may be preferred if the stakeholder can deal with its costs, since the standard deviation of the mean expected time spent in the failure state is nearly divided by 2 compared to the first inspection plan.

$n°$	Δt_{In} (year)	$\mathbb{E}[C_{tot}]$ (€)	$CI(\mathbb{E}[C_{tot}])$ (€)	μ_{t_f} (year)	σ_{t_f} (year)
1	37	184,420	167,783 [44,420; 212,204]	5.02	4.62
2	38	227,859	42,749 [196,679; 239,428]	5.34	2.64

Table 4.14 – Summary of the two selected inspection plans

4.4.5 Conclusion

This illustration has shown the capability of the methodology to optimise an inspection plan to deal with:

- Various degradation processes (One or bi-dimensional, stationary or not);
- Various assumptions on the management procedure (system or component approach);

independently from the assumptions made on the inspection, maintenance and failure costs.

It proved that genetic algorithms are well suited to this problem since the objective functions are only piecewise derivable. And the use of a multi-objective approach has been shown useful to avoid unacceptable solutions such as: *don't know, don't care*.

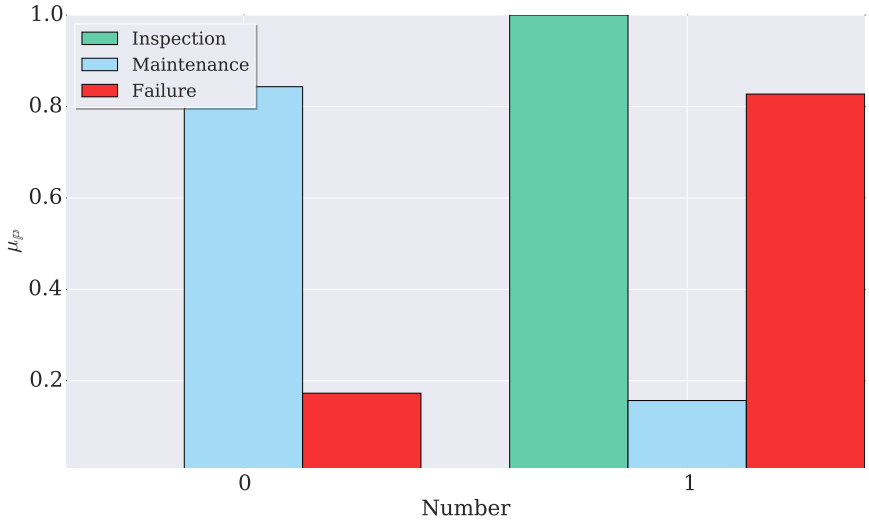

Figure 4.21 – Probabilistic distributions for the number of maintenances, repairs and inspections with an inspection interval of 38 years.

The tools presented in Chapter 2 were used to analyse the probabilistic distributions for the number of inspections, maintenances and repairs of some candidates extracted from the Pareto front in order to help the stakeholder to choose between them.

Last but not least, the computational cost for the most complex optimisation (system approach) is only up to a few hours.

4.5 Conclusion

This chapter introduces first the basics on genetic algorithms which are used to solve the optimisation problems defined later on. Revealed by the literature review (see Section 1.4.2.1.2), the presented NSGA-II algorithm demonstrates its appealing properties such as its *elitism*.

The optimisation problems defined in the second part are composed by:

- A mono-objective definition which aims at minimising the expected total cost;
- A multi-objective definition which aims at minimising both the expected total cost, its confidence interval and the expected time spent in the failure state.

Generic cost functions for the inspection, maintenance and repair actions based on the IMRM description are proposed, independently from any modelling.

In order to prove the capability of the optimisation method to find *when* and *how* the structure should be inspected to optimise the objective functions, the illustration presented in Chapter 2 which models the degradation of balconies is resumed. Several cases are performed, from a simple one-dimensional model of the degradation with an optimisation at a building level to a complex two-dimensional non-stationary degradation index at a system of several buildings level.

The result of such optimisation is a Pareto front with many different solutions. The tools derived from the decision tree used as a life-cyle model, and proposed in Chapter 2, are used to analyse the interesting potential solutions. It thus gives valuable indications to the stakeholder on which plan is the most suitable considering his constraints.

Indeed the obtained results are dependent onh the objective functions introduced in this manuscript. The different Pareto fronts presented were all pretty scattered which means that every candidate solutions were leading to different conclusions. It tends to prove the usefulness of the proposed objectives since they allow for the choice of many different inspection strategies with really different impacts.

In the end, this illustration proves that the methodology proposed in this chapter fulfills the thesis objectives presented in Chapter 1.

CONCLUSION

Summary and main contributions

According to Chapter 1, the research performed in this thesis aimed at :

1. Proposing a methodology for the optimisation of inspection plans:
    - Not driven by a unique objective to be reached;
    - As independent as possible of the different assumptions that could be made to model inspection, failure and maintenance;
    - Able to deal with structures of different sizes, submitted to spatially correlated degradation process or not;
    - Independent from the degradation process and the corresponding degradation indexes;
    - As simple as possible with an affordable computational cost.
2. Allowing the use of any existing data which would be relevant in order to calibrate the degradation model or to update the inspection plan computed with the methodology mentioned above.

Predicting the evolution of a degradation index

Chapter 2 dealt with the prediction of a degradation index dependent on a degradation process spatially correlated. The inputs of the degradation model may also be non-gaussian, spatially correlated and correlated between each other. It has been shown that the numerical simulation of such input data keeps on being an active research field. This manuscript proposed to combine the *translation field* (i.e. Nataf transformation) together with the quantile autocorrelation function and the Karhunene-Loeve decomposition in order to obtain such random fields. HoweveWhr the author acknowledges the method developed by Perrin et al. (2013) which is more suited to such problems, although much harder to use.

Based on the resulting degradation predictions, an adaptive design of experiments handling the spatial variability has been proposed. Despite the first objective of this thesis, this ADoE is directly related to the degradation index chosen in this thesis, yet it proves that dealing with spatial variability is affordable if the degradation index is suited to this case.

The degradation predictions also are an input of the IMRM based on a classical decision tree which also needs models for inspections, failures and maintenance. Since it uses these models without being dependent on them, this IMRM complies with the first objective of this thesis. Moreover it also fulfills the second objective since the simple form of a decision tree allows for the derivation of many valuable criteria which may help the stakeholders to take a decision.

Updating the predictive model

Chapter 3 aimed at answering to the last objective of the thesis. Bayesian statistics were found to be the best tool to calibrate or update a degradation model since their inputs may come from various sources (e.g. direct measurement, structure specifications, expert judgement, ...). The inverse problem has been developed further in order to take into consideration the model inputs which may also be measured with uncertainties. A case study built from real measurements has been used in order to discuss the potential of such approach in the context of ageing RC structures inspected through NDTs. Despite that the degradation is not measurable by NDTs, the Bayesian approach has shown its potential and calls for the results of on-going research dealing with NDT measurements of carbonation and chloride ingress.

Optimisation of the inspection plan

Chapter 4 was the final step of the methodology. It uses the IMRM potentially calibrated through a Bayesian scheme in order to optimise the exploitation cost and its uncertainties. It has shown that considering one or several buildings with different modelling does not impact the capability of the overall methodology to handle different assumptions. The solution of a multi-objective optimisation being a set of potential candidates, i.e. a *Pareto* front, many possible solution that could be chosen. The approach used in this manuscript, neither new nor usual, makes use of the indicators derived from the IMRM in order to help the stakeholder to select which candidate fulfils its own and potentially subjective criteria. The methodology thus completes the answer given to the first objective of the thesis.

Future work

The proposed optimisation methodology has been applied on a numerical case (though its inputs are at least inspired from reality) yet in order to fully validate it an industrial application would be appealing. However from the proposed application several perspectives have

been drawn.

Predicting the evolution of a degradation index

The degradation index considered in this manuscript is linked with the degradation considered: the carbonation process. Using other degradation indexes dedicated to other degradation processes (e.g. concrete cracking, steel fatigue) may lead to a need of updating the proposed adaptive design of experiments. Indeed, this ADoE was developed in order to improve the estimate of a probability of maintenance/failure directly related to the interpolation quality of the degradation trajectories. It would not be suited to the case of maintenance actions being decided upon localised degradation (e.g. critical crack on a steel structure).

Optimisation of the inspection plan

The last part of the methodology uses the stakeholder constraints which may be diversified. A simple approach for the management of several structures has been illustrated. It has been shown that dealing with a constraint on the number of maintenance needs the simulation of the decision tree in order to account for interactions. Through these simulations much more complex constraints may be modelled (e.g. choosing between the structures to be repaired in agreement with a budget constraint).

The IMRM was used to optimise *when* and *how* the structure is to be inspected. Another perspective is to include more accurate models of maintenance and repair actions (e.g. different repair methods, localised maintenance action), information on the construction and the deconstruction costs. The IMRM would thus become a so-called *life-cycle* model.

BIBLIOGRAPHY

Baik, H.-S., H. Jeong, and D. Abraham (2006). Estimating transition probabilities in markov chain-based deterioration models for management of wasterwater systems. *Journal of Water Resources Planning and Management*, 132, 15–24.

Barker, C. and M. Newby (2009). Optimal non-periodic inspection for a multivariate degradation model. *Reliability Engineering and System Safety*, 94, 33–43.

Barone, G. and D. Frangopol (2014). Life-cycle maintenance of deteriorating structures by multi-objective optimization involving reliability, risk, availability, hazard and cost. *Structural Safety*, 48, 40–50.

Bary, B. and A. Sellier (2004). Coupled moisture - carbon dioxide - calcium transfer model for carbonation of concrete. *Cement and concrete research*, 34, 1859–1872.

Bastidas-Arteaga, E. (2010). *Contribution for sustainable management of reinforced concrete structures subjected to chloride penetration*. Ph. D. thesis, ECOLE DOCTORALE SCIENCES POUR L'INGENIEUR, GEOSCIENCES, ARCHITECTURE.

Bastidas-Arteaga, E. and F. Schoefs (2012). Stochastic improvement of inspection and maintenance of corroding reinforced concrete structures placed in unsaturated environments. *Engineering structures*, 41, 50–62.

Bastidas-Arteaga, E., F. Schoefs, A. Chateauneuf, M. Sanchez-Silva, and B. Capra (2010). Probabilistic evaluation of the sustainability of maintenance strategies for rc structures exposed to cholride ingress. *International journal of engineering under uncertainty: hazards, assessment and mitigation*, 2, 61–74.

Berchtold, A. (1998). *Chaînes de Markov et modèles de transition*.

Berchtold, A. and G. Ritschard (1997). Stabilité de l'estimation d'une distribution de probabilité. In *Recueil des Résumés des Communications des 29ème Journées de Statistique*.

Bhargava, K., A. Ghosh, Y. Mori, and S. Ramanujam (2006). Analytical model for time to cover cracking in rc structures due to rebar corrosion. *Nuclear engineering and design*, 236, 1123–1139.

Bickenbach, F. and E. Bode (2001). Markov or not markov - this should be a question. *Kiel Institutte for the World Economy*, 1086.

Bocchini, P. and D. Frangopol (2011). A probabilistic computational framework for bridge network optimal maintenance scheduling. *Reliability Engineering & System Safety*, 96, 332–349.

Bocchini, P., D. Saydam, and D. Frangopol (2012). Efficient, accurate and simple markov chain model for the life-cycle analysis of bridge groups. *Structural Safety*, 40, 51–64.

BODE, E. (1998). *Lokale Wissensdiffusion und regionale Divergenz in Deutschland*. Mohr Siebeck Verlag.

Breysse, D., S. Elachachi, E. Sheils, F. Shoefs, and A. O'Connor (2009). Life cycle cost analysis of ageing structural components based on non-destructive condition assessment. *Australian journal of structural engineering*, 9, 55–66.

Caniou, Y. (2012). *Global sensitivity analysis for nested and multiscale modelling*. Ph. D. thesis, Université Blaise Pascal – Clermont II.

Chung, K. (1967). *Markov chains with stationary transition probabilities*. Springer.

de Larrard, T., E. Bastidas-Arteaga, F. Duprat, and F. Schoefs (2014). Effects of climate variations and global warming on the durability of rc structures subjected to carbonation. *Civil Engineering and Environmental Systems, in press*, 3, 153–164. Civil Engineering and Environmental Systems, in press.

Deb, K., S. Agrawal, A. Pratap, and T. Meyarivan (2000). A fast elitist non-dominated sorting genetic algorithm for multi-objective optimisation: Nsga-ii. *Computer science*, 1917, 849–858.

Deby, F. (2008). *Approche probabiliste de la durabilité des betons en environnement marin*. Ph. D. thesis, Université de Toulouse III - Paul Sabatier.

Dubourg, V. (2011). *Adaptive surrogate models for reliability analysis and reliability-based design optimization*. Ph. D. thesis, Université Blaise Pascal - Clermont II.

Duc Le, M. and C. Ming Tan (2013). Optimal maintenance strategy of deteriorating system under imperfect maintenance & inspection using mixed inspection scheduling. *Reliability Engineering and System Safety*.

DuraCrete (2000). Statistical quantification of the variables in the limit state functions. Technical report, The European Union - Brite EuRam III - Contract BRPR-CT95-0132 - Project BE95-1347/R9.

El Maaddway, T. and K. Soudki (2007). A model for prediction of time from corrosion initiation to corrosion cracking. *Cement and concrete composites*, 29, 168–175.

Elachachi, S. and D. Breysse (2007). Sewer assets maintenance management: comparison by two approaches, markovian process, and probabilistic neural networks. In *International Forum on Engineering Decision Making*.

Ellingwood, R. and Y. Mori (1996). Reliability-based service life assessment of concrete structures in nuclear power plants: optimum inspection and repair. *Nuclear Enginnering and Design*, 175, 247–258.

Estes, A. and D. Frangopol (2001a). Bridge lifetime system reliability under multiple limit states. *Journal of Bridge Engineering*, 6, 523–528.

Estes, A. and D. Frangopol (2001b). Minimum expected cost-oriented optimal maintenance planning for deteriorating structures: application to concrete bridge decks. *Reliability Engineering and System Safety*, 73, 281–291.

Faber, M. and J. Sorensen (2002). Indicators for inspection and maintenance planning of concrete structures. *Structural Safety*, 24.

Faber, M. and M. Stewart (2003). Risk assessment for civili engineering facilities: critical overview and discussion. *Reliability Engineering and System Safety*, 80, 173–184.

Faber, M. H., I. Kroon, and J. Sorensen (1996). Sensitivities in structural maintenance planning. *Reliability Engineering & System Safety*, 51, 317–329.

FHWA (2011). Bridge preservation guide - maintaining a state of good repair using cost effective investment strategies. Technical report, U.S. Depatrement of Transportation.

Fink, D. (1997). A compendium of conjugate priors. Technical report, Environmental statistics group, Montana state university.

Forrest, S. (1993). Genetci algorithms: principles of natural selection applied to computation. *Science*, 261, 872–879.

Franco, J. (2008). *Planification d'expériences numériques en phase exploratoire pour la simulation des phénomènes complexes*. Ph. D. thesis, École Nationale Supérieure des Mines de Saint-Étienne.

Frangopol, D., K.-Y. Lin, and A. Estes (1997). Life-cycle cost design of deteriorating structures. *Journal of structural engineering*, 123, 1390–1401.

Fraser, A. (1957). Simulation of genetic systems by automatic digital computers. ii: Epistasis. *Australian journal of biological sciences*, 10, 492–499.

Garnier, V., D. Martini, J. Salin, V. Fardeau, M. Sbartai, D. Breysse, B. Piwakowski, G. Villain, O. Abraham, and J.-P. Balayssac (2014). Non destructive testing of concrete: transfer from laboratory to on-site measurement. In *EWSHM - 7th European Workshop on Structural Health Monitoring, Nantes, France*.

Ghanem, R. and P. Spanos (2003). *Stochastic Finite Elements : A Spectral Approach*. Courier Dover Publications.

Gioffré, M., V. Gusella, and M. Grigoriu (2000). Simulation of non-gaussian field applied to wind pressure. *Probabilistic Engineering Mechanics*, 15, 339–345.

Goldberg, D. (1989). *Genetic algorithms in search optimization and machine learning*.

Grall, A., C. Bérenguer, and L. Dieulle (2002). A condition-based maintenance policy for stochastically deteriorating systems. *Reliability Engineering & System Safety*, 167-180.

Gulikers, J. and M. Raupach (2006). Comparison of a case study calculated by different researchers. *Materials and Corrosion*, 57, 618–627.

Gurley, K.-R. (1997). *Modelling and simulation of non-Gaussian processes*. Ph. D. thesis, University of Notre Dame.

Halton, J. (1960). On the efficiency of certain quasi-random sequences of points in evaluating multi-dimensional integrals. *Numerische mathematik*, 2, 84–90.

Hammersley, J. (1960). Monte carlo methods for solving multivariable problems. *Annals of the New York academy of sciences*, 86, 844–874.

Hansen, J. R. and E. V. Saouma (1999). Numerical simulation of reinforced concrete deterioration: part 2 - steel corrosion and concrete cracking. *Materials journal*, 96, 331–338.

Hastings, W. (1970). Monte Carlo sampling methods using Markov chains and their application. *Biometrika*, 57(1), 97–109.

Hellevik, S., I. Langen, and J. Sorensen (1999). Cost optimal reliability based inspection and replacement planning of piping subjected to co_2 corrosion. *International Journal of Pressure Vessels and Piping*, 76, 527–538.

Holland, J. (1975). Adaptation in natural and artificial systems. *University of Michigan Press, Ann Arbor, MI*.

Hong, H. (1997). Reliability analysis with nondestructive inspection. *Structural safety*, 19, 383–395.

Hong, H. (1999). Inspection and maintenance planning of pipeline under external corrosion considering generation of new defects. *Structural Safety*, 21, 203–222.

Hyvert, N. (2009). *Application de l'approche probabiliste à la durabilité des produits préfabriqués en béton*. Ph. D. thesis, Université de Toulouse.

Kallen, M.-J. (2007). *Markov processes for maintenance optimization of civil infractructure in the Netherlands*. Ph. D. thesis, Delft University of Technology.

Kallen, M.-J. and J. van Noortwijk (2006). Statistical inference for markov deterioration models of bridge conditions in the netherlands. In *Bridge Maintenance, Safety, Management, Life-Cycle Perfor- mance and Cost: Proceedings of the Third International Conference on Bridge Maintenance, Safety and Management*.

Kelton, C. and W. Kelton (1985). Comparison of inference techniques for markov processes estimated from micro vs macro data. Technical report, The University of Michigan.

Kim, S. and D. Frangopol (2011). Optimum inspection planning for minimizing fatigue damage detection delay of ship hull structures. *International Journal of Fatigue*, 33, 448–459.

Leung, C. (2001). Modeling of concrete cracking induced by steel expansion. *Journal of materials in civil engineering*, 13, 169–175.

Loève, M. (1977). *Probability theory*. Springer.

Ma, Y., J. Zhang, L. Wang, and L. Yongming (2013). Probabilistic prediction with bayesian updating for strength degradation of rc bridge beams. *Structural Safety*, 44, 102–109.

Marchand, J. (2001). Modeling the behavior of unsaturated cement systems exposed to aggressive chemical environments. *Materials and structures*, 34, 195–200.

Mattrand, C. (2011). *Approche probabiliste de la tolérance aux dommages - Application au domaine aéronautique*. Ph. D. thesis, Université BLAISE PASCAL - Clermont II.

Metropolis, N. (1987). The beginning of the Monte Carlo method. *Los Alamos Science, Special Issue*.

Metropolis, N., A. W. Rosenbluth, M. N. Rosenbluth, and A. H. Teller (1953). Equations of state calculations by fast computing machines. *J. Chem. Phys.*, 21(6), 1087–1092.

Metropolis, N. and S. Ulam (1949). The Monte Carlo method. *J. Amer. Stat. Assoc.*, 44(247), 335–341.

Molina, F., C. Alonso, and C. Andrade (1993). Cover cracking as a function of rebar corrosion: part 2 - numerical model. *Materials and structures*, 26, 532–548.

Mühlenbein, H. and D. Schlierkamp-Vooser (1993). Predictive models for the breeder genetic algorithm: I. continous parameter optimization. *Evolutionary computation*, 1, 25–49.

Nagel, B. and B. Sudret (2015). Bayesian techniques for model calibration and stochastic inverse problems rsuq-2015-004. Technical report, Chair of risk, safety and uncertainty quantification.

Nielsen, J. and J. Sorensen (2011). On risk-based operation and maintenance of offshore wind turbine components. *Reliability Engineering & System Safety*, 96, 218–229.

Ntzoufras, I. (2009). *Bayesian modeling using WinBUGS*. John Wiley & Sons.

Oh Hwan, B., K. Hyun Kim, and B. Seok Jank (2009). Critical corrosion amount to cause cracking of reinforced concrete structures. *Materials Journal*, 106, 333–339.

Okasha, N. and D. Frangopol (2009). Lifetime-oriented multi-objective optimization of structural maintenance considering system reliability, redudancy and life-cycle cost using ga. *Structural Safety*, 31, 460–474.

Okasha, N. and D. Frangopol (2010). Novel approach for multicriteria optimization of life-cycle preventive and essential maintenance of deteriorating structures. *Journal of Structural Engineering*, 136, 1009–1022.

Onoufriou, T. and D. Frangopol (2002). Reliability-based inspection optimization of complex structures: a brief retrospective. *Computers and Structures*, 80, 1133–1144.

Orcesi, A. and C. Cremona (2010). A bridge network maintenance framework for pareto optimization of stakeholders/users costs. *Reliability Engineering and System Safety*, 95, 1230–1243.

Orcesi, A. and D. Frangopol (2011a). A stakeholder probability-based optimization approach for cost-effective bridge management under financial constraints. *Engineering Structures*, 33, 1439–1449.

Orcesi, A. and D. Frangopol (2011b). Use of lifetime functions in the optimization of nondestructuve inspection strategies for bridges. *Journal of Structural Engineering*, 137, 531–539.

Otieno, M., H. Beushausen, and M. Alexander (2012). Prediction of corrosion rate in reinforced concrete structures - a critical review and preliminary results. *Materials and Corrosion*, 63, 777–790.

Pantazopoulou, S. and K. Papoulia (2001). Modeling cover-cracking due to reinforcement corrosion in rc structures. *Journal of Engneering Mechanics*, 127, 342–351.

Perrin, F. (2008). *Prise en compte des données expérimentales dans les modèles probabilistes pour la prévision de la durée de vie des structures*. Ph. D. thesis, Université Blaise Pascal - Clermont II.

Perrin, G., C. Soize, D. Duhamel, and C. Funfschilling (2013). Karhunen-loeve expansion revisited for vector-valued random fields: scaling, errors and optimal basis. *Journal of Computational Physics*, 242, 607–622.

Phoon, K., S. Huang, and S. Quek (2002a). Implementation of karhunen-loeve expansion for simulation using a wavelet-galerkin scheme. *Prob. Eng. Mech.*, 17, 293–303.

Phoon, K.-K., S.-P. Huang, and S.-T. Quek (2002b). Simulation of second-order processes using karhunen-loeve expansion. *Computers and Structures*, 80, 1049–1060.

Phoon, K.-K., S.-T. Quek, and S.-P. Huang (2004). Simulation of non-gaussian processes using fractile correlation. *Probabilistic Engineering Mechanics*, 19, 287–292.

Puig, B. (2003). *Modélisation et simulation de processus stochastiques non gaussiens*. Ph. D. thesis, Université Paris VI.

Puig, B. and J.-L. Akian (2004). Non-gaussian simulation using hermite polynomials expansion and maximum entropy principle. *Probabilistic Engineering Mechanics*, 19, 293–305.

Rackwitz, R., A. Lentz, and M. Faber (2005). Socio-economically sustainable civil engineering infrastructures by optimization. *Structural Safety*, 27, 187–229.

Raupach, M. (2006). Models for the propagation phase of reinforcement corrosion - an overview. *Materials and Corrosion*, 57, 605–612.

Recek, S., M. Lemaire, and A. Millard (2005). Décomposition en série de karhunen-loéve d'un processus aléatoire par le biais d'un code eléments finis. In *7ème colloque national en calcul des structures*, Giens.

Redaelli, E., L. Bertolini, W. Peelen, and R.Polder (2006). Fem-models for the propagation period of chloride induced reinforcement corrosion. *Materials and Corrosion*, 57, 628–635.

Rouhan, A. and F. Schoefs (2003). Probabilistic modeling of inspection results for offshore structures. *Structural Safety*, 25, 379–99.

Rudolph, G. (1999). Evolutionary search under partially ordered sets. Technical report, University of Dormund - Technical Report No. CI-67/99.

Saetta, A., B. Schrefler, and R. Vitaliani (1995). 2-d model for carbonation and moisture/heat flow in porous materials. *Cement and concrete research*, 25, 1703–1712.

Sahraoui, Y., R. Khelif, and A. Chateauneuf (2013). Maintenance planning under imperfect inspections of corroded pipelines. *International Journal of Pressure Vessels and Piping*, 104, 76–82.

Sakamoto, S. and R. Ghanem (2002). Simulation of multi-dimensionall non-gaussian non-stationary random fields. *Probabilistic Engineering Mechanics*, 17, 167–176.

Schoefs, F. and A. Clément (2004). Multiple inspection modelling for decision making and management of jacket offshore platforms: effect of false alarm. In *First international forum on engineering decision making*.

Schoefs, F., A. Clément, and A. Nouy (2009). Assessment of roc curves for inspection of random fields. *Structural Safety*, 31, 409–419.

Schoefs, F., T. Tran V, E. Bastidas-Arteaga, G. Villain, and X. Derobert (2015). Stochastic characterization of random fields from ndt measurements: a two stages procedure. *Structural Safety*, In press. Structural Safety, in press.

SENSO (2009). Stratégie d'évaluation non destructive pour la surveillance des ouvrages en béton - final report. Technical report, Association Nationale de la Recherche.

Sétra (1996). Iqoa - classification des ouvrages. Technical report, Ministére de l'Ecologie, de l'Energie, du Développement durable et de la Mer Francais.

Sheils, E., A. O'Connor, D. Breysse, F. Schoefs, and S. Yotte (2010a). Development of a two-stage inspection process for the assessment of deteriorating infrastructure. *Reliability Engineering and System Safety*, 95, 182–194.

Sheils, E., A. O'Connor, F. Schoefs, and D. Breysse (2010b). Investigation of the effect of the quality of inspection techniques on the optimal inspection interval for structures. *Structure and Infrastructure Engineering*, 8, 557–568.

Sobol', I. (1967). On the distribution of points in a cube and the approximate evaluation of integrals. *USSR Computational mathematics and mathematical physics*, 7, 86–112.

Sobol', I. (1993). Sensitivity estimates for nonlinear mathematical models. *Math. Modeling & Comp. Exp.*, 1, 407–414.

Soliman, M., D. Frangopol, and S. Kim (2013). Probabilistic optimum inspection planning of steel bridges with multiple fatigue sensitive details. *Engineering Structures*, 49, 996–1006.

Straub, D. (2004). *Generic approaches to Risk Based Inspection planning for steel structures*. Ph. D. thesis, Swiss Federal Institute of Technology Zürich.

Straub, D. and M. Faber (2002). On the relation between inspection quantity and quality. In *3rd European-American Workshop on NDE Reliability*.

Straub, D. and M. Faber (2005). Risk based inspection planning for structural systems. *Structural Safety*, 27, 335–355.

Sudret, B. and A. Der Kiureghian (2000). Stochastic finite element methods and reliability, a state-of-the-art report. Technical Report UCB/SEMM-2000/08, Universty of California, Berkeley.

Talukdar, S., N. Banthia, and J. Grace (2012). Carbonation in concrete infrastructure in the context of global climate change - part 1: experimental results and model development. *Cement and concrete composites*, 34, 924–930.

Taylor, H. F. W. (2004). *Cement chemistry*. Thomas Telford Ltd.

Thiery, M. (2005). *Modélisation de la carbonatation atmosphérique des matériaux cimentaires. Prise en compte des effets cinétiques et des modifications microstructurales et hydriques*. Ph. D. thesis, Ecole nationale des ponts et chaussées.

Val, D., L. Chernin, and M. Stewart (2009). Experimental and numerical investigation of corrosion-induced cover cracking in reinforced concrete structures. *Journal of structural engineering*, 135, 376–385.

Van der Corput, J. (1935). Verteilungsfunktionen i. *Akademie van Wetenschappen*, 38, 813–821.

van Noortwijk, J. (2009). A survey of the application of gamma processes in maintenance. *Reliability Engineering & System Safety*, 94, 2–21.

Vorechovsky, M. (2008). Simulation of simply cross correlated random fields by series expansion methods. *Structural Safety*, 30, 337–363.

Warkus, J., M. Brem, and M. Raupach (2006a). Bem-models for the propagation period of chloride induced reinforcement corrosion. *Materials and Corrosion*, 57, 636–641.

Warkus, J., M. Raupach, and J. Gulikers (2006b). Numerical modelling of corrosion - theoretical backgrounds. *Materials and Corrosion*, 57, 614–617.

Zhang, R. and S. Mahadevan (2000). Model uncertainty and bayesian updating in reliability-based inspection. *Structural Safety*, 22, 145–160.

Zitzler, E., K. Deb, and L. Thiele (2000). Comparison of multiobjective evolutionary algorithms: empirical results. *Evolutionary computation*, 8, 173–195.

Abstract

The development of modern societies has seen the construction of several structures and infrastructures built in reinforced concrete. The management of those structures, potentially large and subjected to important pathologies, aiming at ensuring and guaranteeing their safety and durability has become a true economical challenge. Looking for an optimal inspection, maintenance and repair plan according to safety constraints is one of the possible solutions to address this challenge. This work is bounded by a preventive maintenance context where the concrete degradations may lead to the corrosion of the reinforcements and not to structural failure. The corresponding degradation models are put in an uncertainty context where the spatial variability of the environmental exposure and the concrete properties are accounted for. Based on such predictions, an adaptive design of experiments helps to identify, at a given time, where the structure should be inspected in order to evaluate its degradation state which will indicate the need for maintenance or a repair action. A decision tree therefore allows to predict the probabilistic evolution of the structure state, including the effect of maintenance and repairs. This tree is then used in an optimisation process which aims at finding where and with which inspection technique the structure is to be inspected to minimise both the expectation of the exploitation costs and the associated uncertainties due to the measurement errors, accounting for the stakeholder's constraints.

Keywords: Optimisation, Spatial variability, Inspection, Maintenance, Bayesian statistics

Résumé

La gestion des structures en béton armé dans le but d'assurer leur sécurité et leur durabilité est devenu un challenge économique d'importance notable. La réponse à ce challenge tient en partie dans la recherche d'un plan d'inspection, de maintenance et de réparation (IMR) optimisé en fonction de contraintes de sureté. Ce travail est placé dans un cadre de maintenance préventive, où les dégradations du béton considérées peuvent amener à la corrosion des armatures, non à la défaillance structurelle. Les modèles de dégradation concernés sont placés dans un cadre probabiliste où la variabilité spatiale de l'exposition environnementale et des propriétés matériaux du béton sont prises en comptes. Sur la base de ces prédictions, un plan d'expérience adaptatif permet d'identifier, à une date donnée, où il est intéressant d'inspecter la structure pour évaluer son état qui conditionnera la décision de maintenance ou de réparation. Un arbre de décision permet ensuite de prédire l'évolution probabiliste de cet état incluant les effets des maintenances et réparations. Ce modèle est enfin utilisé dans une procédure d'optimisation qui vise à déterminer quand et avec quel outil cette structure doit être inspectée pour optimiser l'espérance du budget de suivi d'une structure ou d'un parc ainsi que les incertitudes associées liées aux erreurs de mesure, tout en prenant en compte les diverses contraintes spécifiques des gestionnaires d'ouvrages.

Mots-clés: Optimisation, Variabilité spatiale, Inspection, Maintenance, Actualisation Bayésienne